Characterisation of Particulate Matter Emitted from Aviation Gas Turbines and Spray-Guided Direct Injection Gasoline Engines

By

David Mark Walters

Thesis submitted to Cardiff University for the degree of Doctor of Philosophy

School of Engineering

Cardiff University

2014

Declaration and Statements

This work has not previously been accepted in substance of any degree and is not concurrently submitted in candidature for a degree.

Signed..... (candidate) *Date.....*

This Thesis is being submitted in partial fulfilment of the requirements for the degree of PhD.

Signed..... (candidate) *Date.....*

This Thesis is the result of my own independent work/investigation, except where otherwise stated. Other sources are acknowledged by explicit references.

Signed..... (candidate) *Date.....*

I hereby give consent for my Thesis, if accepted, to be available for photocopying and for inter-library loan, and for the title and summary to be made available to outside organisations.

Signed..... (candidate) *Date.....*

Acknowledgements

There are many people who have helped me in the completion of this research project and I would acknowledge the contributions and thank the following:

My supervisors Professor Philip Bowen and Doctor Andrew Crayford for firstly giving me this opportunity and thereafter providing continual encouragement and guidance throughout the past four years.

My industrial sponsors Rolls-Royce and Ricardo for providing funding and access to the facilities and equipment which allowed many of the experiments presented in this Thesis to be conducted. I would also like to give a special thanks to all the employees I have worked with at these companies, particularly Mark Johnson, Jason King and Richard Osborne. Additionally, I would like to acknowledge the funding provided by the European Aviation Safety Agency which allowed many of the aviation related experimentation presented in this Thesis to be conducted.

All of the staff and researchers at the Gas Turbine Research Centre, Low Carbon Combustion Centre, and SR Technics facilities for their help during exhaust sampling experiments.

To the long-term friends I had before starting this research and the new friends I have made during my time at Cardiff University.

Finally, I would like to express my deepest gratitude to all my family, but principally my parents, brother, sister and grandmother for their endless support and belief.

Published and Presented Work

[1] **Walters, D.**, Sevcenco, Y., Crayford, A., Johnson, M., Marsh, R., Bowen, P., Characterising Particulate Matter Line Losses Through a New Proposed Aircraft Exhaust Sampling System, Proceedings of the European Combustion Meeting, Lünd, 2013.

[2] **Walters, D.**, Sevcenco, Y., Crayford, A., Johnson, M., Marsh, R., Bowen, P., Differential Mobility Spectrometer Particle Emission Analysis for Multiple Aviation Gas Turbine Engine Exhaust at High and Low Power Conditions and a Simulated Gas Turbine Engine Exhaust, Proceedings of the ASME Turbo Expo 2014: Turbine and Technical Conference and Exposition, Düsseldorf, 2014.

[3] Crayford, A., Johnson, M., Marsh, R., Sevcenco, Y., **Walters, D.**, Williams, P., Christie, S., Chung, W., Petzold, A., Ibrahim, A., Delhaye, D., Quincey, P., Bowen, P., Coe, H., Raper, D., and Wilson, C., Sample 3 SC.01: Contribution to Aircraft Engine PM Certification Requirement and Standard, European Aviation Safety Authority, 2011.

[4] Crayford, A., Johnson, M., Marsh, R., Sevcenco, Y., **Walters, D.**, Williams, P., Petzold, A., Bowen, P., Wang, J., and Lister D., Sample 3 – SC.02: Contribution to Aircraft Engine PM Certification Requirement and Standard, European Aviation Safety Authority, 2012.

[5] Bowen, P., **Walters, D.**, Crayford, A., Andersson, J., Osborne, R., Parametric Analysis of Particulate Matter from a GDI Research Engine using DMS, Plenary Presentation, Advanced Emission Control Concepts for Gasoline Engines, Bonn, 2013.

[6] **Walters, D.**, Sevcenco, Y., Crayford, A., Johnson, M., Marsh, R., Bowen, P., Particle Emission Diagnostics Under Simulated Gas Turbine Conditions, Poster Presentation, Fibre-Laser of Gas Turbine Exhaust Species: In Plume Imaging of Gas Turbine Exhaust Species, London, 2013.

[7] Sevcenco, Y., **Walters, D.**, Johnson, M., Marsh, R., Crayford, A., Bowen, P., Evaluation of Particulate Line Losses From Simulated Aircraft Exhaust for Different Residence Times and Dilution Conditions, Poster Presentation, European Aerosol Conference, Manchester, 2011.

[8] **Walters, D.**, Sevcenco, Y., Crayford, A., Johnson, M., Marsh, R., , Bowen, P., Evaluation of Surface Area Particulate Line Losses From Simulated Aircraft Exhaust for Different Residence Time Conditions, Poster Presentation, European Combustion Meeting, Cardiff, 2011.

Thesis Summary

Particulate matter (PM) emissions from combustion processes are of concern as evidence increasingly shows the negative impact that airborne concentrations of ultra-fine particulates can have on human health, environmental damage and global climate change.

Aviation gas turbine and automotive engine exhaust contain a polydisperse mixture of solid and liquid, volatile and non-volatile particles in a hot, highly turbulent flow. In recent years it is the potential health implications of these combustion generated particulates which has become the driving force for more stringent PM emission regulations and improved sampling methodologies. This Thesis explores the characterisation of PM produced by current fleet aviation gas turbines and direct injection gasoline (GDI) automotive engines.

Both the automotive Particle Measurement Programme (PMP) which dictates the European regulatory sampling system and the system currently being developed for international aviation industry regulation only consider non-volatile PM in recorded measurements to increase both reliability and repeatability of results. Experiments were performed to evaluate the performance differences between a volatile particle remover (VPR) which adheres to the specifications within the automotive PMP sampling methodology and that of a system which does not. Two sample aerosols were considered; these consisted of an aerosol containing solely volatile particles and another which consisted of solid core volatile coated particles. Mono-disperse size distributions (100, 50, 30 and 15nm) of each aerosol were employed as 'challenge' aerosols during VPR testing where particle size distributions and number concentrations were performed upstream and downstream of the VPR.

GDI engine technology is becoming more prominent in the automotive market primarily due to the potential for increased operation flexibility and fuel reduction benefits. Regulations governing the output of PM from light duty GDI engines will come into force in 2014 resulting in a new phase of research into GDI engine PM

emission and potential reduction or mitigation methodologies. This Thesis examined how PM emissions varied in response to changes to key engine operational parameters at homogeneous and stratified charge combustion modes and multiple engine loadings.

PM produced by aviation gas turbines is currently regulated using SAE Smoke Number (SN). The main shortfall of SAE SN is that it gives little or no indication of PM size, number or mass; particle parameters which would greatly improve the sensitivity and understanding of an exhaust emission assessment. In order to address these inadequacies the International Civil Aviation Organisation (ICAO) plans to implement a new regulatory standard for the sampling and measurement of non-volatile PM in 2016 through the Committee on Aviation Environmental Protection (CAEP). Appointed with the development of this new methodology is the SAE E-31 Committee, a broad consortium which includes academic institutions, aircraft manufactures, aircraft operators, engine manufactures and Government agencies. During the development of the new standard, multiple large scale PM emission sampling tests have been and are continuing to be performed in order to validate the performance of the sample transfer mechanism and the measurement apparatus being considered as replacements for SAE SN. Analysis of PM emissions gathered during European Aviation Safety Agency (EASA) funded research projects (SAMPLE projects) is presented in this Thesis with a focus on how PM varies as a result of sample conditioning (i.e. dilution, line temperature and length), sample line loses, and the emission source.

Gas turbine designers and manufactures are continually researching new combustion technologies as they strive for a competitive advantage in the industry. The introduction of lean-burn combustion regimes into engine combustor design is one such advancement which can provide a significant reduction in pollutant emission formation. In this Thesis analysis of PM emissions generated from the combustor sections of a modern large civil aviation gas turbine, operating in rich and lean burning combustion modes was performed. The use of a traversing sample probe system to acquire exhaust emissions at the exit of the combustor allowed fully annular sample measurements to be made.

Table of Contents

List of Figures

List of Tables

List of Equations

List of Notations

Symbol	Units	Description
A	m^2	Filter spot area
D	-	Data set
d_{50}	nm	Particle size at which an instrument has 50% counting efficiency
d_{90}	nm	Particle size at which an instrument has 90% counting efficiency
D_a	nm	Aerodynamic diameter
DF_{AR}	-	Deposition fraction of particles in the alveolar region
DF_{HA}	-	Deposition fraction of particles in the head airways region
DF_{Total}	-	Total deposition fraction of particles in the respiratory tract
DF_{TR}	-	Deposition fraction of particles in the tracheobronchial region
KA	-	Lower asymptote
KB	-	Upper asymptote
KT	-	Limit of growth
MC	-	Growth rate
MK	-	Point of maximum growth
N	$\#/cm^3$	Particle number concentration
λ	-	Equivalence ratio
P	kPa	Sample pressure
P_3	kPa	Inlet pressure of gas to the turbine section
R_S	-	Absolute reflectance of the stained smoke number filter material
R_W	-	Absolute reflectance of the clean smoke number filter material
T	K	Sample temperature
T_3	K	Inlet temperature of gas to the turbine section

V	m^3	Volume
V_c	m^3	Clearance volume
V_d	m^3	Displaced volume
V_t	m^3	Total volume
w	-	Log-normal parameters
W	kg	Sample mass
η_P	-	Total PM penetration efficiency
σ	-	Standard deviation

List of Abbreviations

APU Auxiliary Power Unit

AQS Air Quality Strategy

ARP Aerospace Recommended Practice

ASK Available Seat Kilometres

ATDC After Top-Dead Centre

BP British Petroleum

BSFC Brake Specific Fuel Consumption

BTDC Before Top-Dead Centre

CA Crank Angle

CAEP Committee on Aviation Environmental Protection

CE Counting efficiency

CH_4 Methane

CO Carbon Monoxide

CO_2 Carbon Dioxide

CPC Condensation Particle Counter

DF Deposition Fraction

DMA Differential; Mobility Analyser

DMS Differential Mobility Spectrometer

DPF Diesel Particulate Filter

EASA European Aviation Safety Agency

EGR Exhaust Gas Recirculation

EPA Environment Protection Agency

ET Evaporation Tube

EU European Union

EU European Union

EVC Exhaust Valve Closed

EVO Exhaust Valve Open

EVVT Exhaust Variable Valve Timing

FOCA Federal Office of Civil Aviation

FP Fuel Pressure

GDI Gasoline Direct Injection

GE General Electric

GPF Gasoline Particulate Filter

GTRC Gas Turbine Research Centre (Cardiff University)

H_2O Water

H_2SO_4 Sulphuric Acid

HC Hydrocarbons

HEPA High Efficiency Particle Air

HES Hot-End Simulator

HPRC High Pressure Combustor Rig

ICAO International Civil Aviation Organisation

ICRA	International Commission on Radiological Protection
ID	Internal Diameter
IF	Inhalation Fraction
IPCC	Intergovernmental Panel on Climate Change
IVC	Inlet Valve Closed
IVO	Inlet Valve Open
IVVT	Inlet Variable Valve Timing
LCCC	Low Carbon Combustion Centre (Sheffield University)
LOSU	Level of Scientific Understanding
MCRE	Multi-Cylinder Research Engine
NaCl	Sodium Chloride
NAEI	National Atmospheric Emissions Inventory
NH_3	Ammonia
NO	Nitric Oxide
NO_2	Nitrogen Dioxide
NO_x	Oxides of Nitrogen
OEM	Original Engine Manufacturers
OPC	Optical Particle Counter
PAH	Poly Aromatic Hydrocarbons
PM	Particulate Matter
$PM_{0.1}$	Particulate matter with an aerodynamic diameter ≤0.1µm
PM_{10}	Particulate matter with an aerodynamic diameter ≤10µm
$PM_{2.5}$	Particulate matter with an aerodynamic diameter ≤2.5µm
PMP	Particle Measurement Programme
PNC	Particle Number Counter
PND_1	Primary Particle Number Diluter
PND_2	Secondary Particle Number Diluter
PTFE	Polytetrafluoroethylene
RF	Radiative Forcing
RQL	Rich-Quench-Lean
SCR	Sector Combustor Rig
SCRE	Single Cylinder Research Engine
SGDI	Spray-Guided Direct Injection
SMPS	Scanning Mobility Particle Sizer
SN	Smoke Number
SN	Smoke Number
SN’	Smoke number of individual exhaust sample
SO_2	Sulphur Dioxide
SOI	Start of Injection
TRL	Technology Readiness Level
TSCI	Transonic Super Critical Injector
UK	United Kingdom
UTRC	United Technologies Research Centre
VG	Volatile Generator

VOC	Volatile Organic Compounds	WHO	World Health Organisation
VPR	Volatile Particle Counter	WOT	Wide-Open Throttle
VPR	Volatile Particle Remover		

Chapter 1

Introduction

Aviation and automotive travel and transportation have become standard components of modern society. The growth of these sectors has led to extensive research and development across all aspects of both industries. Outcomes of this research include furthering our understanding and improving factors such as passenger safety, manufacturing efficiency and the mitigation of any potential economic and ecological impacts which may occur as a result of the industries influence.

There are many ongoing challenges for all involved in these areas, one of which is control of the emission of pollutants into the atmosphere from the combustion processes associated with aviation and automotive engines. This research project investigates a pollutant which has come under increasing scrutiny in recent years, namely PM.

A by-product of combustion processes, PM has become a major concern, primarily due to its negative impacts on human health, but also for its potential impact on global climate change and environmental damage. The aim of this Chapter is to provide the reader with an introduction to some fundamental aspects of PM, a brief history of how and why it has become a topic of current research, and to introduce the research motivations, aims and objectives of this specific research project.

1.1 What is Particulate Matter?

PM is the term given to solid or liquid particles which are held in suspension in an atmospheric aerosol. These particles primarily exist in the nanometre (<100nm) to micrometre (1000nm) size range, with PM produced in controlled combustion systems commonly exhibiting particle size distributions from 5nm to 1µm. PM can also be created naturally, for example, in coastal regions it is common for there to be high airborne concentrations of sodium chloride (NaCl) particles which develop from sea sprays. Alternately, events such as forest fires or volcanic eruptions can release clouds of fine ash particulates which can remain in the atmosphere for a long period of time.

However, it is anthropogenic PM emissions which are of growing concern. The major sources of these emissions in low altitude ambient air are the automotive transport and stationary power generation sectors, while at high altitudes civil air travel is the primary emission source.

1.1.1 Concerns Associated with PM

The primary reason for concern over the emission of anthropogenic PM is the growing evidence that suggests exposure to high concentrations of fine combustion particles can adversely affect human health and the environment. It has long been accepted that PM can be damaging to human health, principally to the respiratory and cardiovascular systems [1]. Although there is still uncertainty on its overall impact, there is no doubt that PM is also a contributing factor to global climate change [2]. A detailed discussion of how these concerns relate to PM produced by aviation gas turbines and automotive engines is provided in the following Chapters.

1.1.2 Sources of PM

Atmospheric PM emissions often comprise of a complex mixture of different particles which are categorised as being either primary or secondary components depending on the nature of their formation. Primary components are particles which are released into the atmosphere directly from a source; whereas secondary components develop

during chemical reactions in the atmosphere. Some examples of primary and secondary components of PM are listed in Table 1.1.

Table 1.1: Examples and descriptions of primary and secondary components of airborne PM, adapted from [3].

Primary Components	**Sources**
Sodium Chloride	Sea salt
Elemental carbon	Elemental carbon (also referred to as black carbon or soot) is formed during high temperature combustion of fossil fuels such as coal, natural gas and oil (diesel and gasoline) and biomass fuels.
Trace metals	Low concentrations of metals such as lead, cadmium, nickel, chromium, zinc and manganese are mainly generated by metallurgical processes such as steel making. They are also found as impurities or additives in fuels which can be released during combustion. Mechanically abrasive processes, such as brake wear also release metallic fragments.
Mineral components	Minerals can be found in course dusts produced from quarrying, construction and demolition work and from wind driven dusts. These may include particulate compounds of aluminium, silicon, iron or calcium.
Secondary Components	**Sources**
Sulphates	Formed by oxidation of sulphur dioxide (SO_2) in the atmosphere to form sulphuric acid (H_2SO_4), this can then react with ammonia (NH_3) to give ammonium sulphate ($(NH_4)_2SO_4$).
Nitrates	Formed by the oxidation of nitrogen oxides (NO_x) such as nitric oxide (NO) and nitrogen dioxide (NO_2). In the atmosphere these form nitric acid (HNO_3), which can further react with NH_3 to give ammonium nitrate ($(NH_4)NO_3$).
Primary and Secondary Components	**Sources**

Organic carbon	Primary organic carbon is mainly produced by the automotive emissions as unburnt fuel or lubrication oil. Other industrial and domestic combustion sources can also release organic compounds into the atmosphere. Secondary organic carbon can be produced from the oxidation of volatile organic components (VOC) such as unburnt hydrocarbons.

Historically, airborne particle concentration measurements in the United Kingdom (UK) have primarily focussed on PM_{10} levels. The PM_{10} classification refers to particles, determined by mass, to pass a sampling inlet with a 50% cut-off efficiency at a 10µm aerodynamic diameter. This selection was made as at the time it was believed this size range would best describe the particles most likely to be deposited in human lungs [4]. Figure 1.1 was produced using data published by the National Atmospheric Emissions Inventory (NAEI) and shows source specific estimates for the output of anthropogenic PM_{10} in the UK. It can be seen that total PM_{10} output has been significantly reduced since 1970 as regulatory limits, improved production practises, and technological advances, particularly in combustion industries, have been introduced.

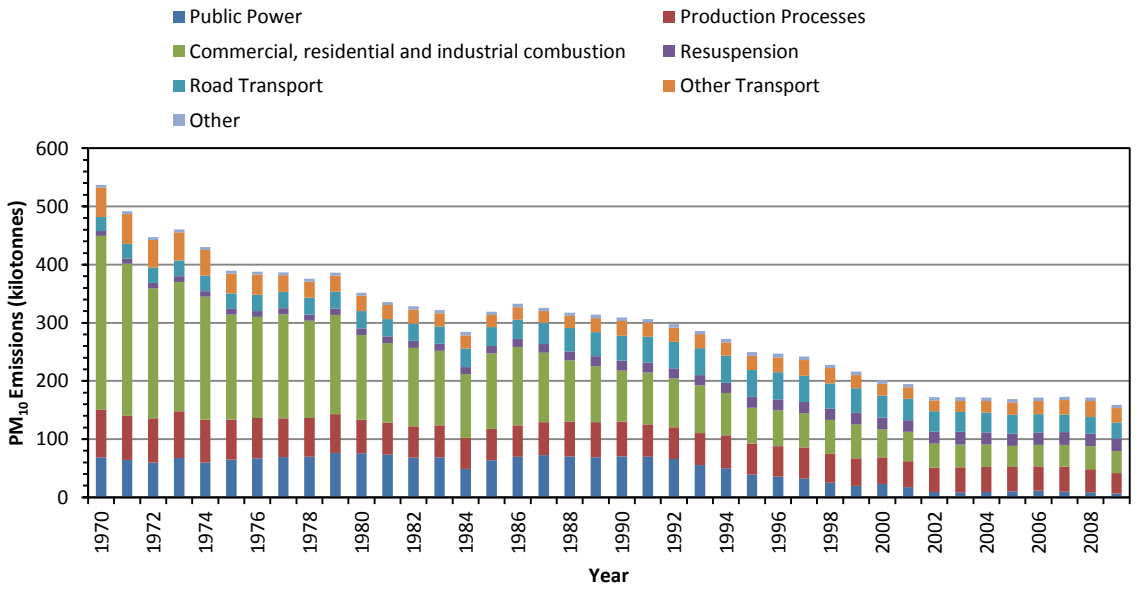

Figure 1.1: Estimated PM_{10} emissions in the UK from 1970 to 2009, produced using data published by the NAEI.

1.1.3 Ambient PM Distributions and PM Size

Ambient PM studies conducted at over a 1000 locations in the United States (US) in the 1970's found that ambient PM concentrations display consistent multi-modal distributions over several physical metrics, such as number, mass or volume concentrations [5]. The trends which were observed then are still relevant today [6], and typically particle diameters of ambient PM span 5 orders of magnitude ranging from 0.001 to 100 micrometres (1 to $1x10^5$nm). Figure 1.2 shows how these multi-modal distributions are distributed across this size range with average values for the concentrations, mean diameters and standard deviations found by Whitby in 1978 [5].

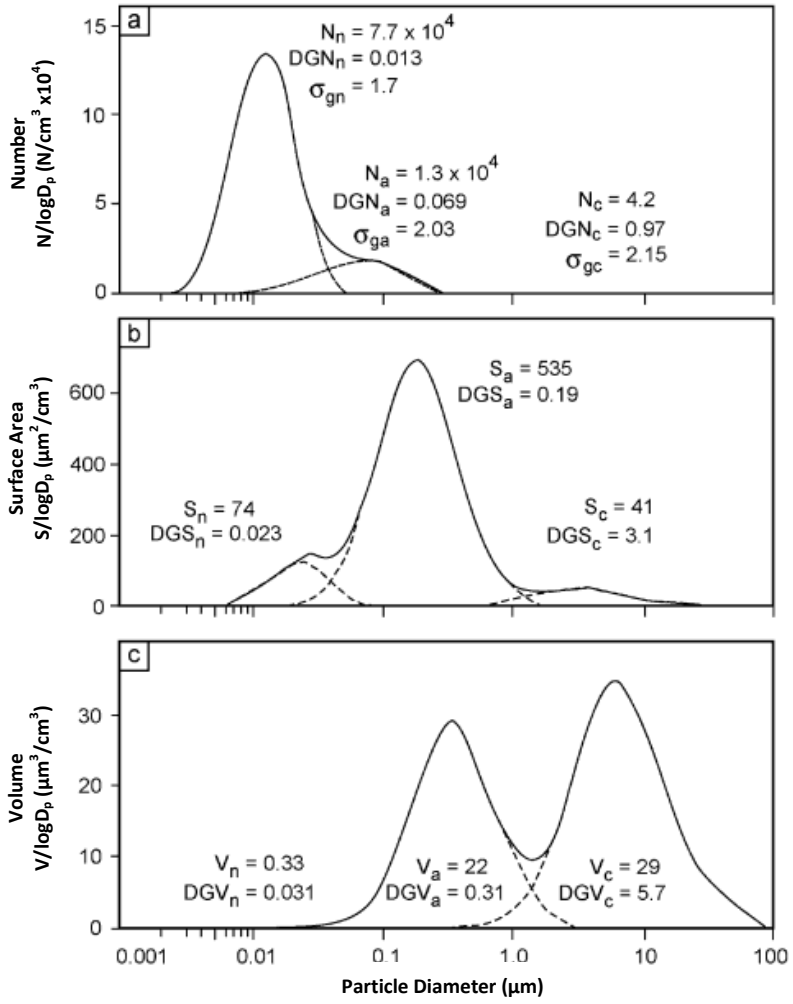

Figure 1.2: Distributions of coarse (c), accumulation (a) and nuclei (n) mode particles displayed in three characteristics: (a) number, N, (b) surface area, S, and (c) volume, V for an average PM size distribution in the US. DGV = geometric mean diameter by

volume, DGS = geometric mean diameter by surface area, DGN = geometric mean diameter by number, and D_p = particle diameter, reproduced from [7].

In panel (a) of Figure 1.2 the highest number of ambient particles is typically below 100nm. The mode present at 10nm is what is commonly associated with a nuclei (or nucleation) mode while the mode present at 70nm is what would be commonly be associated with an accumulation (or agglomeration) mode. The formation mechanisms and particle make-up of these modes will be discussed in detail later in this Thesis. In panel (b) we see that the majority of a distributions surface area is located between 100 and 1000nm. Lastly panel (c) shows that the majority of an ambient PM distributions volume, and consequently most of the mass, is situated in particles with diameters greater than 100nm. It is important to state that these average representations of typical ambient PM distributions may vary depending on the sample location, conditions, and time due to differences in emission sources, atmospheric conditions, topography and the age of the sampled aerosol [8].

Classification of PM is primarily done on a size basis by assuming an aerodynamic diameter (D_a) of the particles as is shown in the NAEI PM_{10} data presented in Figure 1.1. Aerodynamic diameter is defined as the diameter of a sphere, with unit density that has aerodynamic behaviour identical to that of the particle in question. This assumption is made because of the non-uniform morphology that PM often exhibits.

The most common particle size ranges which are used to describe atmospheric concentrations of PM are PM_{10}, $PM_{2.5}$, $PM_{0.1}$, and ultrafine ($<PM_{0.1}$). These references are used to describe total particle concentrations where the size range extends below 10µm, 2.5µm, and 0.1µm respectively. In recent years PM_{10} has become more generally used to characterise total airborne particle concentrations as it encapsulates virtually all total suspended particles. Epidemiology studies have shown that particles in the 2.5 - 10µm size range are inhalable, and therefore sometimes referred to as the ‘thoracic fraction‘, as they are likely to be deposited in the upper regions of respiratory tract such as the nose and throat. Vastly more significance is now placed on particles smaller than 2.5µm, as this is now considered to be the ‘respiratory fraction’ - the fraction which is inhaled into the lungs - of PM size distributions.

PM measurement apparatus and particle detection limits have improved in parallel with the concern over the harmful effects inhaled anthropogenic PM can have on human health, meaning classifications such as $PM_{0.1}$ are becoming far more relevant. Further classifications beyond these popular size classifications are also commonly referenced and it largely depends on the sampling situation and PM source as to which is an appropriate selection. An example of PM classifications as defined by the Environmental Protection Agency (EPA) is shown in Table 1.2.

Table 1.2: PM classification size ranges as defined by the EPA.

EPA definition	Particle size range
Super-coarse	$D_a > 10\mu m$
Coarse	$2.5\mu m < D_a \leq 10\mu m$
Fine	$0.1\mu m < D_a \leq 2.5\mu m$
Ultrafine	$D_a \leq 0.1\mu m$

PM distributions produced during controlled combustion processes, such as those which occur in a gas turbine and internal combustion engines, predominately exists in the ultrafine size region. Figure 1.3 and Figure 1.4 provide a visual representation of the scale of these particles, and the particle size ranges as defined by the EPA, including the aforementioned super-coarse, coarse, and fine particle size boundaries.

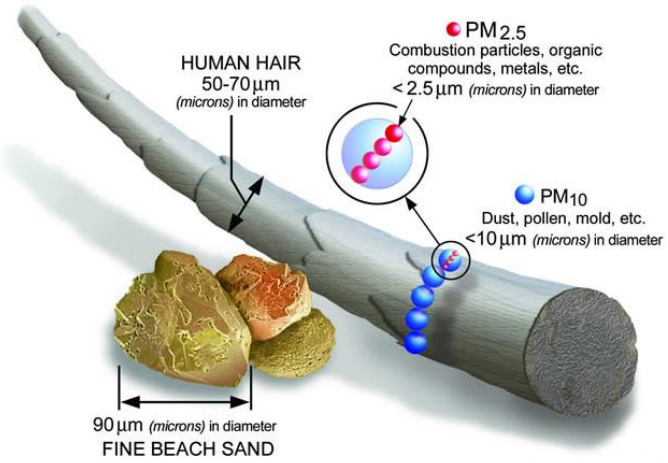

Figure 1.3: Illustration of PM size in comparison to human hair, reproduced from www.epa.gov.

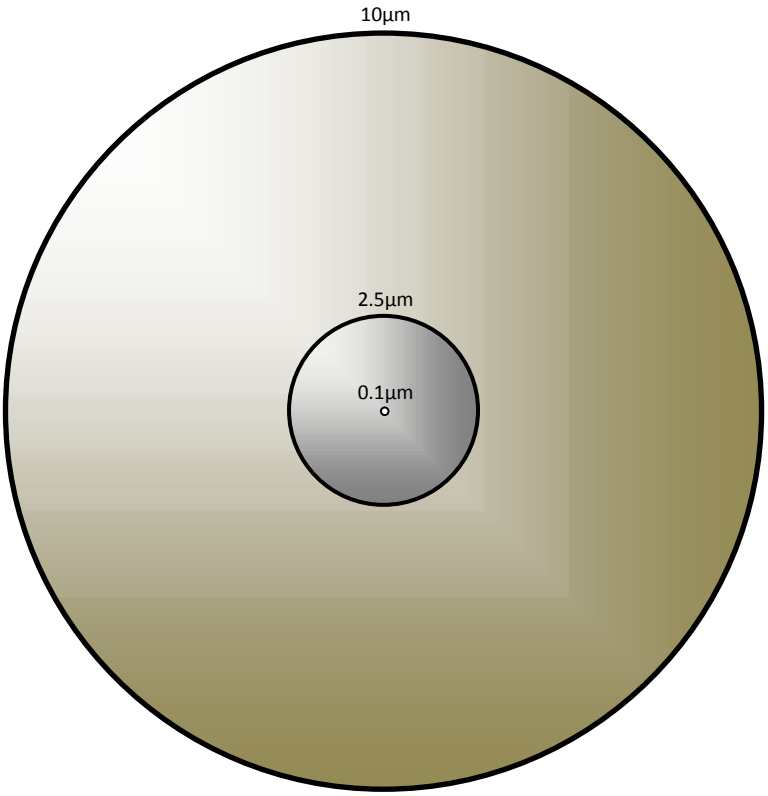

Figure 1.4: Visual representation of main particle sizes used for classification of particulate matter, 10µm, 2.5µm and 0.1µm. Scale: 1cm depicts 1µm.

The aim of theses illustrations is to display the relative size of some of the most abundant particles in a typical PM distribution and in doing so provide an indication of the challenges which can arise when trying to accurately sample, measure, and regulate emissions of this nature.

The disparity between particle classifications is even more apparent when considering PM mass. Figure 1.5 shows a comparison of the masses for a single 0.1, 2.5 and 10µm particle assuming they are spherical and representative of soot particles emitted from a gasoline automotive engine. The difference in mass between the largest and smallest of these particles extends to several orders of magnitude and therefore it is very important to acknowledge that small changes in particle number concentration at the larger end of the PM size spectrum can make an enormous difference to overall recorded mass concentrations.

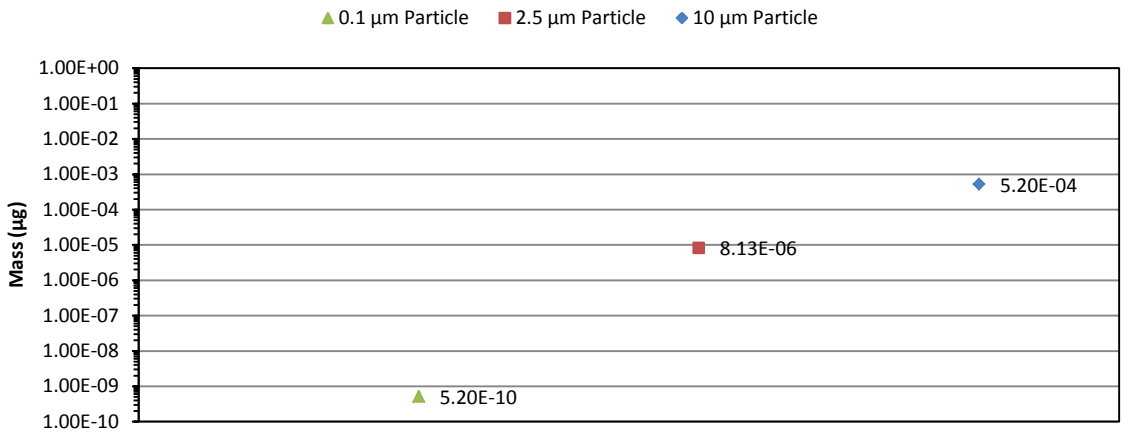

Figure 1.5: Mass comparison for theoretical 0.1, 2.5 and 10µm soot particles.

This relationship between particle size, number and mass can be extremely sensitive to change and for this reason it can be difficult to establish a single measure that can describe PM distributions adequately. In reality it is often the case that an assessment of the sampling situation or system being analysed must be made and a procedure put in place to ensure the measurements recorded accurately reflect the PM that is being sampled.

1.2 History of Air Quality Concerns in the UK

Evidence of PM being recognised as a problem in populated UK cities such as London is documented as long ago as 1661. At this time John Evelyn presented King Charles II with a report on how he believed that smoke pollution within the city would shorten a person's life [9]. However, efforts to control pollution levels were extremely marginal until the 19th Century when a Parliamentary Select Committee was instructed to review and act upon what was becoming an increasing problem in urban areas. This led to the passing of legislation which empowered police officers to take action against individuals emitting what they determined to be excessive levels of 'black smoke'. Actual convictions and implementation of these laws were rare, principally due to the ambiguity of the language used to define expectable emission limits [10].

Following the First and Second World Wars the UK entered into an industrial revolution and experienced increased levels of urbanisation. At this time the main

cause of air pollution was the domestic and industrial burning of coal. The output of smoke continued to be largely unregulated due to difficulties in the implementation of abatement legislation and this resulted in smog formation during cold, calm weather. The most severe of these occurrences, which in now described as the 'Big Smoke' or 'Great Smog', consisted of very high levels of smoke and sulphur dioxide (SO_2) [11]. Lasting from the 5th to the 9th of December in 1952, smoke concentration levels increased to 56 times the standard level in city centre of London leading to a dramatic increase in hospital admissions relating to respiratory problems. Furthermore, it was shown that during, and in the subsequent weeks following the smog, an additional 4000 deaths were recorded compared to normal mortality figures for the time [10]. In a more recent study published in 2004 the authors concluded that the number of deaths directly related to the smog was likely nearer 12,000 through incorporation of deaths caused by slower to develop respiratory conditions such as influenza in the months following December of 1952 into their estimate [12].

Since the Great Smog mitigation of air pollution is taken far more seriously in the UK. As emission sources have evolved, so have the research and legislative efforts placed on combating what is an increasingly complex and problematic issue.

1.3 Air Quality Legislation in the UK

The events of 1952 resulted in widespread public concern which initially went unanswered by the UK Government. However with continued support from some Members of Parliament the Government responded with the formation of the Clean Air Act 1956 [13]. This would be the beginning of defined legislation against airborne PM in the UK. The main objective of this legislation was solely to reduce smoke pollution. This was to be achieved by implementing a prohibition on 'dark smoke', limits on furnace smoke, dust and grit emissions, and the introduction of smoke control areas where low smoke fuels had to be burnt. The legislation was successful in the reduction of both smoke and SO_2 as domestic and industrial properties became more ecologically aware. As time progressed the installation of gas and electricity into domestic properties became more widespread, as did the burning of coals with lower

sulphur content. Industrial facilities also began to relocate to more rural areas and incorporated improved chimney stack design to meet requirements.

In 1968 a revision of the Clean Air Act [14] was published which extended on the established emission reduction and chimney stack height requirements. A quantitative measure was also included to better define 'dark smoke' as being a value greater than 2 on the Ringelmann Chart [15], a rudimental visibility index based on an observer's ability to see through a smoke plume.

The main source of air pollution in the UK has been subject to considerable change since the 1950s and 60s. This has mainly come in the form of a shift from the highest pollutant emitter being domestic and industrial burning of fossil fuels to automotive transport. This transposition has developed as the number of licensed vehicles in the UK has increased from 4 million in 1950 to over 34 million as of 2011 as shown in Figure 1.6.

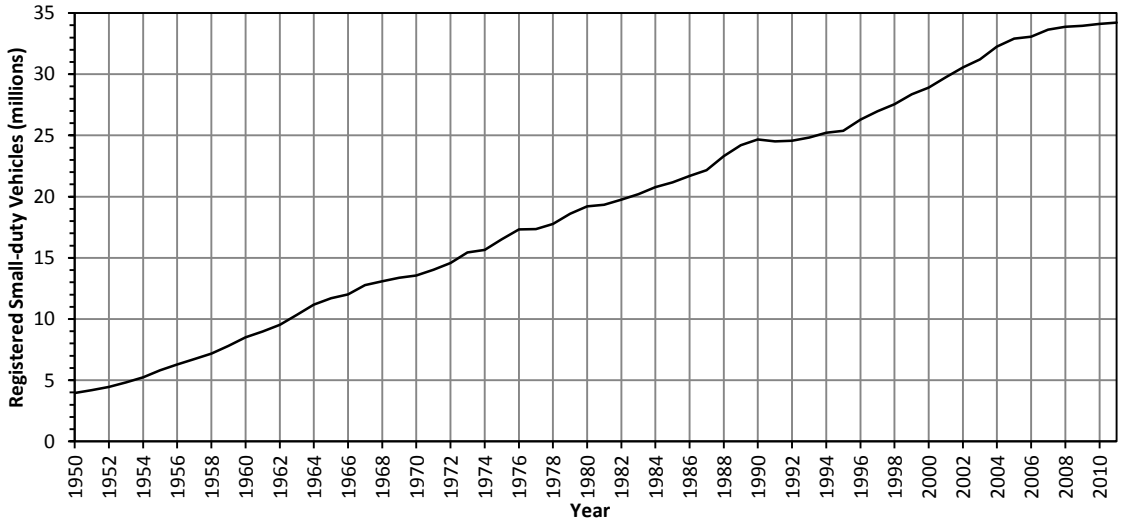

Figure 1.6: Number of registered vehicles in the UK from 1950 to 2011, produced using data published by the Department for Transport.

To combat this change a further revised Clean Air Act [16] was passed in 1993 which combined elements of the 1956 and 1968 framework with the inclusion of additional elements specific to motor vehicle emissions.

Pollution legislation in the UK for the following two decades was dominated by directives put in place by the European Union (EU). These have included several

emission requirements for gaseous and particulate emissions from various sources (1970 - EC Directive 70/220/EEC and 1972 - EC Directive 72/306/EEC for vehicles, 1988 - EC Directive 88/609/EEC for industrial plants, 1989 - EC Directive 89/429/EEC for waste incinerators) and specifications on fuel composition, particularly limiting the content of sulphur (1975 - EC Directive 75/716/EEC) and lead (1978 - EC Directive 78/611/EEC).

The majority of the UK Government's more recent involvement in air quality control has been in the form of setting and monitoring air quality targets, the first instance of which was the publication of the Environment Protection Act of 1990 [17]. This made local authorities responsible for small scale emission sources for the first time and established a system of pollution control for the most potentially polluting industrial processes. In addition to the EU directives which set new vehicle emissions requirements the 1991 Road Vehicle Regulations also set standards for the emission of carbon monoxide and hydrocarbons (HC).

The most comprehensive review of air quality in the UK came after the introduction of the Environment Act 1995 [18] which made it a requirement that the UK Government and devolved administrations produce a national Air Quality Strategy (AQS) containing standards, objectives and measures for improving ambient air quality. The result of this Act was the publication of first national AQS in March 1997. The 1997 AQS included EU air quality targets, in addition to more stringent national targets, and defined 8 pollutants of particular concern, these being:

- Benzene
- 1,3-butadiene
- Carbon monoxide (CO)
- Lead
- Nitrogen Dioxide (NO_2)
- Ozone
- PM_{10}
- Sulphur Dioxide (SO_2)

The airborne concentrations of the listed pollutants were required to be monitored and reviewed on an annual basis with their respective emissions targets being achieved between 2003 and 2008.

Following the initial annual review periods some of the targets set in the 1997 AQS were revised in 2000 with the publication of the AQS for England, Scotland, Wales and Northern Ireland. The revisions included the tightening of the benzene and CO reduction targets to protect vegetation and ecosystems, and the relaxing of concentration limits. PM_{10} targets were also reduced as it was believed national controls alone could not achieve those set in 1997 as estimates placed up to 20% of annual mean particle levels in the UK as originating from emissions in mainland Europe. The AQS published in 2000 also highlighted the need for investigation into the potential health impacts posed by polycyclic aromatic hydrocarbons (PAH) emissions. In 2003 an amendment to the AQS for England, Scotland, Wales and Northern Ireland was made which did include PAHs emissions limits for the first time along with further tightening of targets for benzene, CO and PM. The most recent AQS was published in 2007 and detailed target values for all of the previously described pollutants. It also described a planned way forward for the work and planning that was required to tackle air quality issues. Within this was a new policy framework specifically designed for tackling fine PM emissions.

Currently UK air quality policies and pollutant control and reduction targets are dictated by the EU Ambient Air Quality Directive (2008/50/EC) and were passed into UK law within the 2010 Air Quality Standards Regulations. Air pollution will continue to evolve and there will be an ongoing challenge to better understand the risks which are posed and create solutions to mitigate them. There is little doubt that a part of this process will include the introduction of new emissions regulations and laws being implemented to further improve air quality for the future.

1.4 Research Motivations

There are two main research motivations for the study and better understanding of PM emissions. These are the growing concerns over its negative impacts on human

health and global climate change. There are numerous studies documented in the literature to show that both concerns are valid, and there is also evidence that aviation gas turbine and automotive emissions are direct contributors to the problem.

1.4.1 Specific Aim and Objectives

The aim of this research project is to provide a contribution to the understanding and implementation of gaseous emission sampling methodology, PM characterisation under contemporary and lean burning combustion conditions, and to further establish fast particulate matter measurement techniques. This is to be achieved through the study of PM emissions from aviation gas turbines and spray-guided direct injection (SGDI) gasoline engines, utilising both state-of-the-art PM measurement instrumentation and experimental facilities. Results gained from large scale combustion emission sampling campaigns will further the development of new gaseous and particle sampling methodologies and provide an assessment of how gas turbine combustor and automotive engine operating parameters influence PM production.

In order to accomplish the previously described aim the objectives of this research programme are:

- To highlight the reasoning for PM research, with particular focus on potential danger to human health, and use experimental measurements to reinforce the need for stringent PM regulation.
- To explore the current PM measurement procedures which have been adopted by the diesel automotive industry and discuss their potential application for aviation gas turbine PM measurements.
- To investigate the influence of volatile particles within a sampling system and the effectiveness of current and future removal techniques.
- To use state of the art SGDI gasoline research engines to investigate how engine operating parameters, engine operating modes, and engine loading influence PM production.

- To make DMS measurements on current piezoelectric actuation fuel injection systems and prototype super-heated gasoline injection systems to assess the potential emissions reduction benefits of this new fuel injection technology.
- To take differential mobility spectrometer (DMS) measurements from the exhausts of multiple gas turbine engines, produced by different manufactures and running at numerous operation conditions, in order to establish an assortment of typical particle size, number and mass distributions.
- To investigate and provide a critical assessment of the readiness of the PM sampling methodology being developed by the SAE E-31 Committee.
- To make PM measurements upstream and downstream of the 25m sampling line section proposed by the SAE E-31 Committee in its new sampling methodology. Through the use of existing particle line loss models an assessment of how representable the sample at the analysis suite is compared to the original emission source will be made.
- To make DMS measurements on rich-burn and lean-burn aviation gas turbine engine combustors and to assess the potential emission reduction benefits of lean-burn combustor technology.
- To provide a summary of the main conclusions which can be drawn as a result of all of the previous listed objectives, and discuss areas of this research which could be extended or improved on in the future.

1.5 Thesis Structure

The study of PM produced from two very different combustion technologies has resulted in the potential scope of this this Thesis being fairly broad. An attempt has been made during its development to focus, wherever possible, on similarities and differences associated with PM within current and future aviation and gasoline automotive technologies. However, during the presentation of experimental results this was determined to be inappropriate and therefore for the majority of this Thesis experimental data sets are discussed in isolation prior to overall conclusions being made.

Following an initial review of aviation and automotive engine technologies an assessment of the fundamental principles of combustion exhausts and PM generation will be undertaken (Chapter 1 and Chapter 2). The experimental facilities and apparatus which has been utilised in this research project will also be discussed (Chapter 3). The novel sections of this Thesis will focus on four main areas:

1) The influence of volatile particles on PM sampling systems and application of appropriate removal devices in the automotive and aviation industry standard sampling systems (Chapter 4).

2) Analysis of PM produced by traditional and novel gasoline injection systems and how engine operating modes (homogenous and stratified charge), fuel injection strategies and valve train management can influence PM production for GDI research engines (Chapter 5).

3) The development and appraisal of a new, non-volatile PM and gaseous emissions sampling system for the aviation industry (Chapter 6).

4) Analysis of PM produced by the combustion sections of large current fleet gas turbines engines and how engine operating modes (rich-burn and lean-burn) can influence PM production (Chapter 7).

Following the presentation of the experimental results and their discussion a set of conclusions and an assessment of the successfulness of these novel aspects of this work and the research project as a whole will then be drawn (Chapter 8). This will provide a concise representation of what has been achieved through this work and will also include recommendations and proposals for required future work.

Finally, all the relevant information from this body of work coupled with the research of others which is cited within in this Thesis will be collated. Any supplementary documentation will be included as an appendix.

1.6 Chapter Summary

Sub-micron airborne particles are very common and arise from a multitude of different sources, both natural and anthropogenic. Concerns over the concentration levels of certain types of PM has grown throughout history and resulted in legislation and regulations being put in place to reduce harmful emissions, particularly in combustion related industries.

There are many challenges associated with measuring PM accurately and with good repeatability. This Thesis will investigate how the automotive industry currently achieves PM measurements for diesel engines in the PMP, particularly the methodologies association with volatile particle removal. Additional research into the variation of PM emissions from GDI engines will also be performed. The aviation industry is attempting to address current shortcomings in PM certification with the development of a new emission sampling system, capable of measuring both non-volatile PM number and mass concentrations. PM analysis performed during this development will be presented. The nature of PM produced from different sources in both the aviation and the automotive industry will also be presented to examine how novel combustion technologies and operational configurations are being employed in an effort to reduce overall pollutant emissions output.

Chapter 2

Gas Turbine and Automotive Engine Technologies and Exhaust Emissions

This Chapter aims to provide the reader with a concise review of both aviation gas turbine and internal combustion engines by presenting their fundamental operating principles and technological development. Additionally, the exhaust characteristics of both technologies are investigated, with particular focus placed on the PM emissions within these exhaust.

With regards to PM emissions, firstly a detailed assessment of particle characterisation is given with a subsequent overview of particulate formation mechanisms in combustion engines. The morphology and diverse nature of combustion generated PM is discussed, and the current limitations of PM characterisation methodologies are presented.

The major concerns and impacts of PM emissions are investigated, highlighting the growing evidence on the potential damage PM can cause to the environment and human health.

Current PM regulatory standards for the aviation and automotive industries are discussed with notable aspects of their sampling criteria and research studies which led to their design.

Finally, methodologies for the reduction and removal of PM from combustion exhausts are presented and qualitatively assessed for how applicable they are to meet the newer, more stringent PM regulations and targets.

2.1 Brief Overview of Gas Turbine Technology

Research and development of gas turbine technology began in the early 20th century as an improved form of power generation compared to conventional steam turbines of the time. With advantages such as the elimination of the need for large boilers and water storage systems that were required in order to produce a working fluid, it was believed the gas turbine would offer a more compact and efficient power generation unit [19].

The removal of a direct steam driven turbine means that in a gas turbine there is a need to accelerate the working fluid, commonly air, through the turbine section. To do this a pressure differential between the inlet and outlet of the system is developed using a compressor. The highly compressed air is allowed to expand though the turbine section driving a shaft which can then be used to create power. Assuming no losses any power output developed by this compression and expansion of air through the turbine would only equal that which was absorbed by the compressor. To generate more energy in the working fluid a combustible mixture of fuel and air must be added and ignited prior to it passing through the turbine section. This increases the temperature and gaseous expansion of the working fluid thus leading to a greater power output. This is the fundamental operation of a gas turbine, and establishes its three major components, these being a compressor, combustion chamber and turbine as illustrated in Figure 2.1.

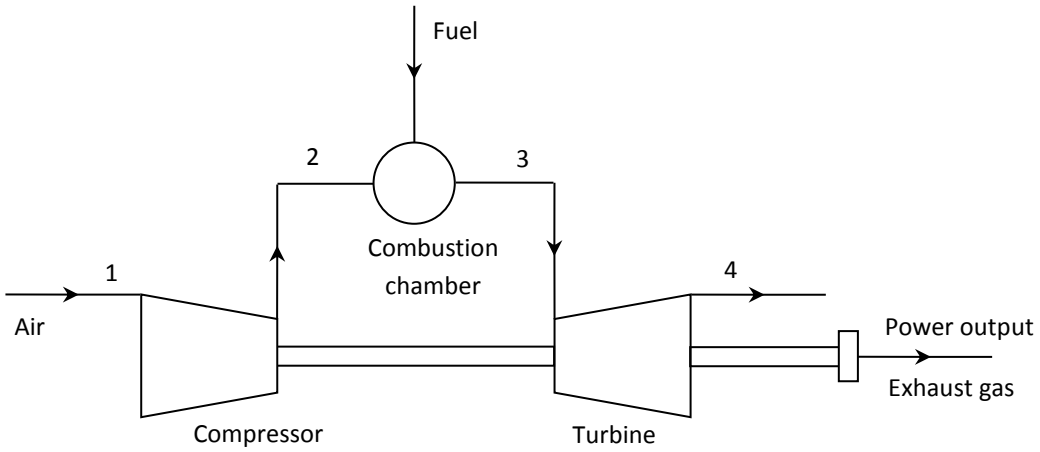

Figure 2.1: Illustration of the principle components of a gas turbine system.

The gas turbine is a system which follows the thermodynamic concept known as the Brayton cycle. The Brayton cycle, Figure 2.2, describes the changes that occur to the working fluid of an engine that adopts the use of a compression, combustion and expansion procedure in order to produce work.

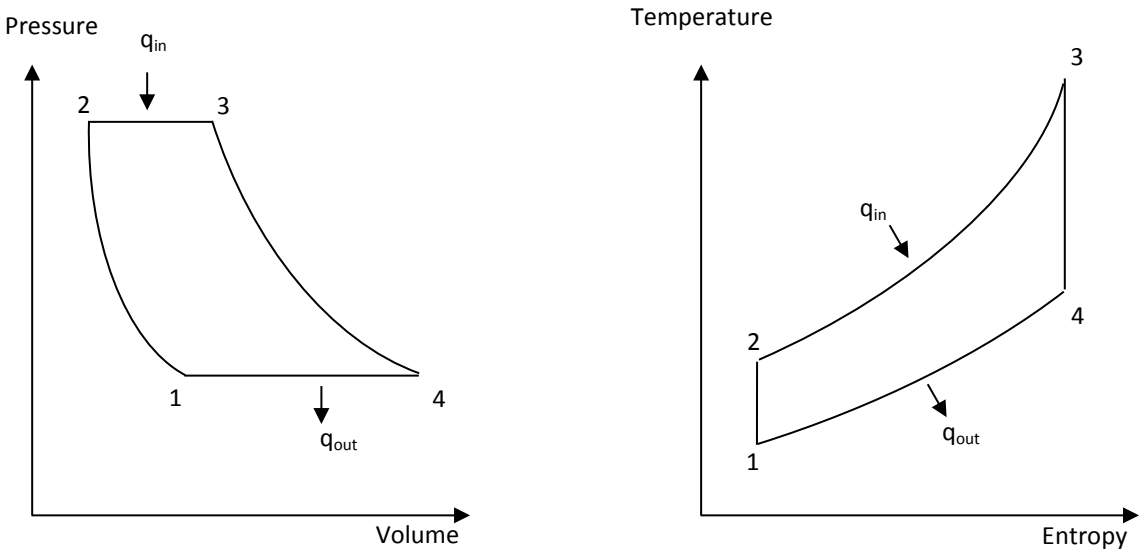

Figure 2.2: Idealised Brayton cycle for a gas turbine engine.

The idealised version of this cycle can be applied to gas turbine engines providing that certain assumptions are made [19], namely:

a) *Compression and expression processes are reversible and adiabatic, i.e. isentropic.*
b) *The change of kinetic energy of the working fluid between the inlet and outlet of each component is negligible.*
c) *There are no pressure losses in the inlet ducting, combustion chambers, heat exchangers, intercoolers, exhaust ducting, and duct work connecting the components.*
d) *The working fluid has the same composition throughout the cycle and is a perfect gas with constant specific heats.*
e) *The mass flow of the gas is constant throughout the cycle.*
f) *Heat transfer in a heat exchanger (assumed as counterflow) is 'complete', so that in conjunction with d) and e) the temperature rise on the cold side is the maximum possible and exactly equal to the temperature drop on the hot side.*

Assumptions *d)* and *e)* imply that the combustion chamber, in which fuel is introduced and burnt, is considered as being replaced by a heater with an external heat source.

2.1.1 Gas Turbines for Aircraft Propulsion

Research into gas turbines for the purpose of aircraft propulsion occurred alongside that of the exploration of gas turbine power generation systems with the first patent for a gas turbine engine granted in 1922 to Maxime Guillaume. The practical theory of using a gas flow to drive enclosed aerofoils was published in 1926 by A.A Griffiths in a report to the Royal Aircraft Establishment titled "An Aerodynamic Theory of Turbine Design" [20]. At the time it was widely regarded that a gas turbine engine with a shaft driven propeller, a turboprop engine, was the best method of generating an aircraft's thrust. Gas turbines from which thrust was developed solely by the jetted exhaust gases of the engine were being developed my multiple researchers in the 1930's, most notably Frank Whittle and Hans von Ohain. It was Whittle who first patented such a design which subsequently became known as a turbo jet [20]. Over the course of the 20th and 21st century gas turbine engine technology has developed at an increasing rate as their potential benefits began to be realised.

Two sectors which have benefited hugely from gas turbine technology are the stationary power generation and aviation transport industries. This research project will focus on gas turbines design for the on the latter of these two industries.

Global statistics published by the International Civil Aviation Organisation (ICAO) show that air traffic capacity, normally represented in available seat kilometres (ASK), has grown from approximately 0.05 to 6.5 billion between 1950 and 2011 as shown in Figure 2.3.

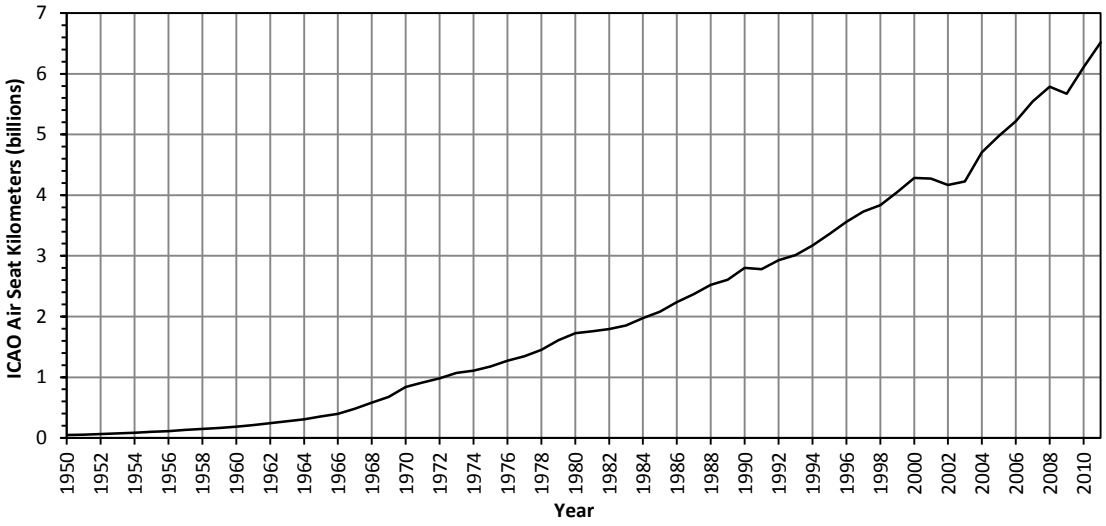

Figure 2.3: Global air traffic development from 1950 to 2011 in billions of air seat kilometres, produced using data published by www.airlines.org.

In order to cope with this rapid demand for air travel an enormous amount of research and development has been placed on the design and manufacture of gas turbines for the use in aviation propulsion.

As was previously illustrated a gas turbine system consists of a compression, combustion and turbine region. Aviation gas turbines will also often include additional intake and nozzle sections, as illustrated in Figure 2.4, which are employed to improve and manage air intake flow and generate thrust.

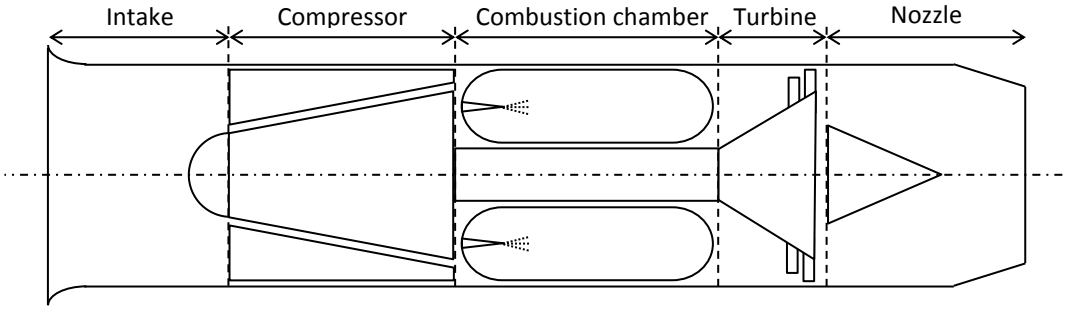

Figure 2.4: Simple schematic showing the fundamental regions of an aviation gas turbine design, adapted from [19].

There are several variations of successful and popular aviation gas turbine engine designs. The most commonly employed systems currently used in the civil aviation industry are the turboprop, turbo jet and turbofan engine configurations.

At a high level a turboprop, illustrated in Figure 2.5, engine operates in a similar fashion to that of a gas turbine which is used for power generation in that the rotary motion developed by the turbine section is mainly transferred to a central drive shaft running through the engine. This shaft, in conjunction with gearbox, is used to drive the compression section of the engine and also delivers rotary motion to a propeller at the engine inlet. The vast majority the engine's thrust is generated from this propeller, with little residual energy within the exhaust gases of the engine. This type of engine has seen widespread usage on predominantly subsonic aircraft, both in military and commercial contexts.

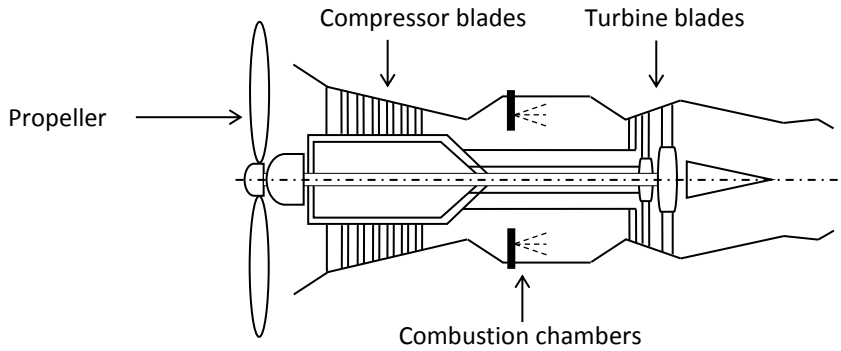

Figure 2.5: Simplified schematic of a turboprop engine, adapted from [19].

A turbojet engine, illustrated in Figure 2.6, generates thrust solely from the jetted exhaust gasses produced in the combustion chambers of the engine. These engines are often used when sustained supersonic speeds are required, and therefore implementation in military fighter aircraft and ballistic missile technologies is common.

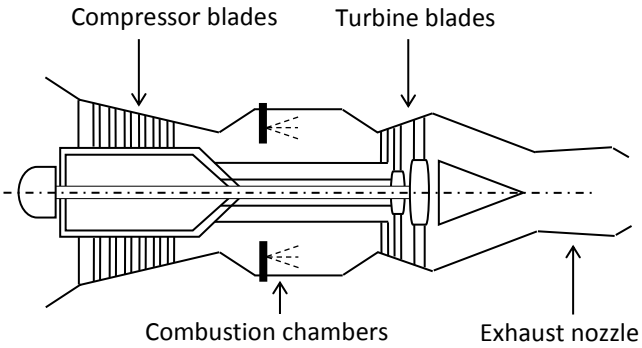

Figure 2.6: Simplified schematic of a turbojet engine, adapted from [19].

The distinguishing feature of a turbofan engine, illustrated in Figure 2.7, is large ducted fans at the engine inlet. These fans pull air from the atmosphere into the compressor blades and also around the exterior of the combustion and turbine section of the engine. This additional airflow is known as by-pass air and an engine's thrust is developed from a combination of this and the exhaust gasses produced during fuel combustion. An engine can have either a low or high by-pass ratio depending on the ratio between the mass flow of by-pass air and air passing through the core of the engine. Turbofan engines have seen major usage in the commercial aircraft sector due to their fuel efficiency and operational stability.

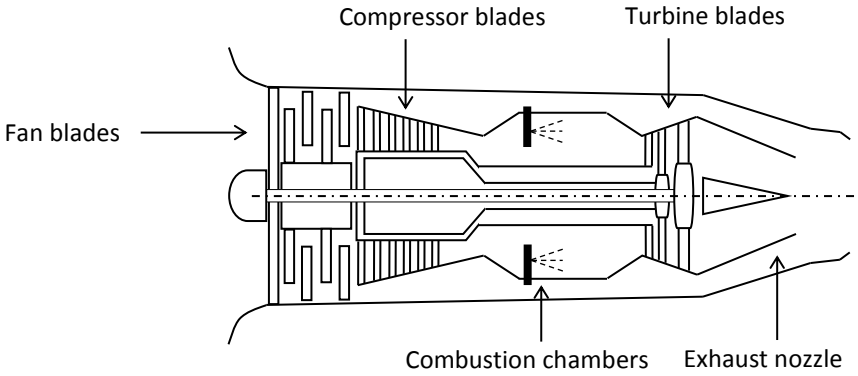

Figure 2.7: Simplified schematic of a turbofan engine, adapted from [19].

2.1.2 Combustor Types and Design Considerations

The evolution of gas turbine combustor technology has resulted in a number of popular design configurations developing. There are five basic concepts that are integral to any combustor design, these being, a primary reaction zone, a secondary

reaction zone, a dilution zone, various wall jets, and management of heat transfer at the combustor boundary, as illustrated in Figure 2.8. In traditional gas turbine combustors fuel and air are injected into the combustion chamber individually. This type of combustor design is known as a diffusion combustor. Although the fuel and air are not pre-mixed prior to entering the primary zone, the combustion reaction does not occur at the interface between the fuel and air as with a tradition diffusion flame. Instead the injection of the reactants, the mixing of the reactants, the entrainment and mixing of the energetic species, and combustion reaction are occurring simultaneously throughout the volume of primary zone [21].

Alternatively, combustor designs can be of a pre-mixed variety in which the reactants have undergone some level of mixing prior to entering the reaction zone. Only systems where the fuel and air have undergone pre-mixing before injection into the primary zone can be classified as truly pre-mixed. Other pre-mixed system variants include; rapidly mixed, non-premixed - where reactants are injected separately but undergo intense mixing preceding the onset of combustion, and spatially injected, non-premixed - where fuel and air are injected at multiple discrete points within the combustion chamber and spread out over a larger area promoting a more disperse mixture region. It is these latter variations which have seen most use in pre-mixed aviation gas turbines designs.

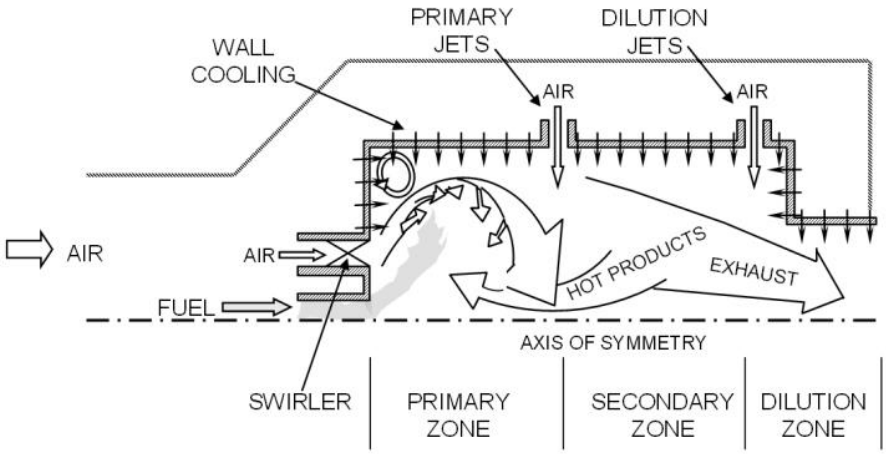

Figure 2.8: Basic combustor features, reproduced from [21].

In a gas turbine combustor the role of the primary zone is to establish a stable combustion region by controlling air-fuel mixing and flame structure. Prior to entering the primary zone the air exiting the compressor is passed through over a series of vanes to induce a turbulent swirling flow. This not only aids the initial mixing process immediately following fuel injection but also creates recirculation zones near to the fuel and air inlet ducts. Recirculation zones help maintain continuous combustion by drawing hot combustion products back towards the reactant injection point. Additional air can also be introduced - labelled as 'primary jets' in Figure 2.8 - to help promote mixing, influence stoichiometry and improve the flame structure within the combustor. These air jets are also designed to direct the flow of the reacting mixture up and downstream of the primary zone in the correct proportions. This ensures that the hot mixtures are entrained in the recirculation zones and that the mixing and combustion process continues into the secondary zone.

The main purpose of the secondary zone is to oxidise CO to carbon dioxide (CO_2) via the kinetic reaction shown in Equation 1.

$$CO + OH \rightarrow CO_2 + H$$

Equation 1: Secondary zone mechanism for the oxidation of CO to CO_2.

In order to maximise the oxidation rate an elevated temperature is maintained, whilst the residence time within the secondary zones is designed to be as long as possible and surplus air is provided into the reaction region to create an overall lean mixture.

Lastly the combustion products enter the dilution zone where the main goal is to cool the mixture to a temperature which will not damage the turbine blades of the engine. Cooling is achieved using dilution air which is injected into the region, leading to a reduction in the mean exhaust temperature and making the final exhaust extremely lean.

There are three main combustor configurations which are generally used in aviation gas turbine engines. These options are illustrated in Figure 2.9, and are known as tubular or 'can', tubo-annular, and annular. The choice of which combustor type and

layout is implemented in a gas turbine design is largely determined by the intended purpose of the engine, and the availability of space in the engine housing.

A tubular combustor design consists of a cylindrical liner mounted concentrically inside a cylindrical casing. The design is rarely used in modern aircraft engine designs due the excessive weight and length required, however for small scale uses it has the benefit of being easier to maintain when compared to the other combustor choices.

In a tubo-annular combustor design tubular liners are arranged in a single annular casing combining the compactness of an annular chamber with the mechanical strength of the tubular chamber. This system became popular as the pressure ratios of modern aviation gas turbines increased.

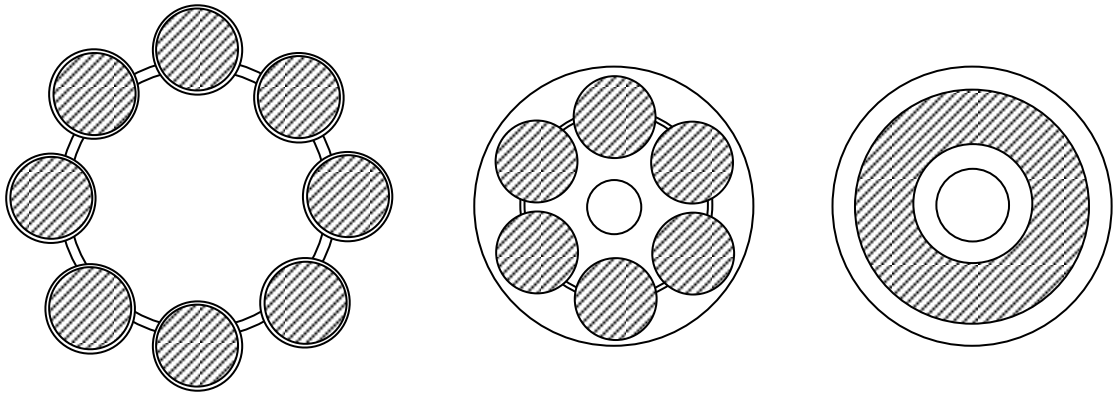

Figure 2.9: Illustration of the main combustor designs adopted in aviation gas turbines, adapted from [22].

Eventually combustor design has developed to a point where fully annular designs have become the standard for civil and commercial aviation transport. The clean aero-dynamic layout allows for a compact combustion chamber with low pressure losses. Combustion systems such as those shown in Figure 2.10 employ advanced fuel injection and wall cooling techniques to further improve fuel and combustion efficiencies thereby reducing operation instability and pollutant emissions.

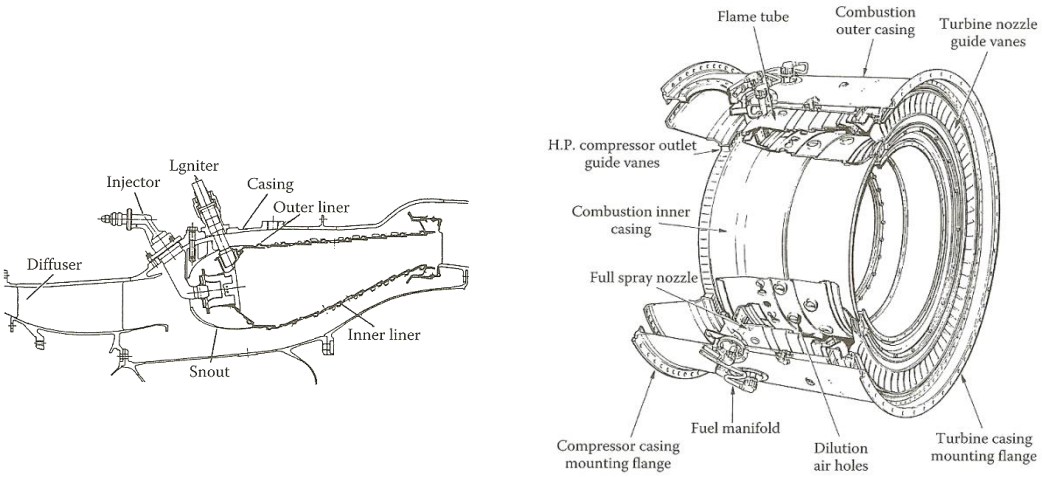

(a) (b)

Figure 2.10: Schematic drawings of (a) General Electric CF6-50 annular combustor and (b) Rolls Royce RB211 annular combustor, reproduced from [22].

The selection of a particular combustor technology or design configuration used in any aviation gas turbine is of course not based solely on individual advantages or disadvantages one option may have over another. There is however an accepted general ranking of the areas which are considered most important in any design. Table 2.1, which is adapted from a study by Rhode in 2002 [23], shows a prioritised list of combustor design considerations.

Table 2.1: Prioritised combustor design considerations for aviation gas turbine engines, adapted from [23].

Design Consideration	Criteria
Safety	
Operability	Take-off to 45,000 ft
Efficiency	99.9%
Durability	6,000 cycles/36,000 hours
Emissions	Best available emissions at 7%, 30%, 85% and 100% power (LTO Cycle) and cruise
Downstream - Turbomachinery - Thermal and Life - Integrity	Minimise the impact of the combustion output

From this ranking structure as would be expected safety and operational robustness are the main consideration in a gas turbine design. The rank given to achieving low exhaust pollutant emissions in aviation applications although not a primary factor in combustor design, due to the necessary importance which is placed upon human safety and accident mitigation, is still something which is crucial to the competiveness and success of an engine design for OEMs as regulatory standards and public awareness of environmental sustainability increase.

2.1.3 Aviation Fuel

The most commonly used aviation fuels in the World are kerosene based. This is due to kerosene being widely available and having beneficial fuel characteristics during the early development of aviation gas turbines. The fuel types which are predominately used in the commercial aviation industry are known as Jet A and Jet A-1 blends. Jet A-1 is used worldwide outside of North America, former Soviet Union and mainland China while Jet A is used in the North America and parts of Canada. The regulatory bodies which set the specifications for Jet A-1 and Jet A are detailed below in Table 2.2.

Table 2.2: Specification required for Jet A and Jet A-1 fuels, adapted from [24].

Regulatory Body	Specifications
Jet A	
USA Standard	ASTM D1655 (Jet A)
Jet A-1	
NATO Code No.	F-35
U.K. Joint Services Designation	AVTUR
British Standard	Defence Standard 91-91
ASTM	D1655 (Jet A-1)
IATA Guidance Material	Kerosene Type

The main difference between the specifications of Jet A and Jet A-1 fuel mixtures are that Jet A-1 must have a freezing point of below -47°C, compared to that of Jet A which must be below -40°C [25]. This makes Jet A-1 more suitable for flying in cold climate

regions, such as those of international flights which cross polar routes during winter. A full description of the typical properties that Jet A and Jet A-1, as manufactured by British Petroleum (BP), are shown in Table 2.3.

Table 2.3: Typical properties of Jet A-1 and Jet A as manufacture by BP [24].

Parameter	**Jet A-1**	**Jet A**
Composition		
Total acidity (mg KOH/g)	0.003	Below 0.010
Aromatics (% vol)	19.5	23.4
Total sulphur (% mass)	0.02	0.07
Mercaptan sulphur (% mass)	0.003	0.0005
Volatility		
Distillation		
Initial boiling point (°C)	156	
Fuel Recovered		
10% vol at °C	167	185
20% vol at °C	172	
50% vol at °C	188	211
90% vol at °C	234	245
Final boiling point (°C)	258	280
Residue (% vol)	1.0	1.0
Loss (% vol)	Nil	Nil
Flash point (°C)	42	51.1
Density at 15°C (kg/m^3)	804	820
Fluidity		
Freezing point (°C)	-50	-51
Viscosity at -20°C (mm^2/s)	3.5	5.2
Combustion		
Specific Energy (MJ/kg)	43.15	43.02
Smoke point (mm)	25	19.5
Naphthalenes (% vol)	1.5	2.9

2.2 Brief Overview of Internal Combustion Engine Technology

By definition a gas turbine could be described as an internal combustion engine, however due to fundamental differences in operating principles the term is most commonly used to describe spark-ignited or compression-ignited reciprocating piston driven automotive engines. As in a gas turbine engine, the purpose of an internal combustion engine is to extract mechanical power from the chemical energy contained within a fuel via the process of combustion.

Internal combustion engines commonly operate in a reciprocating motion, in which a piston travels back and forth enclosed within a cylinder and power is transmitted through a connecting rod to and crank mechanism in order to drive a main rotary shaft as shown in Figure 2.11.

The first marketable internal combustion engine was developed by J. Lenior in the 1860s and operated using coal-gas and air mixtures which underwent no compression before combustion [26], and had a efficiency of 5% at best [27]. After participation in the production of a similar atmospheric engine designs in 1867, Nicolaus Otto proposed a revised engine combustion cycle design which could overcome the shortcomings of previous engines, primarily their low thermal efficiencies and excessive weight. A prototype of his design was produced in 1876 and adopted a four stroke cycle. This included intake and compression strokes prior to the fuel combustion, followed by an expansion and power stroke where work was delivered to the a crank shaft, and lastly an exhaust stroke to remove the combustion gases from the combustion chamber [27]. This series of in-cylinder actions is now commonly known as the Otto cycle.

The majority of reciprocating engines operate in the form described in

Figure 2.12, that being:

a) An *intake stroke* which begins with the opening of an inlet valve to allow a new air-fuel mixture (air only for direct injection gasoline and diesel engines) to be drawn into the cylinder as the piston moves from TDC to BDC.

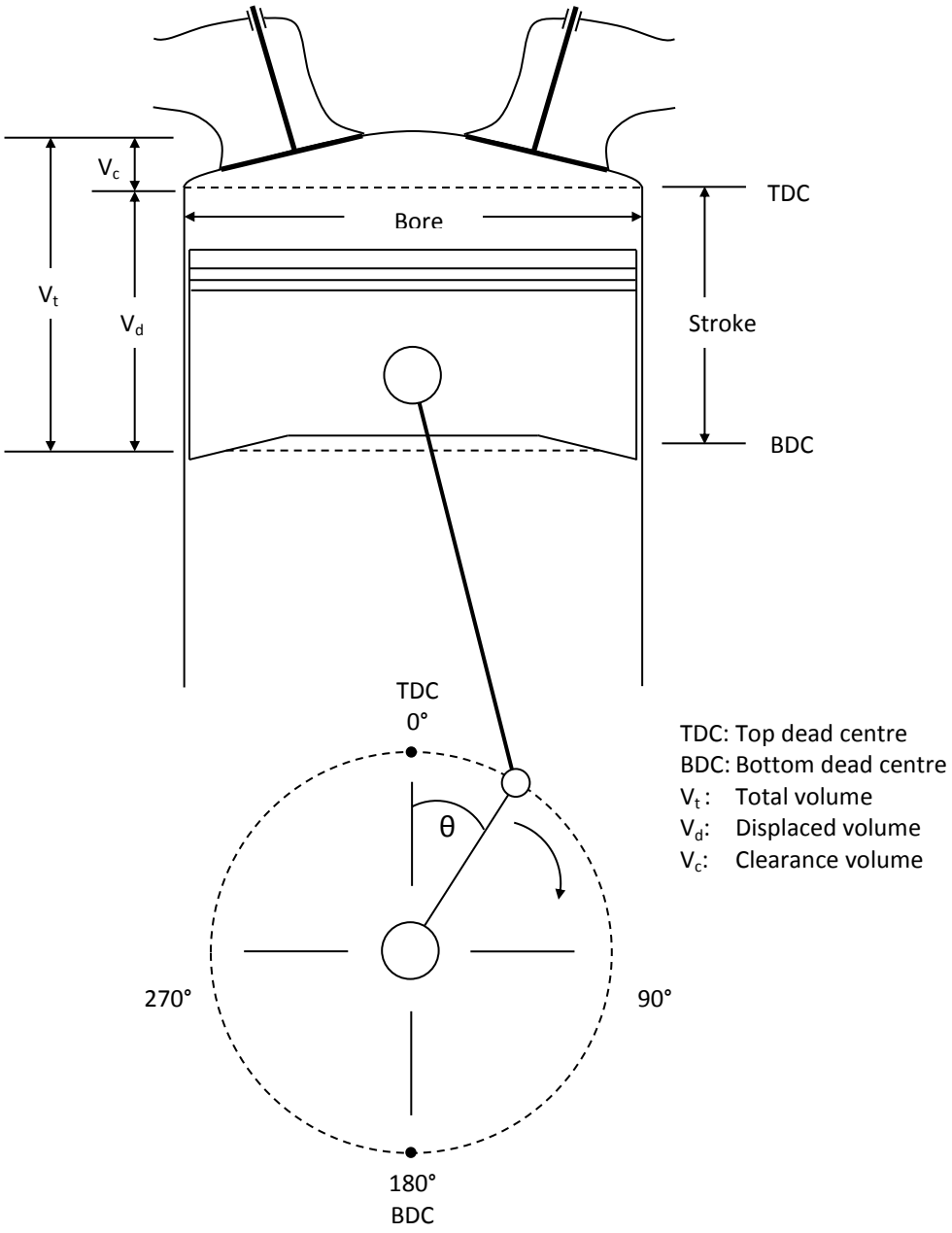

Figure 2.11: Basic illustration of the geometry and descriptive terms of a reciprocating internal combustion engine, adapted from [27].

b) A *compression stroke* in which, with all valves closed, the piston returns from BDC to TDC compressing the air-fuel (or solely air during a late fuel injection engine operating mode) mixture within the cylinder to a fraction of its initial volume. Combustion is initiated either with the discharge of an electrical spark or from the compressive action alone. The rapid burning of the confined mixture causes expansion of the combustion gases and subsequently the pressure in the cylinder increases dramatically.

c) An *expansion stroke* where an engine's power is produced. The high-temperature and high-pressure gases resulting from combustion force the piston down from TDC to BDC, in turn driving the crank shaft. Approximately 5 times as much work is done on the piston on this downward stroke compared to that required during the compression stroke [27].

d) Lastly an *exhaust stroke* is required to expel the combustion gases and lower the cylinder pressure. The piston returns to TDC with the exhaust valve open allowing the gases to exits the cylinder. Finally the exhaust valve is closed and the cycle is ready to be repeated.

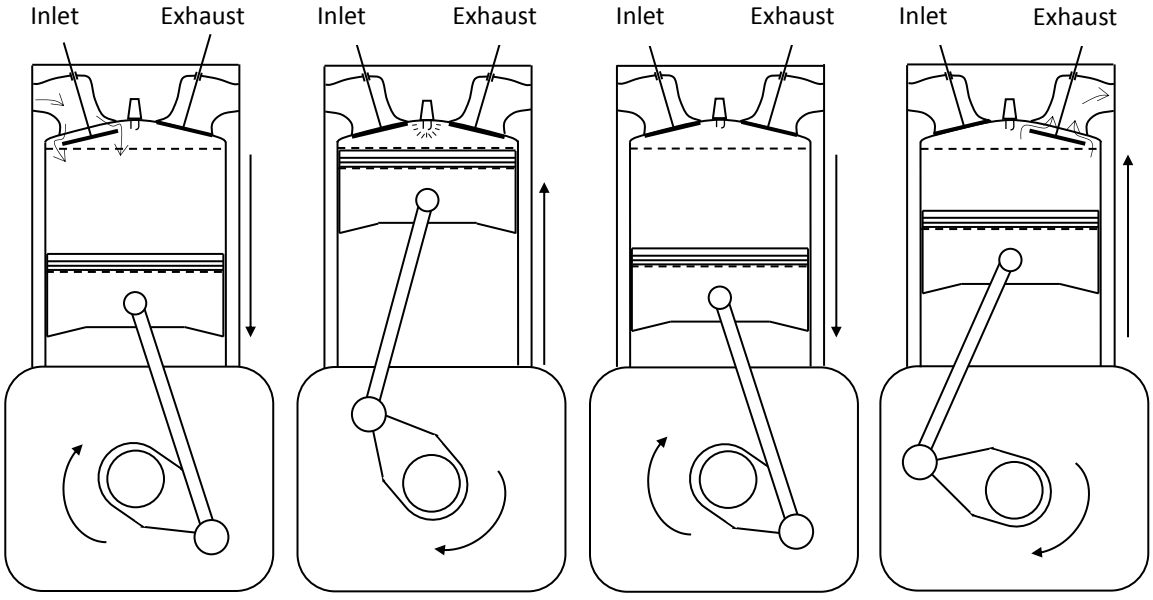

Figure 2.12: Four stroke Otto operating cycle, adapted from [27].

At approximately the same time period as Otto's work a French patent was issued in which the conditions required to achieve maximum efficiency in an internal combustion engine were published [27]. These conditions included:

1) The largest possible cylinder volume with the minimum boundary surface.
2) The greatest possible working speed.
3) The greatest possible expansion ratio.
4) The greatest possible pressure at the beginning of expansion.

Further developments occurred quickly, building on the previous knowledge with the Otto cycle widely adopted as the future with regard to internal combustion engine design.

A notable advancement included the outlining of a combustion cycle in which the combustion of a liquid fuel and air mixture was self-initiated solely during the in-cylinder compression. This concept was published in a patent by Rudolf Diesel in 1892 and claimed higher efficiencies, greater expansion ratios, and reduced knocking [27].

The internal combustion engine has been refined, rather than seen fundamental change since the pioneering research and development of the late 19th Century. Improvements in performance and reliability have been helped by the implementation of electronic control systems and the increased quality of the fuels available to the automotive industry. Research areas such as these are likely to continue to yield future engine development as commercial pressures arising from the cost of petroleum based fuels continues and alternative fuel sources become more viable.

This study focuses on PM produced by spray-guided gasoline injection engines and therefore the majority of this review from this point onwards will concentrate on spark-ignition engines.

2.2.1 Spark-Ignition Engines

Spark-ignition engines are used globally for many applications. Single cylinder varieties can commonly be found in small scale items such as lawn mowers, portable power generation units, and motorcycles while multi-cylinder engines are extensively used within the automotive industry.

In the majority of current fleet spark-injection engines a combustible air-fuel mixture is introduced into the intake system prior to cylinder entry using a carburettor or fuel injection port (alternative in-cylinder injection techniques will be discussed in greater detail in subsequence sections). Although the operating principles of both fuel addition methodologies vary they fulfil the same purpose of controlling the air-fuel mixture (air-

fuel ratio and fuel atomisation properties) depending on the engine operation settings and throttle position.

A typical operating sequence of a spark-injection engine is shown in Figure 2.13:

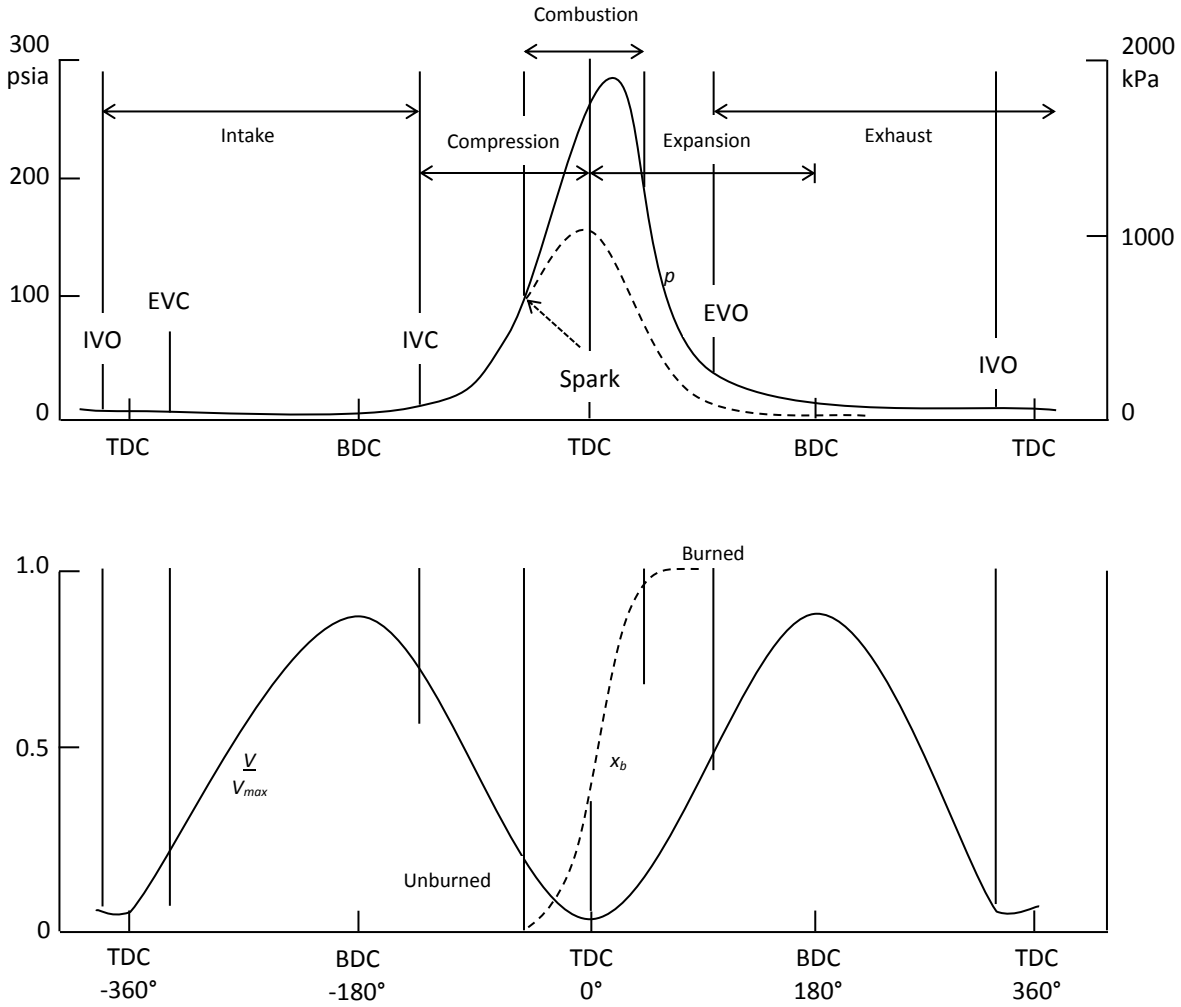

Figure 2.13: Sequence of events in a four-stroke spark-ignition engine operating cycle. Top: Cylinder pressure *p* (solid line), firing cycle (dashed line); Bottom: cylinder volume V/V_{max} (solid line), and mass fraction burned x_b (dashed line), plotted against crank angle, adapted from [27].

This shows several engine variables plotted against crank angle throughout the four-stroke cycle. The initiation of the sequence occurs slightly before TDC when the inlet valve is opened (IVO) allowing the air-fuel mixture to enter the cylinder (air only in direct-injection system). The inlet valve closes (IVC) substantially after BDC, this ensures that high mixture flows can continue at high engine speeds. As the volume of

the un-burnt mixture is compressed the pressure within the cylinder increases, during this phase (normally between 10 and 40 crank angle degrees during homogeneous operation) an electrical spark is discharged from the spark plug. In the following 90° of crank angle the air-fuel mixture is burnt as a turbulent flame propagates away from the spark plug leaving residual combustion gases in the cylinder. The exhaust valve is opened (EVO) towards the end of the expansion stroke allowing the cylinder pressure and exhaust pressure to equilibrate as burned gases flow out of the cylinder and into the exhaust manifold. The piston then displaces the remaining gases from the cylinder on the exhaust stroke, after which with the exhaust valve is finally closed (EVC) just after TDC. There are occurrences when both the inlet and exhaust valves are open, as the valves normally open slowly to avoid noise and excessive wear. The timing of valve opening and closing is tightly controlled to ensure that they are in their fully open positions when piston velocity is at its highest, maximising gaseous flow.

2.2.2 GDI and Fuel Injection Parameters

To meet the increasing demands for higher fuel efficiencies and greater brake power requirements many automotive engine manufactures are implementing fuel injection systems which have been historically used in diesel engines (direct injection). The major advantage of a GDI system is that it is possible to achieve far greater control over the air-fuel delivery and mixing properties. As a result lean, or stratified, combustion modes can be achieved. Direct injection also reduces pumping losses during un-throttled operation and produces lower combustion temperatures as intake air is cooled due to the vaporisation of the liquid fuel. This later fact also allows GDI engines to operate with both a higher specific power and compression ratio. Benefits of the GDI operation go beyond combustion efficiency, with reported reductions in both HC and CO emissions. There are however practical limitations of GDI, such as the need for accurate development of a transition engine mode phase to control when an engine operates using early (homogenous charge operation mode) and late (stratified charge operation mode) fuel injection.

Early GDI technology simply employed wall and air guided direct injection, where in-cylinder mixing was mainly established from the turbulent intake air flow and piston head geometry. This type of direct injection performed fairly poorly due to fuel impingement onto the cylinder walls and the surface of the piston resulting in unfavourable emissions, specific power output and fuel consumption characteristics. More recently SGDI has been introduced to overcome these issues. In these systems it is predominately the injector spray characteristics which determine the process of combustion as ignitable air-fuel charges can be directed and focussed near to the spark plug.

Introducing fuel into the cylinder using a high pressure injector also introduces a wide variety of previously unachievable engine management possibilities, particularly with the advancement of piezoelectrically controlled injectors. These fast opening and closing injectors make is possible to perform multiple injections, introduce variable fuel loads per injection, more accurate and variable (early or late) injection timings or varying fuel injection pressures, all of which provide engine designers greater flexibility in engine mapping.

2.2.3 Automotive Fuel

In a similar fashion to aviation kerosene there are multiple sets regulatory standards surrounding the composition of automotive gasoline. Within the EU strict limits have been placed on particular additives and elements within gasoline, such as the lead and sulphur content. These standards (CEN Standards) and EU Directives have resulted in improved fuel quality and reductions in harmful pollutant emissions. However, adhering to the first CEN fuel standards in 1993 was done on a voluntary basis. Although all fuel suppliers in the EU voluntarily complied with these regulations in 1998 it was made mandatory that all available diesel and gasoline fuels in EU met the specifications set in the relevant EU Directives. Table 2.4 shows the current EU standards for automotive gasoline.

Table 2.4: Standard properties of automotive gasoline in the EU, adapted from [28].

Parameter	Limits	
	Minimum	**Maximum**
Research octane number	95	-
Motor octane number	85	-
Vapour pressure in the summer period (kPa)	-	60.0
Distillation		
Percentage evaporated at 100°C (% vol)	46.0	-
Percentage evaporated at 150°C (% vol)	75.0	-
Hydrocarbon analysis		
Olefins (% vol)	-	18.0
Aromatics (%vol)	-	35.0
Benzene (%vol)	-	1.0
Oxygen content (% mass)		3.7
Oxygenates		
Methanol (%vol)		3.0
Ethanol (%vol)		10.0
Iso-propyl alcohol (%vol)	-	12.0
Tert-butyl alcohol (%vol)	-	15.0
Iso-butyl alcohol (%vol)	-	15.0
Ethers containing ≥ 5 carbon atoms/molecule (%vol)	-	22.0
Other oxygenates (%vol)	-	15.0
Sulphur Content (mg/kg)	-	10.0
Lead Content (g/l)	-	0.005

2.3 Combustion and Exhaust Emissions

Any combustion process of a hydrocarbon fuel can be defined as a relatively rapid chemical combination of hydrogen and carbon in the process fuel with oxygen from the combustion air, resulting in the liberation of energy in the form of heat and light

[29]. Real-world combustion processes are often very complex systems which undergo turbulent and simultaneous mixing and combustion of reactants. Establishing a full understanding of the low level chemistry occurring in these systems can very difficult. In the following sub-chapters some fundamental combustion theory, air-fuel operating regimes, and pollutant exhaust emissions relating to gas turbine and automotive engines are given.

2.3.1 Combustion Chemistry and Operational Modes

The complete combustion of a hydrocarbon in the presence of oxygen will result in only CO_2 and water (H_2O) being produced. This is depicted in Equation 2 and is termed stoichiometric combustion:

$$C_xH_y + \left(x + \frac{y}{2}\right) O_2 \rightarrow xCO_2 + \left(\frac{y}{2}\right) H_2O$$

Equation 2: Complete combustion of hydrocarbon fuel in the presence of oxygen.

Alternatively, if the combustion process were to utilise air as the oxygen source the presence of nitrogen is included in the reaction equation and treated as an un-reactive component.

$$C_xH_y + \left(x + \frac{y}{4}\right) O_2 + 3.76\left(x + \frac{y}{4}\right) N_2 \rightarrow xCO_2 + \left(\frac{y}{2}\right) H_2O + 3.76\left(x + \frac{y}{4}\right) N_2$$

Equation 3: Combustion of a hydrocarbon fuel in the presence of air.

When discussing the reactants entering the combustion zone of a gas turbine or internal combustion engine the parameter most commonly used to characterise the chemistry within the system is known as the air-fuel ratio (AFR), expressed as either a volume or mass basis [30]. As described earlier an air-fuel mixture which contains precisely enough air to fully consume all of the available fuel during combustion is described as having a stoichiometric AFR. As different fuels will produce different stoichiometric AFRs it is convenient when describing combustion processes to express the actual air-fuel mixture using an equivalence ratio (λ), which describes the actual AFR as compared to the perfect stoichiometric case and is calculated using Equation 4.

$$\lambda = \frac{Actual\ AFR}{Stoichiometric\ AFR}$$

Equation 4: Equivalence ratio for a given air-fuel mixture.

In traditional gas turbine combustor technologies which operate using a diffusion flame combustion system, both the fuel and oxidiser are supplied to the reaction zone in an unmixed state. The majority of reactant mixing and combustion take place simultaneously in the primary combustion zone. In this region there is often more fuel than is required to achieve a stoichiometric mixture (λ<1) and the mixture is described as being at a fuel-rich condition. In the context of a gas turbine combustor rich combustion is commonly seen in the primary zone to promote stability and resist blow-out. There are disadvantages associated with operating at fuel-rich or near stoichiometric mixtures which mostly derive from the significantly higher temperatures which are generated. This elevated temperature not only leads to a requirement for advanced cooling methodologies in and around the combustor housing, but also results in high NO_x and PM emissions resulting from the localised fuel-rich zones as illustrated in Figure 2.14.

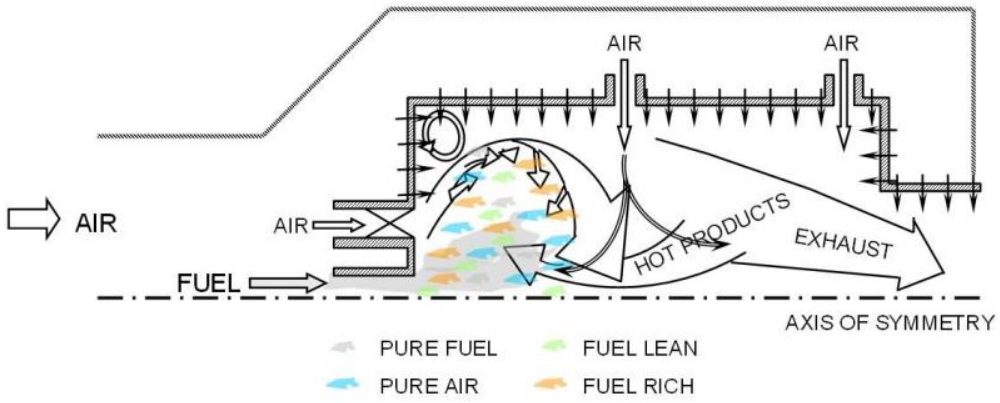

Figure 2.14: Air-fuel mixing in the primary zone of a traditional gas turbine combustor, reproduced from [21].

Conversely to rich combustion a process is considered to be lean when an air-fuel ratio is greater than that needed for stoichiometric combustion (λ>1). This implies that there will be excess oxygen for the reaction cycle and that complete combustion of the fuel can be achieved. The advantage of lean combustion processes is that typically they

have lower emissions compared to systems operating in a fuel rich mode. Emission reductions primarily take the form of reduced NO_x formation, due to lower flame temperatures, and lower hydrocarbon and carbon monoxide release, due to the complete burnout of the fuel. However, achieving a lean combustion system can introduce complications in the form of low reaction rates, susceptibility to extinction, combustion instability, mild heat release, and sensitivity to mixing [31].

The normal outcomes of operating a combustion system in a lean configuration are illustrated in Figure 2.15. This describes how as the equivalence ratio within the combustion system is made more lean (excess air) reductions in the flame temperature and NO, CO, HC and soot emissions are witnessed.

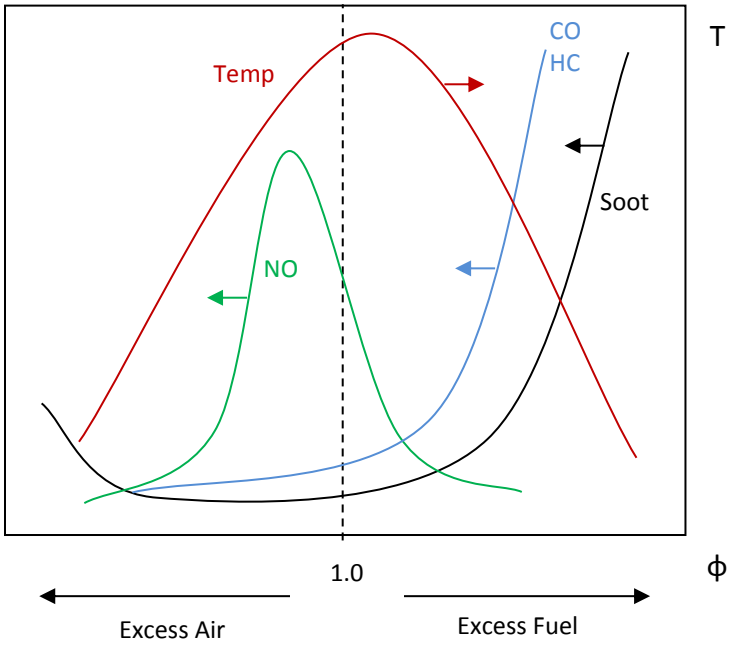

Figure 2.15: Illustration of the typical temperature and pollutant formation rates resulting from changes in AFR for gas turbine combustors, adapted from [31].

In the automotive industry since the introduction of direct injection technology the possibility to operate in rich and lean combustion modes has become much more feasible. In the context of GDI engines the terminology used to describe the combustion operating modes are homogeneous and stratified charge operation. In a homogenous charge operating mode the aim is to create a stoichiometric air-fuel mixture which is evenly distributed throughout the cylinder volume. This is achieved by injecting fuel early in the engine cycle, typically 300° BTDC on the intake stroke. The

mixing of the fuel and air within the cylinder is mainly controlled through the geometry of the piston head and the flow of the intake air. An example of a homogenous charge operating sequence is illustrated in Figure 2.16 where:

(a) Air is drawn into the cylinder during the intake stroke.
(b) Fuel is injected directly into the incoming air flow.
(c) The fuel and air mixture undergoes premixing throughout the duration of the intake and compression stroke resulting in a homogeneous mixture throughout the cylinder volume.
(d) The charge is ignited.

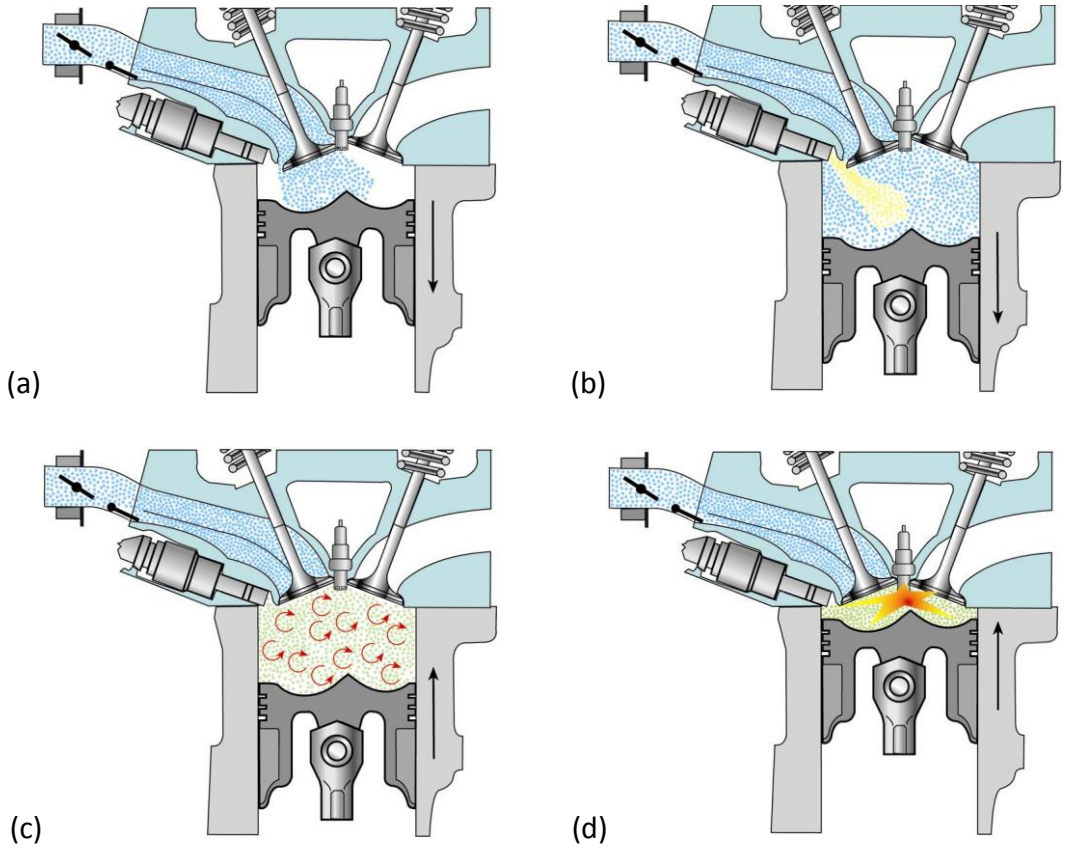

Figure 2.16: Fuel injection and mixing sequence for homogeneous charge combustion operation, reproduced from [32].

In a stratified charge operating mode fuel injection occurs very late in the compression stroke of the engine cycle, typically 30 - 40° BTDC. The aim of this late injection is to create an isolated volume within the cylinder which contains a near stoichiometric or slight rich air-fuel mixture. This area is centred on spark discharge location such that

the surround cylinder volume is extremely fuel lean. Overall AFRs when employing a stratified charge combustion system can be higher than those of a homogeneous charge system. An example of a stratified charge operating sequence is illustrated in Figure 2.17 where:

(a) With the throttle fully open a tumbler flap positioned such that the incoming air flows mainly over the upper edge of the inlet valve. This is done to induce tumble and swirl in the air flow.
(b) As the piston begins its upward movement for the compression stroke the swirling of the air in the cylinder is intensified by the swirl recesses and geometry of the piston head.
(c) When the piston is nearly at TDC continuous swirl has developed.
(d) Very near to the end of the compressions stroke the fuel is injected directly into the swirling air flow. The atomised fuel droplets are drawn towards the spark discharge location.
(e) An ignitable air-fuel mixture develops around the spark discharge location. This isolated volume is what it known as the stratified charge.
(f) The charge is ignited.

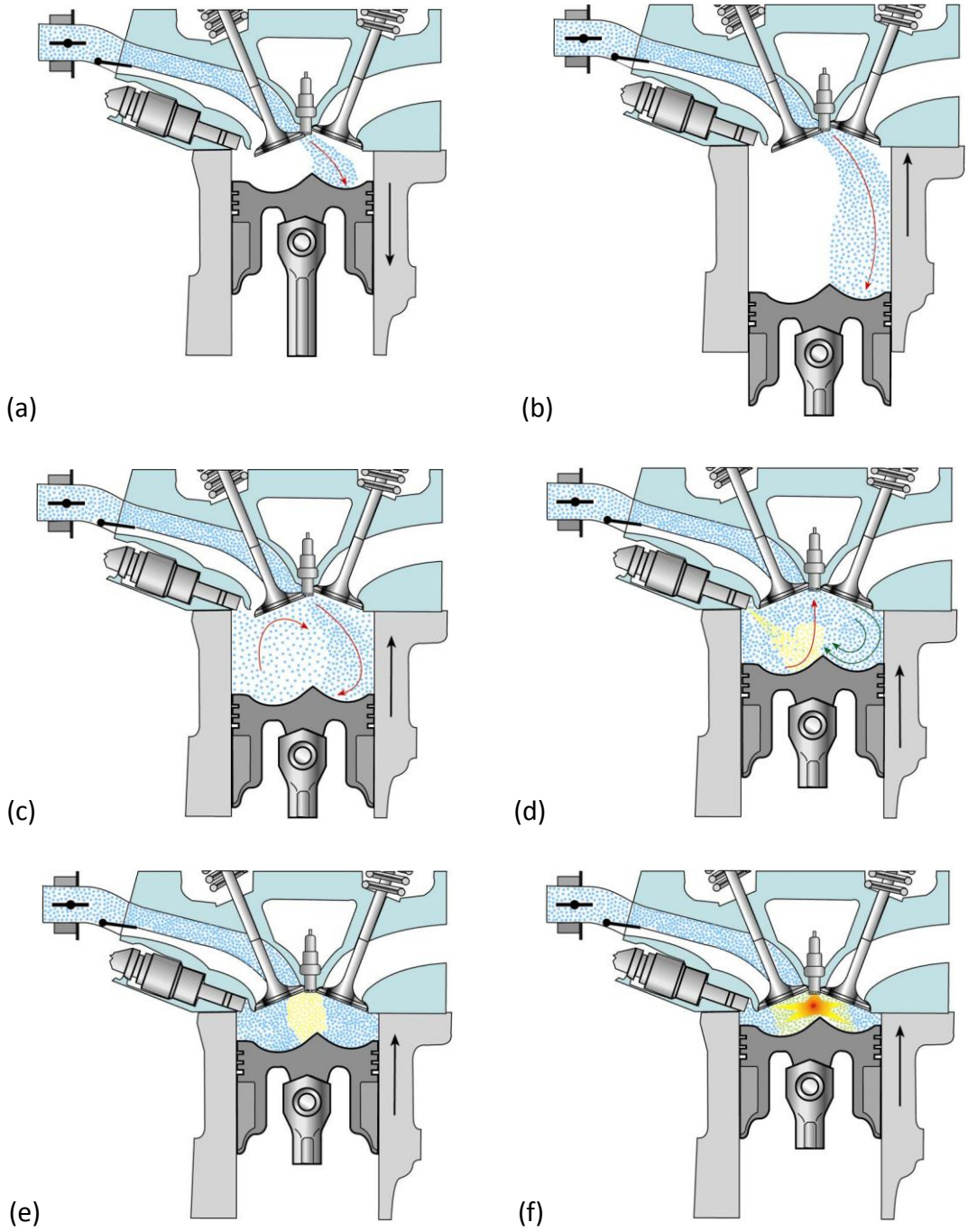

Figure 2.17: Fuel injection and mixing sequence for stratified charge combustion operation, reproduced from [32].

The idealised reactions which were described in Equation 1 and Equation 2 are true for the combustion of highly pure reactants, under very selective combustion conditions. In practice, this type of combustion is not attainable within the combustion zones of gas turbine and internal combustion engines, due to issues with mixing and flame stability. As such the production of pollutant emissions - in addition to CO_2 and H_2O - is

an unavoidable outcome of the combustion of both aviation and automotive fuels and the challenge facing engine manufacturers and regulatory bodies is how these emissions can be reduced to a minimum level. Figure 2.18 illustrates the pollutant emissions and the primary concerns associated with them.

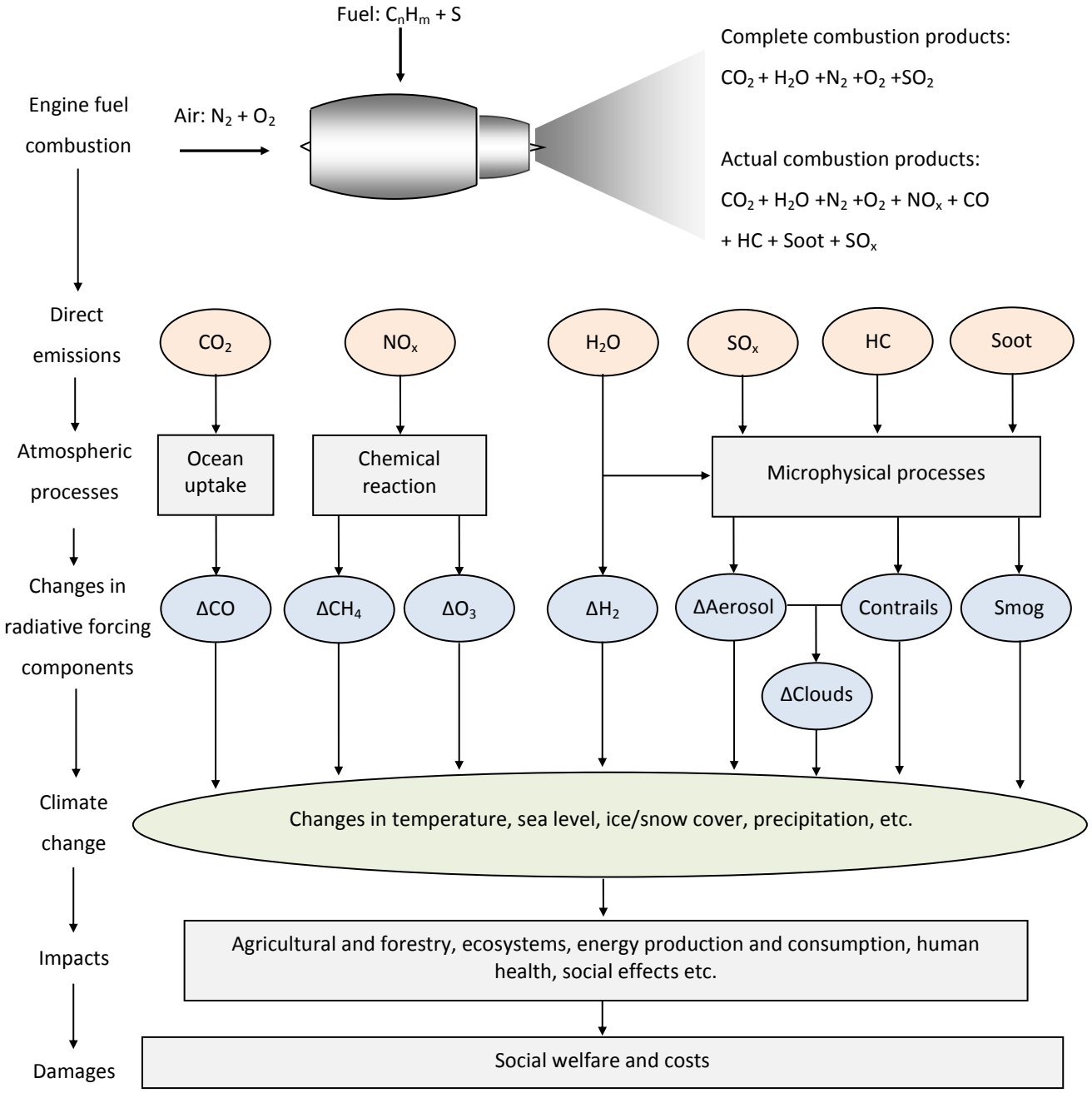

Figure 2.18: Illustration of combustion depicting possible combustion derivatives and affects from aviation and automotive exhaust emissions, adapted from [33,34].

Reduction and mitigation of these emissions has mainly been achieved by the significant progress seen in the development of highly efficient combustion processes and exhaust after treatments. In the following sub-chapter the pollutants which are the primary concern of the EU and UK regulatory bodies will be presented with particular focus placed on particulate emissions and their potential impacts.

2.3.2 Carbon Dioxide and Carbon Monoxide

CO_2 is a naturally occurring compound which is essential in maintaining global temperature as it acts as a greenhouse gas in the upper atmosphere. For this reason monitoring the atmospheric concentration of CO_2 is of particular interest for research into climate change. Anthropogenic emission of CO_2 within the UK currently stands at a total emission of 474.1 Mt for 2012, and provisionally at 463.3 Mt for 2013 [35]. Combustion processes are the main contributors to this figure, with the two largest emitters being energy supply and transport. In 2012 the transport industry was responsible for emitting approximately 116.9 Mt of CO_2 into the atmosphere.

The emission of CO_2 from automotive transport is significantly higher than that of the domestic and international aviation transport in the UK. Of total CO_2 emissions the automotive industry was responsible for ≈63.7 Mt (13.4%) [36] whereas the aviation industry was responsible for ≈27.8 Mt (6%) [37].

2.3.3 Oxides of Nitrogen and Sulphur

Gaseous emissions of nitrogen and oxygen compounds such as NO_2 or NO, commonly referred to as NO_x emissions, are generally produced at high combustion temperatures such as those created in aviation gas turbine combustors and automotive engines. It is the latter which is considered a primary emission source in the UK. NO_x emissions directly related to road transport in the UK in 2010 were quoted as being 34% of total emissions, with England proportioning 75%, Scotland 10%, Wales 7% and Northern Ireland 3% of the total emission releases [38]. Inner-city NO_x concentration can be significantly higher with London figures recently measured at 53% of total NO_x

emissions being produced by vehicles [39]. NO_x emissions from combustion processes are tightly monitored and regulated not only due to the environmental impact they can pose but also as they are an indicator of combustion efficiency.

NO will rapidly oxidise with ozone or radicals in the atmosphere to form NO_2 which has been shown to be damaging to human health, particularly the respiratory system. Exposure to high concentrations can result in nose and throat irritation [40] as-well as a general increase in susceptibility to respiratory infections [41].

2.3.4 Ozone, Benzene, Poly Aromatic Hydrocarbons and Metallic Elements

Ozone in the upper atmosphere is considered beneficial as it absorbs harmful ultraviolet radiation from the Sun. In the lower atmosphere however ozone is considered a pollutant as its oxidative properties can result in it acting as an irritant to humans, causing the respiratory tract or eyes to become inflamed. The formation mechanism for ozone at low altitude is the photochemical reactivity of nitrogen oxides and volatile organic compounds (VOC). Automotive emissions are the main source of these ozone precursors and as such NO_x and VOC reduction methodologies such as exhaust gas recirculation (EGR) and catalytic oxidation are also important in the effort to lower ozone concentrations. Interestingly as ozone can oxidise NO, producing NO_2 and oxygen, urban sites which have high NO_x concentrations will often have lower ozone concentration than rural areas.

Concentrations of the organic chemical benzene are primarily emitted by road transport and domestic combustion in the UK. Benzene is a genotoxic carcinogen which attacks genetic material and therefore even at extremely small concentration levels it still poses a risk to human health. The current acceptable annual mean airborne concentration stipulated in the EU air standard limits is 5 $\mu g/m^3$, which was not exceeded any UK measurement site in 2010 where an annual mean value of 0.9 $\mu g/m^3$ was recorded. These low concentrations have mainly been achieved due to the introduction of automotive catalytic converter technologies.

PAHs are a large group of organic compounds which also have toxic and carcinogenic effects. The main source of emission for these chemicals is again road transport although domestic and industrial combustion processes do also contribute. Annual mean concentration levels in most of the UK remain below the EU target of 1.0 ng/m^3, with exceptions occurring at locations near to industrial installations.

Metallic particles are released into the atmosphere from many sources, most being industrial facilities operating in the mining, combustion, or manufacturing industry. However domestic emissions do also occur from abrasive processes such automotive brake wear. EU Directives cover the emission of nickel, arsenic, cadmium, mercury and lead. All of these elements are controlled due to their toxicity, with concerns mainly over the potential respiratory damage they can cause.

2.3.5 Soot

Carbonaceous solid PM is commonly referred to as soot or black carbon. In addition to containing carbon, soot particles consist of a complex mixture of organic and inorganic chemical compounds generated during the combustion process.

Individual primary particles (spherules) commonly agglomerate creating long 'chain-like' structures. Each of these formations is composed of a number of 10 - 80nm spherules resulting in final agglomerate particle sizes of the order of 10 - 1000nm [42]. Soot makes up a large majority of atmospheric PM, as typically the composition of particulates in combustions exhausts is upwards of 50% soot particles [43].

2.4 Particulate Exhaust Emissions

This research project is focused on the particulate emissions which are generated in the combustion processes associated with gas turbine and internal combustion engines. Combustion PM typically consists of a complex mixture of different particles. However, as has previously been discussed there are many mechanisms for particle generation in the processes involved in aircraft and automotive engines, for example

chemical, electrostatic or abrasive actions can all result in particle formations of varying morphology, toxicity, and chemical reactivity.

2.4.1 Exhaust Particle Formation

The main component of a combustion aerosol which exists in significant numbers following the exit of a gas turbine core or automotive tailpipe, where the exhaust is exposed to what is in effect infinite dilution (open atmosphere), are solid soot particles. The presence of soot in an exhaust stream is a sign of incomplete combustion and often the result of fuel rich zones which have undergone combustion with insufficient air to fully oxidise them.

Soot particles commonly take the form of long chain-like structures which are produced by the agglomeration of carbonaceous spherules (Figure 2.19.a). Each individual spherule can be composed of thousands of nano-crystallite layers (similar to the structure of graphite) which are arranged in an unordered pattern around a central core. The resultant particle structure is often described as being an 'onion-shell' formation (Figure 2.19.b).

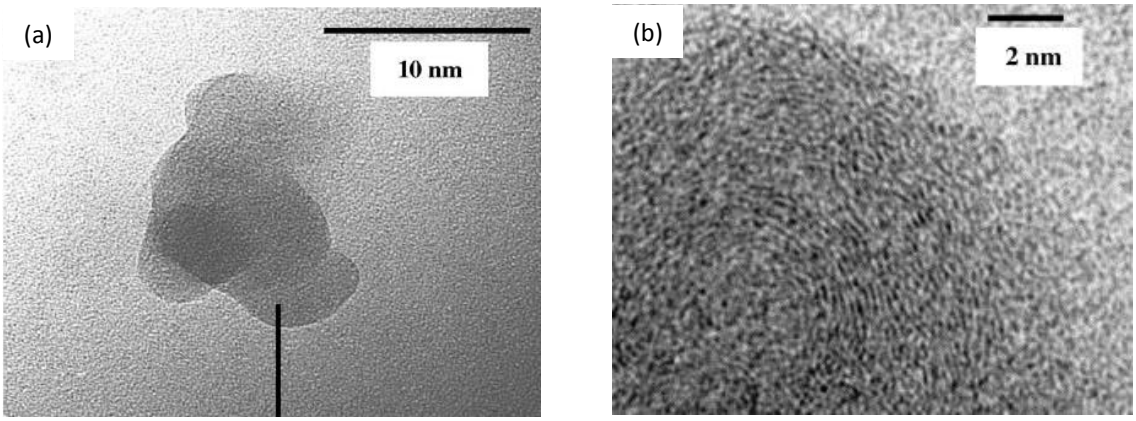

Figure 2.19: Transmission electron microscope (TEM) images of (a) agglomerate of primary carbon particles, and (b) 'onion-shell' stucture of a nano-crystallite particle, reproduced from [44].

The formation of solid soot particles from liquid or vapour phase hydrocarbons has been extensively investigated [45]. Although the process is still not fully understood due to the extremely complex and fast changing chemistry which occurs within the

fuel combustion zone, some fairly established sequential processes and formation mechanisms have been developed. One such soot formation pathway as described by Bockhorn [45] is shown in Figure 2.20.

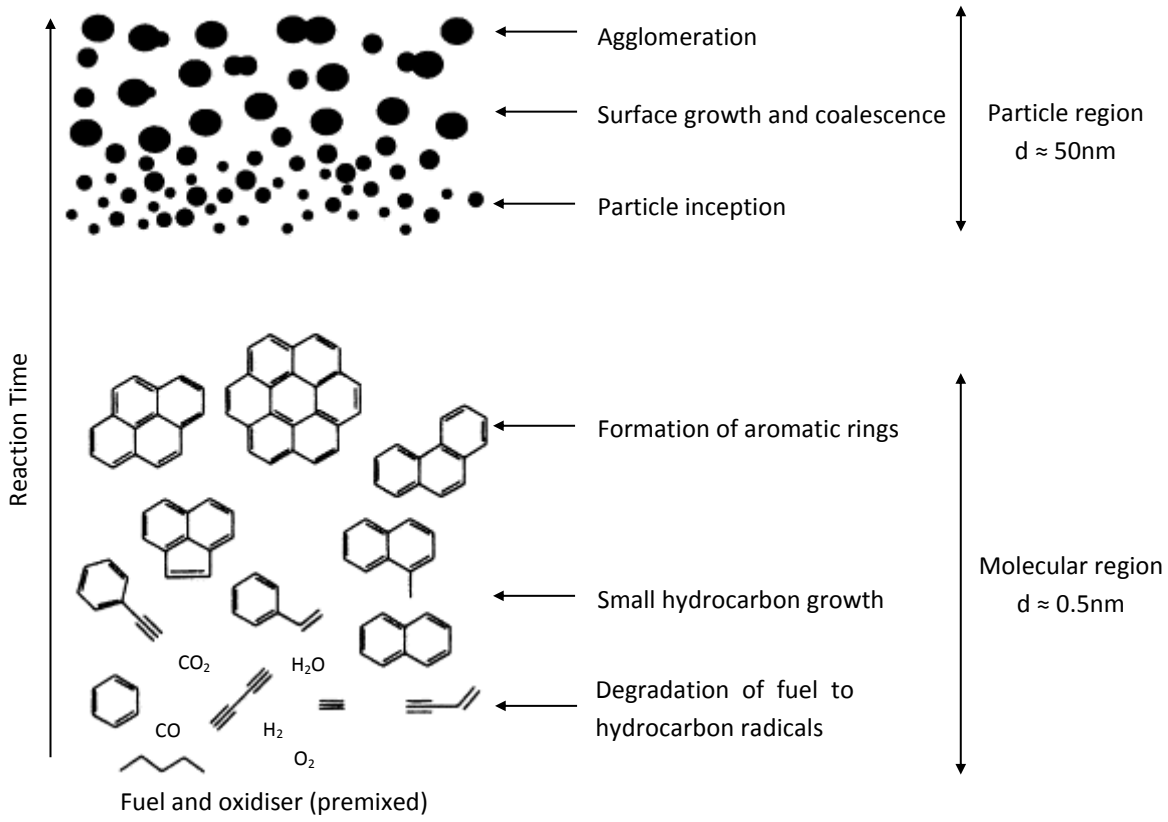

Figure 2.20: Soot formation pathway for a homogeneous premixed flame, adapted from [45,46].

This sequence involves six main processes: pyrolysis, nucleation, coalescence, surface growth, agglomeration and oxidation. The first five of these processes are illustrated schematically in Figure 2.21 while the sixth process, oxidation, where hydrocarbons are converted to CO, CO_2 and H_2O, can occur at any point in the process [43]. In a laminar diffusion flame this sequence may well function in distinct spatially divided points, however in a combustion process that is pre-mixed, or highly turbulent, it is likely that all of the processes will be occurring simultaneously.

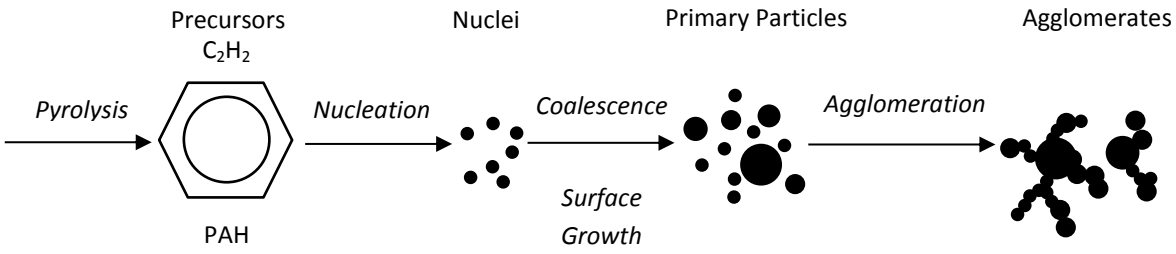

Figure 2.21: Illustration of soot formation processes, adapted from [43].

Initial fuel pyrolysis is the processes by which organic compounds are broken down at their molecular level in high temperature environments. This process occurs without significant oxidation of the compounds even though there may be oxygen species present and is generally an endothermic reaction which leads to overall pyrolysis rates being highly temperature dependent. All fuel can undergo pyrolysis resulting in the production of some species which are precursors to soot production. These species are largely fuel independent and are: unsaturated hydrocarbons, polyacetylenes, PAHs and acetylene [43].

Nucleation, also known as particle inception, occurs as gas-phase reactants undergo transformation into solid particulates. Solid nuclei particles as small as 1.5 - 2nm have been detected in combustion in luminous flames [47], and although most studies in combustion engines associate a nucleation mode with volatile particles below 30 - 40nm, solid core particles have also been discovered in this size range. These particle nuclei individually have little impact on the total mass of a PM distribution during their inception however they can influence the overall mass concentration of a combustion aerosol as they provide sites for surface growth to occur. The nucleation process is mostly localised to the high temperature (1300 - 1600K) primary reaction area. In a gas turbine combustor this is located in the primary combustion zone within a combustor and in a GDI automotive engine it is in close proximity the spark plug. It is in these regions that temperature and concentrations of free radicals and reactive ions are at their highest [47].

Following nucleation, particles begin increasing in mass as they experience the process of surface growth. There is no clear distinction between the end of nucleation and

beginning of the surface growth phase and in reality the two processes are thought to be concurrent [43]. Following inception hot soot particles readily accept gas-phase hydrocarbons, mostly in the form of acetylenes, resulting in an increase in soot mass while the number of particles remains fairly constant. This process continues throughout the primary combustion zones into the cooler, less reactive regions of the combustor or cylinder.

Further particle growth occurs as coalescence and agglomeration mechanisms act upon the primary solid particulates. Coalescence is the process whereby particles collide and become a single entity, thereby reducing overall particle number concentrations while the overall mass concentration is maintained. An assumption is made that during this process the particles involved in the collision are spherical and the resultant particle formation also remains spherical. This differs from the process of agglomerations in which particles stick together rather than completely coalescing. The resultant particle groups typically take the form of chain-like structures as shown in Figure 2.22 although in some cases large clumping of the particles has been observed [43].

Lastly, the process of oxidation involves the conversion of carbon or hydrocarbons into combustion products. Achieving as much oxidation as possible is crucial in the effort to reduce soot production as once carbon has been partially oxidised to CO it will no longer evolve into a soot particulate. The graphite-like structure which soot particles are composed of is thought to make them highly resistant to oxidation after initial inception [48], it is only at very high temperatures, >1300K, that this can be achieved [49]. Oxidation of small particles is dominated by OH in fuel-rich and stoichiometric conditions, while in fuel-lean conditions both OH and O_2 are responsible for initial absorption and subsequent desorption of oxygen from the surface of a particle with the attached fuel component [47].

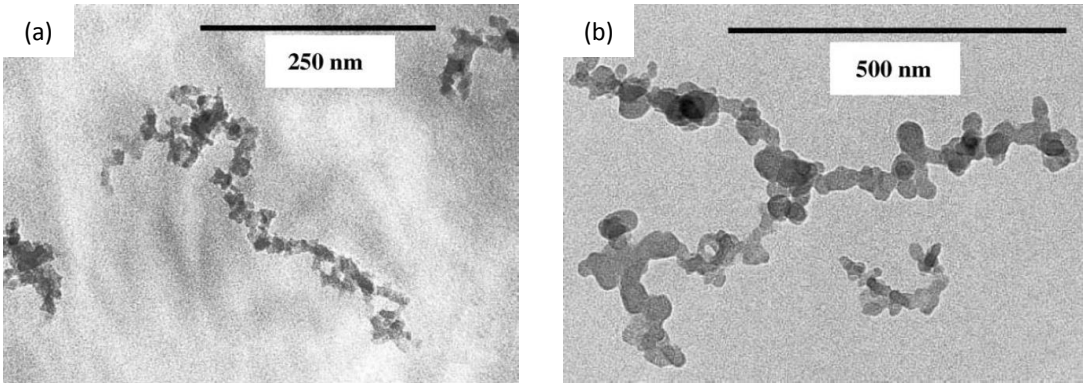

Figure 2.22: TEM images of typical chain-like agglomerate structures of (a) soot generated using the PALAS and (b) Diesel soot particle, reproduced from [44].

Volatile particles may exist as vapour or liquid particles within an exhaust stream and are primarily produced from the fuel source being combusted. The four primary formation mechanisms of organic carbon particulates in automotive combustion are considered to be [27]:

- Flame quenching at the combustion chamber walls.
- Filling of crevice volumes with unburnt mixture.
- Absorption of fuel vapour into oil layers on the cylinder wall during intake and compression strokes followed by desorption of fuel vapour during expansion and exhaust strokes.
- Incomplete combustion in the fraction of the engines operating cycle, occurring due to poor combustion quality (misfires, partial burning, transitions in AFR, EGR or spark timings)

Similar formation mechanisms can be assumed for volatile formation in gas turbine exhaust as the concepts of incomplete fuel combustion, vaporisation of unburned fuel or other lubricants and the combustion process quality are shared for both technologies.

Although volatile production can be an indicator of system performance (poor air-fuel mixing) or maintenance requirements (oil leaks) it becomes a particularly important consideration during any attempt to make quantitative measurement of particle concentrations within an exhaust. Instrumentation which is sensitive to volatiles can

measure massively higher number concentrations of small volatile particles when compared to less sensitive instrumentation which may have a counting cut-off point at ≈25nm. These inflated concentration values can result from very small fluctuations in system performance, such as those which can occur during a transition in operating condition, engine RPM, or fuel composition variability (higher sulphur content) and would not be reflective of the overall particle distributions being produced. Furthermore there is the challenge of preventing or mitigating gaseous volatile material re-condensing within sample lines and resulting in higher particle number concentrations than would otherwise be observed. These challenges will be discussed further in discussions on the PMP developed for the diesel automotive industry, and the equivalent sampling system being developed for the aviation industry.

There are other particle formations which can potentially arise from combustion processes. Sulphur based compounds such as sulphuric acid (H_2SO_4) can originate from fuels and lubrication oils which contain sulphur. In addition to the harmful effects compounds such as H_2SO_4 can have on the environment and human health, there is growing evidence that gaseous sulphuric acid can act as a powerful precursor for the nucleation and growth of solid PM [50]. For these reasons there has for some time been restriction placed on the quantity of sulphur which is considered acceptable in automotive and aviation fuel. The restrictions on sulphur content in automotive fuels are currently stricter than those in the aviation industry.

Metallic particles can also be found in combustion exhausts, from mechanical wear and other abrasive processes. These can be: typical abraded metals like iron, nickel, copper; or metals originating from lubrication oil packages like zinc and calcium; or metals from fuel additives [51].

2.4.2 PM Characterisation

Characterisation of diverse aerosols such as those produced during combustion can prove difficult, and for this reason many classification methodologies have evolved in an attempt to best describe and define PM.

One such categorising method is to purely describe particles as being of either a volatile or a non-volatile nature. This classification has developed due to the increased significance which has been placed on non-volatile emission output targets and also due to the measurement limitations of particular sampling systems and particle detection instrumentation. In reality it is likely that particles derived from the controlled combustion of a hydrocarbon fuel will exhibit a complex morphology, and comprise of a mixture of volatile and non-volatile fractions. It is generally considered that the particle groups which form the bulk of the particles within an engine exhaust are carbonaceous particles (soot), unburnt hydrocarbons, and sulphates; however this can be greatly affected by the operational conditions and the emission source.

Particles produced under controlled combustion conditions will typically have a diameter less than 10µm. An established representation of the particulate distribution produced by an automotive engine which was proposed by Kittleson in 1998 [52] defines a tri-modal distribution where particle number concentration is dominated by a nucleation mode, and mass concentration is dominated by an accumulation mode as shown in Figure 2.23. This type of distribution is not isolated to the automotive industry and has also been witnessed during multiple aero-combustor and gas turbine emission experiments [53,54].

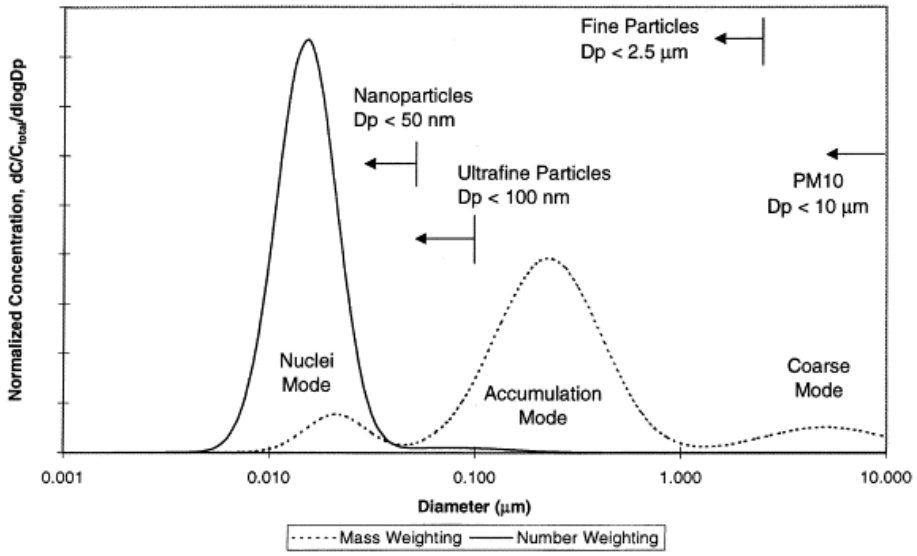

Figure 2.23: Typical engine exhaust particle size distribution as described by Kittleson, reproduced from [52].

The nucleation mode typically has a particle mean diameter of less than 30nm and contains high concentrations of VOCs and sulphur compounds formed during exhaust dilution and cooling. In addition to this trace metal compounds, and primary solid carbon particles in the early stages of development may also be present at this size range. Understanding the composition of nuclei particles is difficult due to the complexity of their formation and the rate at which they can evolve. Often it is the act of exhaust sampling alone which responsible for the re-condensation of the volatile components within the exhaust stream, a topic which will be discussed in detail later in this work.

The accumulation mode is slightly better understood and mostly contains carbonaceous agglomerates. Particles in this size region, typically between 50 and 500nm, have historically been given higher measurement significance as they are more repeatable than the smaller, volatile nucleation mode and represent a large proportion of the mass in a PM distribution. As the majority of current atmospheric PM targets and regulatory standards are mass based it follows that conservation and analysis priority is placed on this size mode.

It is challenging to sample and analyse distributions of this nature as small variations in sampling technique or post processing methodologies can result in significant variance in final number and mass concentration measurements. Applying the appropriate significance to each of these factors is a difficult task and will often involve a degree of compromise.

Excluding SAE smoke number, the most common assessment methods used to define PM distributions are particle size, number and mass concentrations. This is unlikely to change as these metrics are arguably the most informative and measurable at this size range. There is however justification for the inclusion of particle surface area when assessing PM distributions as this can have a large influence on chemical reactivity (a significant factor regarding toxicity and particle interaction with the human body).

2.5 Impact of PM on the Environment

The production of PM in combustion processes is not only monitored to give an indication of the combustion efficiency of the system. In the following sub-sections some of the growing concerns about the wider effects PM emissions may pose on the environment are presented.

2.5.1 Global Climate

The role which PM plays on the Global climate is mainly concerned with the emission of PM from aircraft. Emissions at ground level from automotive engines are far less damaging than those released in the upper atmosphere by aviation gas turbines which are able to have a more direct influence on the atmospheric composition. Indeed, the overall impact on Global climate from PM emissions is dwarfed by that of the emission of CO_2 from the transport sectors. However understanding the potential impacts is still beneficial and can contribute to maintain a sustainable climate.

The term radiative forcing (RF) is used to describe how an exhaust constituent impacts global climate change, a positive forcing result indicating a warming effect and a negative forcing result indicating a cooling effect. The RF components for aviation described by Lee *et al.* [2] arise from the following processes:

- Emission of CO_2, (positive RF).
- Emission of NO_x, (positive RF), this is the sum of three further factors which NO_x emissions highly influence: production of ozone in the troposphere (positive RF), a longer-term reduction in ambient methane (negative RF), and a further longer-term reduction of ozone (negative RF).
- Emission of H_2O, (positive RF).
- Formation of persistent linear contrails, (positive RF).
- Aviation-induced cloudiness (AIC), (potentially a positive RF).
- Emission of sulphate particles, (negative RF).
- Emission of soot particles, (positive RF).

As the emission of soot particles results in a positive RF, while sulphur based particles lead to negative RF the overall impact of aviation PM has on atmospheric temperature is still unclear. The Intergovernmental Panel on Climate Change (IPCC) estimated that aviation represented 3.5% of the total anthropogenic RF in 1992 which was projected to increase to 5% in 2050 [33]. This estimate did not include the majority of the influencing factors created by PM emission, notably those of aviation induced cirrus clouds and contrail formations. A recent review of aviation PM [55] illustrated the results of three studies on the RF components of aviation exhaust and the conclusions stated that compared to other influencing factors (CO_2 emission and ozone production) the impact of PM is low (shown in Figure 2.24). The level of scientific understanding (LOSU) on the influence of PM on RF is quoted as being 'low' and therefore further research is required to fully understand this area.

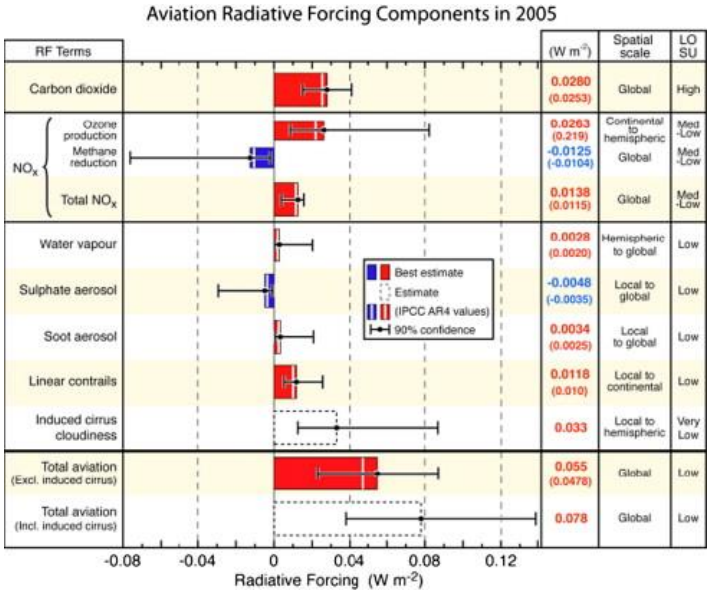

Figure 2.24: RF components associated with aviation emissions, reproduced from [55].

2.5.2 Visibility and Soiling

Particles in the lower atmosphere can degrade visibility directly by creating a loss of contrast between a viewed object and the background. In addition to this the attenuation of the light from the object due to scattering and absorption of light will reduce overall visibility [56]. In areas of high humidity PM can also act as nucleation

source in the same fashion as that previously mentioned for the generation of cirrus cloud in the upper atmosphere. The resulting fogs and haze can further compound the visibility issues associated with high airborne PM concentrations.

The resulting reduction in surface light penetration associated with PM and adversely affected atmospheric conditions do not only impact the population in the area who will be subjected to reduce viability, there is also a potential impact on agricultural crop yields. Estimations from China, a location which experiences severe ground level visibility problems due to PM, were that 70% of current crop yields are reduced by between 5 and 30% due to the haze and air pollution in the atmosphere [57].

Particles which eventually settle on surfaces in and around areas with high atmospheric PM concentrations ultimately also cause nuisance and soiling. These conditions develop particularly around large road networks, airports, quarries and power generation sites. In addition to the unsightliness of particulate coatings on surfaces there is also a risk of de-colourisation and surface damage due to chemical reactivity of the particles and the underlying material.

2.6 Impact of PM on Human Health

There is increasing evidence that high airborne concentrations of fine particles emitted from combustion processes can have negative human health impacts. Particular focus is now being place upon the smallest PM size regions, those concentration of $PM_{2.5}$ (particulate matter with an aerodynamic diameter of less than 2.5μm) and smaller. Globally it is estimated that 0.8 million premature deaths and 6.4 million years of life loss are attributed to anthropogenic $PM_{2.5}$ emissions [58]. In the UK the Committee on the Medical Effects of Air Pollutants (COMEAP) determined that anthropogenic PM caused approximately 29,000 early deaths in 2008 [59].

Apportioning specific health effects to individual constituents or sources of PM is a difficult task due to its complex and heterogeneous nature. Recent attempts have been made to review the available literature [60,61], in which the authors highlight the evidence limitations and uncertainty in as yet being able to isolate elements of PM or

emission sources that closely and unequivocally are related to specific negative health outcomes. However indications are that exposure to high concentrations of $PM_{2.5}$ (particularly trace metals and carbonaceous fractions associated with combustion and transport emissions) are damaging to the respiratory and cardiovascular systems. It has been estimated that in the UK that PM produced by combustion processes alone contribute to approximately 19,000 premature deaths annually [62].

There is unquestionably a risk associated with prolonged exposure to high concentrations of PM produced by automotive engines. As of 2012 the International Agency for Research on Cancer (IARC) and World Health Organisation (WHO) reclassified diesel engine exhaust particles as a Group 1 material, the highest of their carcinogenic classifications [63]. Although this assessment has not currently been extended to particulates produced from gasoline engines, it is fair to assume that as gasoline engine exhaust composition is of a similar nature to that of a modern diesel engine the risks associated remain valid. Similarities in PM size distributions, albeit at lower number concentrations mean there is still high likelihood that elements of gasoline engine PM are carcinogenic.

With regard to PM emissions from aviation gas turbines, the key areas of concern from a health perspective are in the grounds and surrounding areas of large scale airports. The current standard for estimating gas turbine PM emissions in these zones is the First Order Approximation (FOA3) methodology which was introduced in 2007. A comprehensive study on air quality and the public health impacts of UK airports has shown the FOA3 approximation to be lacking [64] and that the number of premature deaths attributed to airport emissions is set to increase from ≈110 currently to ≈230 in 2030, based on projected population demographics, air passenger demand and atmospheric alterations [65].

2.6.1 Ingress of PM into the Human Body

In order for ambient particulates to enter the body they must be inhaled. Understanding how particles interact with the human body during this process has been an important research topic for many years, with particularly focus on particle

deposition in the respiratory tract. This is a crucial element in the development of effective aerosol-inhalation based pharmaceuticals and in order to understand the toxicology risks posed by the inhalation of airborne pollutants.

Ultrafine particulate deposits within the deepest regions of the lungs are of significant concern to researchers as it is thought they pose the greatest risk to human health. Primary concerns are that the smallest particulates have the potential to migrate into the blood stream, where their dangers are no longer isolated to the respiratory system. Particles which are deposited and remain in the lungs can result in localised inflammation and genetic damage which could lead to decreased lung function or cancers. Additionally, the large surface area associated with high concentrations of small particles can mean that the chemical reactivity which the particles may exhibit can occur at a faster rate.

2.6.2 Factors Affecting Particle Deposition and Particle Clearance

It is important to appreciate the complexity involved when making predictions on the deposition of particles in the lungs. Firstly, the properties of the inhaled aerosol will have clear implication on its interaction with the respiratory system. Factors such as particle size distribution, concentration, hydroscopicity, gas-particle interaction, chemical reactivity and surface charge can all influence the deposition theory. The aerosol flow rate must also be considered as this will be a function of lung capacity and breathing frequency. Lastly, the individuality of the human body means that the structure and morphology of the respiratory tract will have a pivotal role on where particles may be deposited.

Many of these properties are well understood in isolation but currently the interaction between them is difficult to define. For this reason it is standard practice when modelling particle deposition in the respiratory system to introduce an inhalation fraction (IF) to describe the aerosol flow and its physical properties. IF is expressed as a ratio of the inhaled aerosol to the total aerosol in the airflow and is sensitive to factors such as aerosol entry point, the orientation of the entry point, flow rate and the

particle size. Equation 5 describes an expression for the IF of a steady breathing rate male with average orientation entry point criteria:

$$IF = 1 - 0.5\left(1 - \frac{1}{1 + 0.00076{D_p}^{28}}\right)$$

Equation 5: Average inhalation fraction.

It is possible to clear particles from the airways and lungs in a variety of ways. Coughing, dissolution, mucociliarly escalation, translocation from the airways to other sites, phagocytosis by macrophages and neuronal uptake are all methods in which the body aims to expel potentially harmful deposits, as shown in Figure 2.25 [66]. Quantitative analysis of the effectiveness of these mechanisms with regards to PM deposition has yet to be fully established within the human body [67].

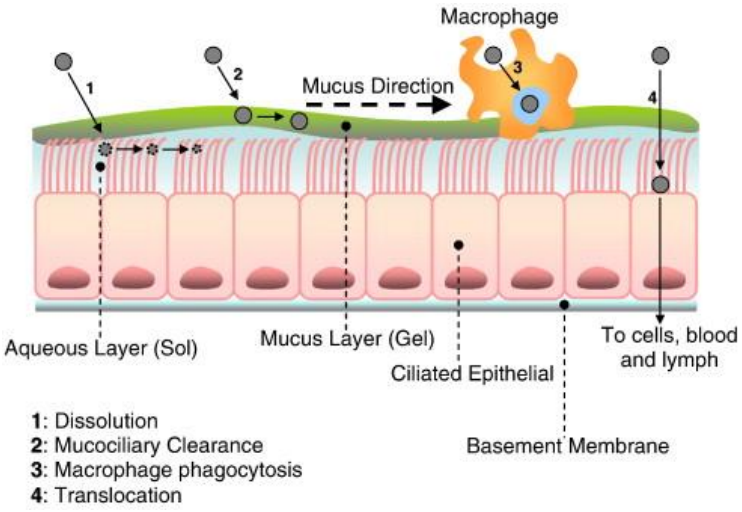

Figure 2.25: Potential pathways determining the fate of inhaled particles, reproduced from [66].

2.6.3 Particle Deposition Mechanisms

The mechanisms which have been proposed for the deposition of particles within the human respiratory tract are broadly divided into two categories. The major deposition mechanisms:

a) Inertial Impaction

Inertial impaction occurs when particulates possess sufficient momentum to maintain a trajectory despite a change in the suspending fluid flow direction. The consequence of this reluctance to follow the airstream flow results in particles colliding with the walls of the respiratory tract. The probability of impaction occurring is increased for large, higher mass particles travelling at high airflow velocity. It follows that due to the bifurcated nature of the upper airway (nasopharyngeal region) large particles (>1μm) are likely to collide and be deposited in the nose, nasal cavity or throat [68].

b) Sedimentation

Sedimentation is the settling of particles on a surface due to the force of gravity. This process is heavily time dependent and therefore acts such as breath-holding increase the likelihood of particle deposition [68]. The National Aeronautics and Space Administration (NASA) has undertaken research into particle lung deposition as influenced by gravity in order to gain a greater understanding of the toxicological potential of inhaled lunar dust in a low gravity environment [69].

c) Diffusion

The process of diffusion, also known as Brownian motion, impacts particles which are sufficiently small that they undergo random motion due to molecular bombardment.

And the minor deposition mechanisms:

d) Interception

When a particle travel close enough to the surface of the respiratory tract it is possible that it will come into contact with airway cilia or simply the airway surfaces themselves. This method of deposition is common for particles with a large surface area, such as fibres like asbestos [68].

e) Electrostatic

Particles which possess an electrostatic charge, opposite in polarity to that held by the surface or portion of the respiratory tract may become deposited due to the force of attraction which is created [68].

2.6.4 ICRP Lung Deposition Model

In 1994 the International Commission on Radiological Protection (ICRP) produced a widely used morphometric lung model which was developed by in-situ determination of particle deposition in the human respiratory tract [70]. Using radiolabelled aerosols the ICRP was able to construct a regional particle deposition theory as a function of particle size and flow rate. The regions, illustrated by Figure 2.26, are the extrathoracic region, also known as the head airways, tracheobronchial region and alveolar region.

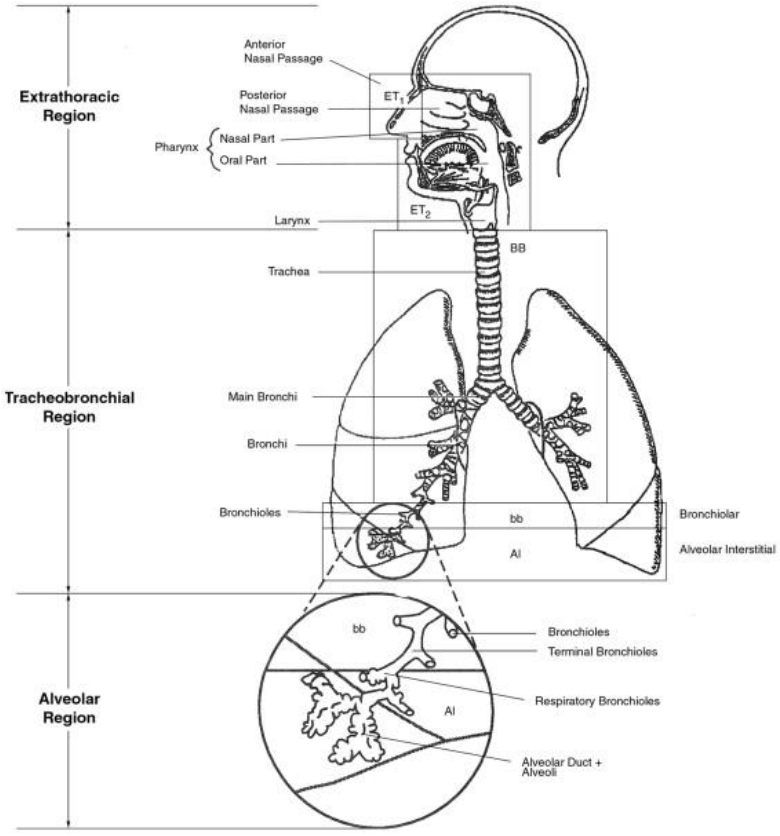

Figure 2.26: Illustration of the major anatomical regions of the human body tract as described by the ICRP, reproduced from [70].

The ICRP model employed the three major deposition mechanisms previously described to establish empirical equations on how particle diameter (D_p) influenced the deposition fraction (DF) within the head airways, tracheobronchial and alveolar regions of the respiratory tract. These formulae are shown below [70]:

$$\mathrm{DF_{HA}} = \mathrm{IF}\left[\frac{1}{1+\exp\left(6.84+1.183\ln \mathrm{D_p}\right)} + \frac{1}{1+\exp\left(0.924-1.885\ln \mathrm{D_p}\right)}\right]$$

Equation 6: Deposition fraction for the head airways region using the ICRP particle inhalation model.

$$DF_{TR} = \frac{0.00352}{D_p}\left[exp\left(-0.234\left(lnD_p+3.40\right)^2\right)+63.9exp\left(-0.819\left(lnD_p-1.61\right)^2\right)\right]$$

Equation 7: Deposition fraction for the tracheobronchial region using the ICRP particle inhalation model.

$$\mathrm{DF_{AR}} = \frac{0.0155}{\mathrm{D_p}}\left[\exp\left(-0.416\left(\ln \mathrm{D_p}+2.48\right)^2\right)+19.11\exp\left(-.482\left(\ln \mathrm{D_p}-1.32\right)^2\right)\right]$$

Equation 8: Deposition fraction for the alveolar region using the ICRP particle inhalation model.

Summation of Equation 6, Equation 7 and Equation 8 provides a total deposition fraction function which is detailed in Equation 9:

$$\mathrm{DF_{Total}} = \mathrm{IF}\left[0.0587+\frac{0.911}{1+\exp(4.77+1.485\ln \mathrm{D_p})}+\frac{0.943}{1+\exp(0.508-2.58\ln \mathrm{D_p})}\right]$$

Equation 9: Total deposition fraction generated using the ICRP particle inhalation model.

Via substitution of particle diameters ranging from 0.001 to 10µm into the previously described equations it is possible to generate deposition fractions for particle size ranges associated with PM, this is shown in Figure 2.27.

Exhausts particulates produced by gas turbine and automotive engines often exhibit high particle number concentrations in the 10 - 100nm (0.01 - 0.1µm) size range, a region that the ICRP deposition model predicts will have the highest deposition fraction in the alveolar region of the repository tract. As was mentioned in previous discussion, with regards to PM size and toxicity it is particles in this size range which possess the ability to access the deepest areas of the lungs and are currently of most concern to researchers.

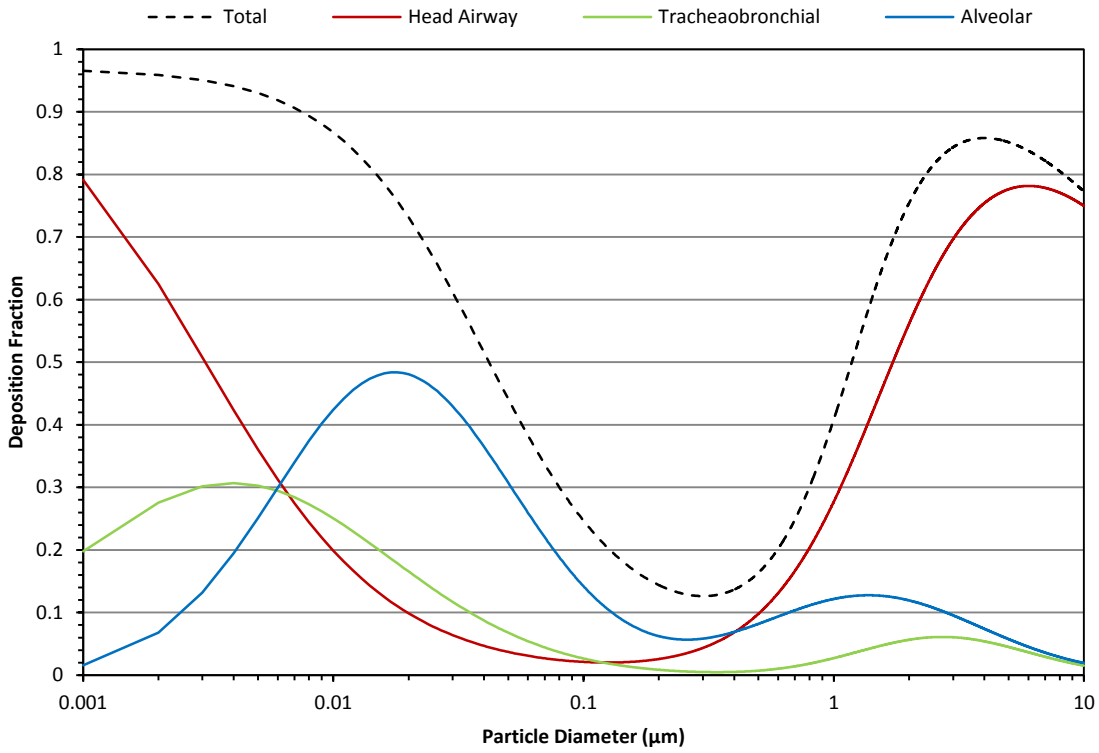

Figure 2.27: Particle deposition fraction profiles for specific respiratory tract sections as described by the ICRP particle inhalation model.

2.7 PM Regulations for Gas Turbine and Automotive Engines

Most emission regulations are now controlled by individual sector specific governing bodies which source direction from local or collaborating Governments. The governing body which publishes standards and recommended practises for the aviation industry is the ICAO. Specifically relating to the gas turbine PM emissions the ICAO defines regulatory standards and measurement requirements through ICAO Annex 16, Volume 2: Environmental Protection – Aircraft Engine Emissions publication [71].

In the automotive industry the leading body on particulate emissions is the UN-ECE GRPE (Working Party on Pollution and Energy) who implemented the PMP Working Group and the PMP Programme. The final results of these investigations were included in UN-ECE Regulation No.83 – Emissions of N^1 and M^1 vehicles [72]. The following sub-sections will discuss some notable aspects of both aviation and automotive PM regulation.

2.7.1 The LTO Cycle

To meet Annex 16 certification requirements, specific emission test points must be considered. The 'Landing and Take-Off Cycle' (LTO cycle) details the percentage of rated thrust an engine must produce, and for how long emissions sampling should occur at each specific thrust condition. Four conditions are considered, these being take-off, climb, approach and taxi, details of which as illustrated in Figure 2.28 and shown in Table 2.5.

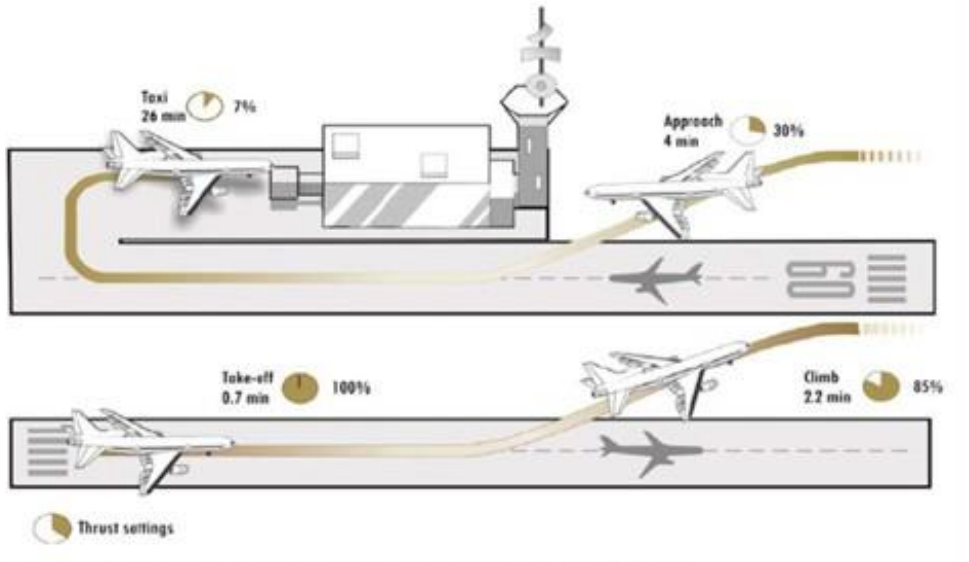

Figure 2.28: Illustration of ICAO exhaust emission certification procedure (LTO cycle), reproduced from www.icao.int.

Table 2.5: LTO cycle operating modes.

Operating mode	Thrust setting (%)	Time in operating mode (minutes)
Take-off	100	0.7
Climb	85	2.2
Approach	30	4
Taxi	7	26

The LTO cycle is intended to replicate the proportion of time an average commercial aircraft will spend at each of the listed engine conditions while completing the low altitude portion of a journey. It is worth highlighting that the main objection of the LTO cycle is to aid in the monitoring of PM emissions from a local air quality standpoint, as the entirety of these regulated emissions are released below 3000 feet. Currently there are no regulatory or measurement standards for cruise emissions occurring above 3000 feet primarily due to the sampling difficulty associated with taking in flight samples. It is however at cruise altitudes where the majority of exhaust emissions occur and thus this can create ambiguity when comparisons are made between short and long haul flights. Table 2.6 shows the percentage of total emissions associated with the LTO cycle criteria for a typical long and short flight.

Table 2.6: LTO relevant emissions results from a long and short haul flight presented as a percentage of the total full journey emissions [73].

	Exhaust Emissions (% of total journey emissions)		
	Fuel	CO_2	NO_x
Short haul (London to Glasgow)	37	37	32
Long haul (Los Angeles to Tokyo)	3	3	2

Although a long haul flight will emit far greater total exhaust emissions, when looking at the LTO cycle in isolation it is the short haul trip which may appear to be more of a concern from a local air quality perspective.

2.7.2 SAE Smoke Number and Gaseous Emissions for Aviation Gas Turbines

Smoke Number (SN) is a dimensionless value used to quantify solid PM emission and is the current regulatory standard for aviation gas turbine engine exhaust smoke measurement. It is defined by the SAE ARP1179D [74] and is determined by the relative reflectance of a standard filter paper following exposure to the engine exhaust in question, under set experimental conditions. SN is rated on a scale of 1 to 100 where higher smoke densities produce larger SN ratings.

The measurement procedure for determining SN involves first calibrating a reflectometer using a coloured tile of known reflectance. The reflectance of each sample filter paper, manufactured by Whatman Ltd (size No. 4), is then recorded prior to use to give an absolute reflectance of the clean filter material, R_w. A filter which has been inserted into a holder of defined geometry is then exposed to a sample flow of 14L/min ±0.5L/min for sufficient time (no less than 1 min) that a fully charged representative sample is achieved. Consecutive samples must be taken at each measurement condition, at which 16.2 kg/m^2 ±0.7 kg/m^2 of exhaust gas must passed through each filter, until at least 3 samples are obtained which agree within ±3 smoke numbers. Alternatively, at least 3 samples can be taken within a range of 12 to 21 kg of exhaust gas/m^2 of filter paper, with samples required above and below 16.2 kg of

exhaust gas/m^2 of filter paper. A stained filter is then retested using the reflectometer to achieve an absolute reflectance of the sample spot, R_s. The smoke number of an individual exhaust sample (SN') can then be found [74]:

$$SN' = 100[1 - \frac{R_s}{R_w}]$$

Equation 10: SAE smoke number for individual exhaust samples.

In order to have comparative sample measurements a sample mass per unit area is commonly used:

$$\frac{W}{A} = 3.483\frac{PV}{AT}$$

Equation 11: Comparative measure of smoke samples on a mass per unit area basis.

Where: A = Filter spot area (m^2)

W = Sample mass (kg)

P = Sample pressure (kPa)

T = Sample temperature (K)

V = Measured sample volume (m^3)

The gaseous species regulated by ICAO are also considered by the SAE measurement dictated by ARP1256D [75] are CO, CO_2, NO, NO_2, HCs and gaseous H_2O, however these will not be the focus of this research project.

2.7.3 European Emissions Standards for Light Duty Vehicles

As the UK is a Member State of the EU a significant portion of the emissions targets and regulations it must adhere to are derived from European Directives. In the case of automotive emissions the directives are summated in the European Emissions Standards, typically referred to as EURO standards. EURO Standards are produced for both diesel and gasoline engine vehicles and are further separated by vehicle type (heavy or light duty). There have been several iterations of the EURO standards with

the newest set - EURO6 - coming into effect in September of 2014. A historical overview of the EURO standards is shown in Table 2.7 [28].

Table 2.7: Historic and future European Emission Standards for light duty vehicles, modified from [28].

Stage	Date	CO	HC	HC + NO_x	NO_x	PM	PN
				g/km			#/km
Compression Ignition (Diesel)							
Euro 1 †	07. 1992	2.72 (3.16)	-	0.97 (1.13)	-	0.14 (0.18)	-
Euro 2, IDI	01. 1996	1.00	-	0.70	-	0.08	-
Euro 2, IDI	01[a]. 1996	1.00	-	0.90	-	0.10	-
Euro 3	01. 2000	0.64	-	0.56	0.50	0.05	-
Euro 4	01. 2005	0.50	-	0.30	0.25	0.025	-
Euro 5a	09[b]. 2009	0.50	-	0.23	0.18	0.005[f]	-
Euro 5b	09[c]. 2011	0.50	-	0.23	0.18	0.005[f]	$6.0x10^{11}$
Euro 6	09. 2014	0.50	-	0.17	0.08	0.005[f]	$6.0x10^{11}$
Positive Ignition (Gasoline)							
Euro 1 †	07. 1992	2.72 (3.16)	-	0.97 (1.13)	-	-	-
Euro 2	01. 1996	2.20	-	0.50	-	-	-
Euro 3	01. 2000	2.30	0.20	-	0.15	-	-
Euro 4	01. 2005	1.00	0.10	-	0.08	-	-
Euro 5	09[b]. 2009	1.00	0.10[d]	-	0.06	0.005[f]	-
Euro 6	09. 2014	1.00	0.10[d]	-	0.06	0.005[f]	$6.0x10^{11}$ [e,g]

At the Euro 1 – 4 stages, passenger vehicles >2500 kg were type approved as Category N1 vehicles

† Values in brackets are conformity of production (COP) limits

a. Until 30.09.1999 (after that date DI engines must meet the IDI limits)

b. 01.2011 for all models

c. 01.2013 for all models

d. and NMHC = 0.068 g/km

e. Applicable only to vehicles using DI engines

f. 0.0045 g/km using the PMP measurement procedure

g. $6.0x10^{12}$ 1/km within first three years from Euro 6 effective dates

2.7.4 The Particle Measurement Programme

The PMP was developed as an international collaboration to provide new PM measuring techniques which would complement or replace the existing regulations which focused solely on particle mass measurement. The main driver for the introduction of improved measurement capabilities was the growing consensus that particles in the ultrafine size range (<100nm diameter) posed the greatest risk to human health and these were not accurately reflected in the mass measurements which were currently in place.

The PMP operated by firstly undertaking a comprehensive assessment of a wide range of measurement instruments and sampling systems. This sought to address key PM properties including mass, number, active surface area and chemistry along with appropriate dilution methods, sample conditioning and consideration of the cost and logistical aspects involved with the introduction of a new sampling methodology. Following the evaluation of these initial performance and application criteria the best performing systems were determined and put forward for an inter-laboratory experimentation.

In order to establish a measure of the repeatability and reproducibility of measurements taken at the nine collaborating laboratories a reference vehicle and reference particle measurement system were selected. These were termed the ‘Golden Vehicle’ and ‘Golden Particle Measurement System’. A Peugeot 407 2.0 HDi was selected as the standard test vehicle as it was compliant with the then current EURO4 standards and included the most mature Diesel Particle Filter (DPF) technology available at the time. The specifications of the Golden Vehicle and schematic diagram of the Golden Particle Sampling system are shown in Table 2.8 and Figure 2.29 respectively.

Table 2.8: Specifications of the Golden Vehicle used to develop the PMP.

Golden Vehicle	Diesel with DPF
VI Number	VF36DRHRH21028953
Vehicle Model/Reg	Peugeot 407 – AG04 NYM
No. of Cylinders	4
Aspiration	Turbocharged
2 or 4 Stroke	4
Fuel Delivery	Common rail D.I.
Capacity (cc)	1997
Test Inertia (lbs)	3500
Kerb Weight (kg)	1590
Transmission	6 speed manual
Catalyst #1	Oxidation Catalyst
Catalyst #2	Si-C DPF

A schematic of the Golden Particle Measurement System is shown in Figure 2.29:

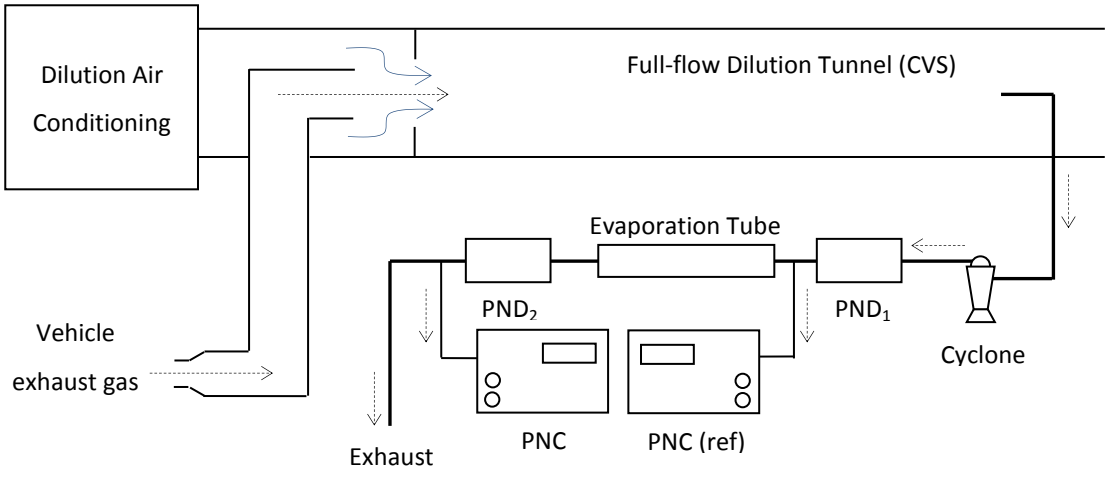

Figure 2.29: Schematic of the Golden Particle Measurement system methodology.

As can be seen in Figure 2.29 the Golden Particle Measurement System comprises of the following fundamental operating principles [76]:

- Efficient dilution air filtration - A standard full-flow Constant Volume Sampler (CVS) equipped with highly efficient dilution air conditioning filters for particles and hydrocarbons.
- Size pre-classification - A sampling probe and cyclone pre-classifier which serve to protect the downstream system components from particle contaminations and set a nominal upper size limit for the particle size measured to be 2.5µm.
- Hot dilution - A first particle number diluter (PND_1) which heats the sample aerosol to 150°C while introducing adequate diluting in order to evaporate volatile material and reduced the partial pressures of the gas phase species to prevent re-condensation at the diluter exit.
- Evaporation - A low particle loss evaporation tube (ET) in which the sample is heated to 300°C and held for approximately 0.2 seconds while semi-volatile particles are evaporated. Any particles that remain in the aerosol after this point are considered to be solid particles. This definition of 'solid particles' is analogous to the definition of regulatory gaseous hydrocarbons: defined as those materials that are measured by flame ionisation detector (FID) downstream of a filter heated to 192°C.
- Cold dilution - Immediately after exiting the ET the sample enters a second particle number diluter (PND_2), where it is cooled as dilutant is introduced: the partial pressures of the gas phase species are further reduced at this point to prevent re-condensation, the concentration of particle present should also be controlled such that they are below 10^4 N/cm^3 and thermophoretic losses are minimised.
- Particle number counting - A particle number counter (PNC) with a strictly controlled counting efficiently curve receives the sample as is exits PND_2. This sets a nominal lower limit of 23nm to the size range measured. The cut off limit and counting efficiency curve is considered necessary to exclude the possible confounding of measurement data by low volatility hydrocarbons manifesting

as a nucleation mode present below 20nm while including the primary carbon sphere size of approximately 20nm.

Results from the PMP measurement system showed repeatability and reproducibility in the order or 20 - 30% for both number and mass measurement across all laboratory tests. It also established the volatile removal efficiency for the combination of primary hot dilution, heated evaporation tube, and secondary cold dilution stages. The latter findings have led to the creation of a set of requirements that any commercially available Volatile Particle Remover (VPR) must adhere to in order to be deemed PMP compliant. These requirements and experimental results obtained using both PMP complaint, non-complaint, and other volatile removal techniques will be discussed in greater detail in Chapter 4.

2.8 PM Reduction Methodologies

Reducing PM emissions has clearly been an ongoing challenge for many years. This has resulted in a number of interesting and novel PM mitigation techniques and technologies being produced. Figure 2.30 outlines a high level breakdown of the most important parameters which are critical to the reduction of PM with relation to gasoline engines.

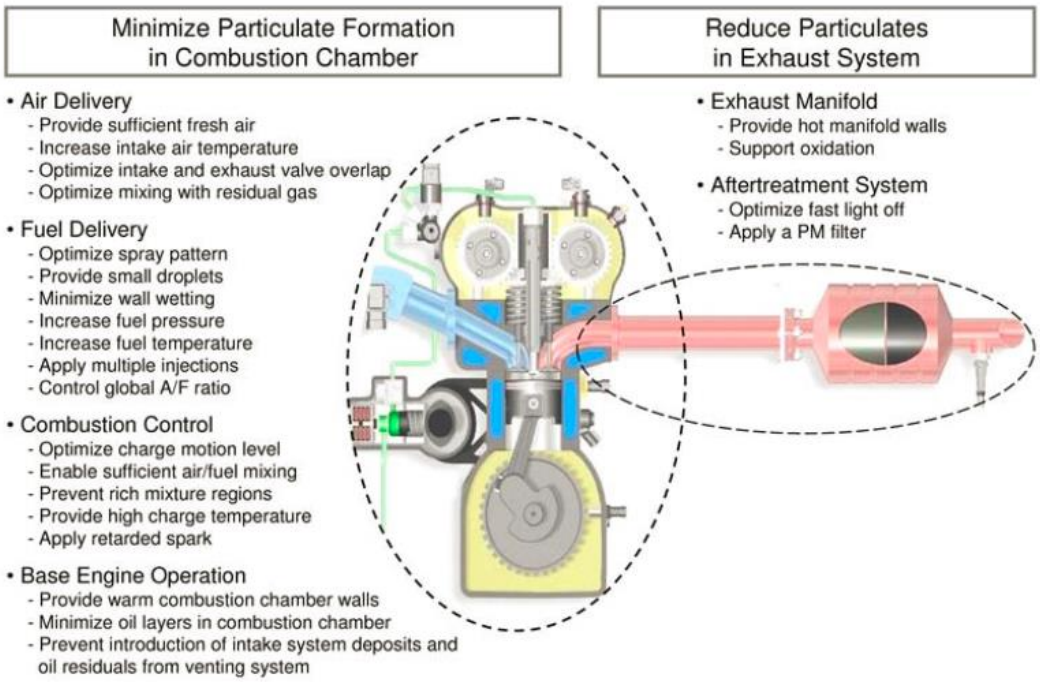

Figure 2.30: Parameters concerned with the reduction of PM emissions for a gasoline engines, reproduced from [77].

Certainly not all of the parameters shown in the Figure 2.30 are also relevant for aviation gas turbines but there are some common themes between the two systems. PM emissions emitted by gas turbine engines are arguably more difficult to reduce than those emitted by automotive engines as the working environment of a gas turbine is far more hostile and sensitivity to change than that of an automotive engine. For this reason many of the after treatment techniques employed in the automotive industry to reduce emissions, i.e. catalysts and filters, are not feasible in the aviation industry. There are however developing methodologies in both sectors which go beyond just reduced fuel consumption, improved operational practices, and robust engine maintenance.

2.8.1 Engine Management and Fuel Injection Characteristics

Optimisation of the input parameters of any combustion system play a critical role in controlling exhaust characteristics. In a gas turbine combustor the primary influencing

parameters on PM - smoke and un-burnt hydrocarbons (UHCs) - production are the combustor inlet temperature, pressure, and fuel spray characteristics.

Increasing inlet air temperature to the combustor is seen as advantageous in that it aids the soot-burnout process; however it can also accelerate the onset of soot-formation. Balancing these factors in order to achieve a net reduction in smoke is usually employed [22].

Soot production is most severe at high pressures due to a combination of chemical and physical effects. The flammability limits are extended at elevated pressures meaning that soot formation may occur in regions at high pressure which would have been too rich to burn at low pressure [22]. The increased pressure also accelerates the chemical reactivity rates within the combustor, meaning that a larger proportion of injected fuel is likely to be combust earlier, towards the front of the combustor in fuel-rich zones. Much of the negative physical impacts on fuel injection characteristics are limited to pressure atomisation systems with the drawback far less pronounced for airblast atomisers [78].

Establishing the correct air-fuel mixing quality is influenced by the successful atomisation and subsequent evaporation of liquid fuel within an adequate amount of air. It has been shown that through improved atomisation and resultant reduction in droplet size, soot formation can be reduced. There is a practical limit to this reduction as if the fuel particle size becomes too small, the penetration of the fuel spray into the combustor will be negatively impacted, ultimately leading to increased PM production [79].

2.8.2 Particulate Filters and Catalysts

Filters have been used for many years as a physical means to capture particles from aerosols. As EU automotive emissions standards have become more stringent, particularly since the introduction of PM number concentration limits in the EURO5b standards which came into effect in 2009, DPFs have become a mandatory installation on new light-duty diesel vehicles.

These devices are typically made from ceramic and consist of a monolithic wall-flow structure within which is a network of flow channels known as cells [80]. The porous nature of the ceramic material, coupled with the effective surface area of the cell network, allows PM to be filtered as exhaust gasses pass through the DPF. The filtration efficiency of current DPFs can be greater than 99% after a thin layer of soot has been deposited on the cell walls [81,82]. Eventually soot accumulation within a DPF will negatively impact the performance of the filter and the engine as exhaust back pressure is increased. Consequentially fuel consumption would increase and in severe cases can even lead to engine stalling. For these reasons a DPF must undergo a process of regeneration to remove the soot, commonly achieved through oxidation of the particulates.

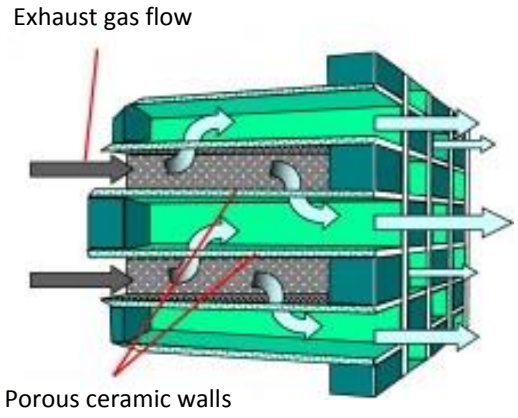

Figure 2.31: A schematic of a wall-flow DPF, adapted from [80].

Regeneration can be achieved actively, by increasing the local temperature of the DPF, or passively, using catalysts and increased exhaust gas temperatures. Active regeneration using localised heating elements periodically is advantageous in that the lifecycle of the DPF can be more tightly monitored and controlled as part of the engine management system. However, the additional energy input associated with these processes will result in overall higher fuel consumption. In contrast passive regeneration using the catalytic processes to produce more powerful oxidants, such as NO_2, can be achieved during normal driving conditions [83].

As the EURO5b Standards limited PM number output to only diesel combustion engines, filtration technology has been heavily tailored to the respective engine designs and exhaust criteria. The EURO6 Standards introduced in September of 2014

will include GDI combustion engines within the PM number restrictions and therefore particle filters designed for gasoline engines, Gasoline Particle Filters (GPFs) are now becoming more widely available. Although studies have shown particle emissions can be reduced via selective engine mapping and fuel injection strategies, the only proven technology that would effectively bring the particle number emissions of GDI vehicles below the $6x10^{11}$ #/km EURO6 threshold is wall flow particulate filters optimised for gasoline vehicles [84–86]. It is therefore likely that light-duty GDI vehicles will begin to implement GPFs in near future.

Direct filtration of gas turbine exhaust gases is not feasible and therefore PM reduction must be achieved through other means. Careful engine management and rigorous maintenance is currently the most widespread method of PM control for aviation gas turbines. Any introduction of new technology within the aviation gas turbine sector can prove difficult as designs require extensive research and associated quality assurance testing phases to ensure engine reliability. However, there are some examples within the literature of catalytic coatings being applied to areas of the combustion and exhaust zones of engines to promote oxidation of PM and improve overall combustion efficiency [87].

Catalytic technologies have been employed by the automotive industry since the 1970s to reduce pollutant emissions. The three-way catalyst (TWC), so called as it was able to oxidise CO, HCs and reduce NO_x emissions, is still in widespread usage today. The maximum performance efficiency of a TWC lies within a narrow operational window for which air-fuel ratio must be approximately stoichiometric (14.6 ±0.05) [88]. This poses a challenge to future GDI engine technologies which have a key benefit of being able to operate fuel-lean. Operation in this format can result in excess 0_2 which inhibits the reduction of NO_x. There has been some progress in developing alternative catalysts methodologies for the simultaneous reduction of NO_x and HCs, however they have seen limited success. Selective catalytic reduction (SCR) with NH_3 has also been reported as a possible solution should NOx emission regulations prove difficult to meet for GDI vehicles [89].

2.9 Chapter Summary

This Chapter has presented a review of both gas turbine and automotive engine technologies and an overview of the combustion exhaust which each commonly produce. Particular attention was paid to the particulate emissions which are generated within these exhausts and the formation mechanisms surrounding their production.

These particles are known to be harmful and have the potential to damage the environment and human health via a number of different mechanisms. In the case of human health the respiratory system is most at risk from particulate damage, additionally deposition of particles in the lungs can also lead to particles entering the blood stream and negatively impacting other organs in the body, particularly the heart. Many attempts have been made to model particulate deposition in the lungs, primarily for the pharmaceutical industry. The ICRP Model which was examined in this work showed that particles between 10 and 50nm, a size region commonly associated with combustion particles will be most likely to reach the deepest areas of the lungs.

Issuing regulations and limitations of particulate emissions across industrial sectors and individual emission sources has been very effective in reducing the ambient PM in the U.K. The new PM regulations which are currently being debated for aviation gas turbines and the Euro Standards which the automotive industry must adhere to are becoming increasing stringent. For this reason alternative means of particulate emission mitigation are being devised such as the use of catalytic removal mechanisms and the implantation of particulate filtration technologies (DPFs and GPFs).

Chapter 3

Facilities, Experimental Rigs and PM Measurement Instrumentation

Within this research project several industrial and research based facilities were used to conduct experimental testing. These sites provided the opportunity for extensive PM related and direct exhaust sampling from multiple combustion sources to take place. A wide variety of PM and gaseous emissions sampling and measurement equipment was employed to gather and process experimental results.

In this Chapter a discussion of the facilities, experimental rigs and apparatus which have been used most prominently to produce the results which are presented in later Chapters is provided.

3.1 Gas Turbine Research Centre: Port Talbot, UK

The Gas Turbine Research Centre (GTRC) is an academic research facility located in Port Talbot, South Wales. The centre is owned by Cardiff University and was formally opened in 2007 after a 4 year development phase following relocation from QinetiQ.

The GTRC comprises of three main experimental rigs, these being a sector combustor rig (SCR), high pressure combustor rig (HPCR), and large scale atmospheric spray rig. The HPCR was employed during this research to generate a simulated gas turbine exhaust. This function of the rig has been used extensively in the past in the production of EU funded PM sampling methodology reports [53,90,91].

3.1.1 High Pressure Combustor Rig and the Hot End Simulator

The HPCR unit is capable of providing a pre-heated airflow of 5 kg/sec at a temperature of 900K and 16 bar using a compressor and a gas-fired non-vitiating heater. Its modular design makes multiple combustion based experimentation achievable. Currently the GTRC has an array of optical, combustion instability, gas turbine exhaust simulator, auto-ignition and wall-cooling sections which can be installed onto the HPCR.

These attributes make the HPCR an ideal intermediate testing stage for the study of gas turbine exhaust as it allows for representative data without the requirement for a full scale engine or very high pressure (≈50 bar) combustion rig test, yet simulates actual gas turbine operating parameters more closely than low pressure combustion testing units. The unit also allows a higher degree of testing flexibility than that possible in larger scale experimentation. Experiment start-up and shutdown is faster, and combustion characteristics can be altered more rapidly by controlling the air and fuel input independently. Sampling from a representative aircraft exhaust is also a cost effective solution to gas turbine research where operational costs can become extremely high.

The particular combustion section option used in the creation of a simulated gas turbine exhaust was the Hot-End Simulator (HES). A schematic of the complete rig is

shown in Figure 3.1 where gaseous flow travels from left to right and a photograph of the rig installed in the HPCR is shown in Figure 3.2. Pre-heated, pressurised combustion air is introduced to a Rolls-Royce Tay aerospace combustion can contained within a bespoke pressure casing. Liquid fuel is introduced using an airblast atomiser, a modified version of the type used in the actual engine configuration. The required operating pressure is maintained in this upstream section using a choke plate, a water-cooled assembly consisting of a matrix of holes. The HES section follows this choke plate and is designed to reduce the temperature and pressure of the exhaust stream by removing heat rather than work. This is achieved using a series of heat exchanger units which are intended to simulate the pressure stages in the turbine section of a gas turbine engine. The pressure in each of the three stages, referred to as high pressure, intermediate pressure and low pressure, is maintained using a selection of trim plates, with varying cross-sectional area, and containing a matrix of holes. Temperature of the exhaust gases is controlled using a water-cooling circuit.

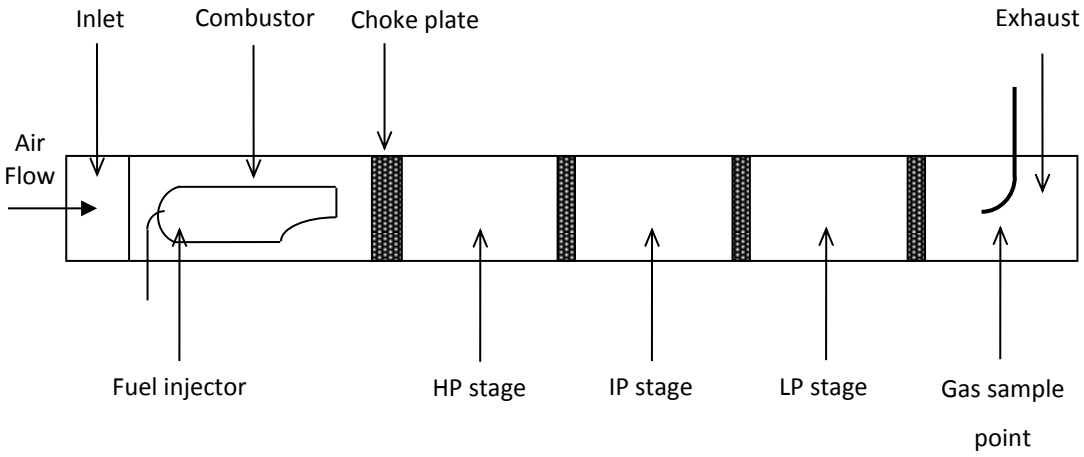

Figure 3.1: Schematic of the combustion system, HES and gas sampling probe assembly.

Figure 3.2: Photograph of the HES and gas sampling probe assembly.

3.2 Rolls-Royce: Derby, UK

The Rolls-Royce facility in Derby, UK, is involved with many aspects of the company's global operations however it is now predominantly used for gas turbine engine research and design, manufacture, and testing. The site houses state of the art full scale and individual engine component testing apparatus and experimental rigs, some of which were utilised in the generation of experimental results presented in this Thesis. Due to confidentiality and intellectual property agreements detailed photographs of the testing environments cannot be provided however descriptions and schematic depictions of the experimental arrangements are given.

3.2.1 Fully Annular Combustor Rig

The combustor annular rig, shown in Figure 3.3, is designed in a similar fashion to the HPRC and HES rig. High pressure, high temperature air is delivered from a compressor to the full annular combustor and fuel injection zone of a specific gas turbine while manipulation of exhaust back pressure can simulate engine loading profiles. The rig is used to conduct experimentation and testing on many aspects of combustor design such as fuel burning strategies and efficiencies, acoustic resonance and emissions analysis. The particular combustor rig which was used for testing was capable of providing pressurised heated inlet air flows representative exiting the compression

stage of a gas turbine engine. Emissions were captured using a multi-point traversing probe which was capable of rotating 360° around the annulus of the combustor exit plane. In order to do this the sample line was designed to be able to move with the probe while still maintaining experimental robustness.

Figure 3.3: Photograph of the combustor exit on a Rolls-Royce fully annular combustor rig, reproduced from [92].

3.3 Low Carbon Combustion Centre: Sheffield, UK

The Low Carbon Combustion Centre (LCCC) is operated by the University of Sheffield and targets research experimentation in many areas of combustion. These include power generation, fuel optimisation, alternative and renewable fuel opportunities, energy efficiency, and emissions reduction. Within this body of work the facility proved ideal for small scale aviation gas turbine exhaust generation.

3.3.1 Auxiliary Power Unit Test Bed

An auxiliary power unit (APU) is a small gas turbine engine which is commonly used on large aircraft to perform functions other than propulsion. These include electricity production for main engine starting and appliance use within the aircraft, also mechanical operations such as hydraulic pump control and air conditioning may also be run from the APU.

The particular APU available at the LCCC test bed is a Rolls Royce Artouste Mk113 which saw use in the RAF Victor Bomber (retired in 1993). The APU consists of a two stage turbine connected to a centrifugal compressor through a single shaft. The Artouste combustor is an annular, radial flow combustor with a fuel flinger injector as shown as a schematic diagram in Figure 3.4 and a photograph of the APU test bed in Figure 3.5.

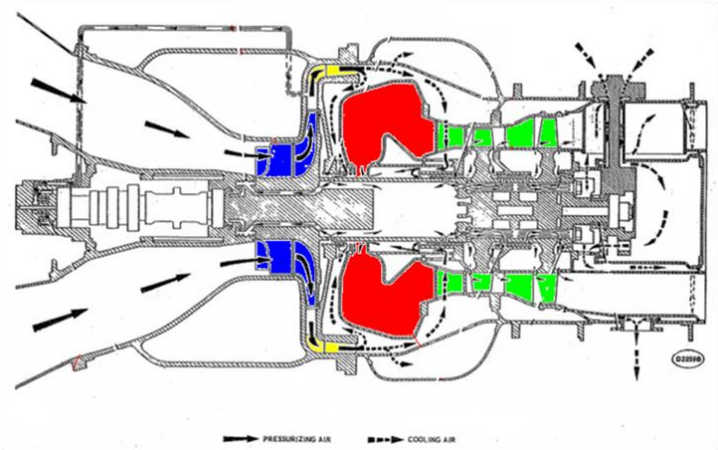

Figure 3.4: Schematic of the Rolls Royce Artouste APU, reproduced from [93].

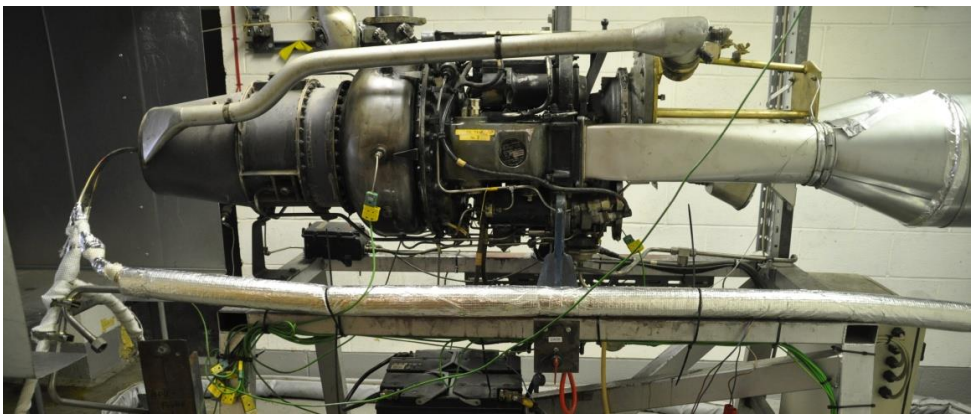

Figure 3.5: Photograph of the Rolls-Royce Artouste APU located on the LCCC test bed.

3.4 SR Technics: Zürich, Switzerland

The SR Technics aircraft engine servicing centre is located at Zürich Airport, Switzerland. The facility provides engine maintenance support to companies such as Airbus and Boeing. Maintenance cycles will commonly involve safety inspections,

standard cleaning, and replacement of fuel seals or aging components, followed by a rigorous operational running check.

In conjunction with the Federal Office of Civil Aviation (FOCA) SR Technics has fitted a traversing exhaust sampling probe directly behind one of its main engine testing beds. During non-critical maintenance testing phases of engine running the retractable probe can be lowered into the exhaust stream.

Figure 3.6: SR Technics engine test bed and Sample III SC.02 [94] team.

3.5 Ricardo Technical Centre: Shoreham-By-Sea, UK

Ricardo is a leading provider of product innovation, engineering solutions, clean technology and strategic consulting; however the primary focus of the Shoreham Technical Centre is automotive research and development. The Shoreham site is the head office and largest of Ricardo's international network of technical facilities. Opened in 1919, it is Ricardo's longest established location for engineering, design, and development test facilities. The site offers extensive state of the art testing facilities for research into internal combustion engines and systems including gasoline, diesel and gaseous fuelled engines of all sizes. Additional engine refinement and certification analysis into areas such as acoustic and exhaust emissions are also available. These facilities and testing equipment are amongst the most advanced in the global markets in which the company operates.

3.5.1 Multi and Single-Cylinder SGDI Hydra Research Engines

Ricardo have developed SGDI gasoline variants of their established Hydra engine design in an attempt to meet the growing demand for industrial and academic research into automotive fuel economy, emission reduction and performance benefits. The versatility of the Hydra engine design allows for extensive upgradeability as well as testing flexibility, elements which proved highly beneficial when studying particle emissions which can exhibit significant variability dependent on engine operating details. Two variations of Ricardo's Hydra engine models were utilised during this work; these being the multi-cylinder (4 cylinder) SGDI engine (MCRE) and the single-cylinder SGDI engine (SCRE). The SGDI combustion system which is installed in these engines is the result of a collaborative effort between Ricardo and PETRONAS. The specifications of these engine designs are given in Table 3.1.

Table 3.1: Ricardo test engine specifications, reproduced from [95].

Engine Parameter	Description
Type	4 stroke
Combustion system	Spray guided gasoline direct injection
Bore x Stroke (mm)	86 x 86
Swept volume (cm^3)	500 for SCRE, 2000 for MCRE
Compression ratio	11.5:1 for NA SCRE, 10.7:1 Boosted SCRE and MCRE
Injector	Piezoelectric actuation, outwardly opening pintle or novel piezoelectric actuation, super-critical fuel
Maximum fuel pressure (bar)	230
Valvetrain	Twin VVT, two stage valve lift on SCRE only
Ignition system	35mJ coil plug
Air motion	0.9 tumble ratio at maximum valve lift of 9mm

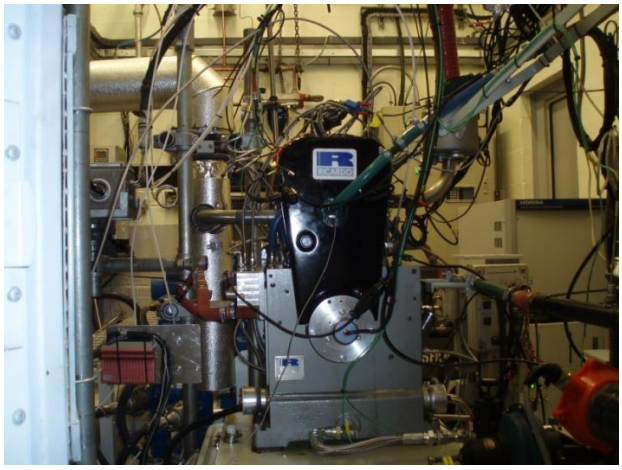

Figure 3.7: Photograph of the single-cylinder spray guided direct injection engine installed on a Ricardo test bed.

Internally, the engine cylinder heads featured a traverse orientation spark plug and injector layout, i.e. the axis of the spark plug and the fuel injector was perpendicular to the crankshaft axis. The fuel injector was positioned between the intake valves while the spark plug was positioned between the exhaust valves, shown in the cross-section Computer Aided Design (CAD) model in Figure 3.8. The engines were fitted with pistons which incorporated a bowl shape within the piston-head, optimised for lean stratified SGDI operation. The reasoning for the inclusion of a bowl into the piston-head is to delay the onset of piston crown fuel impingement thus increasing the spray penetration length during late injection [95].

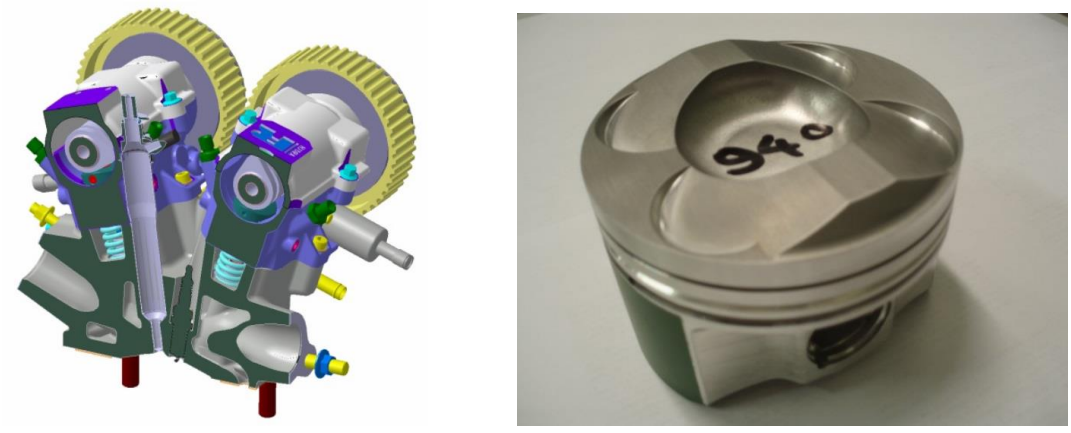

(a) (b)

Figure 3.8: (a) Cross-section view of the spray-guided cylinder head system, reproduced from [95], and (b) photograph of a piston used during Hydra engine experiments.

3.6 Particle Detection and Measurement Instruments

The production and sale of particle measuring devices is a fast growing industry. As discussed in Chapter 2 the understanding of the impact combustion PM emissions can have on human health and climate change has resulted in increased legislative limits and subsequently monitoring requirements being applied to emission outputs. Research institutes and industrial organisations are therefore placing resources into the study and development of new measurement apparatus with higher repeatability, resolution and accuracy. In the following pages the instrumentation which was utilised for particle characterisation during this work are presented.

3.6.1 Optical Smoke Number

Smoke number is the current aviation regulatory standard for PM emissions in the aviation industry and has traditional been measured using the filter based technique outlined in the previous Chapter. The Rotadata Optical Smoke Meter (OSM) was developed as an instrument in the late 1980's to obtain real time (1Hz) smoke number measurements on combustor rigs. Conventional Smoke Number measurements using the ICAO Annex 16 filter method are time consuming (>1min per filter) which is not compatible with performing traverse combustor measurements.

The Optical Smoke Meter measures smoke by passing a sample through a light path and measuring the attenuation of the light at a photodetector. The basic principle of an OSM is to measure the extinction of visible (green) light (using an LED emitting light at a wavelength of 565nm) through a volume of smoke. The amount of light that gets transmitted through to the detector is a measure of the amount of smoke particles that are in the sample. Multiple back-to-back filter comparison combustor tests during the OSM instrument development provides the correlation between the extinction curve and Smoke Number.

The inlet sample and cell are kept heated at 55°C to minimise the risk of water condensation and ensure a stable environment. A schematic of the OSM design is shown in Figure 3.9.

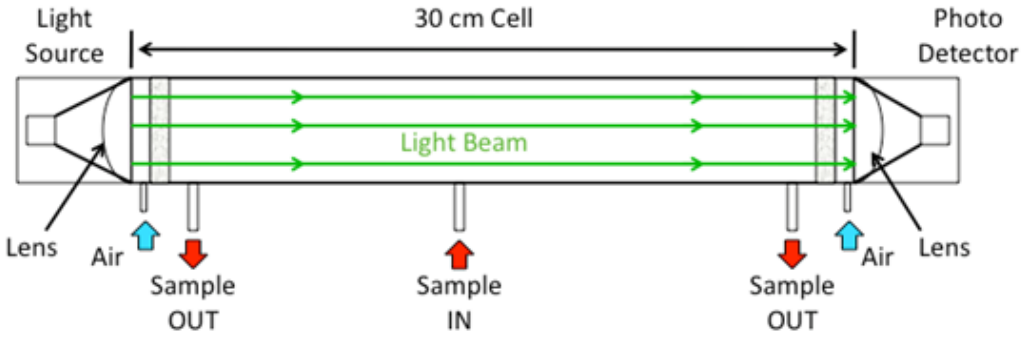

Figure 3.9: Schematic of OSM detection chamber, reproduced from [96].

Utilising green light absorbance for Smoke measurement has the unwanted interference of NO_2 absorption. This is overcome by operating two Rotadata OSM's in parallel, one with a particle filter to measure the NO_2 absorbance contribution only. The subtraction of the filtered OSM voltage output from the unfiltered OSM, provides the smoke-only contribution measurement required for PM emission certification.

3.6.2 Condensation Particle Counter

Traditionally counting the number of small particles in an aerosol was achieved with an optical particle counter (OPC) which uses photo-sensitive detectors to observe the scattering of a light source, as particles are drawn through a classification chamber. The scattering intensity and geometry is then interpreted to provide a number count and in some instances particle size estimation by selecting a calibrated refractive index of the emission source. An example of such a setup can be seen in Figure 3.10, which shows a schematic cross section of the Grimm 1.109 OPC model. The operating range of an OPC is in the micro meter region, typically between 0.3µm to 10µm [97], as particles must be of a large enough size to provide a detectable signal. This makes OPCs a good method of gaining real-time measurements of fairly course particles, but they lack the sensitivity to measure the ultrafine PM which is routinely produced in controlled combustion processes.

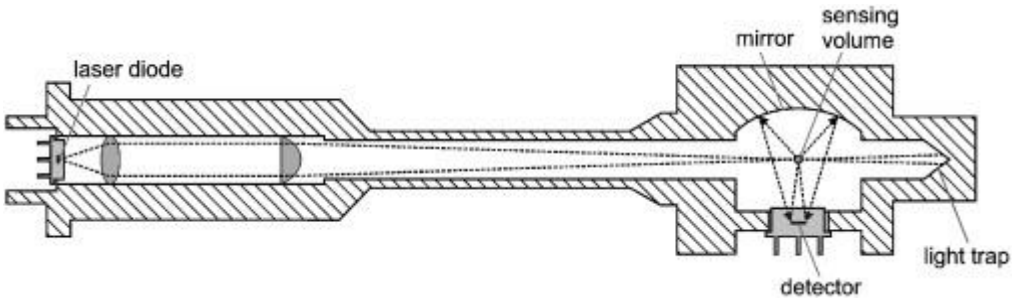

Figure 3.10: Schematic cross section of the classification chamber of the Grimm 1.109, reproduced from [98].

Condensation Particle Counters (CPCs) address the issue of this particle detection limit by exposing sampled particles to a super-saturated condensation chamber containing a working fluid (commonly butanol or water vapour). In this environment the solid particles act as a nucleation source allowing liquid droplets to adhere to their surface enlarging them to a detectable size using optical arrangements similar to that used in an OPC. Modern CPCs, such as the TSI 3788, are capable of measuring particle sizes to a lower size limit of 2.5nm making them ideal for counting ultrafine particles.

3.6.3 Differential Mobility Analyser and Scanning Mobility Particle Sizer

A differential mobility analyser (DMA) classifies particles according to their electrical mobility meaning particles of specific sizes can be separated from a size distribution contained within an aerosol. This is achieved by first neutralizing a sampled aerosol using a radioactive source such that they have a Fuchs equilibrium charge distribution. As particles enter the classification chamber of a DMA they are exposed to an electric field created by a high voltage rod at the centre of the cylindrical column. The aerosol particles, being oppositely charged, interact with the electric field at a rate dependent on their charge-drag ratio (electrical mobility). At the base of the classifying chamber only particles of a specific electrically mobility, and therefore specific size, will enter the narrow collection area with excess particle particles and sheath air being exhausted. This mechanism for classifying particles using electrical mobility is illustrated in Figure 3.11.

A scanning mobility particle sizer (SMPS) is essentially a combination of a DMA and CPC which allows for full particle size distributions to be collected. This is achieved by changing the voltage of the DMA central rod and therefore changing which particle size range is entering the collection chamber. Sweeping through a range of voltages allows a complete particle size range, within the lower and upper bounds of the instrument range, to be covered.

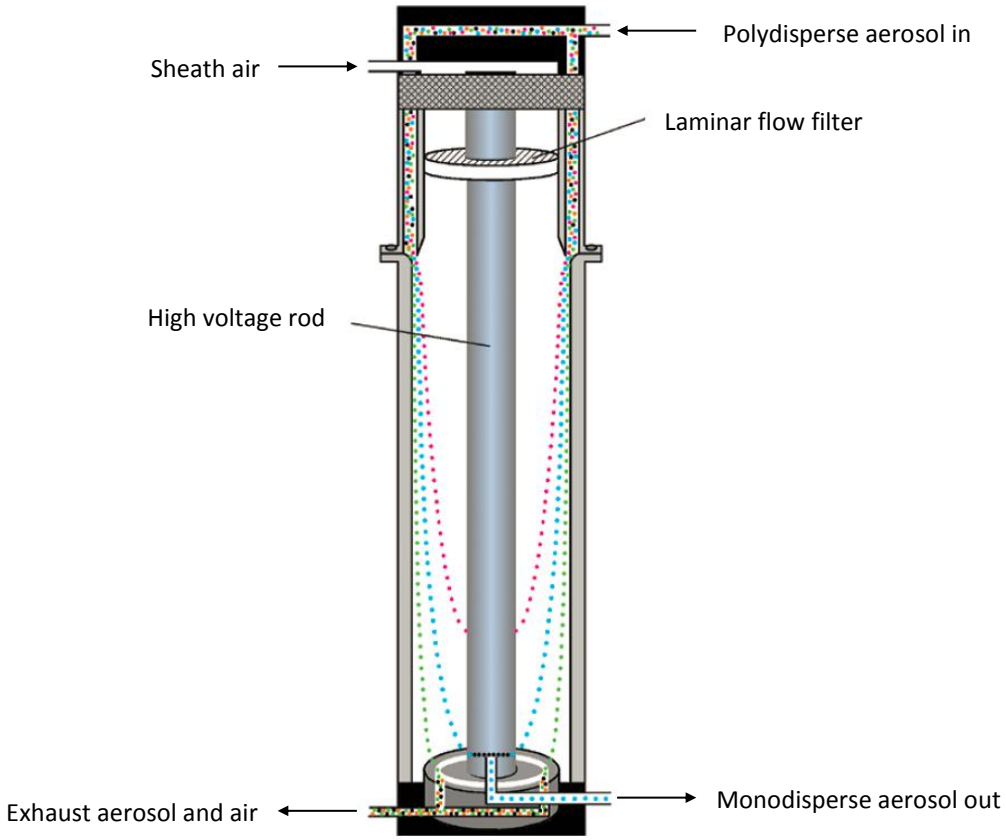

Figure 3.11: Illustration of the operating mechanism of a DMA, adapted from [99].

3.6.4 Differential Mobility Spectrometer

A DMS operates on a similar principle to that of a DMA in that particles are classified according to their electrical mobility. In the case of many of the results presented in this Thesis the DMS system which was used extensively was the DMS500 MKII fast particle analyser, produced by Cambustion Ltd. In contrast to an SMPS system which scans through discreet particles sizes in order to build up a full PM size distribution a DMS is able to classify a particle size range simultaneously.

The DMS500 consists of a corona diffusion charger mounted on top of the main classification column. Particles which enter the corona diffusion charger they inherit a charge which is largely proportional to their surface, although doubly and triply charged particles can also develop. As in a DMA the particles are then subjected to a strong electrical field emitted from a high voltage electrode at the centre of the classifying column as they travel down the classification chamber in a flow of sheath air. This causes the particles to be deflected and to follow a trajectory dependent on their aerodynamic drag-charge ratio towards the outer circumference of the classification chamber. Unlike a DMA there is not one particle collection point in a DMS, instead there are multiple high sensitivity electrometer rings surrounding the outer circumference of the classifying chamber. As particles reach the outer edge of the classifying chamber they come into contact with one of the 22 electrometers. The measuring range of the DMS500 for all of the research presented in this Thesis was 5 - 1000nm, this size range is divided logarithmically such that each of the electrometers is apportioned a specific detectable measurement range. Changes in amperage which are detected by the electrometers when charged particles come into contact with them are interpreted as particle number count using an inversion matrix generated by Cambustion during system calibration. Several calibration inversion matrices exist for each DMS500 unit, each designed to be emission source, or analysis methodology specific. It is this parallel size measurement process which makes the DMS500 capable of a 10Hz, (200ms) $T_{10\text{-}90\%}$ response time.

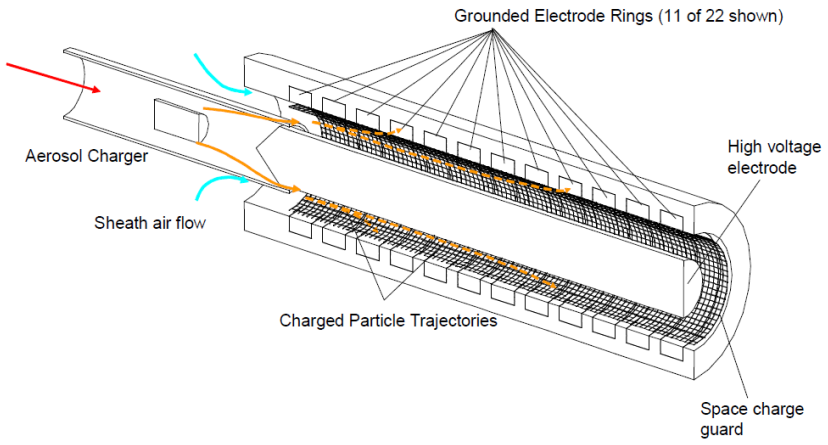

Figure 3.12: Schematic of the DMS500 classifying chamber design, reproduced from [100].

When measuring at a particle detection range of 5 - 1000nm the DMS500 operates at sub-atmospheric pressure (250mb). This is a requirement to move the point in space of the mobility inversion [101] and additionally improves the instrument time response, reduces particle agglomeration and ensures less sensitivity to engine exhaust pressure fluctuations [100]. The instrument samples at a rate of 8 slpm through a 5m heated Polytetrafluoroethylene (PTFE) sample line for direct exhaust sampling. At the sample line tip is the first of a built in two-stage dilution system, as shown in Figure 3.13. First stage dilution consists of up to 4:1 dilution with metered, High Efficiency Particle Air (HEPA) filtered, pre-warmed air. The main purpose of diluting at this point is to limit any condensation of water vapour in the instrument. The sample pressure is reduced to 250mb using a critical orifice which gives a concentration reduction equivalent to 16:1 [100].

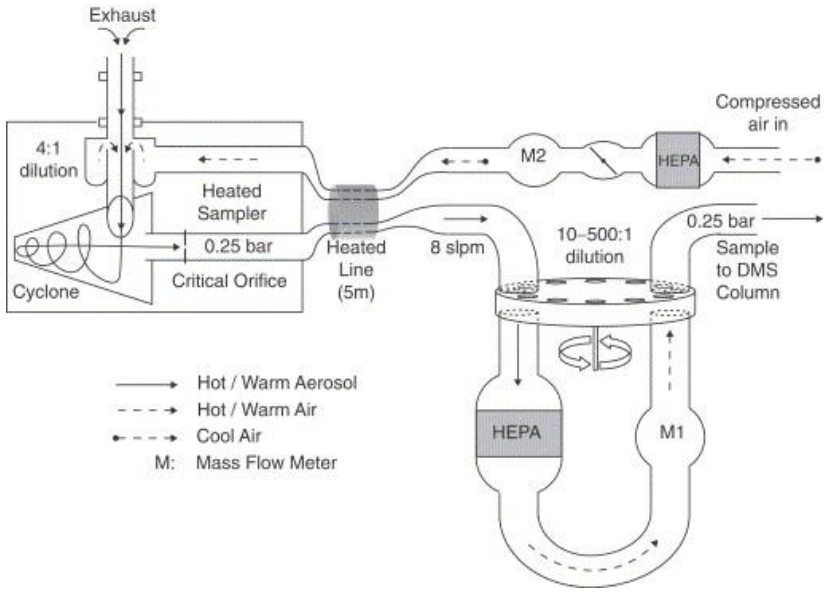

Figure 3.13: Illustration of the DMS500 sampling system, reproduced from [100].

Secondary dilution can also be applied to the sample within the instrument following transportation through the 5m heated sample line. This dilution is applied using a mechanical rotary disc diluter which is bespoke to the DMS500. The design of this dilution system is such that the majority of the 8 slpm sample flow is HEPA filtered after passing through one of the several holes in the diluter disc. The newly filtered flow then passes through a hole on the opposite side of the rotating disc in the opposite direct. As the disc rotates small volumes of the sampled aerosol are

transported from the unfiltered stream to the filtered stream therefore reducing the concentration of the sampled aerosol to a ratio dependent on the speed of rotation of the rotary disc. Correction for both dilution systems is made in real-time based upon the primary flow of air supplied as first-stage dilution and the flow of the main air through the secondary diluter after HEPA filtration; additionally correction for the secondary diluter is made from the feed-back motor speed [100]. The maximum PM concentration which can be analysed using the DMS500 is dependent to a certain extent on particle size. When operating at the instruments maximum possible dilution ratio (3000:1) higher number concentrations can be sampled which are shown in Figure 3.14.

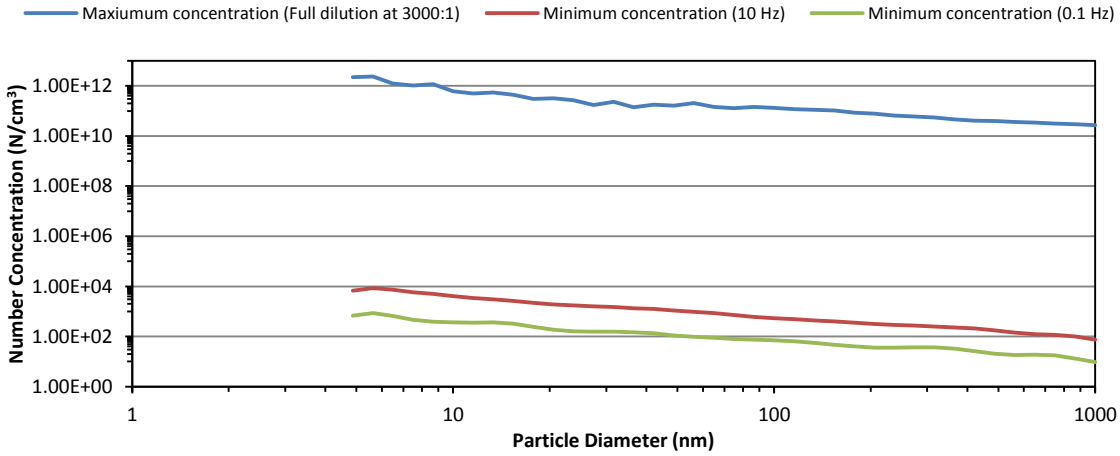

Figure 3.14: Maximum sampling number concentration when fully diluted and the instrument noise sensitivity at 10 and 0.1Hz sampling frequency of the DMS500, data provided by Cambustion Ltd.

The sensitivity of the DMS500 is also particle size dependent and is defined as the smallest signal which exceeds the peak to peak noise, or if peak to peak noise is not defined, this is the smallest signal which can be identified from the noise with a 99% confidence [102]. Figure 3.14 shows the noise level of the instrument when operating in a 10Hz (no averaging of data) and a 0.1Hz (data average for 10 seconds) capacity. The highest noise levels occur when sampling at the highest frequency (10 Hz) and reduce as the data averaging time for a sample is increased. All measurements presented in this Thesis were sampled at a rate of 10Hz and output as an averaged sample rate a rate of 1Hz (10 individual measurements averaged every second) as this

was considered sufficient to capture any transient PM phenomena and provided a better signal-to-noise ratio than the higher 10Hz sample rate [103].

An assessment of instrumental noise level is conducted each time the DMS500 is 'auto-zeroed' using the bespoke instrument software. This process evaluates the noise variance on each of the electrometer rings when sampling HEPA filtered sheath air and produces a chart similar to that shown in Figure 3.14. This allows the operator to determine what aerosol concentration is required to ensure experimental accuracy and can be used as an indicator of when the instrument requires cleaning.

3.7 DMS500 Data Processing and Presentation

Much of the experimental results and data presented in this Thesis are in the form of traditional scatter charts however there are some key features about the DMS500 and similar PM size detection instruments which mean it is convenient to present PM data in a particular fashion. Additionally, the methodologies used by the DMS500 to interpret other parameters about a sampled aerosol are important to understanding the generated results discussed in later Chapters.

3.7.1 Generating PM Size Distributions

The DMS500 outputs particle size distributions in a continuous spectral function generated from its electrometer readings and inversion matrix interpretation. An example of such spectrum for a small portion of the DMS500 measurement range is illustrated in Figure 3.15:

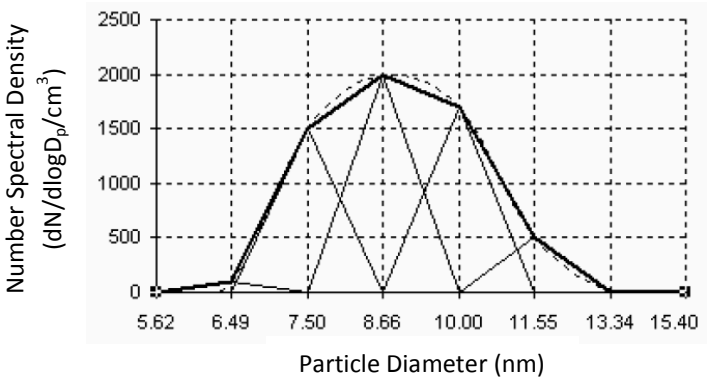

Figure 3.15: Example of the output of the DMS500 consisting of a continuous spectrum (dashed line) and a discrete linear approximation (solid line), reproduced from [104].

The reason for expressing concentration as a size spectral density ($dN/dlogD_p/cm^3$) is that it allows easy integration over any size range to give the total particle concentration. Applying dN/dlogDp as the chosen area under the graph gives N [104]:

$$N = \int_{Dp1}^{D_{p2}} \frac{dN}{dlog(D_p)} dlog(D_p)$$

Equation 12: Integration of continuous spectral density function to determine number concentration across a size range.

3.7.2 Mode Finding

The DMS500 employs sophisticated real-time mode finding algorithms to interpret the raw PM size spectrum data as discreet log-normal nucleation and agglomeration modes whenever possible. Optimisation and construction of these modes is based upon a Bayesian statistical framework. Bayes' theorem states that a set of data (D) described by parameters (w) [104]:

$$P(w|D) = \frac{P(w)P(D|w)}{P(D)}$$

Equation 13: Posterior probability function derived from Bayes' theorem.

In the case of the DMS500 the input parameters are lognormal (number concentration, mean and standard deviation) and the measured electrometer currents. P(D|w) is the posterior probability to be maximised, and is known as the 'likelihood' representing

the probability of the measured electrometer currents given a set of parameters. This function makes an assessment true instrument noise based upon the electrometer zero offset values. The P(w) term is known as the 'prior probability' and represents the prior knowledge about the system and the sampled aerosol before data is examined. This can be used to loosely bind the particulate modes to be within a range of sizes and geometric standard deviations by specifying the probability in regions of space. These probability maps, an example of which is shown in Figure 3.16, are contained within calibration files specific to the type of aerosol and instrument and are produced during DMS500 calibration [100]. P(D) is a normalisation constant which can be ignored.

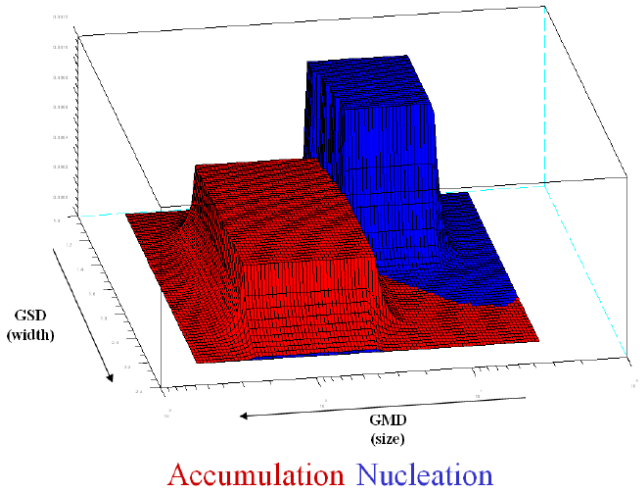

Figure 3.16: Prior probability map for diesel aerosol, reproduced from [104].

In this research project unless otherwise stated the DMS500 results presented consist of raw particulate size and number concentrations.

3.8 Particle Generation

In addition to sampling the exhausts produced by gas turbine and automotive engines, in this research project additional aerosols were generated for specific experiments. These aerosols were mainly used to investigate the effects of VOCs may have on sampling theory, and were also used in some cases as a particle generation source for instrument comparisons.

3.8.1 Solid Particles

In order to simulate soot particles a PALAS GFG 1000 solid graphite particle generation system, shown in Figure 3.17, was used. The unit operates by arcing electricity across two graphite rods in an inert atmosphere of argon gas. During the electrical discharge particles of graphite are produced, the size and concentration of which can be manipulating by varying the electrical current, discharge frequency and gaseous dilution ratio.

Figure 3.17: PALAS GFG 1000 used for the generation of solid graphite aerosol.

3.8.2 Volatile Particles

The calibration procedure for a VPR calls for the removal of >99% removal efficiency of 30nm tetracontane ($CH_3(CH2)_{38}CH_3$) particles with an inlet concentration of >10,000 particles per cm^3. A report of VPR calibration produced by the AEA Environment & Energy [105] described a methodology of creating an aerosol rich in volatile particles with the schematic shown in Figure 3.18.

The volatile particle generator operates by heating the solid or liquid volatile components within the crucible to a sufficient temperature that evaporation occurs. Volatile particulates are transported from the crucible by introducing filtered air into the saturated environment establishing a flow into the cold filtered bypass air stream. The temperature difference between the bypass air and volatile saturated crucible air flow causes condensation as the volatile particles return to the particle phase from the gaseous phase. By manipulating the bypass and crucible airflows and the temperature

applied to the crucible it is possible to adjust the particle concentration and mean particle diameter of the aerosol produced.

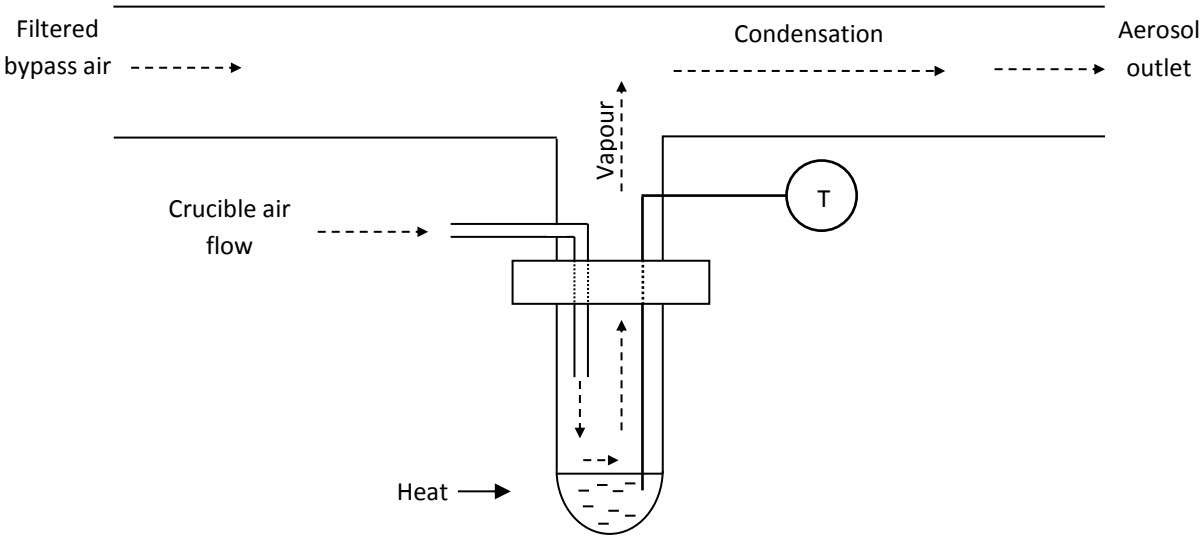

Figure 3.18: Schematic of condensation aerosol generator, adapted from [105].

The volatile particle generator produced by Cardiff University as part of the Sample III experimentation campaign was based upon the design principles shown in Figure 3.18 with the addition of advanced control elements. A schematic of the bespoke volatile generator design and photographs of the produced generator are shown in Figure 3.19 and Figure 3.20.

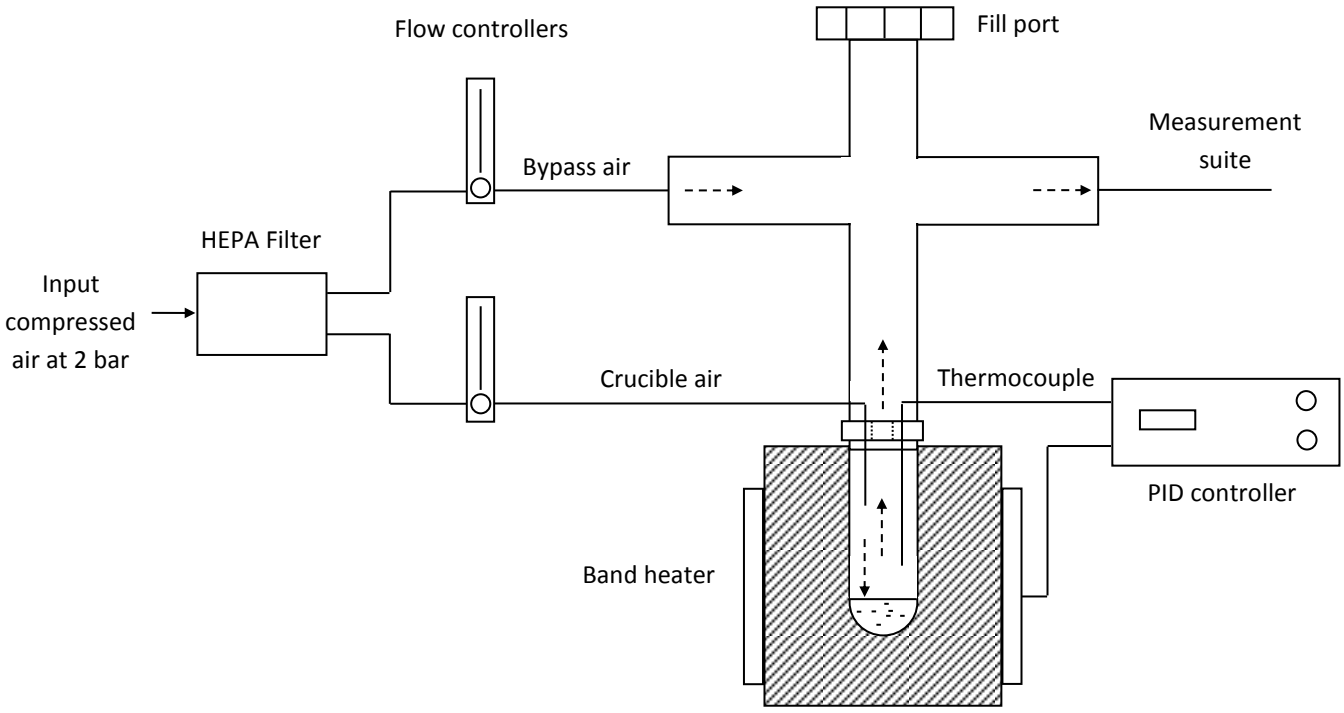

Figure 3.19: Schematic of bespoke volatile particle generator design.

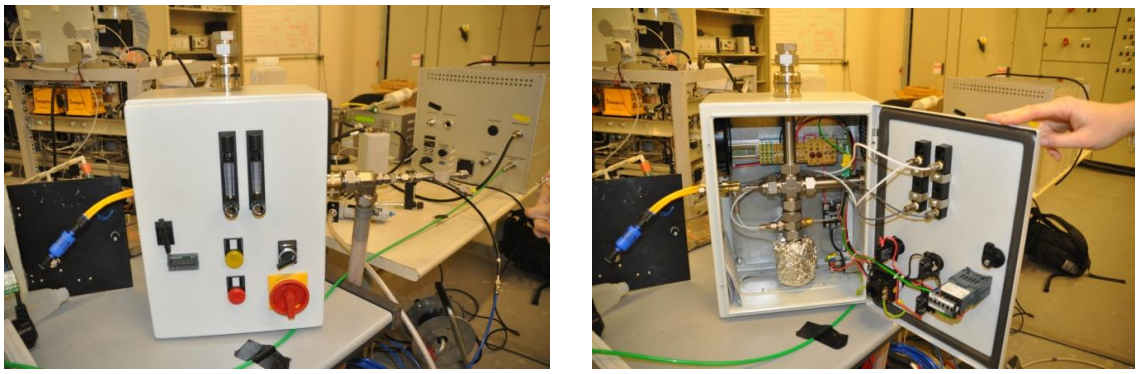

Figure 3.20: Photographs of bespoke volatile particle generator.

3.9 Chapter Summary

In this Chapter the industrial and academic facilities used and experimental campaigns which were performed during this research project has been presented with details relevant to the experiments which were performed at each location.

Research into PM emissions from aviation gas turbines was performed using the HPCR and HES combustion rig at the GTRC in Port Talbot, a small scale Rolls-Royce APU at the LCCC in Sheffield, multiple large scale gas turbines at SR Technics in Zürich, and

Rolls-Royce in Derby, and finally two configurations of a fully annular gas turbine combustor section at Rolls-Royce in Derby.

Research into PM emissions from light duty GDI engines was performed exclusively using two configurations of the Ricardo Hydra research engine at the Ricardo Technical Centre in Shoreham-By-Sea.

Several PM sampling instruments and other testing equipment have been used during this research project. Much of the PM analysis presented in this Thesis focuses on the number concentration, mass concentration and particle size distributions generated using the DMS500 which is manufactured by Cambustion Ltd. in Cambridge. The benefits of using this instrument were that it allowed a fairly broad PM sampling range which was respective of aviation gas turbine PM and automotive PM (5 - 1000nm), and its fast response (10Hz) and sensitivity ensured transient changes in PM distributions could be recorded.

Chapter 4

Volatile PM and Coatings of Volatile Material on Solid Core Particles

Both the PMP and the exhaust sampling system being currently being developed to become the new standard for the regulation of gas turbine emissions specify that only non-volatile particulates are to be included in recorded PM measurements. This is primarily due to the fact that in both the automotive and aviation industry the formation of volatile exhaust components can be highly dependent the operating parameters and sampling methodologies employed. The sensitivity of the volatile PM to change can make reliable and repeatable PM measurements difficult to obtain, further complicating the task of setting appropriate emission standards.

Volatile removal methodologies and commercial volatile particle removal apparatus (VPRs) have been developed to meet the requirements of combustion exhaust sampling. In this Chapter a discussion of volatile particles and the current specifications removal devices must meet to be considered PMP compliant is presented.

Following this are the results of two experiments designed to investigate how the performance of a compliant and non-compliant PMP VPR differ when supplied with a variety of 'challenge' aerosols. These aerosols included mono-disperse distribution sizes (100, 50, 30 and 15nm) of $CH_3(CH_2)_{38}CH_3$ (tetracontane) and a combination of volatile material and mono-disperse distribution sizes (100, 50, and 30nm) of solid particles. These experiments allowed an assessment of the VPRs volatile removal efficiency for solely volatile and solid core volatile coated particulate aerosols.

4.1 Volatile Particles

Exhaust emissions from aviation gas turbines and automotive engines comprise of a complex mixture of gases and particles. It has also been shown that typically exhaust particle number distributions in both such engines are of bi-modal nature, exhibiting nucleation and agglomeration modes. Although there are uncertainties about the distinctness of these modes - discussed in later Chapters - there is little doubt that a large percentage of small size exhaust particulates are of a volatile or semi-volatile state.

Volatile particles such as hydrocarbons and sulphur containing compounds can exist in both the gas and liquid phase within an exhaust stream depending on its physical properties. Hydrocarbons are predominantly produced due to incomplete combustion of the primary fuel source; however other petroleum based products which are used within an internal combustion engine, such as lubrication oil, can also induce volatile particle formation. H_2SO_4 and sulphate particles originate from chemical reactions involving SO_2 gas. Limiting the sulphur content of the fuel therefore significantly reduce these sulphate formations. Figure 4.1 shows an example of a sulphate formation (bright sphere) produced by a diesel engine, and a much smaller volatile particle formation produced by a direct injection spark-ignited engine.

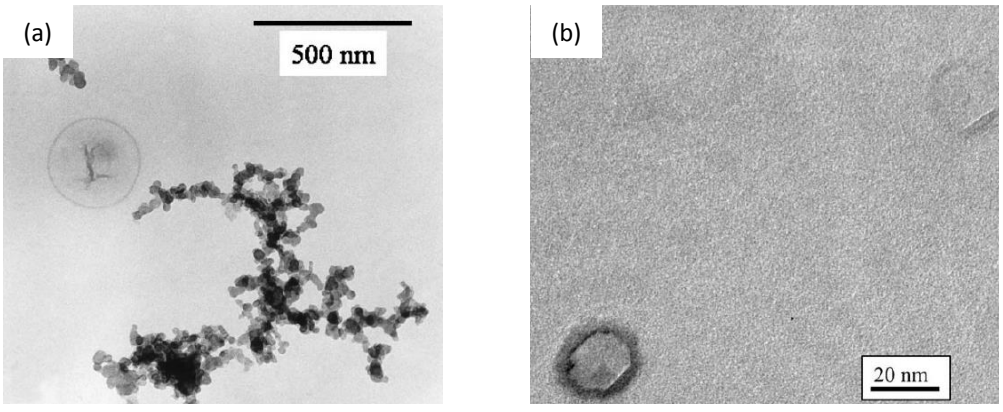

Figure 4.1: Volatile formations produced by (a) a diesel engine , reproduced from [44], and (b) a direct-injection spark-ignition engine, reproduced from [106].

The presence of ultrafine (<20nm) volatile particulates in a combustion exhaust increases the likelihood of complex aggregates forming where solid core particles can act as nucleation points and become coated in a volatile outer layer. There is evidence

that it is these types of particulates which pose the greatest risks to human health [107].

A major conclusions of the PMP was that the unpredictable nature of volatile particle formation, coupled with the sensitivity which volatile particles have to temperature and dilution characteristics, meant that in order to achieve a robust particle sampling and measurement methodology the system should be designed to be not be impacted by the presence of volatile compounds. It was the conclusion of the PMP that by considering only the non-volatile fraction of a PM distribution the emissions characteristics of test conditions would be more repeatable, comparable and representative of typical operating conditions. This has the additional benefit of simplifying the analysis of PM emissions and also aids in the setting adequate and enforceable emission legislation.

The PMP therefore stipulates that it is necessary that all volatile material in the exhaust stream is removed prior to making number, size, and mass measurements. With the introduction this non-volatile PM (nvPM) standard, candidate volatile removal devices have been proposed and were examined within the PMP to establish how to remove the >99% volatile material required with the smallest impact on composition of the sampled aerosol.

4.2 Volatile Particle Removers

The term ‘volatile particle removal’ is a broad definition of an after treatment process which has been established over several years in various industries (e.g. incinerators and sewage management). Catalytic volatile removal devices have been used in the automotive industry for the oxidation of UHCs in the tailpipe exhaust since the 1970s.

VPRs can therefore take many different forms dependent on the role they are required to fulfil. The introduction of the PMP has resulted in a number of commercially available VPRs designed to remove volatile particles from a sampled aerosol with the required temperature, dilution, and sample conditioning specifications outlined in the PMP. These systems have mainly been intended to make nvPM number concentration

measurements for the exhausts of diesel reciprocating engines fitted with ceramic DPFs. Other non-compliant PMP systems do exist however it is likely that until VPRs are officially adopted in other non-automotive exhaust sampling roles, the majority of commercially available products will be best suited to this sector. With the expansion of the EURO6 Standards to include GDI emissions in the particle number restrictions, and the development of similar PM sampling proposals in the aviation industry, it is likely that VPR technology will become more widespread and flexible in regard to emissions sources.

4.2.1 PMP Compliant VPRs

As described in Chapter 2 for a VPR to be PMP compliant it must have three distinct elements; a heated primary dilution phase (PND_1), a heated evaporation tube phase (ET), and lastly a cold secondary dilution phase (PND_2). This is simply illustrated in Figure 4.2:

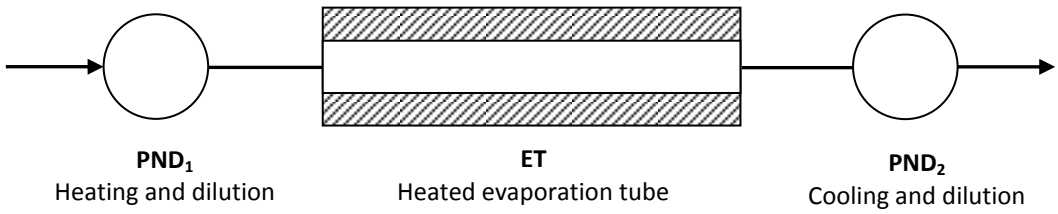

Figure 4.2: Schematic of the design requirements for a PMP described VPR.

In addition to having a valid construction, a PMP compliant VPR must also meet a required level of volatile particle removal efficiency. This specification is derived from the redrafted UN Regulation No.83 documentation produced by the PMP workgroup and stipulates that a greater than >99% reduction of 30nm $CH_3(CH_2)_{38}CH_3$ (tetracontane) particles with an inlet concentration of >10,000 particles per cm^3 must be achieved [72].

4.2.2 Solid Particle Concentration Reduction Factor

A solid particle concentration reduction factor (PCRF) must also be generated in order to meet PMP specifications. The purpose of a PCRF is to compensate for particle

penetration losses within the system, and therefore takes into account both dilution and upstream and downstream particle number concentration.

For each nominal dilution setting and particle diameter, the ratio of upstream number concentration to downstream number concentration should be calculated as:

$$f_r(d_i) = \frac{N_{in}(d_i)}{N_{out}(d_i)}$$

Equation 14: Particle concentration reduction factor.

where $N_{in}(d_i)$ is the upstream particle number concentration for particles of diameter d_i; $N_{out}(d_i)$ is the downstream particle number concentration for particles of diameter d_i; and d_i is the particle electrical mobility diameter (30, 50 or 100nm)

For each nominal dilution setting the mean particle concentration reduction factor:

$$\overline{f_r} = \frac{f_r(30nm) + f_r(50nm) + f_r(100nm)}{3}$$

Equation 15: Mean particle concentration reduction factor.

Additionally, at each nominal dilution setting the VPR is required to deliver PCRFs for particles of 30nm and 50nm electrical mobility diameters, that are no more that 30% and 20% higher respectively, and no more than 5% lower than those for particles of 100nm electrical mobility diameter. This can be summarised by the following:

$$1.3 > \frac{f_r(30nm)}{f_r(100nm)} > 0.95$$

Equation 16: Particle concentration reduction factor validation criteria for 30nm particle.

$$1.2 > \frac{f_r(50nm)}{f_r(100nm)} > 0.95$$

Equation 17: Particle concentration reduction factor validation criteria for 50nm particle.

4.3 Volatile-Only Particle Removal

As an introductory phase to this research project, an examination of the volatile removal efficiency of two commercially available VPRs was undertaken. As well as the removal efficiency of volatile material only, this study also included the capability of these devices to remove volatile material coating from solid core particles.

These objectives were achieved by measuring the concentrations and particle size distributions of a 'challenge' aerosol upstream and downstream of the tested VPR, to determine any variability between the original and final composition of the 'challenge' aerosol. The particle measurement and generation apparatus used in this experimentation were the TSi CPC, GRIMM SMPS, PALAS GFG 1000 soot generator and the bespoke Cardiff University volatile particle generator (VG) all of which have been described in the preceding Chapter.

Although the certification requirements for a VPR to be PMP compliant are non-ambiguous, the methodologies on how these requirements are obtained are less stringently defined. This has meant that VPR manufacturers have employed different solutions in the production of their technologies. These differences are mainly in the form of dilution techniques; however some are more novel and take a wholly different approach to volatile particle removal. The VPRs which have been utilised in this research project include:

- Volatile removal using heated evaporation dilution introduced eductor dilutor technology (DEKATI system).
- Volatile removal using heated evaporation dilution introduced using mass flow recirculation (GRIMM system).
- Volatile removal using chemical catalytic processes (the bespoke University of Minnesota system, this is not examined in this experimentation but is discussed later in Chapter 5).

The first of the tested VPR systems was the DEKATI Engine Exhaust Diluter (EED) which complies with all the requirements for VPR validation within the PMP and UN Regulation No.83 documentation. The design of the DEKATI EED system is very simple and does not include any moving parts. Primary and secondary dilution is provided

using ejector diluters constructed out of stainless steel. Primary dilution is supplied at a ratio of 10:1 and at a temperature of 150°C and is introduced into the sample aerosol prior to the ET. The ET temperature can be varied between 300 and 400°C. Cold (20°C) secondary dilution is introduced at a ratio of 10:1 resulting in an overall dilution ratio of 100:1. The DEKATI EED is designed exclusively to fulfil the VPR role of an exhaust sampling system, and does not integrate any particle measurement equipment. User integration with the DEKATI EED is achieved entirely using the LCD front mounted control panel where dilution evaporation tube characteristics can be specified.

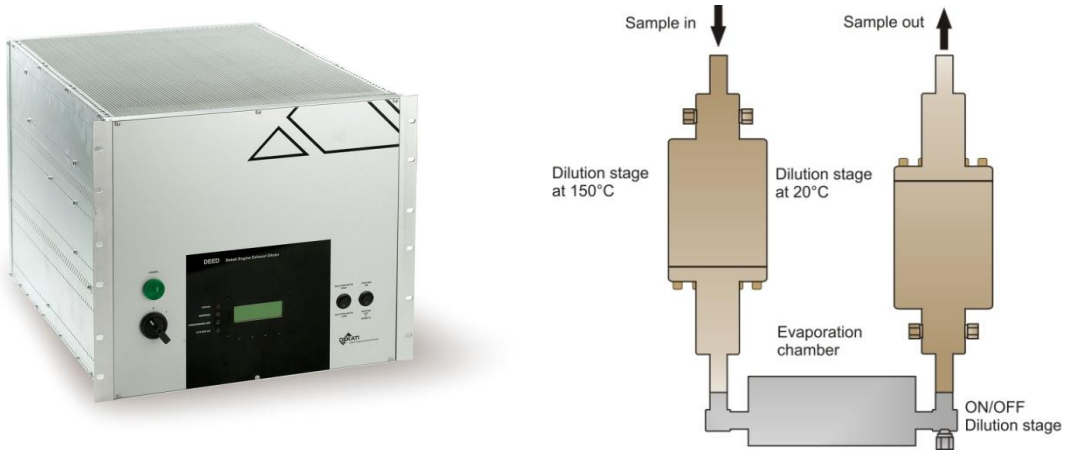

Figure 4.3: (a) Photograph and (b) schematic diagram of the DEKATI EED, reproduced from [108].

The second VPR appraised was the GRIMM Emission Sampling System (ESS) which does not adhere to the VPR requirements set out by the PMP, as it does not follow the design requirement that the dilution and the ET are stand-alone sections of any system design. Instead the GRIMM ESS employs hot (200°C) primary dilution at the probe tip, as shown in Figure 4.4.

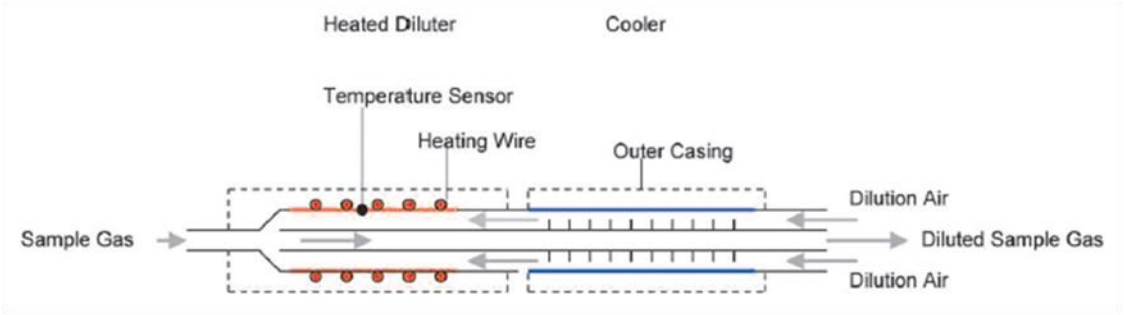

Figure 4.4: Schematic of the GRIMM Emission Sampling System sample probe and primary dilution setup, reproduced from [109].

The GRIMM ESS employs a novel solution to introduce dilution whereby excess exhaust sample is taken at a rate of 9 L/min, dried, filtered and re-heated to a maximum of 200°C before being re-introduced to the sample flow at the probe tip. A similar process is also used for the introduction of 9 L/min of secondary dilution, although the sample is assumed to be dry at this stage and therefor no additional drying section is included in the design. The total dilution of the GRIMM ESS system is dependent on the sample flow which is being drawn. For a 100:1 dilution ratio 1 L/min of sample flow is required, alternatively, for a higher 1:961 total dilution ratio the sample flow can be reduced to 0.3 L/min. The user is supplied with a control unit in order to set heating and flow points, however, the unit is designed to be utilised with a GRIMM SMPS system, a combination which allows real-time assessment of particle size distributions. Within the context of this research project, the unit was used with an SMPS installed.

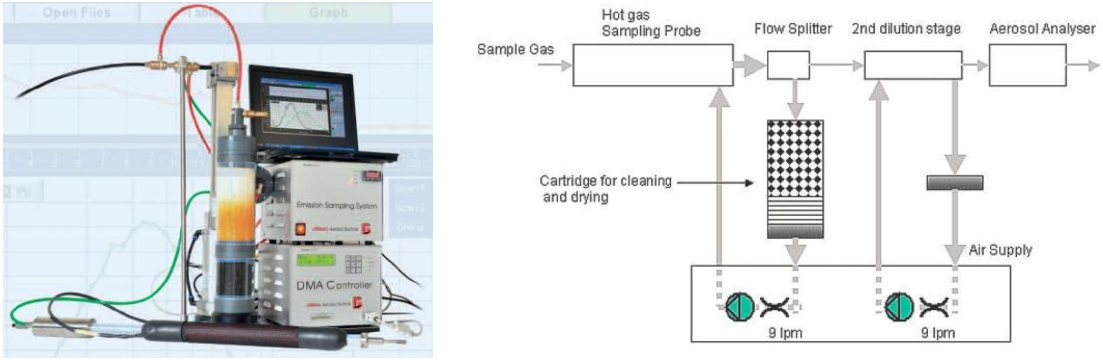

(a) (b)

Figure 4.5: (a) Photograph and (b) schematic of the GRIMM ESS, reproduced [109].

A schematic diagram of the sample set-up used for the first configuration of these experiments, which involved the creation of a solely volatile particle 'challenge' aerosol, is shown in Figure 4.6. The procedure used during this set of experiments involved supplying the VG with HEPA filtered air to create a densely volatile particle loaded aerosol. This aerosol was then size-selected using the DMA system to produce mono-disperse aerosols of 100, 50, 30 and 15nm. Each of these challenge aerosols were then individual introduced into the VPR while measurements of the up and downstream concentrations and size distribution of the 'challenge' aerosol were recorded. In post processing of the recorded data, two minute stable period of up and downstream number concentrations were used to produce average concentration measurements.

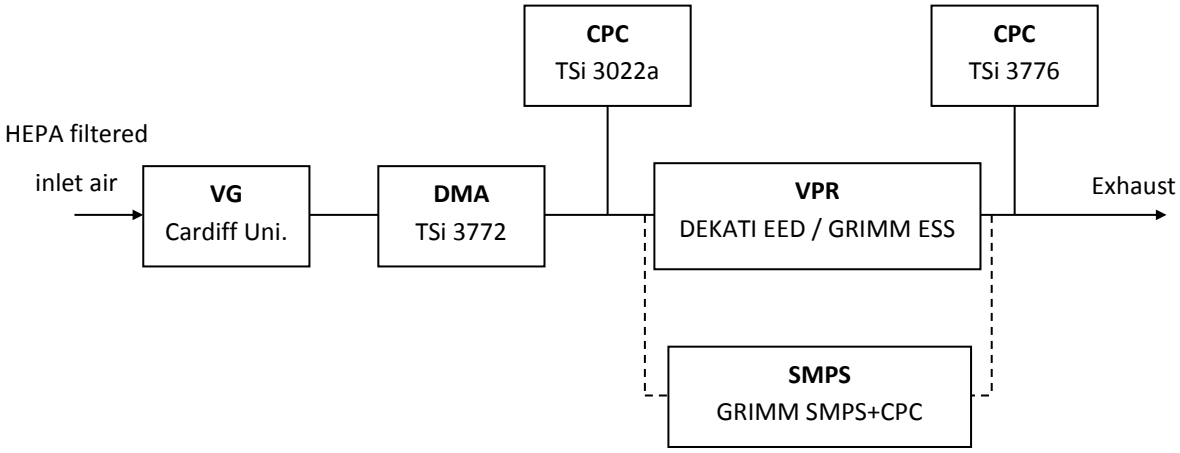

Figure 4.6: Schematic diagram of the volatile removal experiments using only volatile loaded challenge aerosol.

Results gathered when evaluating the performance of the DEKATI EED system and GRIMM ESS VPR systems are presented according to the 'challenge' aerosol being supplied (100, 50, 30, and 15nm volatile only particles).

4.3.1 Results: 100nm Volatile-Only 'Challenge' Aerosol

The performance of the DEKATI EDD VPR system was excellent when appraised against the 100nm challenge aerosol comprising of only volatiles. For volatile material with an average concentration of 1.06×10^5 N/cm^3 (approximately 10 times that required by the

PMP standard) the unit was still able to reduce the recorded particle count to 9.36x10^3 N/cm^3, a reduction of 92%. The size spectral analysis the GMD of the original upstream aerosol was calculated by the SMPS system to be 88nm. The GMD downstream aerosol was calculated to be 12nm. It is concluded therefore that the remaining volatile material was likely to have reduced in size dramatically however the residence time or ET temperature was not high enough to fully evaporate these large volatile particles.

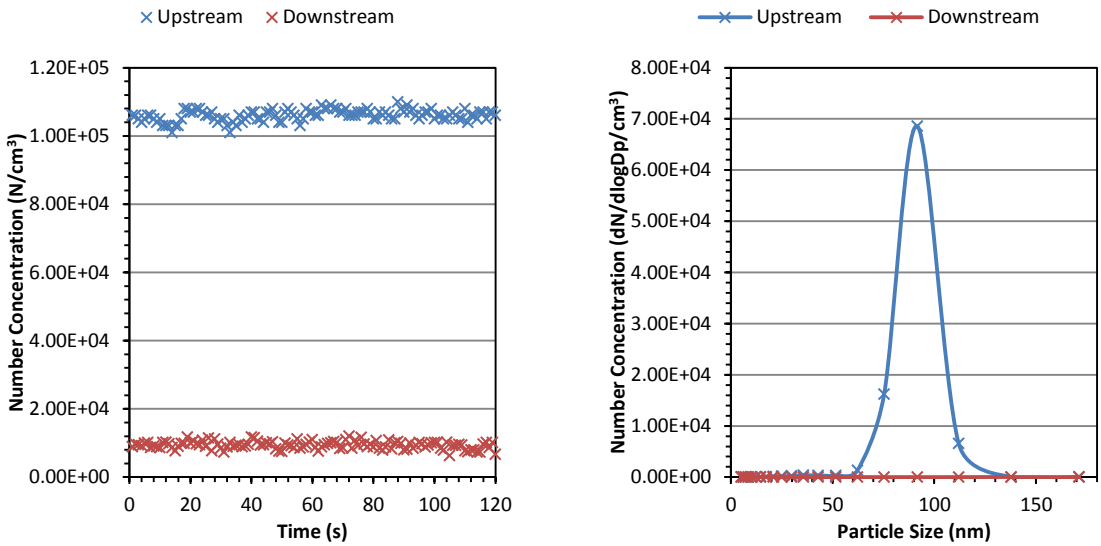

Figure 4.7: (a) Number concentrations recorded up and downstream of the DEKATI EDD, (b) SMPS particle size spectra recorded up and downstream of the DEKATI EDD when supplying 100nm volatile particle 'challenge' aerosol.

The number concentration data which was recorded during testing with the GRIMM ESS was unusual in that the downstream number concentrations were found to be higher than those upstream of the VPR. Initially the measured number concentration was 1.18x10^5 N/cm^3 and increased to 1.70x10^5 N/cm^3 following the VPR. The size spectral analysis of this test condition also showed that whilst a significant reduction of the initial size mode (GMD 87nm) was recorded, this was accompanied by a significant increase in the concentration of smaller particles following the VPR (GMD 14nm). Without an ET in the GRIMM ESS the dilution temperature of only 200°C is unlikely to be high enough to fully evaporate this high concentration of volatile material. The result of this is that the particulates have shrunk and fractured into smaller size particle fractions covering a broad size range of 5 to 60nm.

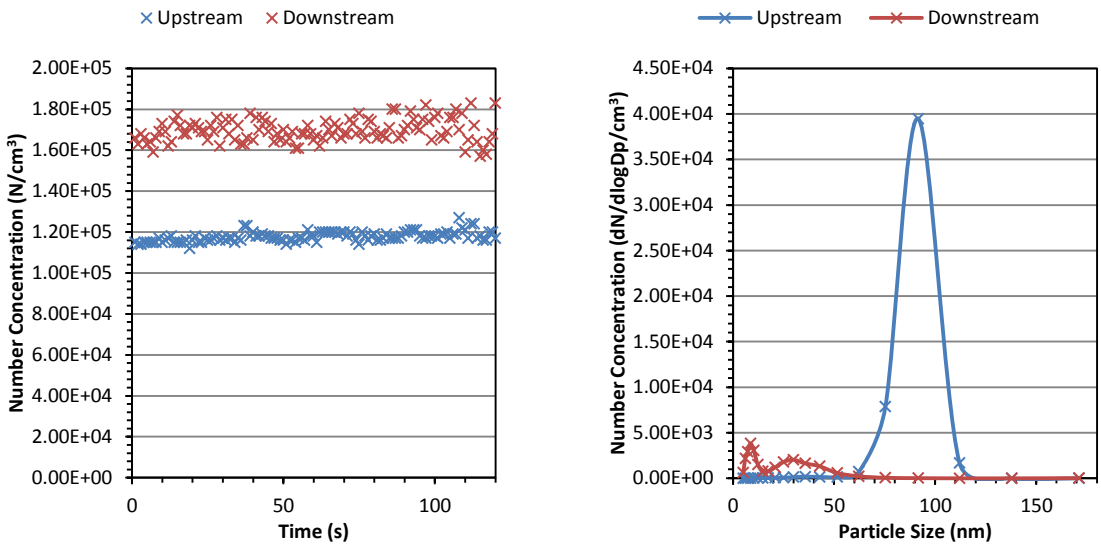

Figure 4.8: (a) Number concentrations recorded up and downstream of the GRIMM ESS, (b) SMPS particle size spectra recorded up and downstream of the GRIMM ESS when supplying 100nm volatile particle 'challenge' aerosol.

4.3.2 Results: 50nm Volatile-Only 'Challenge' Aerosol

For the 50nm volatile-only challenge aerosol the DEKATI EDD was able to remove 99.9% of the volatile material reducing the upstream number concentration from 8.32×10^4 N/cm^3 to 1.27×10^2 N/cm^3 downstream of the VPR. This reduction in concentration is evident in the up and downstream size distributions of the challenge aerosol. Originally delivered to the VPR with GMD of 45nm and a mode peak at ≈42nm there is no longer any apparent size mode of similarly high concentration detected following the VPR.

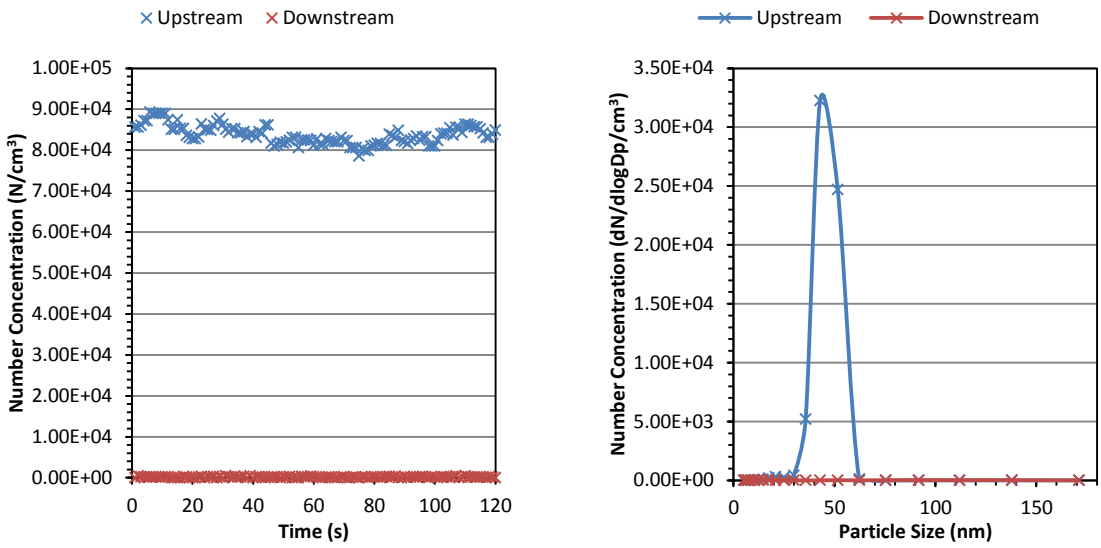

Figure 4.9: (a) Number concentrations recorded up and downstream of the DEKATI EDD, (b) SMPS particle size spectra recorded up and downstream of the DEKATI EDD when supplying 50nm volatile particle 'challenge' aerosol.

The GRIMM ESS performs better during this condition than that of the 100nm challenge aerosol and was able to remove approximately 66% of the upstream volatile material decreasing the particle number concentration from 9.25×10^4 to 3.14×10^4 N/cm^3. The remaining volatile fraction appears to again have been reduced in size considerably from the initial 43nm GMD to a final 9nm GMD. As for the 100nm challenge aerosol condition, due to the GRIMM ESS operating at a lower evaporation temperature than the DEKATI EDD, it is unable to fully evaporate or shrink these very high concentrations of volatile material.

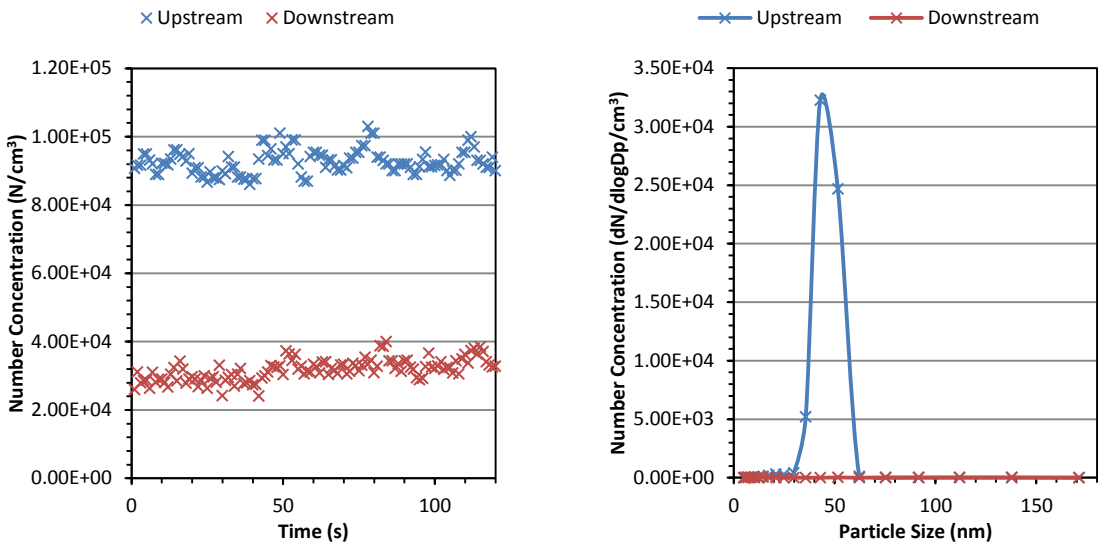

Figure 4.10: (a) Number concentrations recorded up and downstream of the GRIMM ESS, (b) SMPS particle size spectra recorded up and downstream of the GRIMM ESS when supplying 50nm volatile particle 'challenge' aerosol.

4.3.3 Results: 30nm Volatile-Only 'Challenge' Aerosol

The 30nm challenge aerosol is noteworthy as it is the specified challenge aerosol particle size in the PMP for which a VPR must remove >99% of the volatile material to be considered a PMP compliant system. At this experiment condition the DEKATI EED was able to perform this challenge, removing 99.97% of the challenge aerosol.

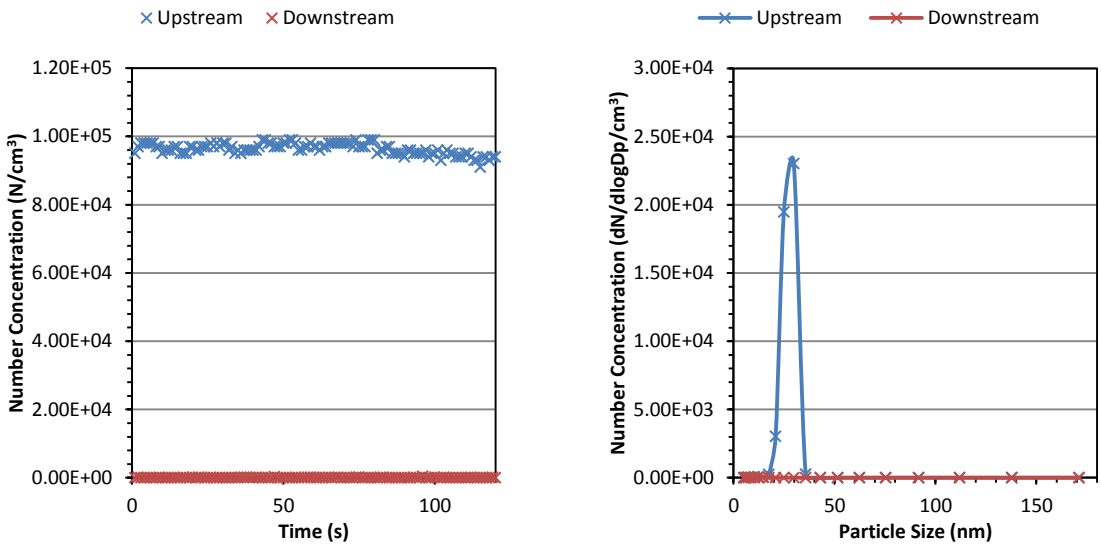

Figure 4.11: (a) Number concentrations recorded up and downstream of the DEKATI EDD, SMPS particle size spectra recorded up and downstream of the DEKATI EDD, (b) when supplying 30nm volatile particle 'challenge' aerosol.

At this size the GRIMM ESS was also now able to deliver excellent removal efficiency with a reduction in volatile material of 99.76%.

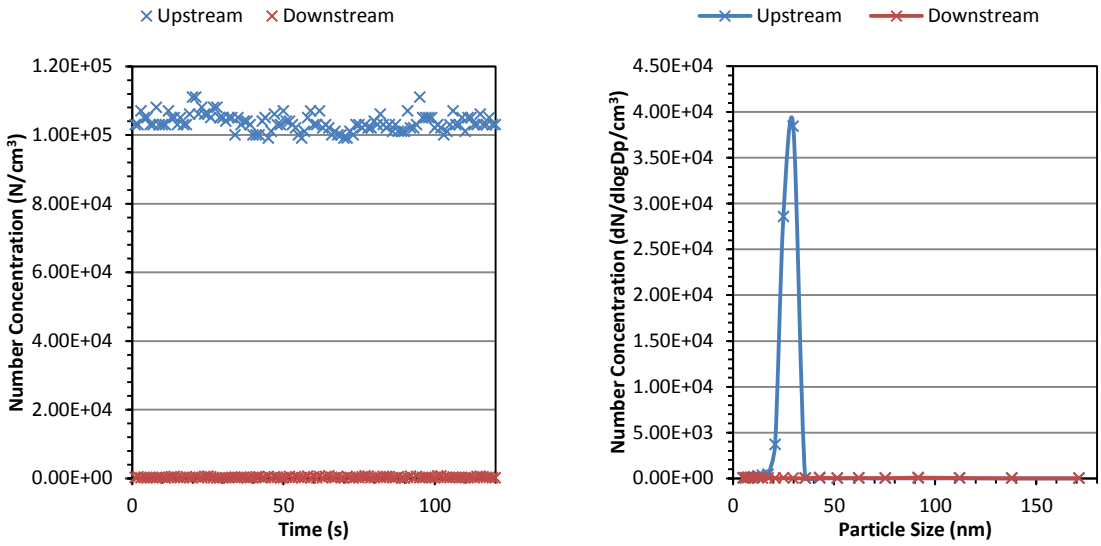

Figure 4.12: (a) Number concentrations recorded up and downstream of the GRIMM ESS, (b) SMPS particle size spectra recorded up and downstream of the GRIMM ESS when supplying 30nm volatile particle 'challenge' aerosol.

Based on this test condition alone both VPR systems would therefore classify as being PMP complaint, however as was previously described the design structure of the GRIMM ESS does not constitute as being a compliant system.

4.3.4 Results: 15nm Volatile-Only 'Challenge' Aerosol

The last test challenge aerosol of 15nm proved more difficult to achieve stable test periods and sufficient number concentrations above 10000 N/cm^3 were unachievable. However the test results which were obtained still provide an indication of the volatile removal potential of these VPRs at small particle sizes. The DEKATI EDD was found to be capable of removing 99.5% of the volatile 'challenge' aerosol.

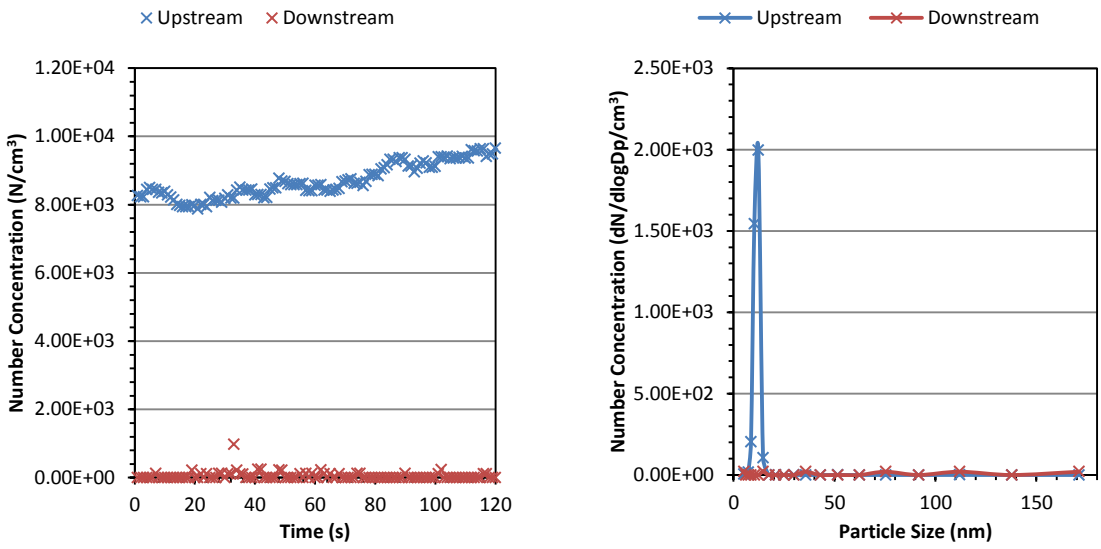

Figure 4.13: (a) Number concentrations recorded up and downstream of the DEKATI EDD, (b) SMPS particle size spectra recorded up and downstream of the DEKATI EDD when supplying 15nm volatile particle 'challenge' aerosol.

An initial concentration of 1.91x10^3 N/cm^3 of 15nm volatile material was delivered to the GRIMM ESS and it was successful at removing 99.9% of it with the downstream concentration measured at 1.92x10^0 N/cm^3.

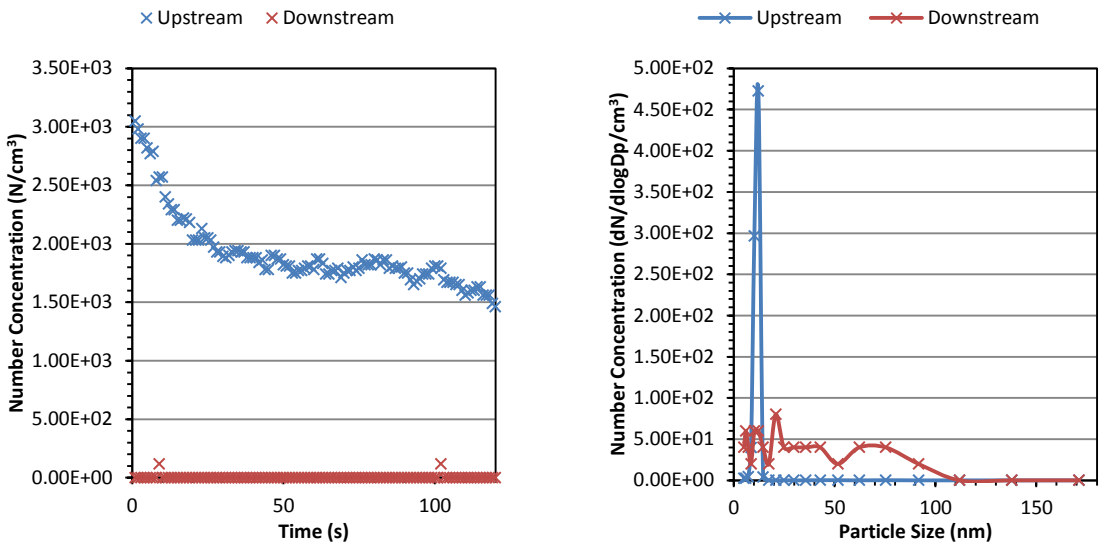

Figure 4.14: (a) Number concentrations recorded up and downstream of the GRIMM ESS, (b) SMPS particle size spectra recorded up and downstream of the GRIMM ESS when supplying 15nm volatile particle 'challenge' aerosol.

Table 4.1: Summary of the volatile-only 'challenge' aerosol number concentrations and GMDs measured up and downstream of the test VPR.

Sample position relative to tested VPR	Concentration (N/cm^3)	GMD (nm)
DEKATI EDD		
	100nm	
Upstream	$1.06x10^5$	88
Downstream	$9.36x10^3$	12
	50nm	
Upstream	$8.32x10^4$	45
Downstream	$1.27x10^2$	35
	30nm	
Upstream	$9.62x10^4$	27
Downstream	$2.63x10^1$	10
	15nm	
Upstream	$8.81x10^3$	11
Downstream	$4.02x10^1$	40
GRIMM ESS		

	100nm	
Upstream	$1.18x10^5$	87
Downstream	$1.70x10^5$	14
	50nm	
Upstream	$9.25x10^4$	43
Downstream	$3.17x10^4$	9
	30nm	
Upstream	$1.04x10^5$	27
Downstream	$2.47x10^2$	22
	15nm	
Upstream	$1.91x10^3$	11
Downstream	$1.92x10^0$	2

4.4 Volatile Coated Solid Core Particle Removal

Recognising that volatile compounds can exist not only as stand-alone particulates but also as agglomerates and coatings on solid particles (e.g. soot) should be an important consideration when evaluating the effectiveness of a volatile removal system. Figure 4.15 shows of a TEM image of such a particle formation in which a volatile particle (ammonium sulphate) has combined with an agglomerated soot particulate in a diesel automotive exhaust.

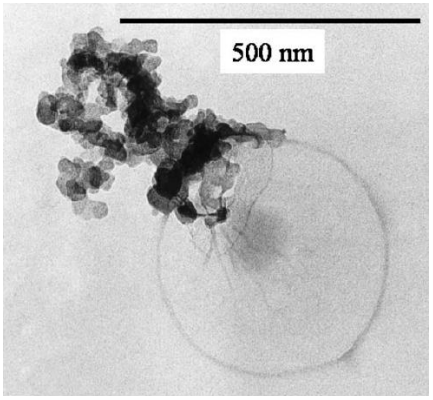

Figure 4.15: Aggregate of an ammonium sulphate particle and an agglomerated soot particle, reproduced from [44].

To examine how the removal efficiency of a VPR may be affected by such particle formations soot particles produced by the PALAS GFG 1000 soot generator were coated with a surface of volatile material (tetracontane) prior to their entry into the VPR system. The same two VPRs were used for this experimentation, those being the DEKATI EED and the GRIMM ESS.

Using a DMA three original soot particle diameters were investigated; 100, 50 and 30nm. At the flow rate and sample conditions required sufficient qualities of 15nm soot particles were not achievable and have therefore not been considered. Each soot size distribution was individually passed through Cardiff University VG within the crucible airflow ensuring the particles were exposed to a region saturated with a high concentration of tetracontane vapour. To detect if a coating had been applied to the soot particles a SMPS was used to provide a size distribution upstream of the VPR, downstream SMPS measurements were then subsequently made to gauge what impact the VPR had on the 'challenge' aerosol. In addition to particle size assessment number concentration measurements were also taken upstream and downstream of the VPR using a CPC. A schematic diagram of the experimental setup is shown in Figure 4.16.

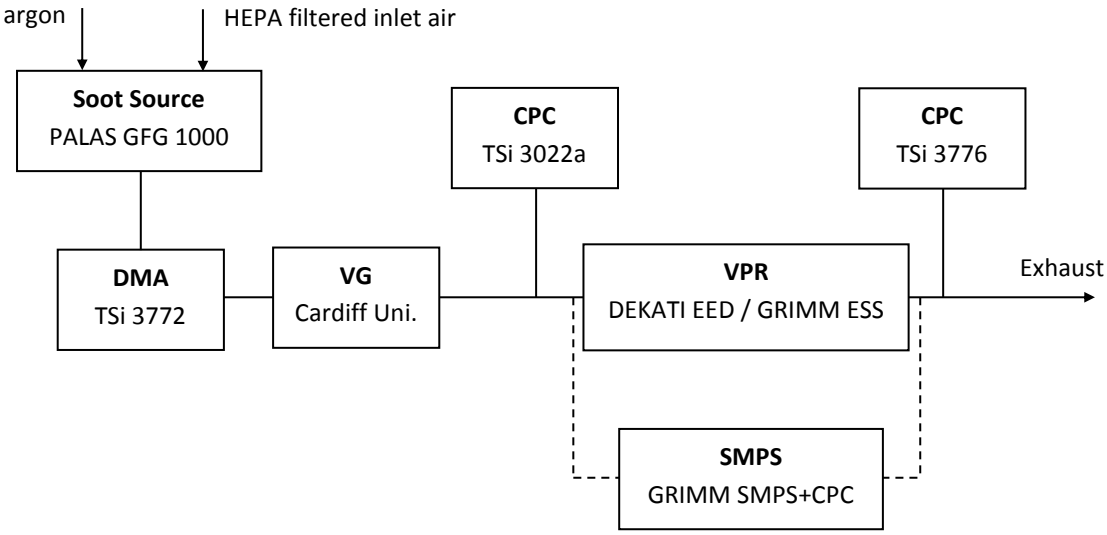

Figure 4.16: Schematic diagram of volatile removal experiment using volatile coated solid core 'challenge' aerosol.

Results gathered when evaluating the performance of the DEKATI EED system and GRIMM ESS VPR systems will again be presented dependent on the 'challenge' aerosol being supplied (100, 50, and 30nm solid core volatile coated particles).

4.4.1 Results: 100nm Volatile Coated Solid Core 'Challenge' Aerosol

From the upstream size spectrum of the 'challenge' aerosol it is clear that there is significant growth of the ≈100nm solid particles after they have passed through the VG. On exiting the DEKATI EDD the number concentration of the challenge aerosol has been reduced from $2.60x10^5$ to $9.68x10^4$ N/cm^3. The size spectral analysis of this new aerosol composition shows that the remaining particle distribution consists mainly of particles in the ≈60nm size region (GMD of 64nm).

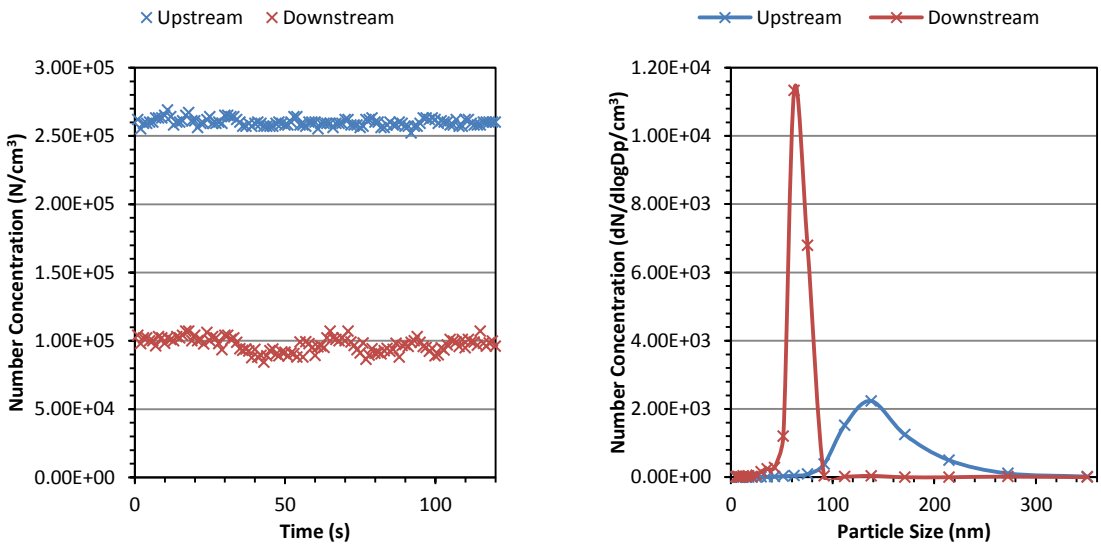

Figure 4.17: (a) Number concentrations recorded up and downstream of the DEKATI EDD, (b) SMPS particle size spectra recorded up and downstream of the DEKATI EDD when supplying 100nm volatile coated solid core particle 'challenge' aerosol.

The upstream and downstream number concentrations measured when delivering 100nm volatile coated particle to the GRIMM ESS were of approximately the same magnitude. The upstream PM size distribution is unlike that observed during all other volatile coated PM test conditions apart from that of the 50nm GRIMM ESS 'challenge' aerosol test condition. These two VPR validation experiments were performed on at a

later time period than the others present and this is considered to be the reason for the variability. The final result of the PM coating was that much larger particles are produced across a size range of 150 to 350nm. The downstream PM size distribution indicates that particles of a similar size were being introduced into the VG however it appears that an increased level of agglomeration occurred (larger particles). Input parameters were identical for the PALAS soot generator and VG however ambient conditions may have occurred

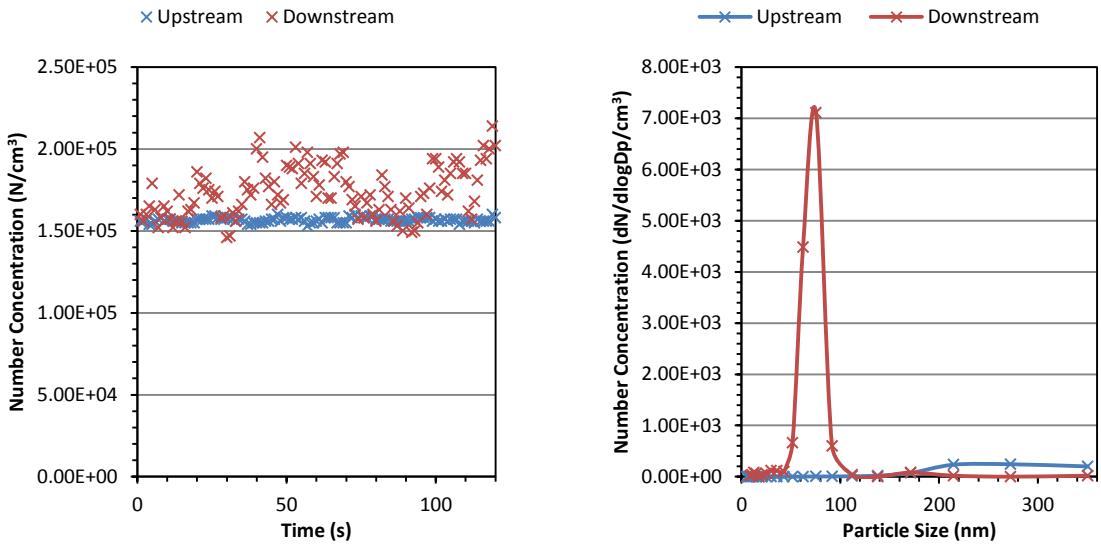

Figure 4.18: Number concentrations recorded up and downstream of the GRIMM ESS (left), SMPS particle size spectra recorded up and downstream of the GRIMM ESS (right) when supplying 100nm volatile coated solid core particle challenge aerosol.

4.4.2 Results: 50nm Volatile Coated Solid Core 'Challenge' Aerosol

Consistent with the 100nm challenge aerosol when ≈50nm solid particle were introduced through the supply air of the VG, the resulting aerosol size distribution showed considerable particle growth. The DEKATI EDD was again successful at removing the majority of the coated volatile material and the suspended volatile material with a reduction in the measured aerosol of 99.9%.

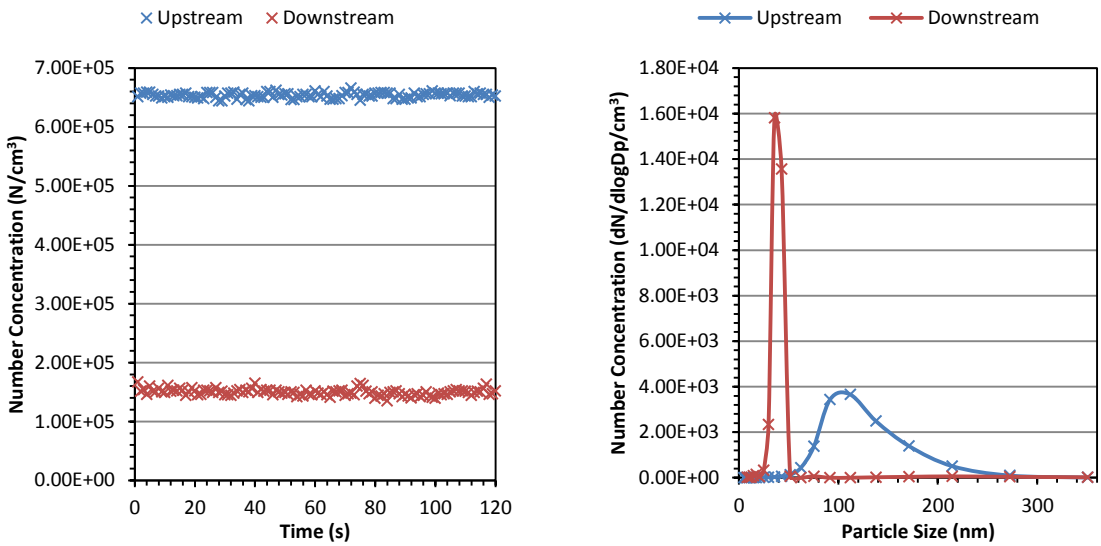

Figure 4.19: (a) Number concentrations recorded up and downstream of the DEKATI EDD, (b) SMPS particle size spectra recorded up and downstream of the DEKATI EDD when supplying 50nm volatile coated solid core particle 'challenge' aerosol.

As was earlier discussed the upstream size distribution of the 50nm volatile coated solid core 'challenge' aerosol is different from that seen in other conditions. The end result of appraisal with this aerosol is consistent though previous test conditions in that the downstream size distributions indicate that the volatile coating has been removed and the solid core particle remain.

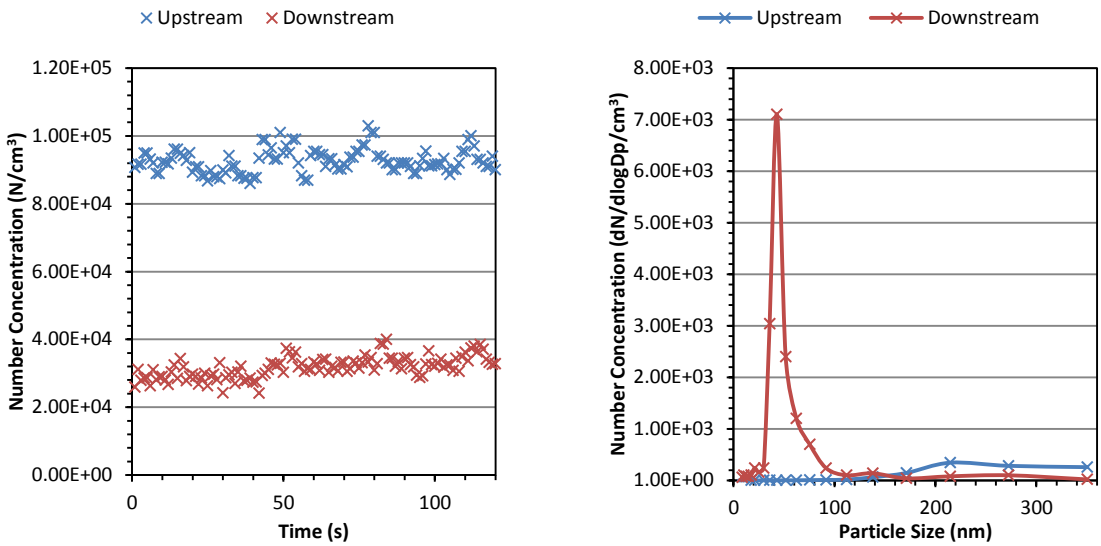

Figure 4.20: (a) Number concentrations recorded up and downstream of the GRIMM ESS, (b) SMPS particle size spectra recorded up and downstream of the GRIMM ESS when supplying 50nm volatile coated solid core particle 'challenge' aerosol.

4.4.3 Results: 30nm Volatile Coated Solid Core 'Challenge' Aerosol

The up and downstream size spectra show that following the DEKATI EDD the particle size distribution has returned to approximately that of the solid 30nm particles which were introduced into the VG.

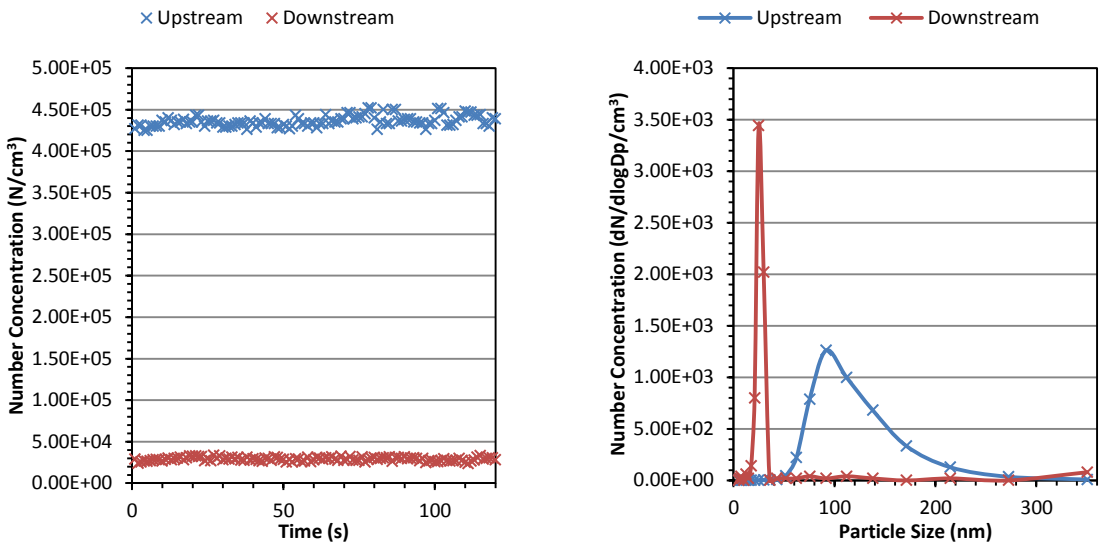

Figure 4.21: (a) Number concentrations recorded up and downstream of the DEKATI EDD, (b) SMPS particle size spectra recorded up and downstream of the DEKATI EDD when supplying 30nm volatile coated solid core particle 'challenge' aerosol.

The PM size distribution measured downstream of the GRIMM ESS when supplied with the 30nm volatile coated solid core particle aerosol show that the volatile PM coating and only particle of ≈35nm remain.

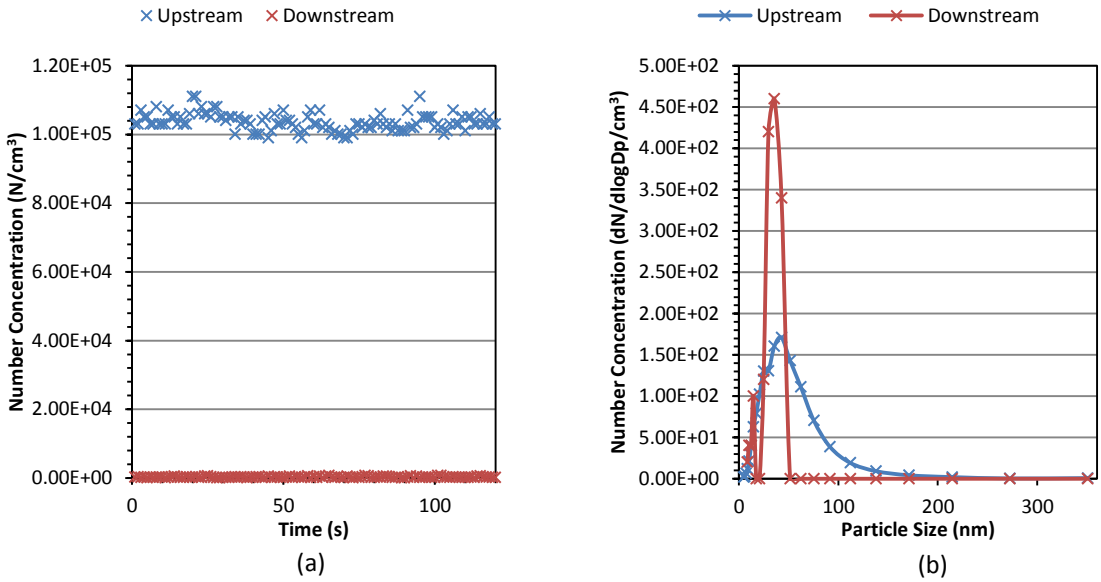

Figure 4.22: (a) Number concentrations recorded up and downstream of the GRIMM ESS, (b) SMPS particle size spectra recorded up and downstream of the GRIMM ESS when supplying 30nm volatile coated solid core particle 'challenge' aerosol.

Table 4.2: Summary of the volatile coated solid core particle 'challenge' aerosol number concentrations and GMDs measured up and downstream of the test VPR.

Sample position relative to tested VPR	Concentration (N/cm^3)	GMD (nm)
DEKATI EDD		
	100nm	
Upstream	$2.60x10^5$	138
Downstream	$9.68x10^4$	64
	50nm	
Upstream	$8.32x10^4$	110
Downstream	$1.27x10^2$	38
	30nm	
Upstream	$9.62x10^4$	104
Downstream	$2.63x10^1$	27
GRIMM ESS		
	100nm	
Upstream	$1.18x10^5$	244
Downstream	$1.70x10^5$	66
	50nm	
Upstream	$9.25x10^4$	228
Downstream	$3.17x10^4$	44
	30nm	
Upstream	$1.04x10^5$	34
Downstream	$2.47x10^2$	24

4.5 Chapter Summary

This Chapter has discussed the objectives and relevance of the PMP and why the removal of volatile material from a combustion exhaust is necessary in order to make reliable PM measurement, particularly concerning number concentration measurements. Removing volatile PM can be accomplished through a variety of methods; the most commonly employed being the use of high and low temperature dilution and exposing the sample to a high temperature evaporation tube for an appropriate residence time.

In this Chapter, two commercially available VPR systems, one which met the PMP specification and one which did not, were evaluated to determine how they performed when exposed to very high concentration of volatile material. The results showed the DEKATI EDD system was able to remove 90% of the 100nm and greater than 99% of the 50, 30 and 15nm volatile only 'challenge' aerosols. The GRIMM ESS system did not perform so well as the DEKATI EDD increasing the number concentration of the 100nm challenge aerosol initially following exposure to the VPR. Size spectral analysis showed that this result occurred because the volatile material was only reduced in size and likely to have fractured into smaller particle formations within the VPR. As the GRIMM ESS relies solely on hot dilution (200°C) to evaporate the volatile material compared the DEKATI EDD which employs hot dilution (150°C) and an evaporation tube (350°C), this poor performance at very high particle concentrations was not unexpected. When the particle size of the challenge aerosol was decreased to 50, 30 and 15nm the GRIMM ESS removal efficiency improved resulting in 66%, 99.8 and 99.9% volatile removal respectively.

One of the requirements for a VPR to be PMP compliant is that it must be able to remove >99% of a 10000 N/cm^3 concentration of 30nm tetracontane aerosol. The volatile remove effectiveness of the DEKATI EDD VPR was therefore expected to meet or surpass these requirements for the solely volatile aerosol. In fact both the DEKATI EDD and the GRIMM ESS achieved this requirement and therefore it is only there based on these experiments it is only the design specification of the GRIMM ESS which prevents it being considered PMP compliant.

Downstream of both VPRs the solid particles appear to have reduced in size compared to their initial input sizes (100, 50 and 30nm). It is possible that this reduction could have developed as a direct result of the temperature gradient between the primary and secondary dilution stages of the VPRs. Alternatively as the PALAS GFG 1000 has been previously shown to produce agglomerate particle formations [44], in these experiments the volatile coating which was applied to them may have caused the structure to collapse and contract in size.

Future studies which included TEM analysis of the upstream and downstream aerosol formations would be beneficial in determining an accurate aerosol composition profiles.

Chapter 5

PM Characterisation for Spray-Guided GDI Research Engines

In 2014 vehicles with direct injection gasoline engines will have to adhere to the EURO6 Standards on the emission of PM. In this Chapter analysis of PM emissions from GDI research engines gathered during experimental testing campaigns conducted at the Ricardo Technical Centre will be presented. Multi and single-cylinder variations of a Ricardo Hydra engine were used to investigate how PM emissions correlated with key engine operational parameter, and furthermore how these characteristics varied with PM emissions generated during homogeneous and stratified charge operating modes.

During single-cylinder research engine experiments two fuel injection systems were used to evaluate and appraise how PM production differed when using a conventional gasoline injector and a state-of-the-art super-critical gasoline injection system. PM measurements were performed using DMS500s in conjunction with Ricardo's on site gas analysis and solid particle counting system. This allowed a comparison to be made between a PMP compliant particle measurement system and fast-response particle measurement equipment more suited to transient exhaust emissions.

The findings of this Chapter were presented via an invitation paper at a specialist gasoline vehicle emissions conference - Advanced Emission Control Concepts for Gasoline Engines - in 2013 [110].

Section A

5.1 PM Sampled from Single-Cylinder Research Engine

Experimentation with the SGDI SCRE, a variant of the Ricardo Hydra engine family, were undertaken over at the Ricardo testing and manufacturing facility located in Shoreham-By-Sea, Brighton. This test campaign provided an opportunity to investigate PM emissions from an engine which was representative of current GDI technologies, while also providing the flexibility to install conventional and novel fuel injectors and operate at multiple engine combustion modes and loading conditions.

In addition to PM characterisation using the DMS500, a PMP compliant measurement system was also installed into the sampling setup allowing simultaneous particle number concentration measurements to be made using two DMS500s and the Horiba Solid Particle Counting System (SPCS).

The setup for this experimentation included the SCRE being installed on a dynamometer in order to accurately drive the engine at predetermined RPM and load values. Exhaust exiting the manifold of the engine travelled down an insulated tail pipe prior to a stainless steel 3/8” sampling line branch off. This line was then split using a Swagelok ‘T-joint’ fitting to supply both the Cardiff University and Ricardo DMS500 units with undiluted exhaust.

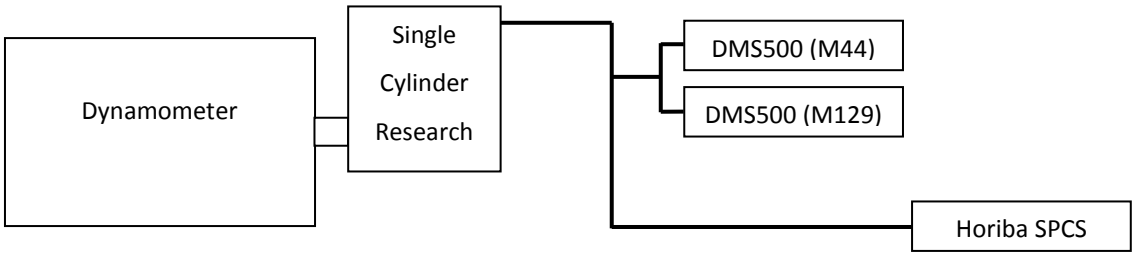

Figure 5.1: Schematic of the SCRE experimental setup.

Both DMS500s were operated with a 5:1 primary dilution ratio using HEPA filtered compressed air. Further dilution was applied using their respective internal rotary diluters when it was so required in order to keep particle number concentrations within the dynamic range of the instrument. The units were operated with the same

input settings and the recorded data processed using the equivalent versions of the each unit's bi-modal distribution inversion matrix, full details of the setup parameters are shown in Table 5.1.

Table 5.1: DMS500 settings for SCRE testing.

Input Parameter	
Charger sheath temperature	40°C
Sample block temperature	80°C
Line temperature	120°C
Remote cyclone temperature	120°C

Results gained from PM sampling when the engine was fitted a conventional GDI fuel injector will be present first, followed by those obtained while using the novel super-heated fuel injection system. Each of these data-sets will be further sub-divided to show the results gained during homogeneous and stratified charge testing conditions. A summary of all the results obtained from PM sampling with the SCRE will then follow and will include comparisons and discussion of the two injection systems.

5.2 Piezoelectricly Actuated Outwardly-Opening Fuel Injector

Initial experimentation with the SCRE was conducted while utilising a piezoelectricly actuated outwardly-opening pintle fuel injector manufactured by Bosch, a photograph of which is shown Figure 5.2. Development of this injector technology was undertaken as a joint venture between Ricardo and Bosch with ambitions to advance turbo-charged, direct injection gasoline engine systems. The injector has seen some adoption in current fleet GDI automotive technology, notable in the GDI variants of the Mini Cooper series.

Figure 5.2: Piezoelectricly actuated outwardly-opening pintle fuel injector manufactured by Bosch.

PM analysis was performed for both homogeneous and stratified charge engines modes while operating at three engine load conditions which are described hereafter as low, medium and high load. The specific parameters of these conditions are listed in Table 5.2.

Table 5.2: Engine settings for each test condition during experimentation with the SCRE fitted with the Bosch injector.

Test Condition	Speed (rpm)	Load (bar)
Low	2000	2
Medium	1821	4.84
High	2000	10

5.2.1 Results: Homogeneous Charge Operation

5.2.1.1 Low Load Condition (2000 rpm, 2 bar)

At the lowest engine loading condition the total number concentration measured by both DMS500s compared very well with each another, with both instruments showing the same trends across the sample time period.

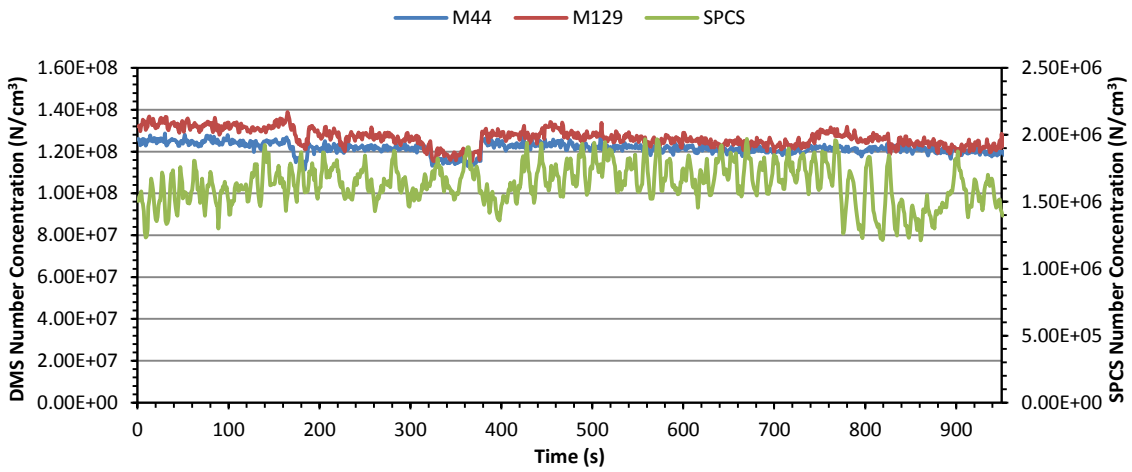

Figure 5.3: Total number concentrations recorded by DMS500s and SPCS at homogeneous charge low load condition.

There is however some variation in the particle size spectra produced by from each measurement PM instruments as shown in Figure 5.4. The DMS500 M44 model (Cardiff University owned DMS500) interpreted the data set as a mono-modal particle distribution with a peak position at approximately 20nm. The DMS500 M129 model (Ricardo owned DMS500) on the other hand interpreted the data as a bi-modal distribution with peak positions at approximately 10 and 24nm. This variability between DMS500 models was also noted in the gas turbine emissions testing performed in at the SR Technics facility in Zürich when sampling with the M44 and the M125 DMS500 units and is discussed in the following Chapter.

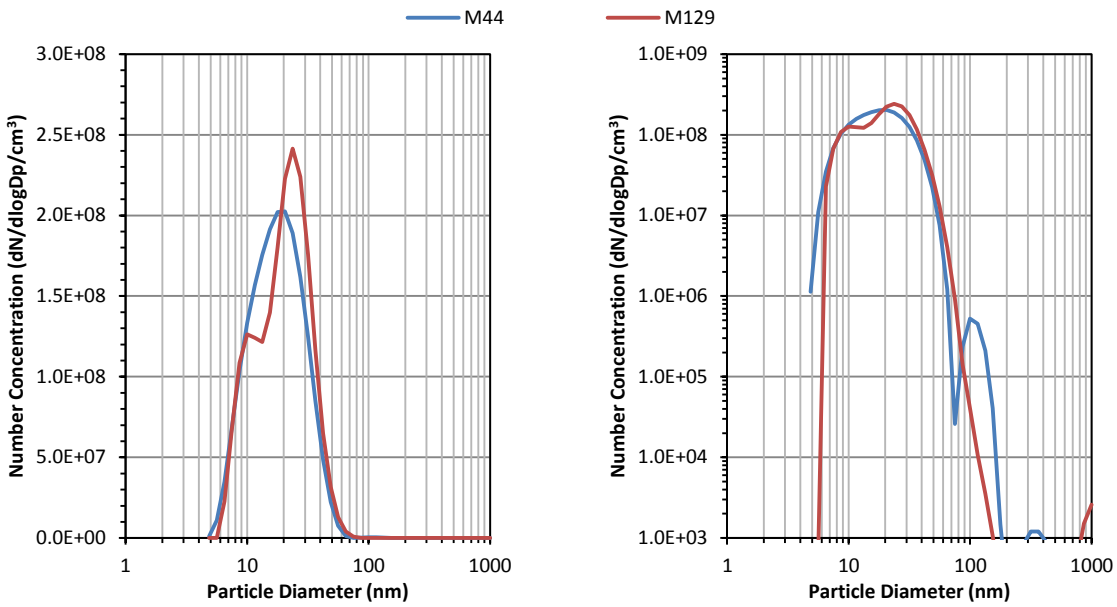

Figure 5.4: DMS500 size spectra at homogeneous charge low load condition: (a) linear y-axis scale, (b) logarithmic y-axis scale.

In an attempt to make the most representative comparison between the DMS500 and SPCS particle number measurements an allowance was required to take into account the counting efficiency and lower cut point of the TSI 3790 CPC which was installed in the SPCS. The cut point of this CPC was 23nm (as stipulated in the PMP) and the instrument is quoted as having a counting efficiency of 50% ± 12% at 23nm (d_{50}) and a 90% counting efficiency at 41nm (d_{90}). There are studies in the literature which have examined the counting efficiency of the TSI 3790, however there is very limited information on modelling the counting efficiency of a CPC for any given particle diameter. In order to generate a multiplication factor for each of the particle diameter sizes measured by the DMS500 a logistic function was designed such that at 23 and 41nm particle diameters the same counting efficiencies were produced as those quoted in the TSI 3790 documentation. The final expression for the generation of the counting efficiencies (CE) used as multiplication factors for the DMS500 data sets is shown in Equation 18:

$$CE = KA + \frac{KB}{((1 + KTexp^{-KC(T-2KM)})^{\frac{1}{KT}}}$$

Equation 18: Logistic function used to generate counting efficiency estimates for TSI 3790 at particle sizes relevant to DMS500 operational range.

where: KA = Lower asymptote (0)

KB = Upper asymptote (1)

KT = Limit of growth (1)

KC = Growth rate (0.14)

MK = Point of maximum growth (11.4)

It should be noted that this logistic function performs better for particles larger than ≈15nm. However as the SPCS does not include particles below 23nm in its count output, this function does provide adequate estimates for counting efficiencies in the size region of interest (23 - 1000nm).

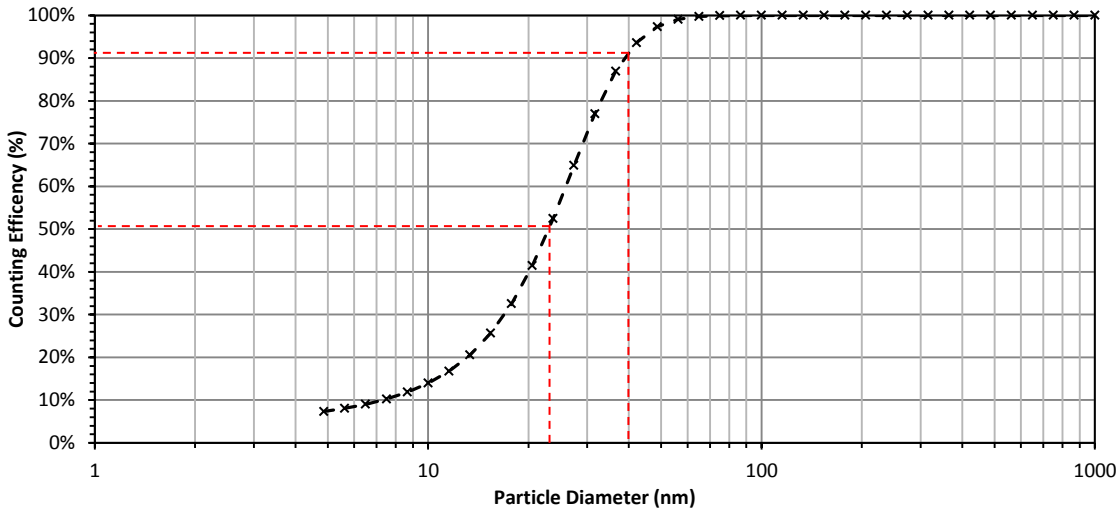

Figure 5.5: Estimated counting efficiency curve for the TSI 3790 CPC generated using a logistic function designed to have d_{50} and d_{90} positions at approximately 23 and 41nm respectively.

The counting efficiencies generated at each of the particle diameters associated with DMS500 size measurements were used as multiplication factors on the actual measured data recorded at each test condition. In a further effort to make the DMS500 and SPCS more comparable, all DMS500 number concentration

measurements below the counting limit of the SPCS (23nm) were removed from the final corrected total number concentration results.

The DMS500 number concentrations showed good agreement for the low load condition irrespective of the slight difference in the particle size spectra they produced. The number concentration measured by the SPCS was approximately 1 order of magnitude lower than that of the both DMS500s, even following the attempts to compensate for measured differences between techniques. Possible reasons for this discrepancy are discussed following the presentation of results for all sampled conditions (Section 5.2.3).

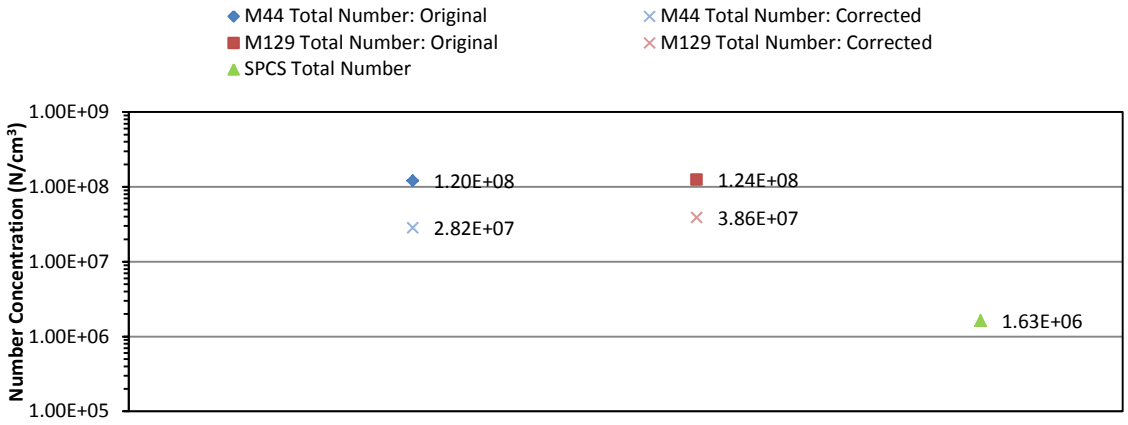

Figure 5.6: Original and corrected DMS500 and SPCS total number concentrations at homogeneous charge low load condition.

5.2.1.2 Medium Load Condition (1821 rpm, 4.84 bar)

At the medium load condition very good agreement of the number concentration measurements of both DMS500s was observed throughout the test condition. Similar trends in the emissions profile were also detected by the SPCS although as with was observed during the low load conditions number concentrations are significantly lower than those recorded by the DMS500s.

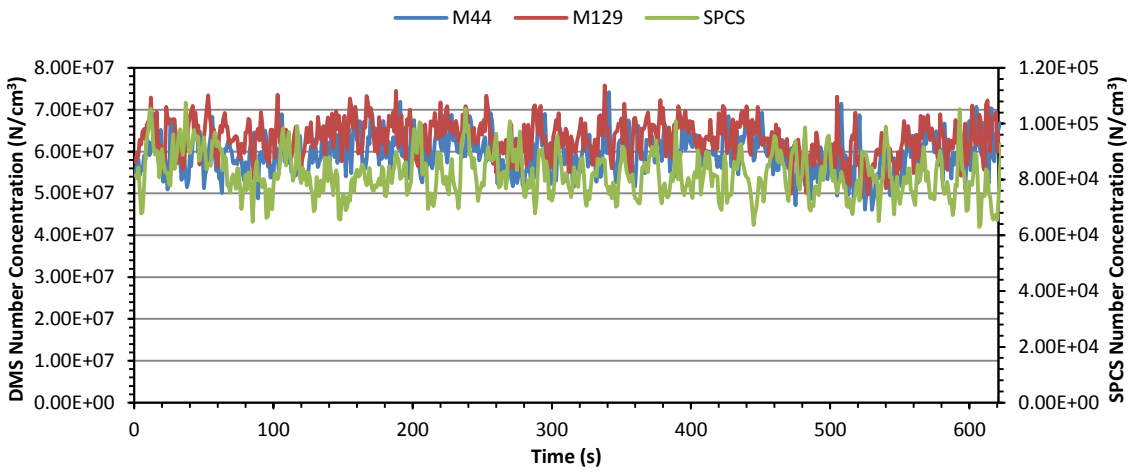

Figure 5.7: Total number concentration recorded by DMS500s and SPCS at homogeneous charge medium load condition.

The particle size spectra produced by both instruments at this condition are almost identical and display a large nucleation mode peak at approximately 7.5nm. Particle emissions of this size are almost certainly of a volatile nature which is likely to have developed from unburnt hydrocarbons. Although the spectra are dominated by these small particles there are also a fairly high proportion of larger particulates present with concentration values of the order of $1x10^7$ dN/dlogDp/cm^3 throughout the 20 - 100nm size range.

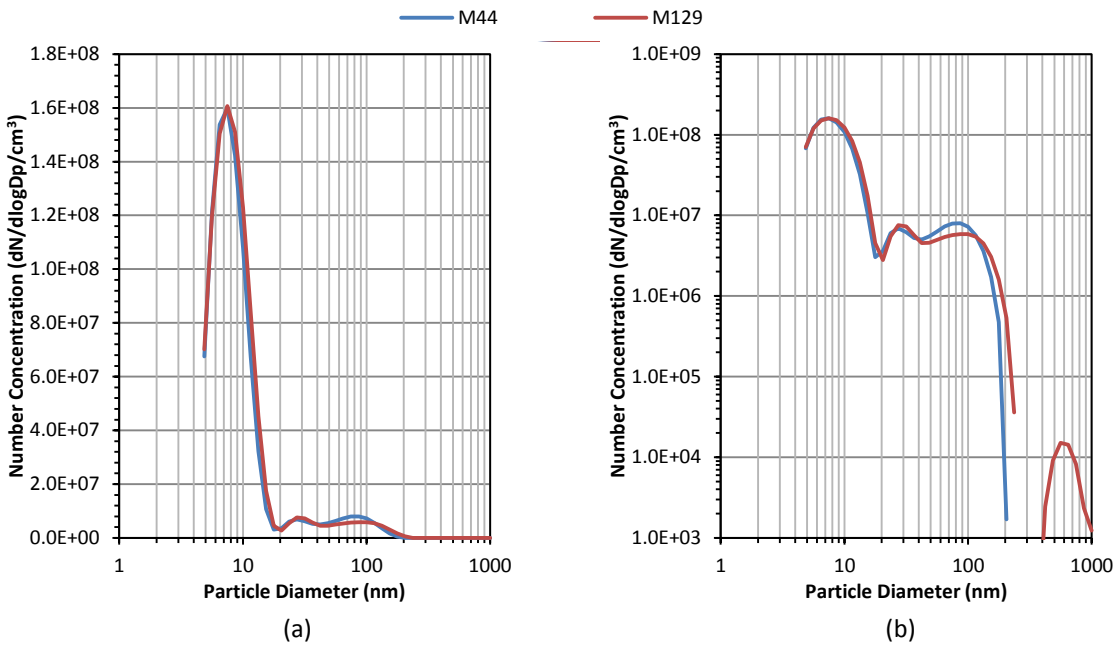

Figure 5.8: DMS500 size spectra at homogeneous charge medium load condition: (a) linear y-axis scale, (b) logarithmic y-axis scale.

Because there are so many sub-23nm particles measured at this condition the difference between the uncorrected DMS500 and SPCS results would be expected to the larger than that of the previous condition. Figure 5.9 shows this to be the case, although even after a significant reduction in the total number concentration following correction of the data-sets, there is still a large difference between the DMS500 and the SPCS data points.

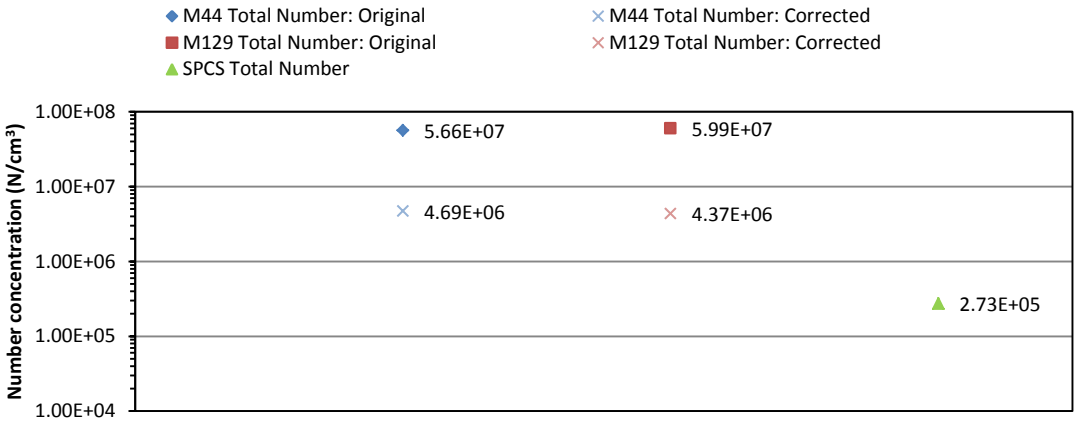

Figure 5.9: Original and corrected DMS500 and SPCS total number concentrations at homogeneous charge medium load condition.

5.2.1.3 High Load Condition (2000 rpm, 10 bar)

The final homogeneous condition from which PM was sampled was that with the highest engine loading experienced during this experimental campaign. The total number concentrations which were measured by both DMS500s again show good agreement and are reduced compared to those the two previous homogeneous conditions (low and medium loading). The number concentrations are increasing slightly throughout the test condition however at these concentrations the increase is very low. SPCS number concentrations at this condition are very low and consistent with near ambient emissions levels.

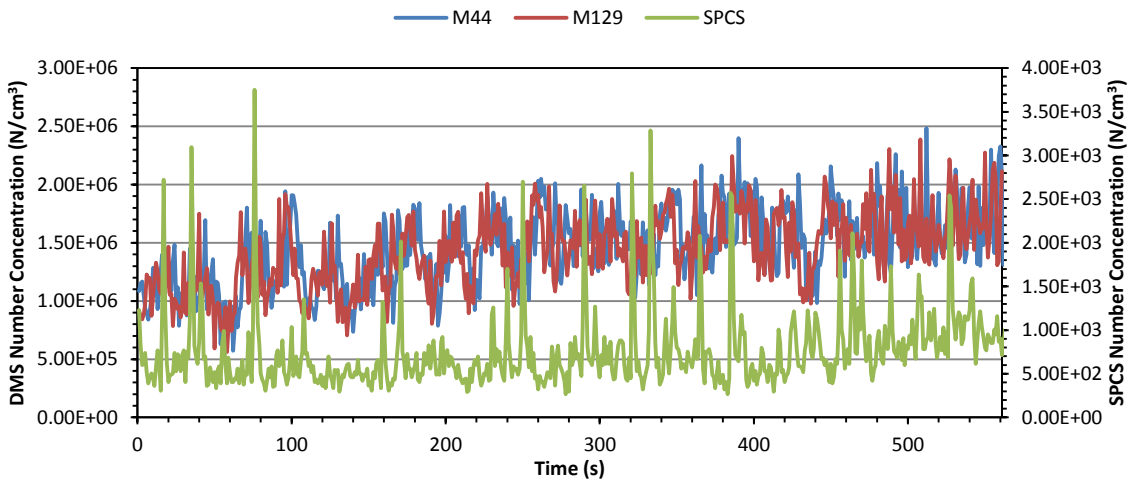

Figure 5.10: Total number concentrations recorded by DMS500s and SPCS at homogeneous charge high load condition.

The particle size spectra produced at this condition, shown in Figure 5.11, are unusual and are thought to have developed partly as a result of the DMS500 fitting algorithms. The bi-modal spectrum which was produced by the M44 is more likely to represent a particle size distribution of this nature as it is more consistent with previous results (nucleation mode at ≈10nm and agglomeration mode at ≈85nm). It is unlikely that the DMS500 would have the sensitivity to represent three particle size modes at close proximity i.e. 10nm, 28nm and 85nm as shown by the M129 instrument.

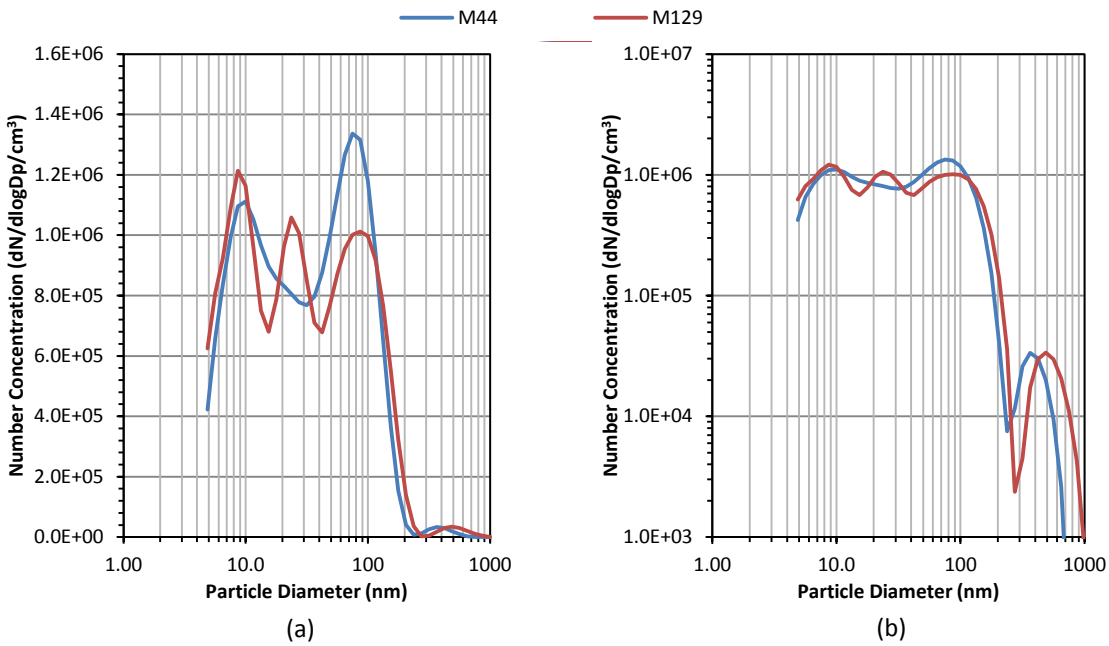

Figure 5.11: DMS500 size spectra at homogeneous charge high load condition: (a) linear y-axis scale, (b) logarithmic y-axis scale.

Figure 5.12 shows that as was observed for the size spectra of the low and medium load conditions the SPCS number concentration at this condition is far lower than those of the corrected DMS500 data.

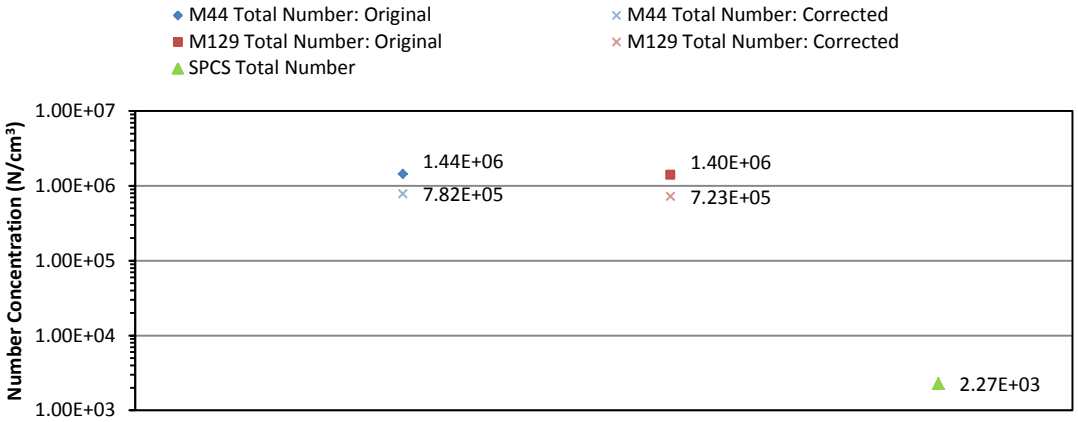

Figure 5.12: Original and corrected DMS500 and SPCS total number concentrations at homogeneous charge high load condition.

5.2.2 Results: Stratified Charge Operation

5.2.2.1 Low Load Condition (2000 rpm, 2 bar)

During stratified charge operation there was an expectation that PM emissions could be more unstable than those seen at the homogeneous charge conditions as the late fuel injection can result in occurrences of inadequate air-fuel mixing periods. The particle number concentrations which were recorded for the low load condition did exhibit more variability than those measured for the same condition during homogeneous charge operation. Average number concentrations of the both DMS500s were approximately 7.1×10^6 N/cm^3 however there are many data points where concentrations as high as 3.87×10^7 N/cm^3 were recorded.

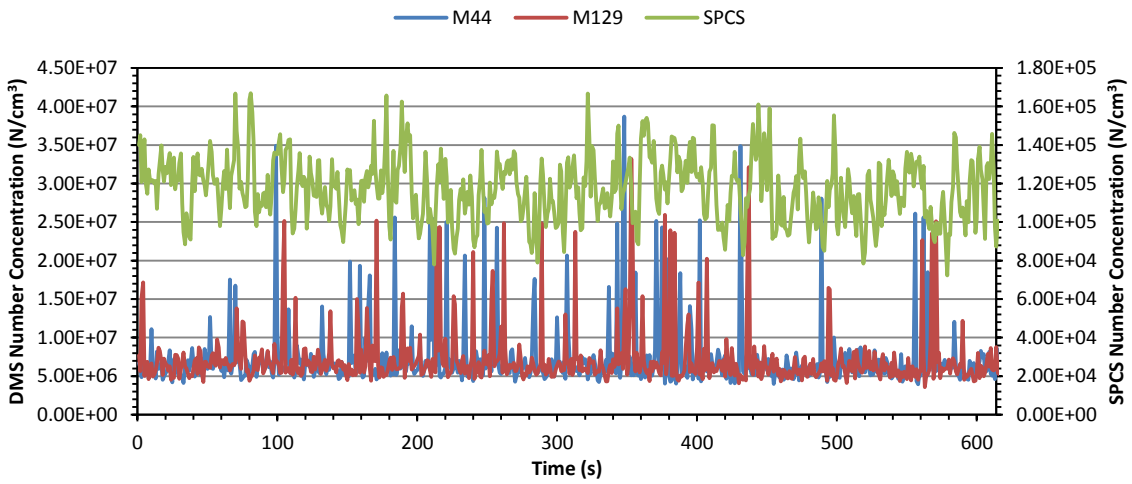

Figure 5.13: Total number concentration recorded by DMS500s and SPCS at stratified charge low load condition.

The size distributions produced at this condition is representative of at during high load homogenous charge operation. Overall concentration levels are slightly higher across the entire particle range and as was previously discussed the presence of a tri-modal distribution with peak positions positioned so closely to be considered an element of the DMS500 fitting algorithm.

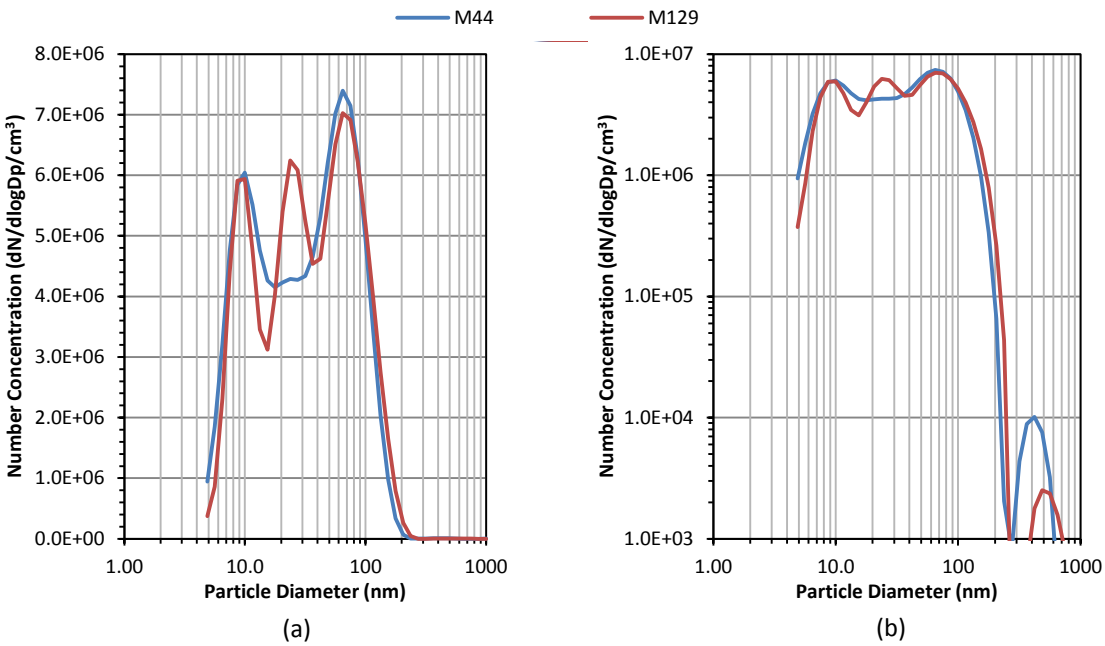

Figure 5.14: DMS500 size spectra at stratified charge low load condition: (a) linear y-axis scale, (b) logarithmic y-axis scale.

Total number concentrations are far lower for stratified charge operations at this low load condition than those produced at the same engine settings operating in a homogenous charge mode. The concentrations measurements produced by the DMS500s continue to be higher than those of the SPCS.

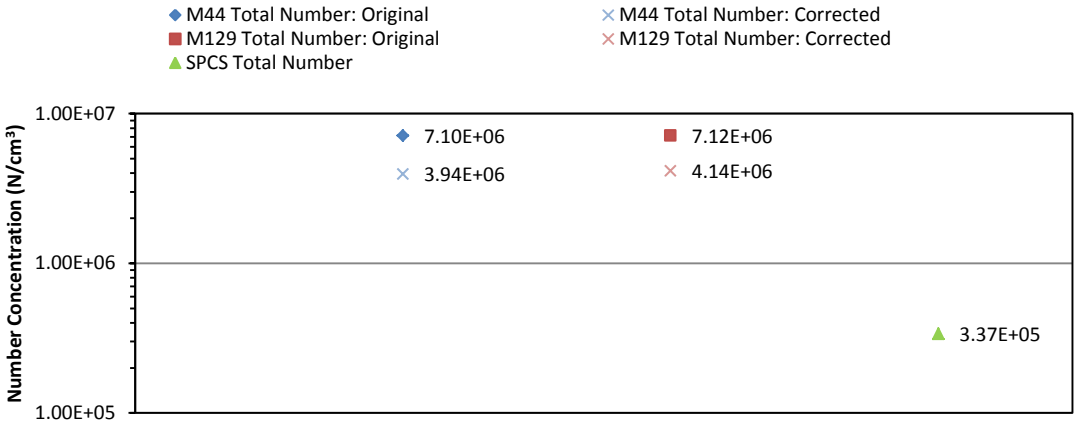

Figure 5.15: Original and corrected DMS500 and SPCS total number concentrations for stratified charge low load condition.

5.2.2.2 Medium Load Condition (1821 rpm, 4.84 bar)

At medium load the number concentrations measured by both DMS500s were consistent and showed less variation than that seen during the low load operation. Similarly the SPCS measurements across the sample period remained fairly stable.

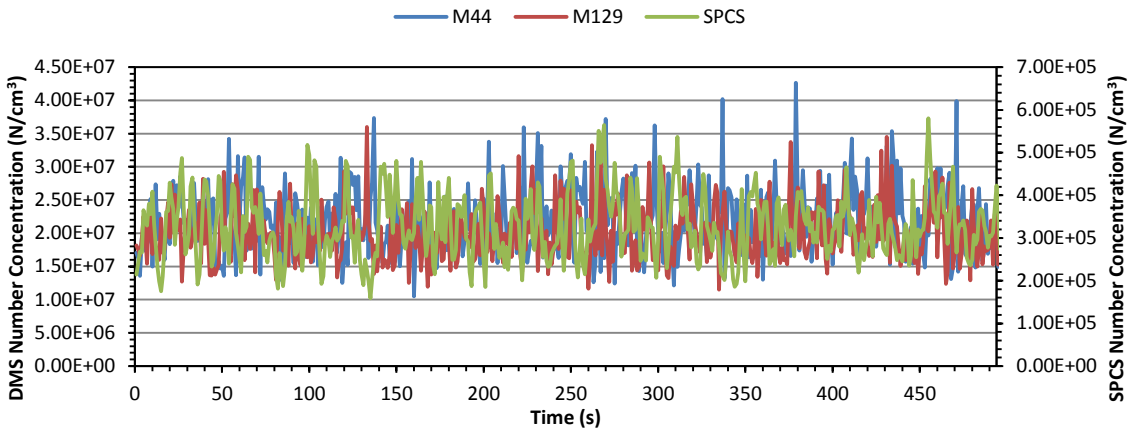

Figure 5.16: Total number concentration recorded by DMS500s and SPCS at stratified charge medium load condition.

There is a significant difference between the particle size spectra produced at this stratified charge condition compared to that of the homogeneous charge operation mode. Here we observe a largely bi-modal signal (some tri-modality occurring again from the M129) with peak positions at ≈20nm and ≈75nm. The number of sub-20nm particles drastically reduced compared to the homogeneous charge condition with no noticeable presence of the high concentration ($1.6x10^8$ dN/dlogDp/cm^3) small mode located at 7.5nm. Particles of this size would commonly be associated with volatile exhaust compounds, such as un-burnt fuel, and therefore as this condition is leaner than its homogenous charge counterpart, the loss of this high concentration of small particles is consistent with reduced volatile emission.

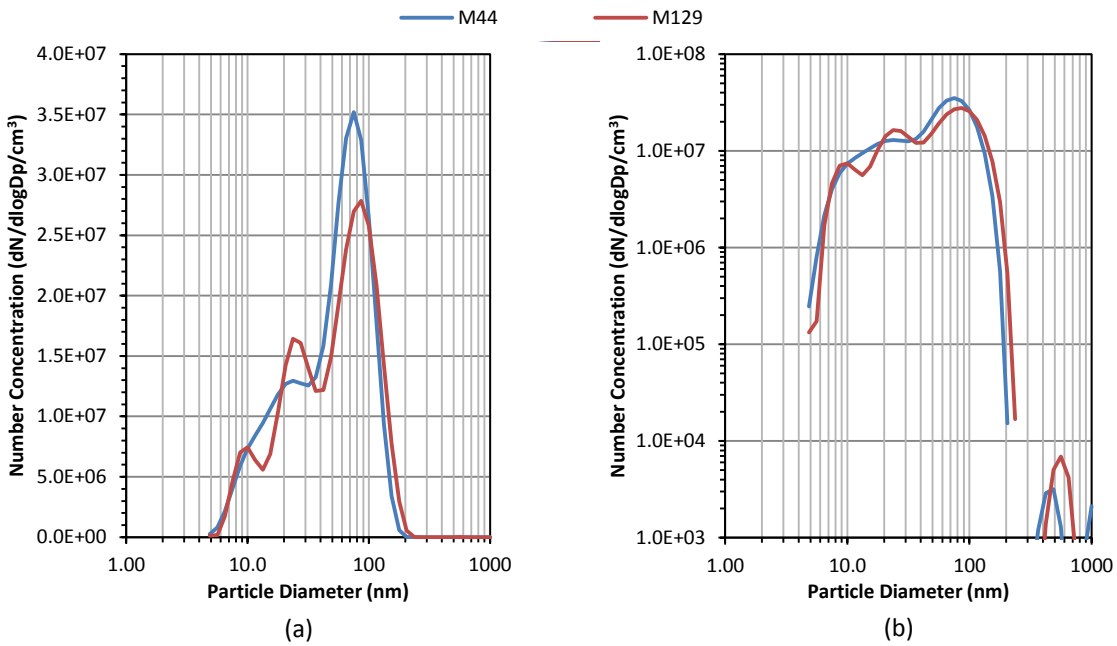

Figure 5.17: DMS500 size spectra at stratified charge medium load condition: (a) linear y-axis scale, (b) logarithmic y-axis scale.

As there are less sub-23nm particle produced at this condition, the original and corrected DMS500 number concentration results displayed in Figure 5.18 remain similar.

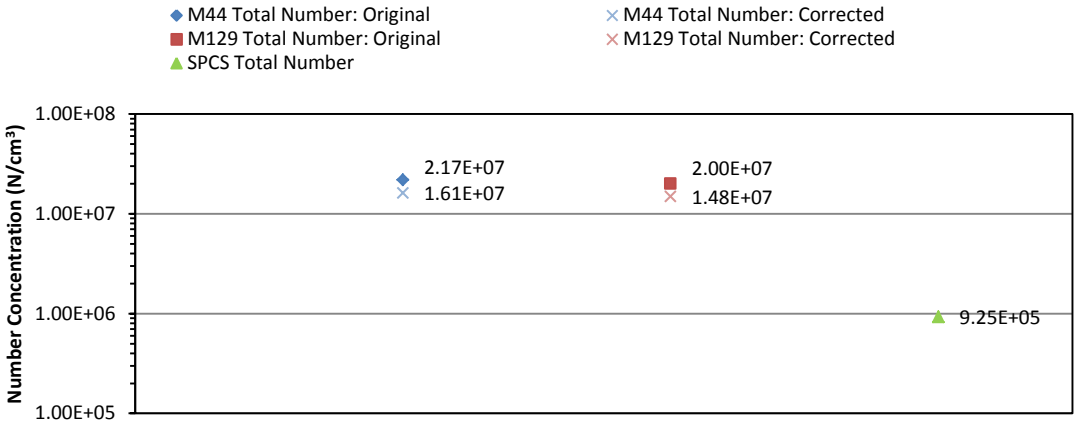

Figure 5.18: Original and corrected DMS500 and SPCS total number concentrations at stratified charge medium load condition.

5.2.2.3 High Load Condition (2000 rpm, 10 bar)

Finally at high loading the measured DMS500 number concentrations are again stable with some fluctuation from an average of ≈2x10^{7} N/cm^{3}. The SPCS and DMS500s were in agreement with regards to these fluctuations, and as with other sample conditions the number concentration measured by the SPCS were lower than those of the DMS500s.

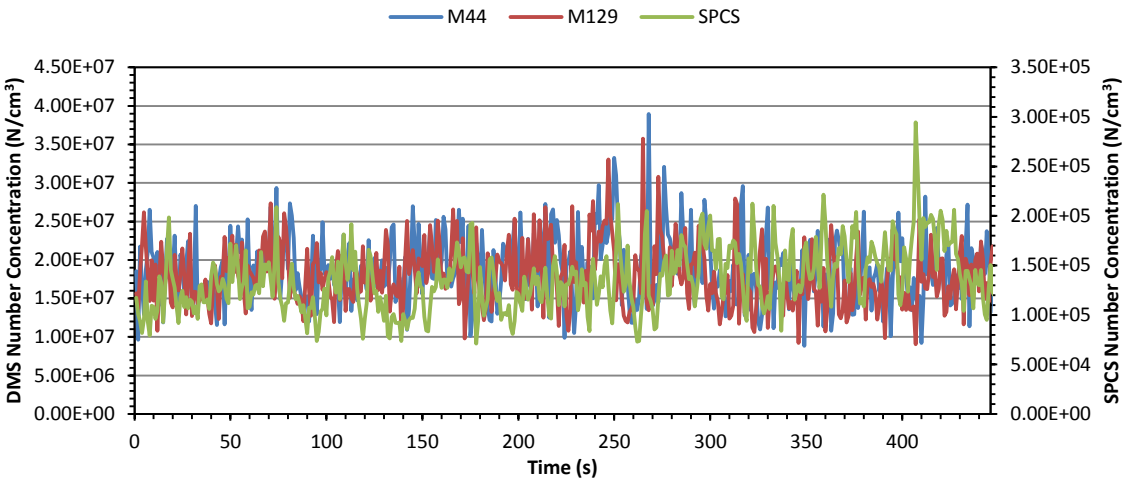

Figure 5.19: Total number concentration recorded by DMS500s and SPCS at stratified charge high load condition.

There is some consistency between the size spectra produced at the high loads for stratified and homogeneous charge operation, mainly in the multi-mode peak locations (≈10 and 65nm). At this condition concentration measurements are higher and more heavily weighted to the smaller particle sizes.

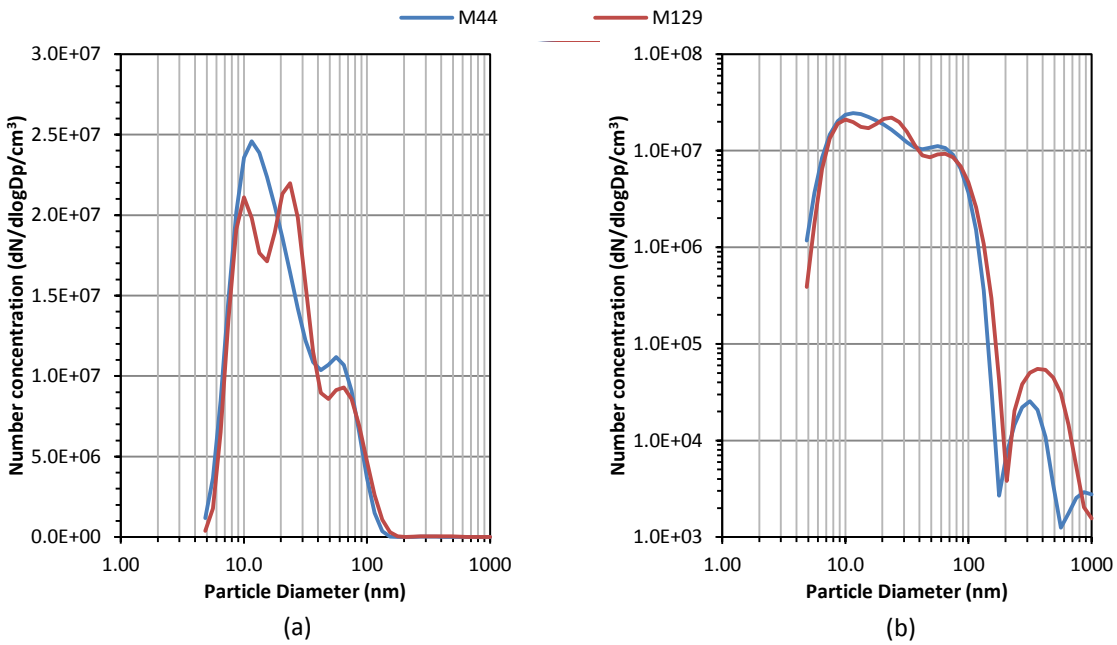

Figure 5.20: DMS500 size spectra at stratified charge high load condition: (a) linear y-axis scale, (b) logarithmic y-axis scale.

The total number concentrations produced overall during stratified charge operation as opposed to homogeneous charge operation are slightly higher at this load condition however following the application of the correction factors they are more comparable.

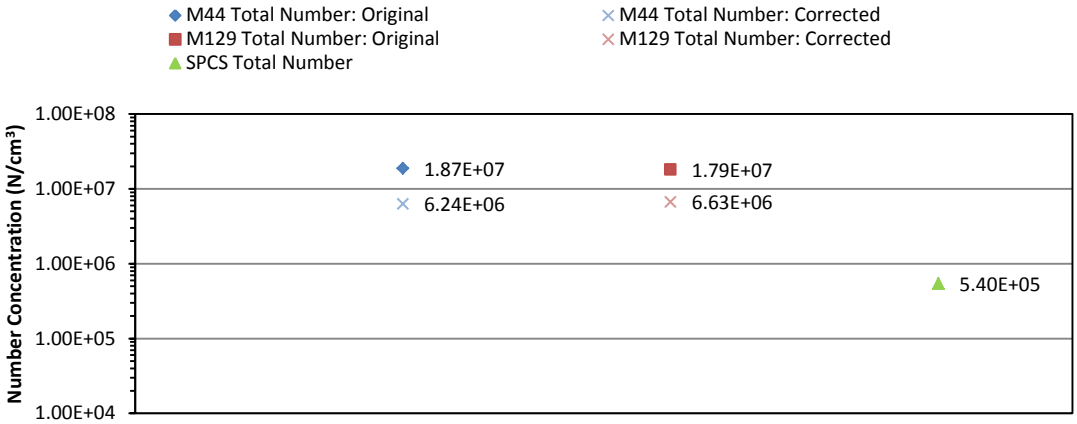

Figure 5.21: Original and corrected DMS500 and SPCS total number concentrations at stratified charge high load condition.

5.2.3 Summary of Piezoelectricly Actuated Outwardly-Opening Fuel Injector Results and Volatile Removal using Catalytic Stripper

While operating in a homogeneous charge mode as the load on the engine was increased the trend observed was that the PM number concentration decreased. This was true for the measurements recorded using the both DMS500s and the SPCS and is shown in Figure 5.22.

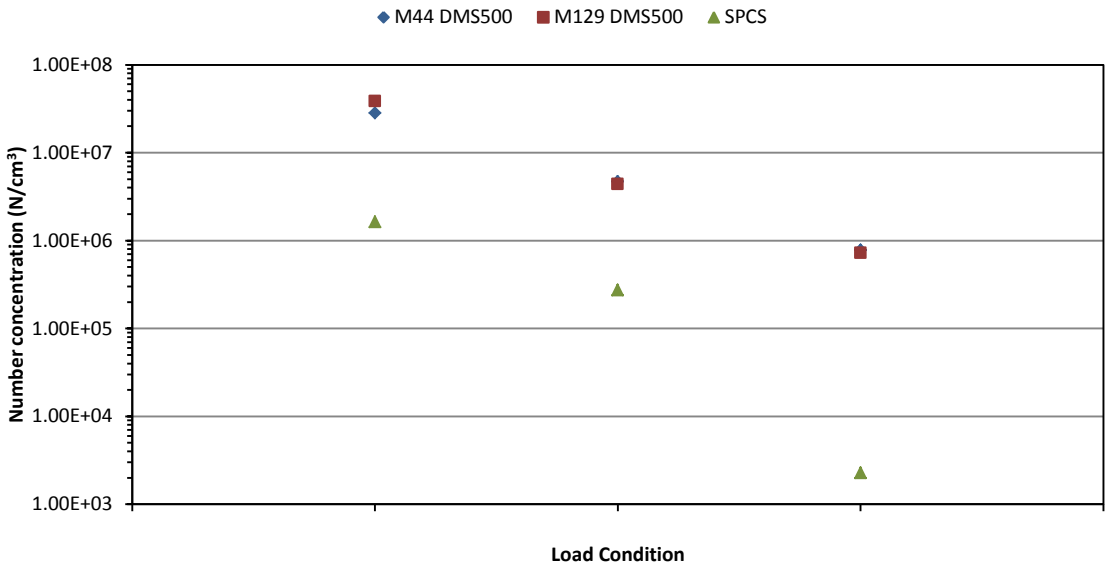

Figure 5.22: Total number concentration recorded by DMS500s and SPCS for homogeneous charge operation at all load conditions.

During stratified charge operation the PM number concentration produced remained fairly consistent across all engine loadings as shown in Figure 5.23. The increase observed at the medium load condition may be as a result of reduced engine rpm rather the engine load.

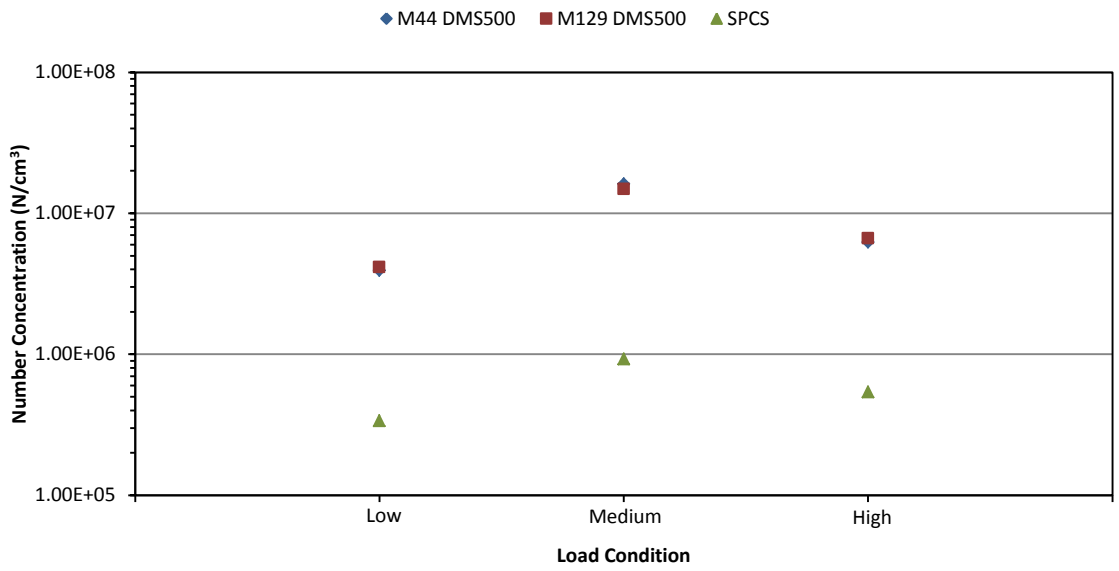

Figure 5.23: Total number concentration recorded by DMS500s and SPCS at stratified charge operation at all load conditions.

Although an allowance for CPC counting efficiency loses and removal of particles counts below 23nm there was still a discrepancy between the DMS500 and SPCS results. This is believed to be due to the SPCS being insensitive to volatile material whereas the DMS500 is not. Most volatile material would be expected to be in the smaller size regions (<23nm) however from the experimental results presented in Chapter 4 it is clear there is a possibility for volatile particles to exist above this size and for volatile coatings to occur in combustion exhausts.

In an attempt to remove any volatile material prior to the DMS500 measurement a catalytic stripper (CS) was installed upstream of the Cardiff University (M44) DMS500 sampling location. The CS aims to chemically remove volatile particulates from an aerosol through oxidation and absorption. The sampled aerosol is first heated to induce evaporation of volatile particles allowing subsequent oxidation of the resulting gases. Inorganic compounds, such as sulphates, are absorbed onto a barium washcoat and stored as barium sulphate ($BaSO_4$):

$$H_2SO_4 \rightarrow H_2O + SO_2$$

$$SO_2 + ½O_2 \rightarrow SO_3$$

$$BaO + SO_3 \rightarrow BaSO_4$$

When the storage capacity of this washcoat trap is exceeded it can then be regenerated by heating the unit to 450 to 500°C in a gaseous blend of 95% nitrogen and 5% hydrogen.

The CS which was used within this experimental programme was a prototype unit developed by the University of Minnesota shown in Figure 5.24 [111], the specification of which is detailed in Table 5.3:

Table 5.3: Design specifications of 10 L/min CS.

Property	
Length	100mm
Diameter	32mm
Channel dimensions	1.116 x 1.116 x 110mm
Channel density	350 channels/in^2
Wall thickness	5.5 mil
Washcoat loading	1223 g/cm^3
Washcoat density	1500 g/cm^3

Figure 5.24: Photograph of bespoke 10 L/min CS.

Particle number concentration measurements were repeated at low, medium and high load conditions for homogeneous and stratified charge operating modes. The results of these experiments are summarised in Figure 5.25.

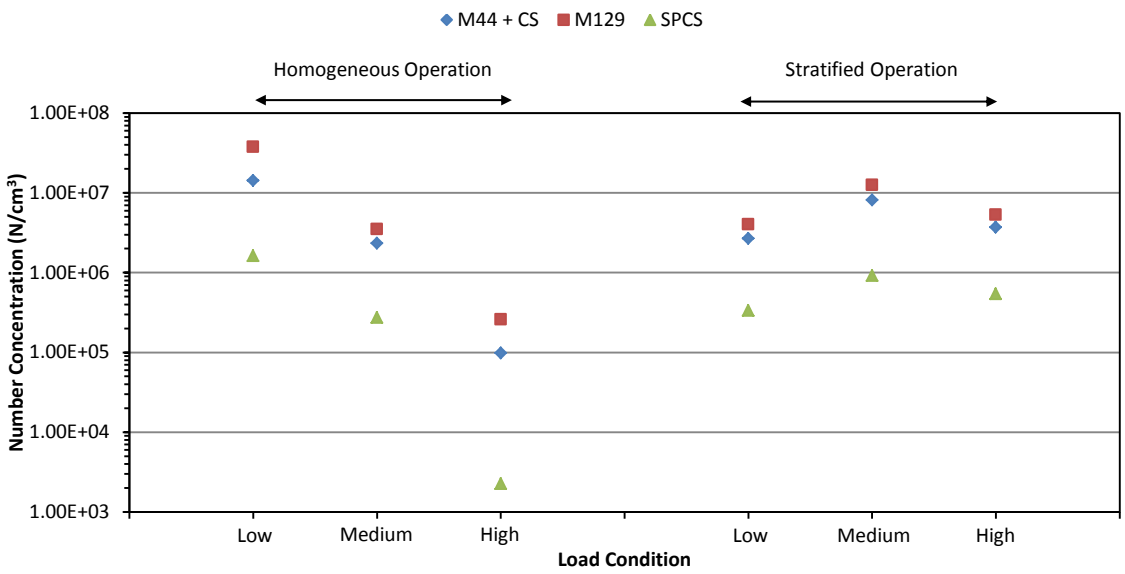

Figure 5.25: Total number concentration recorded by DMS500s (with and without CS upstream) and SPCS at homogenous and stratified charge operation at all load conditions.

A decrease in the recorded number concentration was observed by the DMS500 fitted with the CS upstream of its sample inlet (M44). These results were also corrected for penetration losses within the CS and therefore this reduction is considered to have developed as a direct result of volatile PM removal. However the discrepancy between the DMS500 and SPCS results still remains significant.

5.3 Piezoelectric Actuated Super-Critical Fuel Injector

In an effort to further improve the fuel efficiency and emission reduction benefits which can be achieved with SGDI GDI technology novel approaches to fuel injection are being explored. One such innovation currently being produced by Transonic Combustion Ltd. is a fuel injection system which can deliver supercritical gasoline directly into an engine combustion chamber at high pressure. The Transonic Super-Critical Injector (TSCI), an image of which is shown in Figure 5.26, in conjunction with a custom fuel pump, fuel heater and fuel delivery rail systems, is able to pressurise and heat gasoline up to 300 bar and 320°C respectively.

Figure 5.26: Prototype super-critical fuel injector manufactured by Transonic Combustion Ltd., image supplied by Chris de Boer, V.P. of Research and Development for Transonic Combustion Ltd.

A supercritical fluid is any substance at a temperature and pressure above its critical point; they are not considered to be a solid, liquid, or a gas. Fluids in a supercritical state possess unique properties such as having no surface tension, excellent potential to solvate other materials, and the ability to form nano-particles with sizes that can be controlled to a very high tolerance level. Supercritical fluids also possess rapid mass transfer properties with diffusion coefficients more than ten times that of a liquid near the critical point [112].

Gasoline consists mainly of a blend of C_4 and C_{12} hydrocarbons, and contains hundreds of different molecules. Under the conditions generated by the TSCI gasoline exists as a superheated fluid and therefore during injection into the cylinder the fuel plume maintains the attached supercritical properties. The benefit of injecting a supercritical fluid into the cylinder as opposed to atomisation of liquid gasoline is that air-fuel mixing is a more efficient process [113]. Furthermore, as the fuel plume requires no additional heat to vaporise liquid droplets there is not a negative heat transfer from the cylinder charge [112].

PM sampled from the SCRE when fitted with the TSCI was performed in the same fashion as that of the Bosch injector with characterisation occurring at multiple engine loadings and operating modes. The low and high load test conditions are identical to that of the Bosch injector and the medium condition is slightly high load and slightly lower rpm.

Table 5.4: Engine settings for each test condition during experimentation with the SCRE fitted with the TSCI.

Test Condition	Speed (rpm)	Load (bar)
Low	2000	2
Medium	1500	6.5
High	2000	10

5.3.1 Results: Homogeneous Charge Operation

5.3.1.1 Low Load Condition (2000 rpm, 2 bar)

The stability of the number concentrations measured with both DMS500s and the SPCS were consistent throughout the lowest load testing condition. The Ricardo M129 unit showed approximately a 39% offset from the Cardiff University M44 DMS500, this increase in number concentration is reflected in the particle size spectra which produced from each instrument (Figure 5.28). SPCS number concentrations were again found to be reduced when compared to the DMS500.

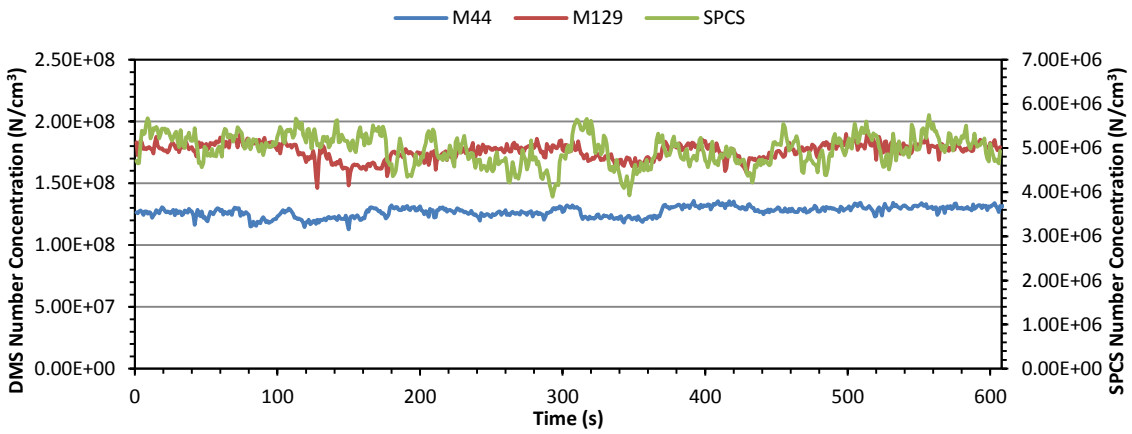

Figure 5.27: Total number concentrations recorded by DMS500s and SPCS at homogeneous charge low load condition.

The M44 and M129 continue to produce varying size spectra at this load condition with the M44 indicating a mono-modal distribution with peak position at ≈20nm and the M129 indicating a bi-modal distribution with peak positions at ≈10 and ≈24nm

respectively. As is expected for automotive emissions PM concentrations are mainly distributed in the 10 - 100nm region.

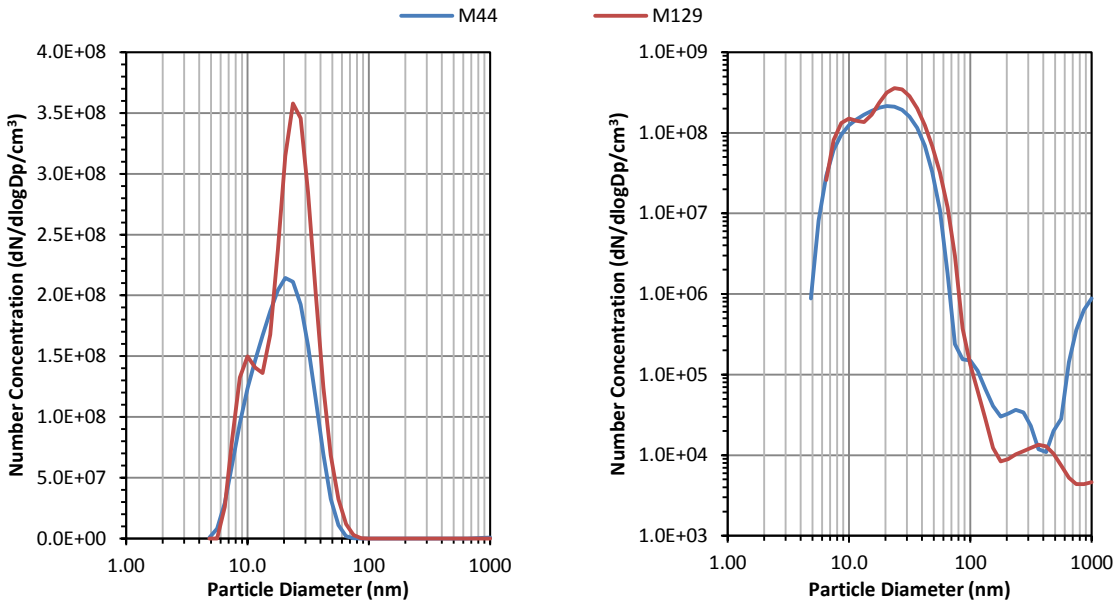

Figure 5.28: DMS500 size spectra at homogeneous charge low load condition: (a) linear y-axis scale, (b) logarithmic y-axis scale.

As with the results gained when the SCRE was fitted with the Bosch injector there is a large difference between the uncorrected DMS500 number concentrations and that of the SPCS. When the relevant corrections are applied to the measured data the discrepancy is reduced and the DMS500 to SPCS comparison for this condition is far better than any of those produced with the Bosch injector at homogenous charge conditions.

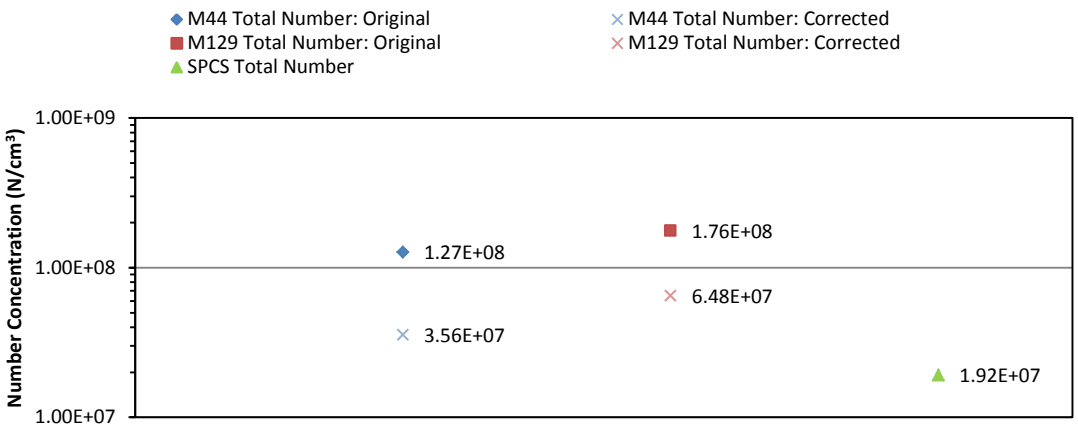

Figure 5.29: Original and corrected DMS500 and SPCS total number concentrations at homogeneous charge low load condition.

5.3.1.2 Medium Load Condition (1500 rpm, 6.5 bar)

At the medium load condition the number concentration recorded showed some variability with sudden spikes in the measured concentrations being displayed on all measurement instruments.

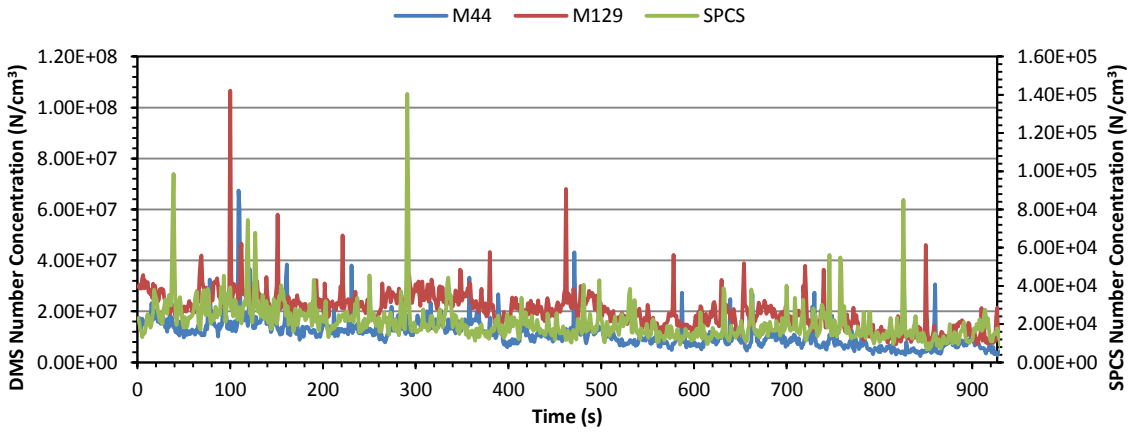

Figure 5.30: Total number concentration recorded by DMS500s and SPCS at homogeneous charge medium load condition.

The size spectra of the PM distributions shown in Figure 5.31 may indicate a reason for the instability in number concentrations as there is a dominant small particle sized mode present. As was early discussed particles at these size ranges are likely to be VOCs which are prone to fluctuations in magnitude and can therefore have a negative

impact on test condition reproducibility. Both DMS500s indicated the presence of this small sized mode at ≈5nm and also showed moderate concentration of particles likely to be a carbonaceous fraction, in the 20 - 50nm region.

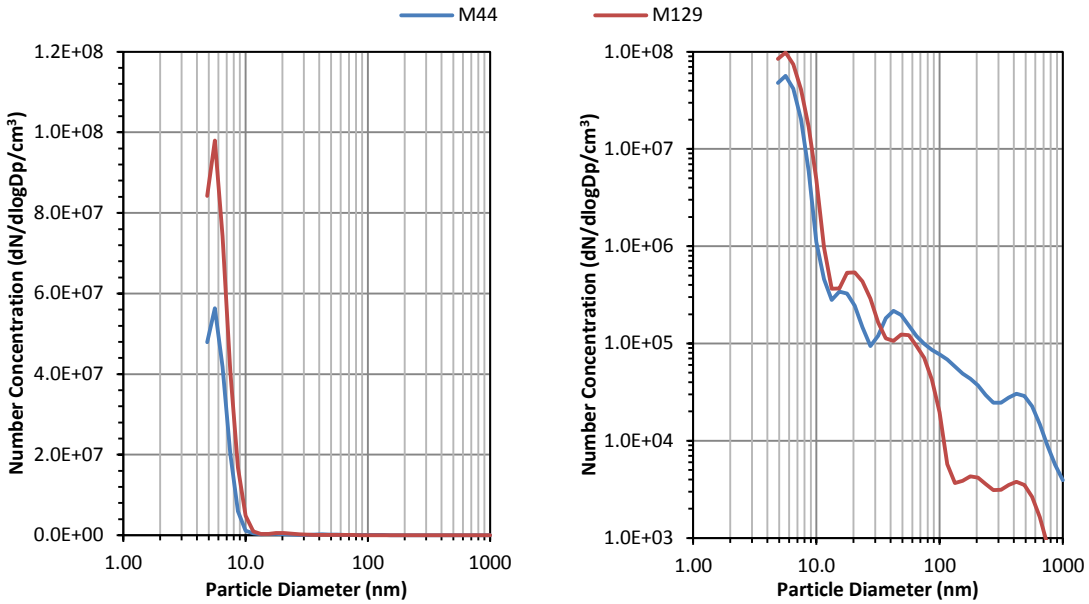

Figure 5.31: DMS500 size spectra at homogeneous charge medium load condition: (a) linear y-axis scale, (b) logarithmic y-axis scale.

At this condition the high concentration of small sized particles has resulted in there being a large offset between the corrected and uncorrected DMS500 values. Following the application of the correction methodology the DMS500 number concentrations are more consistent with that recorded by the SPCS.

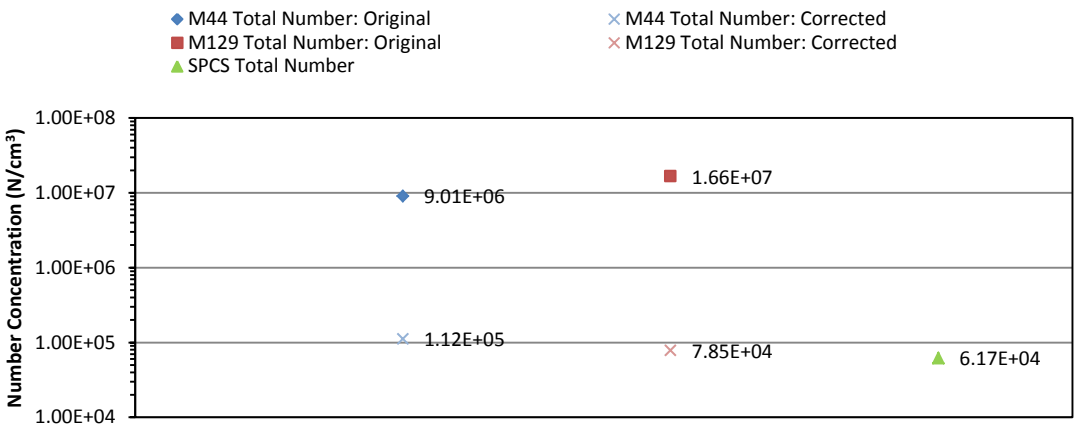

Figure 5.32: Original and corrected DMS500 and SPCS total number concentrations at homogeneous charge medium load condition.

5.3.1.3 High Load Condition (2000 rpm, 10 bar)

The sample stability at the highest load homogeneous charge condition is poor with fluctuations in the measured number concentrations recorded by all devices and a large offset between the M44 and M129 DMS500s at the start of the test period. A similar fluctuating signal was also observed at the highest load condition when the SCRE was fitted with the Bosch injector; however the initial offset in the DMS500 measurements is unusual. The comparability of the two instruments is noted to be very good at other test conditions which may suggest that this incident was caused by something specific to the M129 system. It is possible that during the transition phase to the new condition a residual fraction of hydrocarbons settled in the M129 sample line and evaporated throughout the course of the testing period resulting in the decreasing number concentration recorded. The presence of a large quantity of hydrocarbon emission at this condition is likely as the size spectral analysis shown in Figure 5.34 displays very high number concentrations of small sized particles. The stability of the SPCS measurements when compared to those the DMS500s is a good example of why the automotive industry currently, and the aviation industry intends in the future, to only measure and legislate for nvPM emissions.

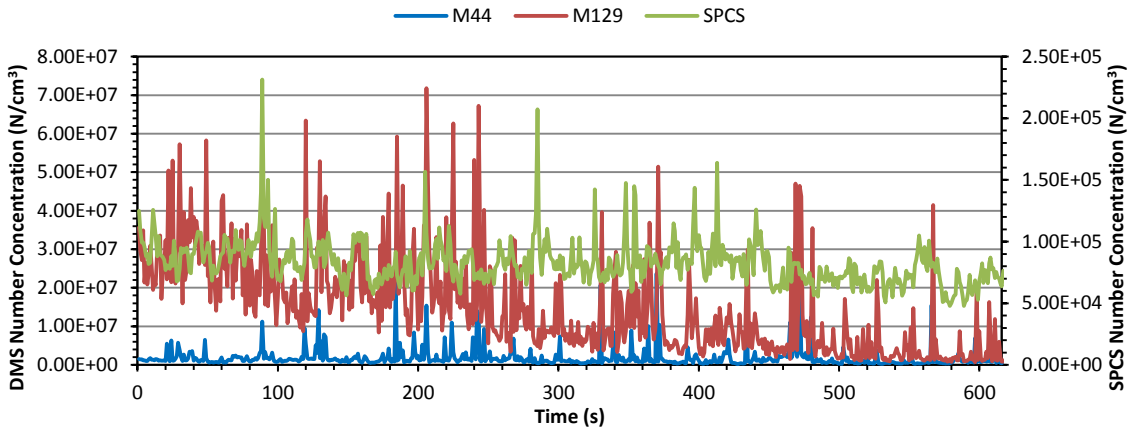

Figure 5.33: Total number concentration recorded by DMS500s and SPCS at homogeneous charge high load condition.

As was observed at medium load condition, the PM size spectra for exhaust produced when using the TSCI consisted mainly of small size particles. also shows that the offset in the number concentrations measured by the M44 and M129 DMS500s throughout the test condition is caused by the presence of a larger number of small particles which would be consistent with volatile particle evaporation in the sample line.

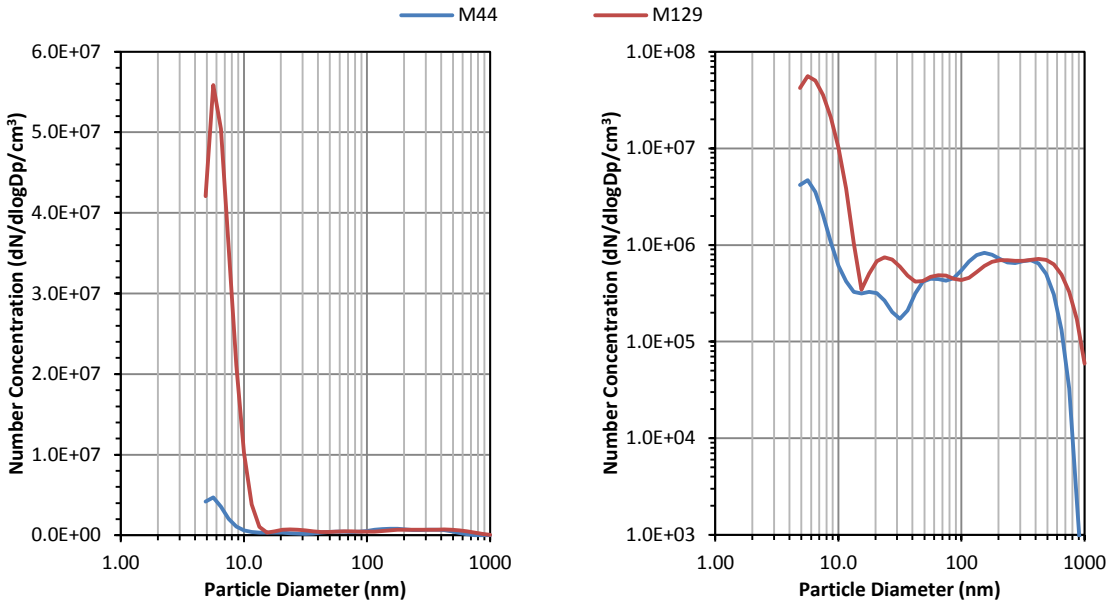

Figure 5.34: DMS500 size spectra at homogeneous charge high load condition: (a) linear y-axis scale, (b) logarithmic y-axis scale.

The final corrected DMS500 number concentrations are again higher than the result recorded by the SPCS however the difference is again improved when compared to the results generated when the SCRE was fitted with the Bosch injector.

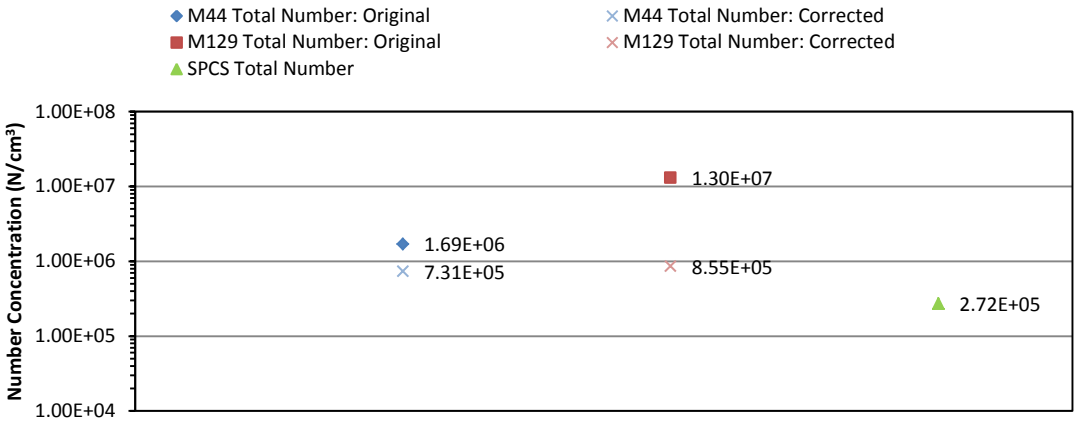

Figure 5.35: Original and corrected DMS500 and SPCS total number concentrations at homogeneous charge high load condition.

5.3.2 Results: Stratified Charge Operation

5.3.2.1 Low Load Condition (2000 rpm, 2 bar)

The stability throughout the low load test condition was again good with some minor fluctuation recorded by both DMS500s.

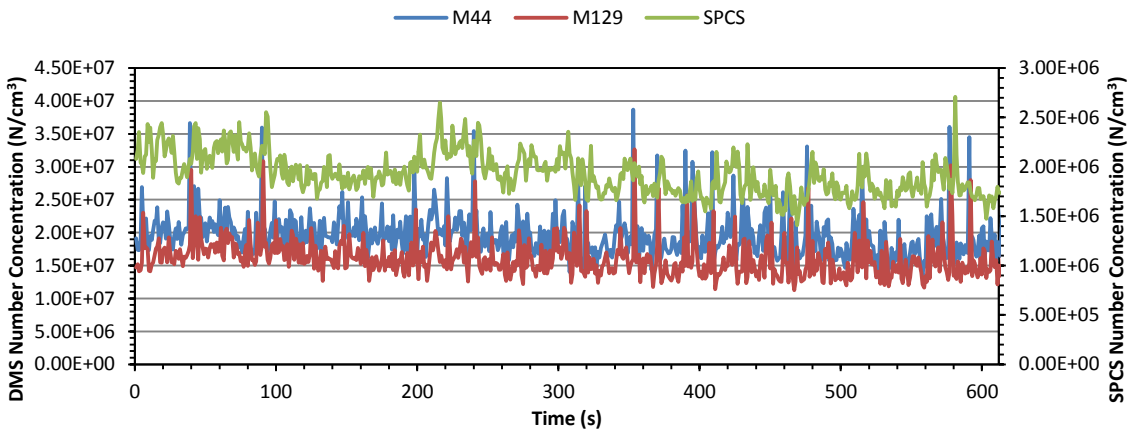

Figure 5.36: Total number concentration recorded by DMS500s and SPCS at stratified charge low load condition.

In contrast to the size spectra produced when operating the SCRE at the homogeneous charge low load condition with the TSCI here it was observed that a high number of larger sized particles developed in the accumulation mode. When operating homogenously the largest concentrations of particle were of the order of 20nm diameter, whereas here the highest concentrations of particles are approximately 100nm in diameter. This increase in particle size indicates that there is likely to be more soot being produced at this condition that that previously measured when operating homogenously.

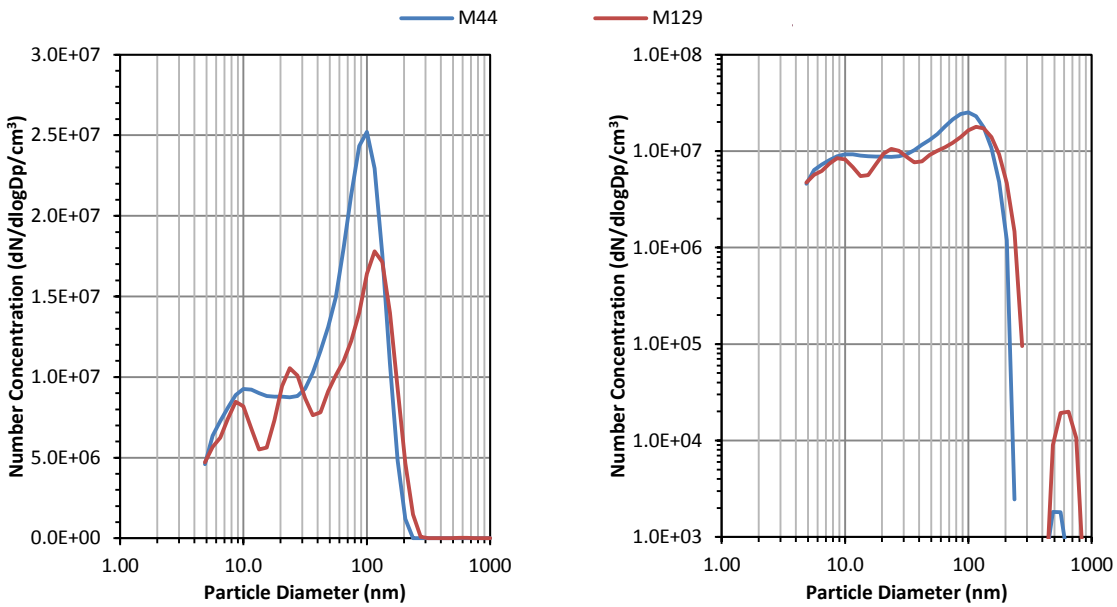

Figure 5.37: DMS500 size spectra at stratified charge low load condition: (a) linear y-axis scale, (b) logarithmic y-axis scale.

The fact that there were far less sub-23nm particles generated at this condition meant that the corrected DMS500 measurements are only slightly reduced when compared to the original data sets.

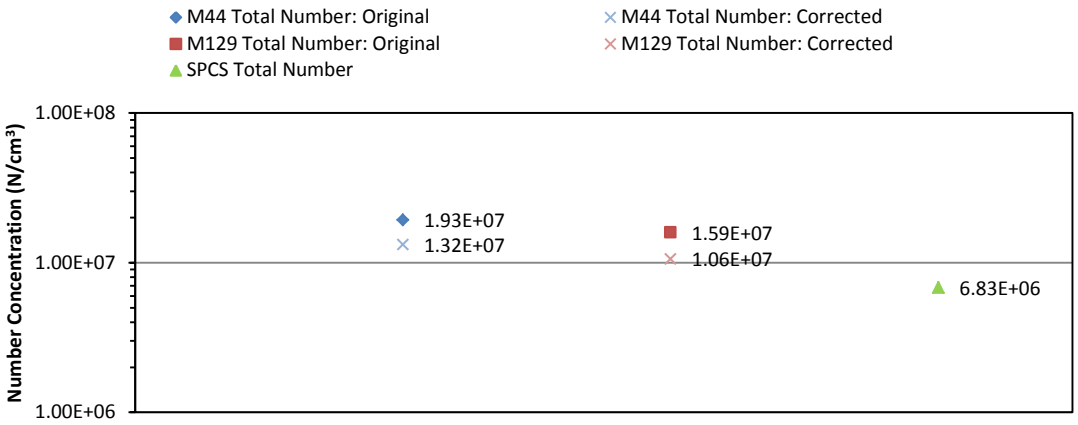

Figure 5.38: Original and corrected DMS500 and SPCS total number concentrations at stratified charge low load condition.

5.3.2.2 Medium Load Condition (1500 rpm, 6.5 bar)

At the medium load conditions the stability throughout the experiment was good with all sampling devices generating number concentration measurements which indicated the same trends. The SPCS number concentration as in all other tested conditions is reduced when compared to the DMS500 results.

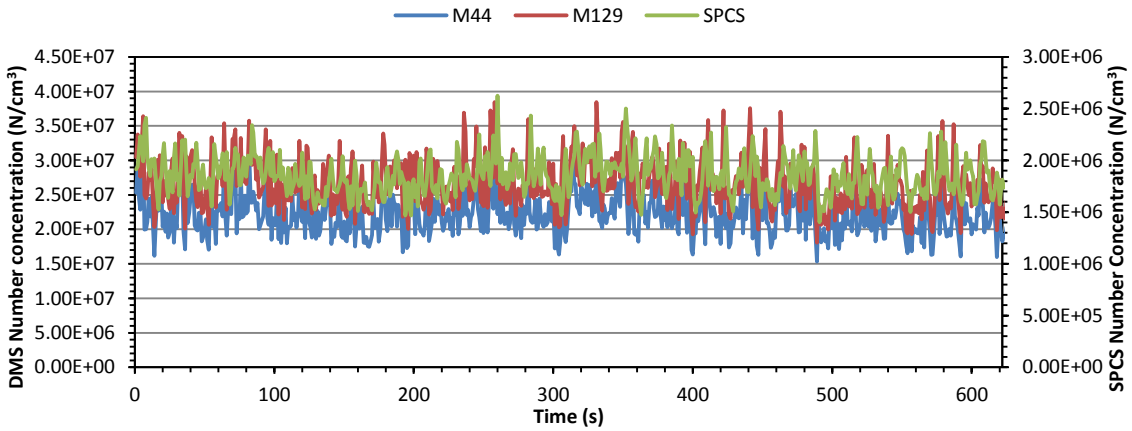

Figure 5.39: Total number concentration recorded by DMS500s and SPCS at stratified charge medium load condition.

Operating in a stratified charge mode has had a dramatic effect on the PM size distribution produced at this condition. The number of small particulates has been

significantly reduced when compared to the previous homogeneous charge condition and the result is a bi-modal spectrum.

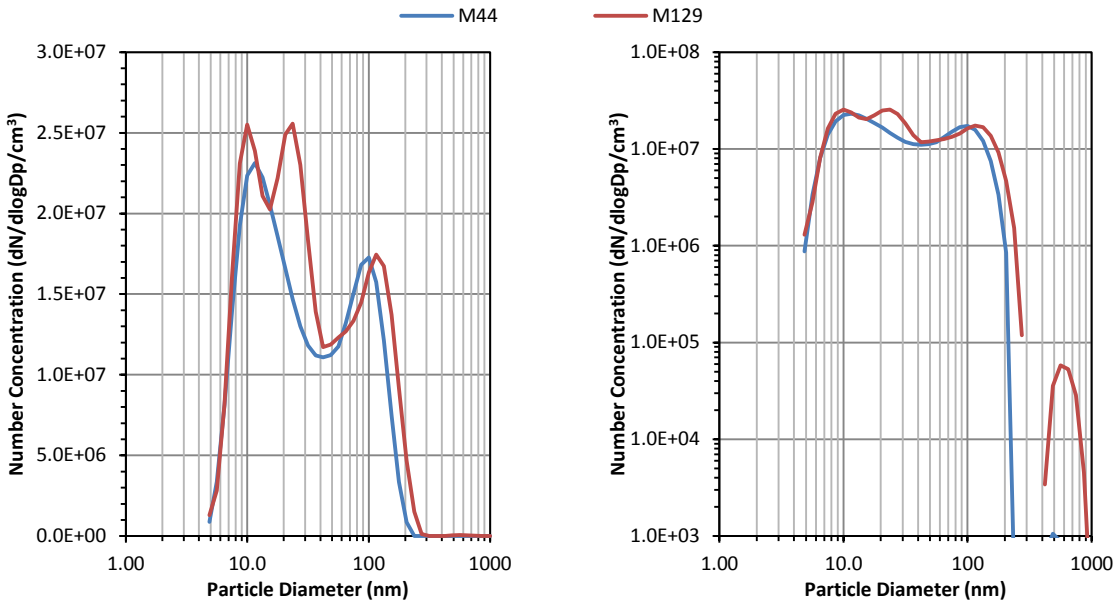

Figure 5.40: DMS500 size spectra at stratified charge medium load condition: (a) linear y-axis scale, (b) logarithmic y-axis scale.

Figure 5.41 shows that final corrected DMS500 are comparable to those of the SPCS.

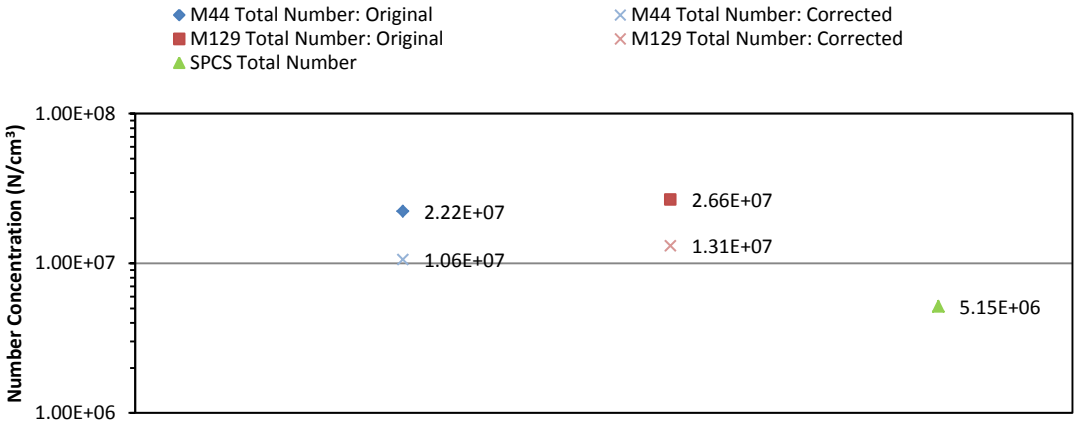

Figure 5.41: Original and corrected DMS500 and SPCS total number concentrations at stratified charge medium load condition.

5.3.2.3 High Load Condition (2000 rpm, 10 bar)

Figure 5.42 shows that DMS500 and SPCS measurements taken at the highest engine loading were stable throughout the sampler period and displayed the same general trends.

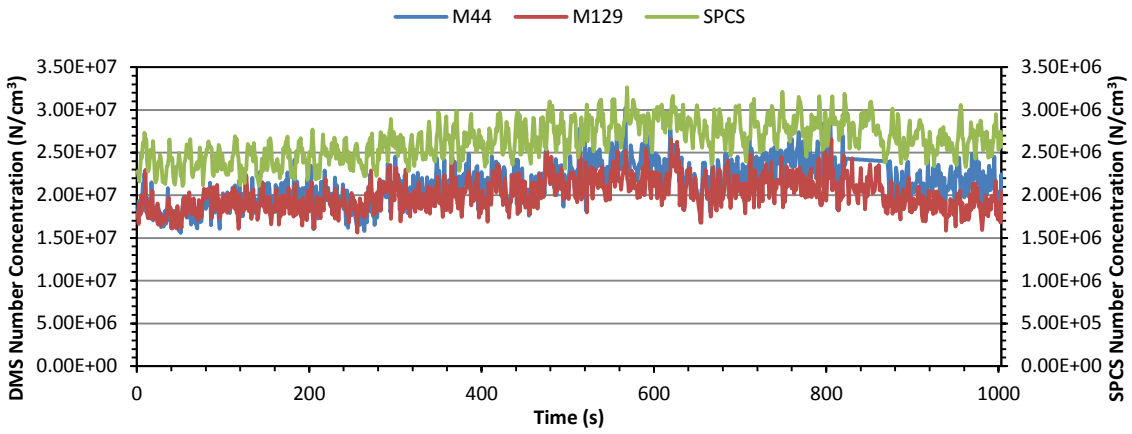

Figure 5.42: Comparison of total number concentration recorded by DMS500s and SPCS for stratified high load condition.

The size spectra shown in Figure 5.43 indicate the presence of higher soot production at this higher load condition as there is a large agglomeration mode.

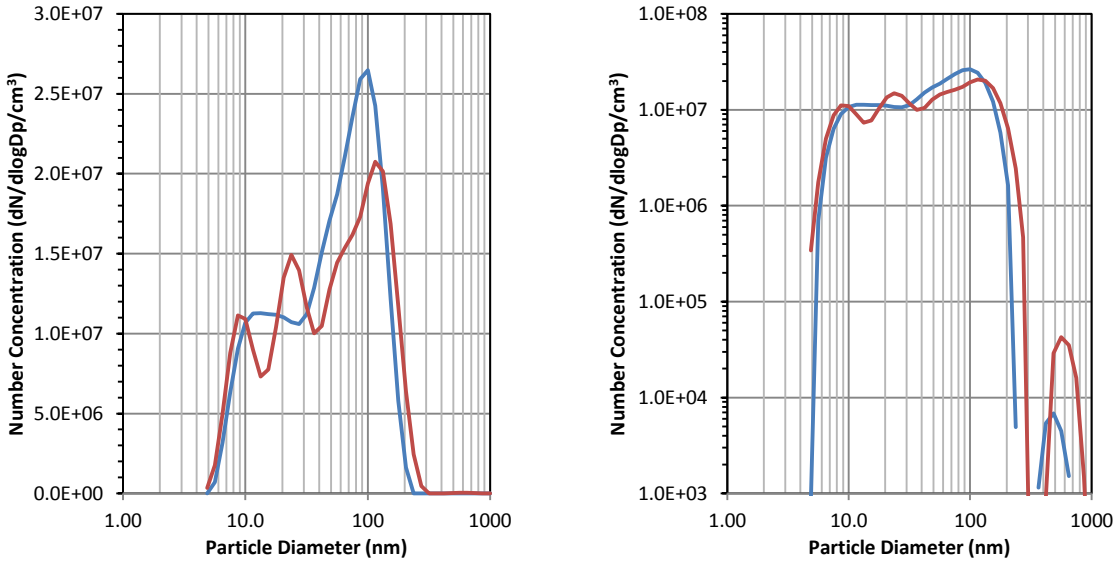

Figure 5.43: DMS500 size spectra at stratified charge high load condition: (a) linear y-axis scale, (b) logarithmic y-axis scale.

Final corrected DMS500 number concentrations are comparable to that produced by the SPCS.

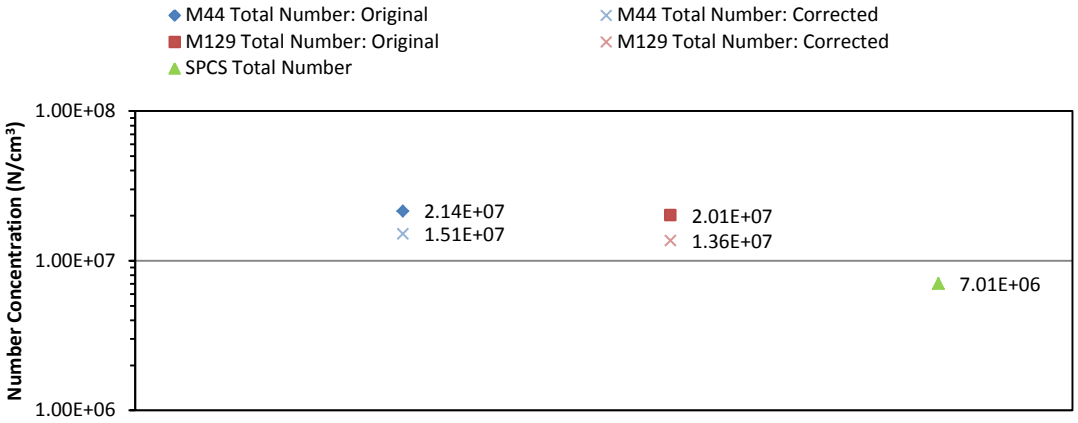

Figure 5.44: Original and corrected DMS500 and SPCS total number concentrations for stratified high load condition.

5.3.3 Summary of Piezoelectric Actuated Super-Critical Fuel Injector Results

During homogenous charge operation the highest observed number concentrations were measured during the lowest load condition. In this engine mode the PM generation appears to be sensitive to engine RPM in addition to engine load as the lowest concentrations were measured during the medium load condition which was operated.

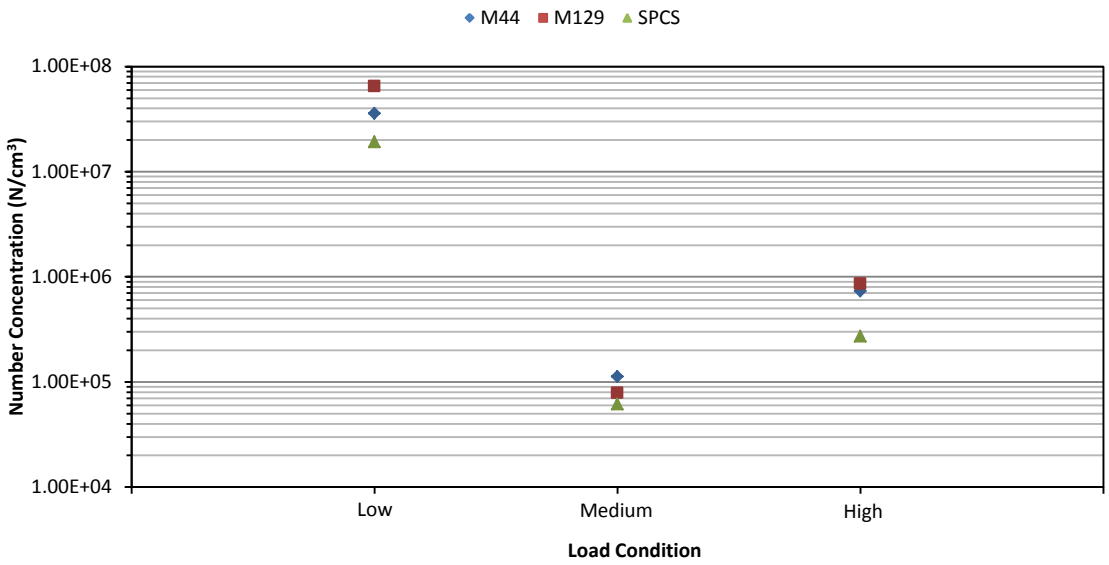

Figure 5.45: Total number concentration recorded by DMS500s and SPCS at homogeneous charge operation at all load conditions.

As was observed in during stratified charge operation using the Bosch fuel injector there is not a significant change in the PM number concentrations produced across the engine load range.

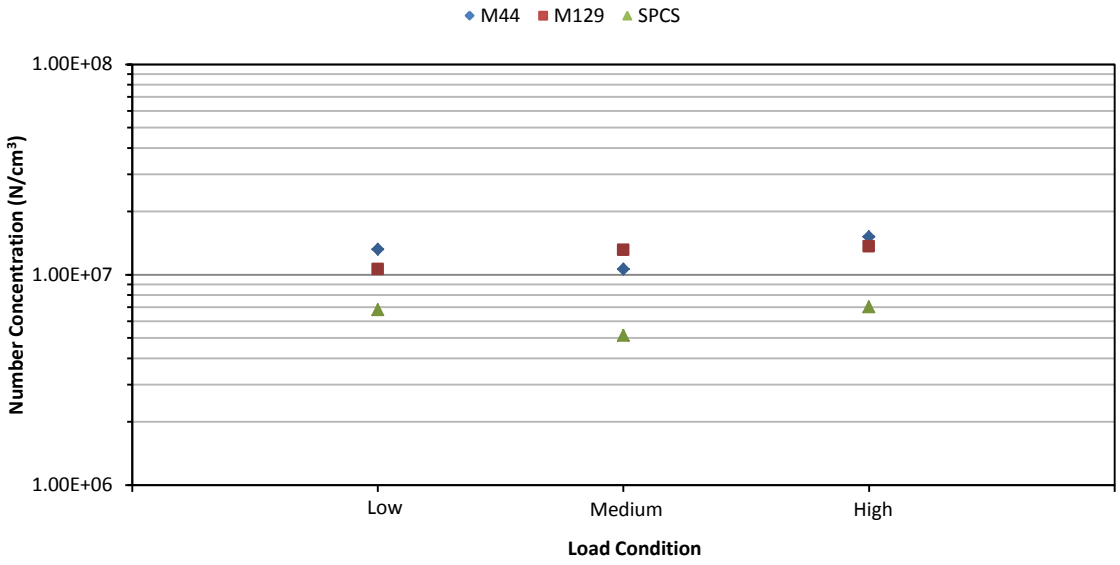

Figure 5.46: Total number concentration recorded by DMS500s and SPCS at stratified charge operation at all load conditions.

5.4 Summary of Single-Cylinder Engine Testing Results

Various PM distributions were successfully sampled from the exhaust of a SCRE at the Ricardo Technical Centre while it was operated with a standard and novel fuel injection system at both homogeneous and stratified charge operating conditions.

PM distribution from both the Bosch and Transonic fuel injection systems proved to be highly dependent on the engine operating load conditions. The potential change in the PM production which occurred from relatively small increases in engine load or RPM were dramatic and as a result the PM number concentration reflect these changes.

PM number concentration recorded at the same load conditions for both fuel injectors (low and high) at homogeneous and stratified charge operation modes are shown in Figure 5.47 and Figure 5.48. When operating in a homogeneous charge mode the PM number concentrations were highest at low load conditions when for both the Bosch and Transonic fuel injectors. At higher engine loads PM concentrations were reduced significantly.

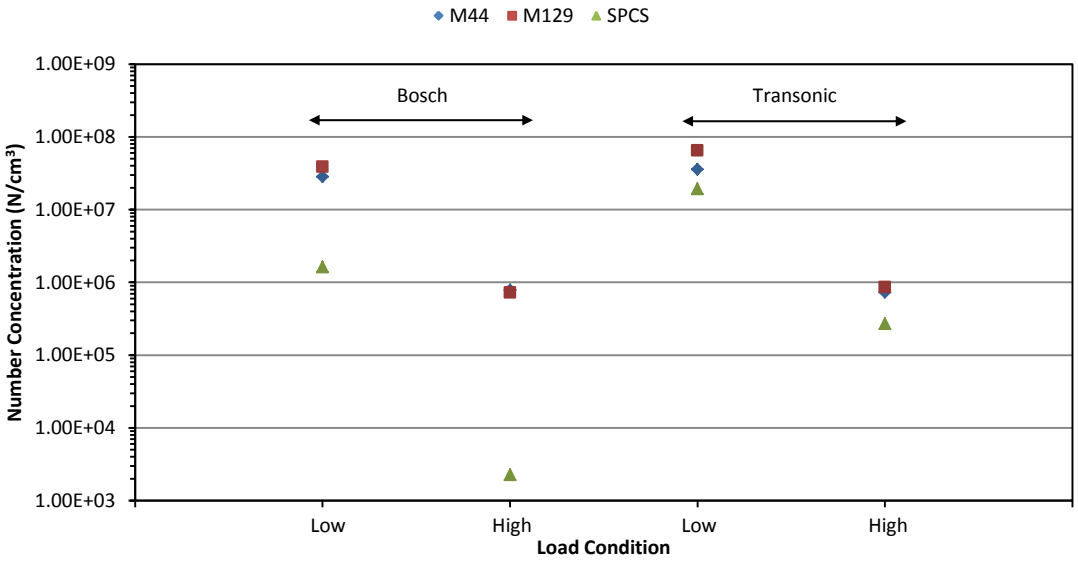

Figure 5.47: Total number concentration recorded by DMS500s and SPCS at homogeneous charge operation for Bosch and Transonic injectors at high and low load conditions.

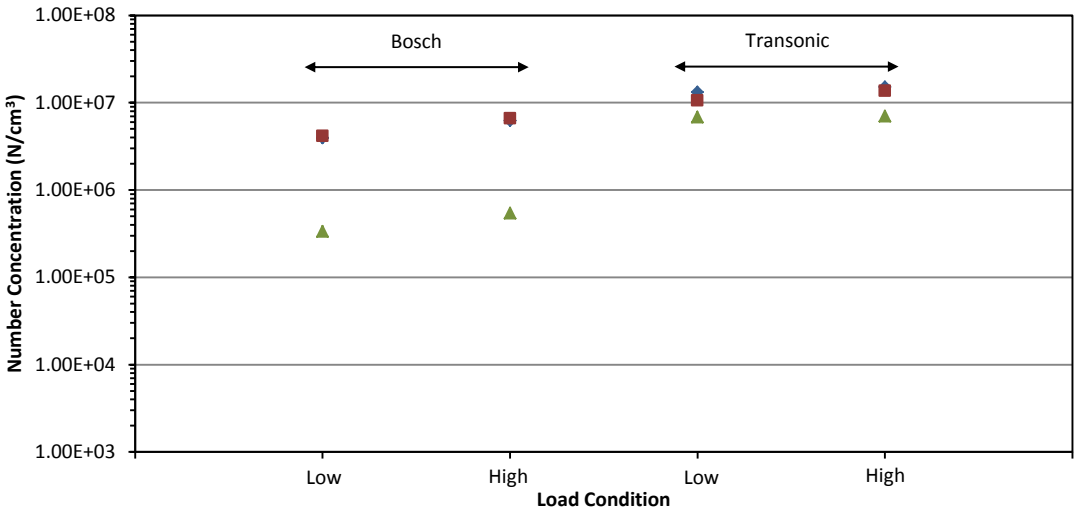

Figure 5.48: Total number concentration recorded by DMS500s and SPCS at stratified charge operation for Bosch and Transonic injectors at high and low load conditions.

PM number concentration measurements made using the DMS500 were found to be consistently higher than those measured by the SPCS. This was expected as the SPCS system is insensitive to volatile PM and was further downstream of the emission source (PM line losses). However, attempts made to correct for the most influencing of these factors (volatile PM) using a CS still resulted in a disparity in PM number concentration for results generated using the Bosch fuel injector.

Although moderate PM emission reduction benefits have been reported for the Transonic injection system [112] in this series of experiments PM number concentrations produced by the Bosch and Transonic fuel injection system were comparable.

Section B

5.5 PM Sampled from Multi-Cylinder Research Engine

The variability of PM production, whether derived from engine operating parameters or sampling methodologies, can make it extremely challenging to achieve repeatable and comparable measurements. To develop further understanding of how primary engine operational parameters influence the production of PM in SGDI gasoline engines, experiments were performed the Hydra MCRE . Both homogeneous and stratified charge engine modes were examined, with the following engine parameters investigated during the study:

- Fuel injection pressure
- Start of injection timing
- Number of injections
- Level of exhaust gas recirculation

PM analysis was performed while each of the specified engine parameters was varied at several engine loadings dependant on the engine operating mode. Four engine loadings were examined while operating under homogenous charge conditions; these will be referred to as low, medium, high and very high load. A summary of these engine conditions is shown in Table 5.5:

Table 5.5: Engine loading conditions tested at homogeneous charge operation.

Engine Property	Low	Medium	High	Very High
Speed (rpm)	1500	2000	2000	2500
Load (bar)	2.62	2	5	10
Coolant Temp. (°C)	90	90	90	90
Oil Temp. (°C)	90	90	90	90
Lambda	1	1	1	1
Ignition	Optimised for 50% MFB at 8°CA ATDC			

While operating in a stratified charge capacity three engine loadings were studied, which are nominally identical in to the low, medium and high load conditions. These were also used during homogenous charge experiments. A summary of these conditions engine conditions is shown in Table 5.6.

Table 5.6: Engine loading conditions tested at stratified charge operation.

Engine Property	Low	Medium	High
Speed (rpm)	1500	2000	2000
Load (bar)	2.62	2	5
Coolant Temp. (°C)	90	90	90
Oil Temp. (°C)	90	90	90
Throttle	WOT	WOT	WOT
Ignition	Optimised for best BSFC; approximately 23°CA BTDC		

Each of the parameters was varied independently of the other engine settings in an attempt to isolate effects. The results generated from these experiments will be presented separately prior to proving an overall summary.

5.6 Fuel Injection Pressure

Fuel injection pressure is a pivotal element of any direct injection fuel delivery system as it usually - not necessarily so for superheated injected fluids which can be relatively insensitive to injection pressure - has major influence on the atomisation characteristics of the fuel. It is therefore expected that the combustion efficiency within the cylinder will be affected by the injection pressure as combustion efficiency is dependent on the mean fuel droplet size.

To investigate how fuel injection pressure influenced PM emissions when operating in a homogeneous charge mode, the pressure at which fuel was injected into the engine cylinders was varied between 40 and 200 bar. This was performed while operating at a low, medium, high and very high engine loading. Inlet and exhaust cam timings and the start of injection timing remained constant during each fuel injection pressure

condition. When operating the engine in stratified charge mode only three engines loading where examined; these being a low, medium and high load. A full operating parameter test matrix is shown in Table 5.7 for homogenous charge mode conditions and in Table 5.8 for stratified charge mode conditions. PM analysis was undertaken using the DMS500 at each of these five test conditions and at each of the previously described engine loadings.

Table 5.7: Fuel injection settings for homogeneous charge mode operation conditions.

Test Point	Engine Parameters			
	FP	**iVVT**	**eVVT**	**SOI**
1	40	20	20	300
2	80	20	20	300
3	120	20	20	300
4	160	20	20	300
5	200	20	20	300

Table 5.8: Fuel injection settings for stratified charge mode operation conditions.

Test Point	Engine Parameters			
	FP	**Number of Injections**	**EGR Rate**	**SOI**
1	40	2	27	37
2	80	2	27	37
3	120	2	27	37
4	160	2	27	37
5	200	2	27	37

At each of the fuel pressure test points the MCRE was allowed to stabilise its running for 5 minutes to ensure exhaust emissions were representative of that particular operating condition, rather than an artefact of changing the engine operating parameters. DMS500 sampling was then commenced for 1 minute periods, an average of which was subsequently be post processed to provide size spectral analysis, number concentration and mass concentration data on the PM emissions.

5.6.1 Results: Homogeneous Charge Operation

5.6.1.1 Low Load Condition (1500 rpm, 2.62 bar)

The DMS500 size spectra created during sampling of the low load homogeneous test condition showed a dominant number concentration peak occurring at a 6 - 7nm size region, and an addition larger particle size peak at 80 - 90nm. This is consistent with a large proportion of volatile material in the small size region and a smaller quantity of larger solid carbonaceous particles in the exhaust stream. As the fuel injection pressure is increased the larger accumulation mode decreases in concentration, while there is a slight increase in the concentration of the smaller particle mode.

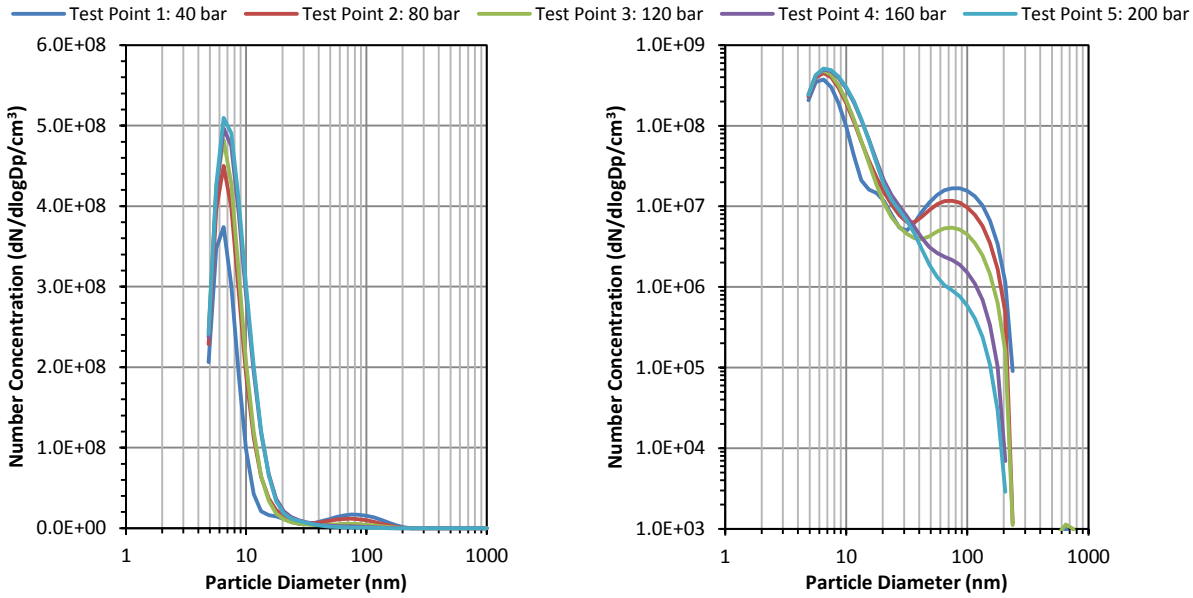

Figure 5.49: DMS500 size spectra for variable fuel injection pressures at homogeneous charge low load condition: (a) linear y-axis scale, (b) logarithmic y-axis scale.

Figure 5.50 shows that total number concentration increases steadily as fuel injection pressure was increased with a 65% change between the initial and final test point. In contrast, total mass concentrations decreases as the fuel pressure increases. The drop in total mass can be explained by the decrease in larger particles throughout the fuel injection pressure variation. If the dominant peak at 6nm is of an organic hydrocarbon nature consisting mainly of unburnt hydrocarbons, which increases over the experimental range, this may suggest that as the fuel pressure is increased the

combustion process is becoming more efficient in the reduction of soot formation, yet less efficient in the complete combustion of fuel.

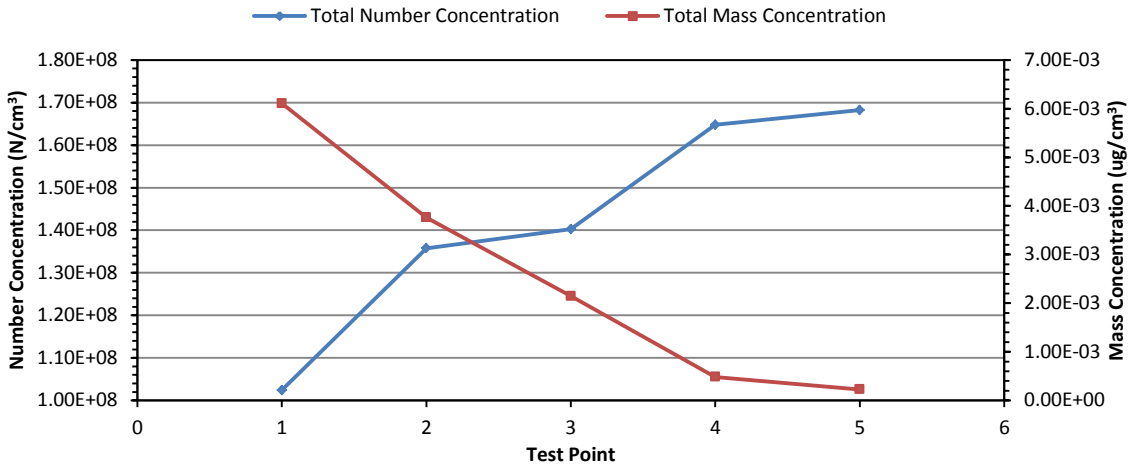

Figure 5.50: Number and mass concentrations measured for variable fuel injection pressures at homogeneous charge low load condition.

5.6.1.2 Medium Engine Loading (2000 rpm, 2 bar)

Test results from varying the fuel injection pressure while operating at medium engine loading also show that as the fuel injections pressure into the cylinder is increased the generation of larger sized particles (between 50 and 100nm) decreases. This consequentially leads to a significant reduction in the measured total mass concentration. However, number concentration does remain fairly stable over the test range with a less prominent increase in the lower size mode. There may be an indication that of a tri-modal size spectrum appearing with peak positions at 6-7nm, 18nm, and 80nm.

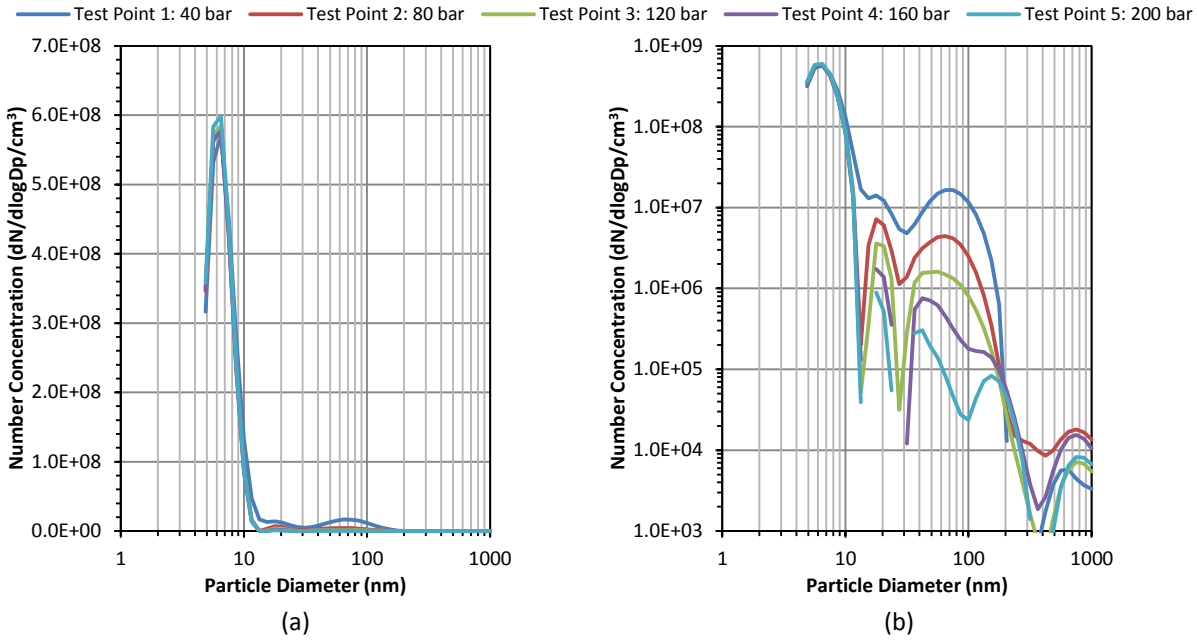

Figure 5.51: DMS500 size spectra for variable fuel injection pressures at homogeneous charge medium load condition: (a) linear y-axis scale, (b) logarithmic y-axis scale.

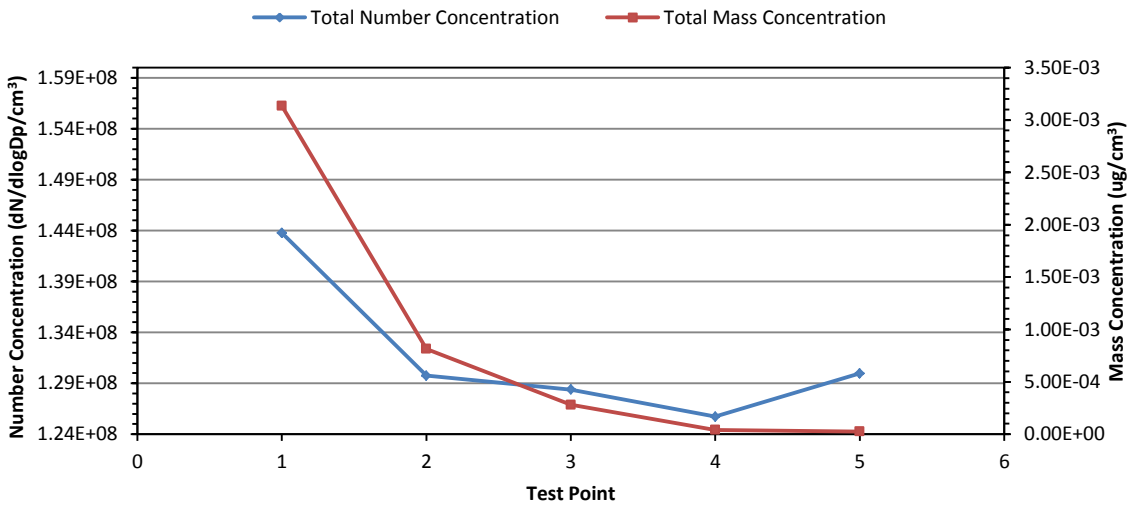

Figure 5.52: Number and mass concentrations measured for variable fuel injection pressures at homogeneous charge medium load condition.

5.6.1.3 High Engine Loading (2000 rpm, 5 bar)

As the engine loading is increased further the development of what appears to be a tri-modal PM size spectrum develops with peak positions at 6 - 7nm, 18nm, and 80nm as was suggested in the results for the medium load condition. Across the complete size

spectrum number and mass concentrations can be seen to decrease as the fuel injection pressure is increased. Total number concentrations are lower than the previous two load conditions, however with the development of larger size particles the total mass concentration increases relative to previous conditions.

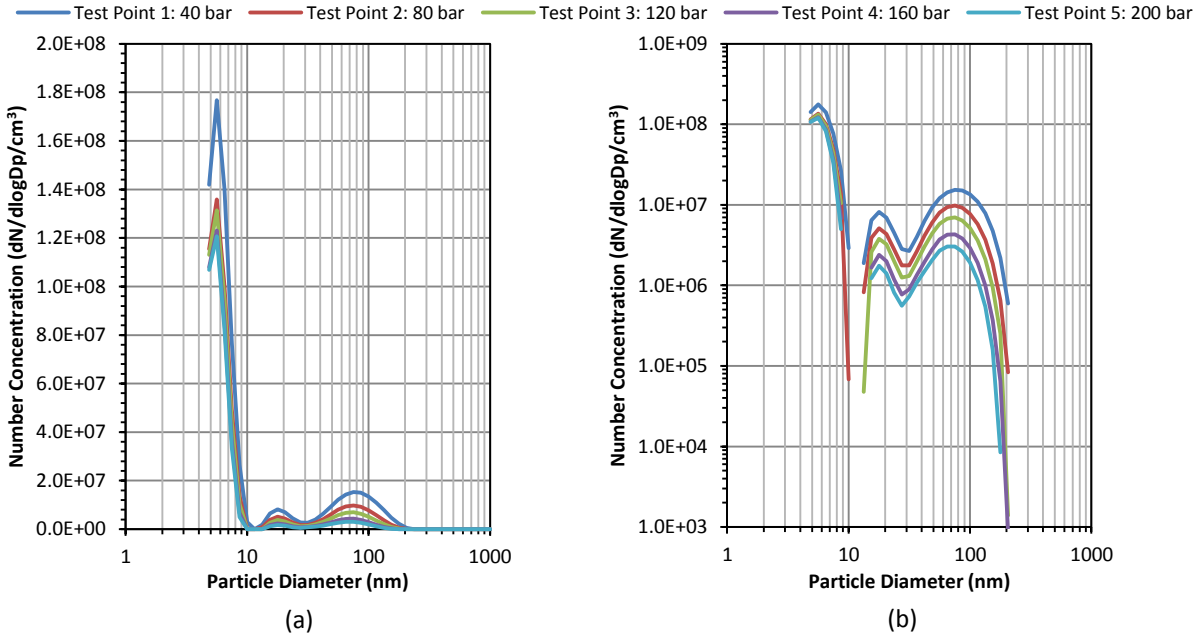

Figure 5.53: DMS500 size spectra for variable in fuel injection pressures at homogeneous charge high load condition: (a) linear y-axis scale, (b) logarithmic y-axis scale.

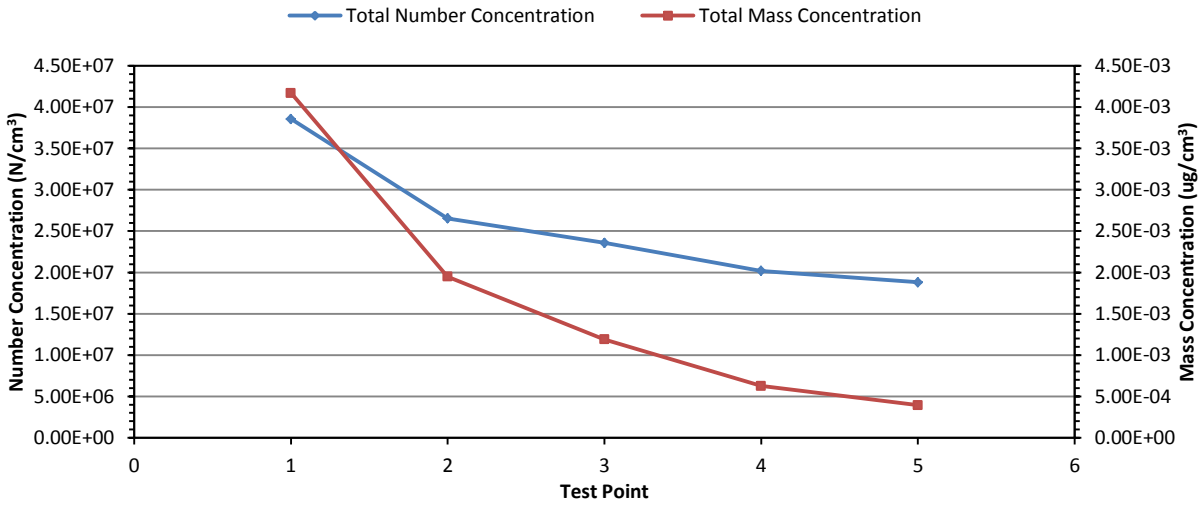

Figure 5.54: Number and mass concentrations measured for variable fuel injection pressures at homogeneous charge high load condition.

5.6.1.4 Very High Engine Loading (2500 rpm, 10 bar)

Total number concentrations are lower by an order of magnitude for the highest loading condition compared to those previously whereas total mass concentration has risen slightly as the presence of the larger size modes (12nm and 65nm) have become more pronounced. Although the tri-modal size spectrum is still present, the peak positions of the three size modes has shifted towards a smaller size range. The smallest size mode appears now to be beyond the measuring capability of the DMS500 therefore true number and mass concentration may be higher than those measured.

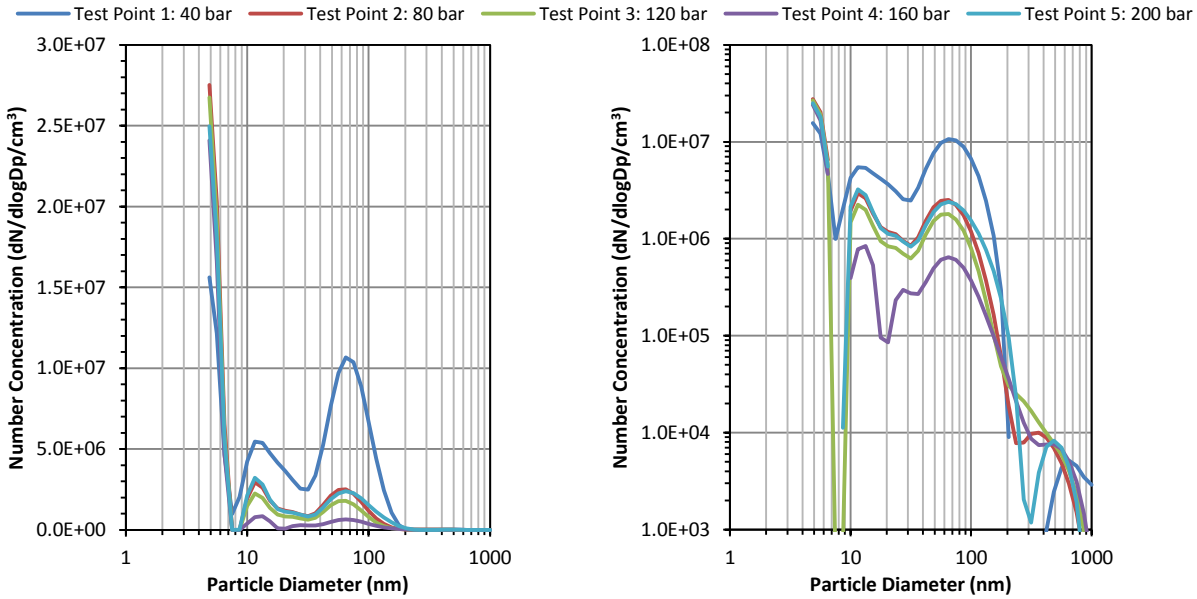

Figure 5.55: DMS500 size spectra for variable fuel injection pressures at homogeneous charge very high load condition: (a) linear y-axis scale, (b) logarithmic y-axis scale.

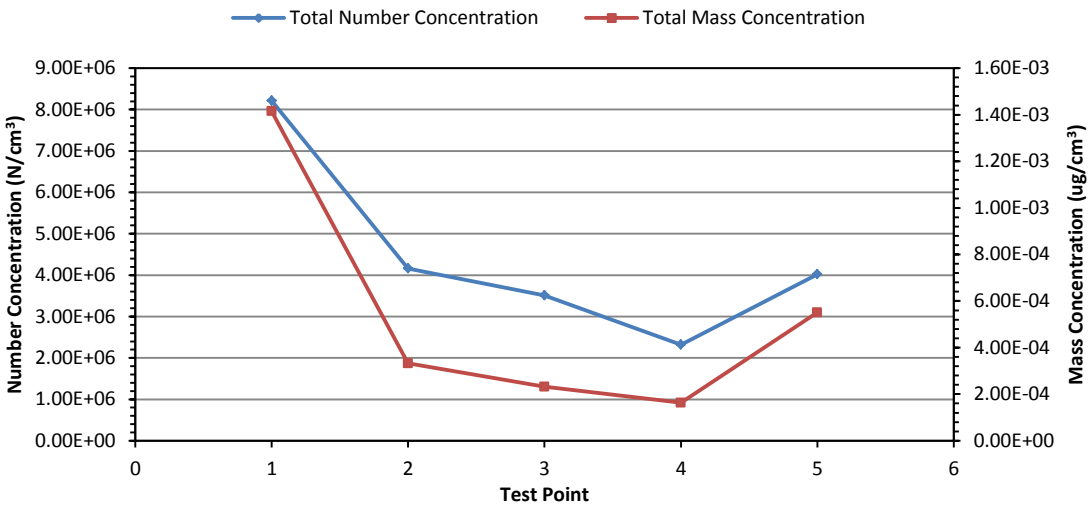

Figure 5.56: Number and mass concentrations measured for varying fuel injection pressures at homogeneous very high load condition.

A summary of all the PM number and mass concentration which were recorded at each of the engine test conditions are shown in Table 5.9.

Table 5.9: Summary of all number and mass concentrations at each engine load and fuel injection pressure condition during homogeneous charge operation.

Test Point	Total Number Concentration (N/cm^3)	Total Mass Concentration ($\mu g/cm^3$)
	Low Load	
1: 40 bar	1.02×10^{8}	6.11×10^{-3}
2: 80 bar	1.36×10^{8}	3.76×10^{-3}
3: 120 bar	1.40×10^{8}	2.15×10^{-3}
4: 160 bar	1.65×10^{8}	4.82×10^{-4}
5: 200 bar	1.68×10^{8}	2.55×10^{-4}
	Medium Load	
1: 40 bar	1.44×10^{8}	3.14×10^{-3}
2: 80 bar	1.30×10^{8}	8.15×10^{-4}
3: 120 bar	1.28×10^{8}	2.80×10^{-4}
4: 160 bar	1.26×10^{8}	4.18×10^{-5}
5: 200 bar	1.30×10^{8}	2.60×10^{-5}
	High Load	
1: 40 bar	3.86×10^{7}	4.17×10^{-3}
2: 80 bar	2.65×10^{7}	1.95×10^{-3}

3: 120 bar	2.36×10^{7}	1.19×10^{-3}
4: 160 bar	2.02×10^{7}	6.26×10^{-4}
5: 200 bar	1.88×10^{7}	3.93×10^{-4}
	Very High Load	
1: 40 bar	8.21×10^{6}	1.41×10^{-3}
2: 80 bar	4.16×10^{6}	3.32×10^{-4}
3: 120 bar	3.51×10^{6}	2.31×10^{-4}
4: 160 bar	2.32×10^{6}	1.63×10^{-4}
5: 200 bar	4.02×10^{6}	5.51×10^{-4}

When all of the PM number and mass concentration data sets for each loading condition are plotted on the same chart the apparent trend which is observed is that as the engine loading is increased from the low to very high condition the recorded PM number and mass concentration are reduced. The higher fuel injection pressure settings appear to further reduce both PM number and mass output, with the exception of low load condition. As earlier stated, the presence of high concentrations of very small particles may suggest a significant presence of organic carbon, possibly unburnt fuel, which is not being fully utilised due to the low engine loading.

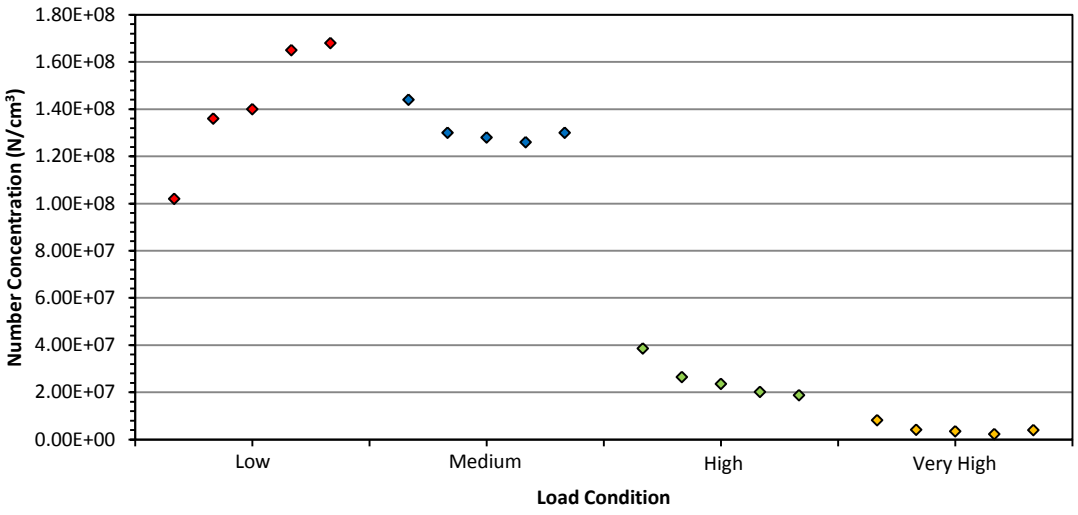

Figure 5.57: Total number concentration for low, medium, high and very high engine load condition during homogenous charge fuel injection pressure testing.

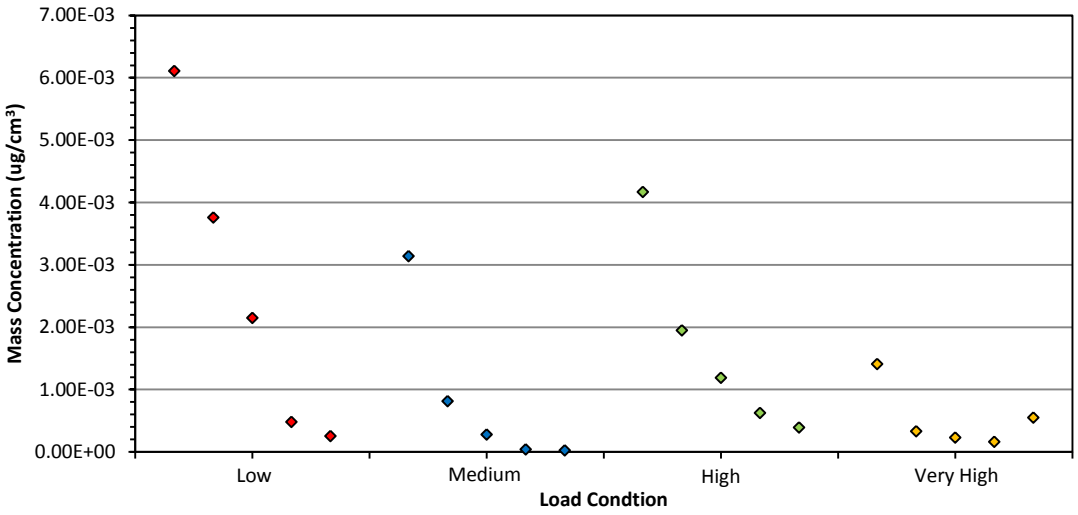

Figure 5.58: Total mass concentration for low, medium, high and very high engine load condition during homogeneous charge fuel injection pressure testing.

5.6.2 Results: Stratified Charge Operation

5.6.2.1 Low Engine Loading (1500 rpm, 2.62 bar)

The PM size spectra produced at low engine loading while operating in a stratified charge configuration suggest that as the fuel injection pressure is increased the number of larger particles, at approximately 80nm, decreases. There is also some fluctuation in the number of smaller sized particles which are produced. These changes in size and number concentration are again reflected in the observed mass concentration produced at each of the testing conditions. There is a general trend that the mass concentration decreases throughout the experiment as the larger particle concentrations diminish.

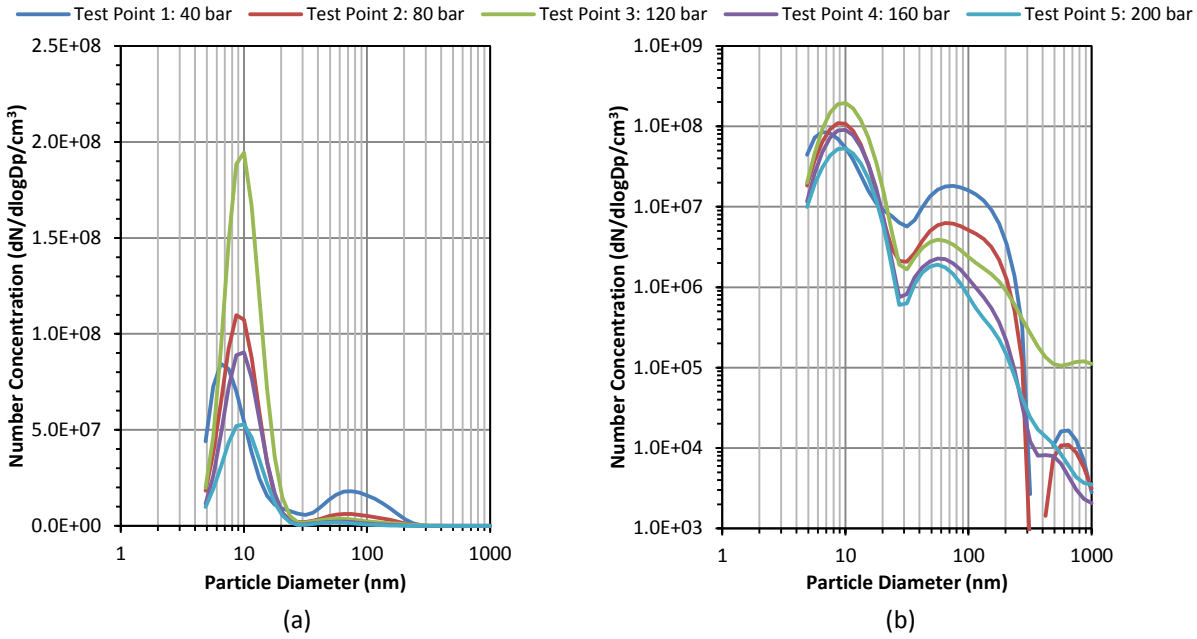

Figure 5.59: DMS500 size spectra for variable fuel injection pressures at stratified charge low load condition: (a) linear y-axis scale, (b) logarithmic y-axis scale.

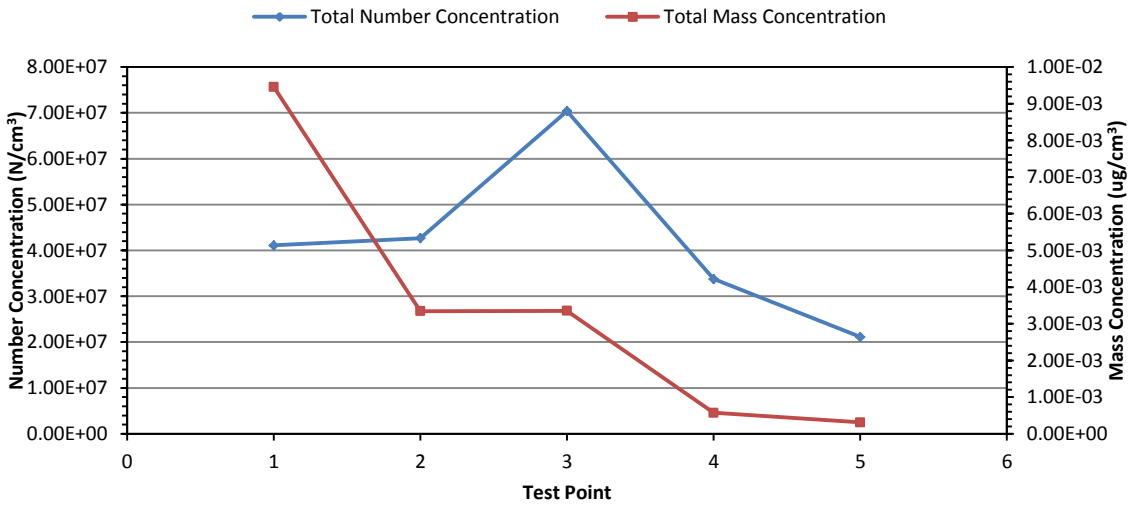

Figure 5.60: Number and mass concentrations measured at varying fuel injection pressures at stratified charge low load condition.

5.6.2.2 Medium Engine Loading (2000 rpm, 2 bar)

A similar bi-modal size spectrum can be seen for the medium load experiments although the peak positions have shifted towards a larger particle size range. Test Point 1 is significantly different from that seen during the rest of the test range which

may be due to a less stable engine operation which can occur during stratified charge modes. Excluding this anomaly the trend seems to be that increasing the fuel pressure is resulting in lower number and mass concentrations across the complete size spectrum.

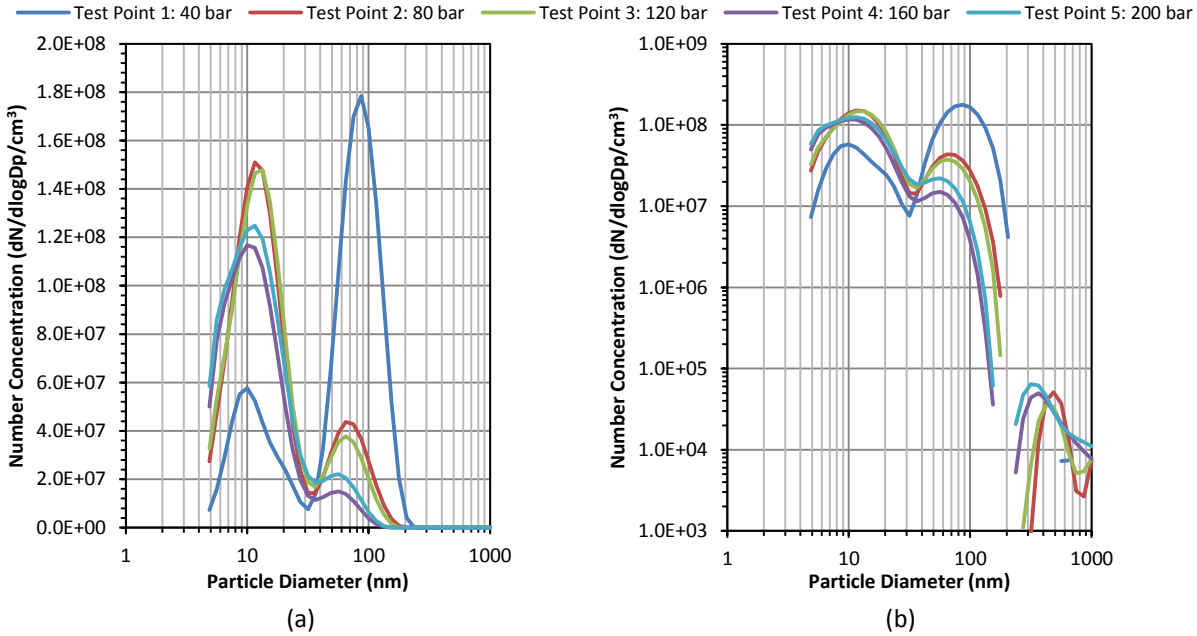

Figure 5.61: DMS500 size spectra for variable fuel injection pressures at stratified charge medium load condition: (a) linear y-axis scale, (b) logarithmic y-axis scale.

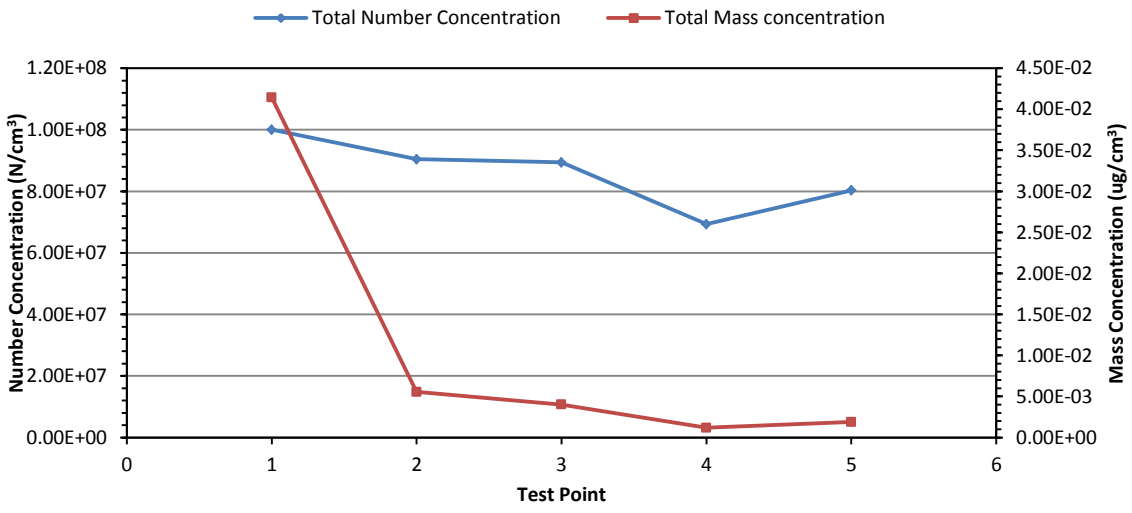

Figure 5.62: Number and mass concentrations measured for variable fuel injection pressures at stratified medium load condition.

5.6.2.3 High Engine Loading (2000 rpm, 5 bar)

Testing on High engine loading produced significantly differently results that those previously seen with a very large reduction in the number of smaller particles being detected. Total number and mass concentrations are similar to those seen in the previous test conditions but the composition which creates these values appears to be very different.

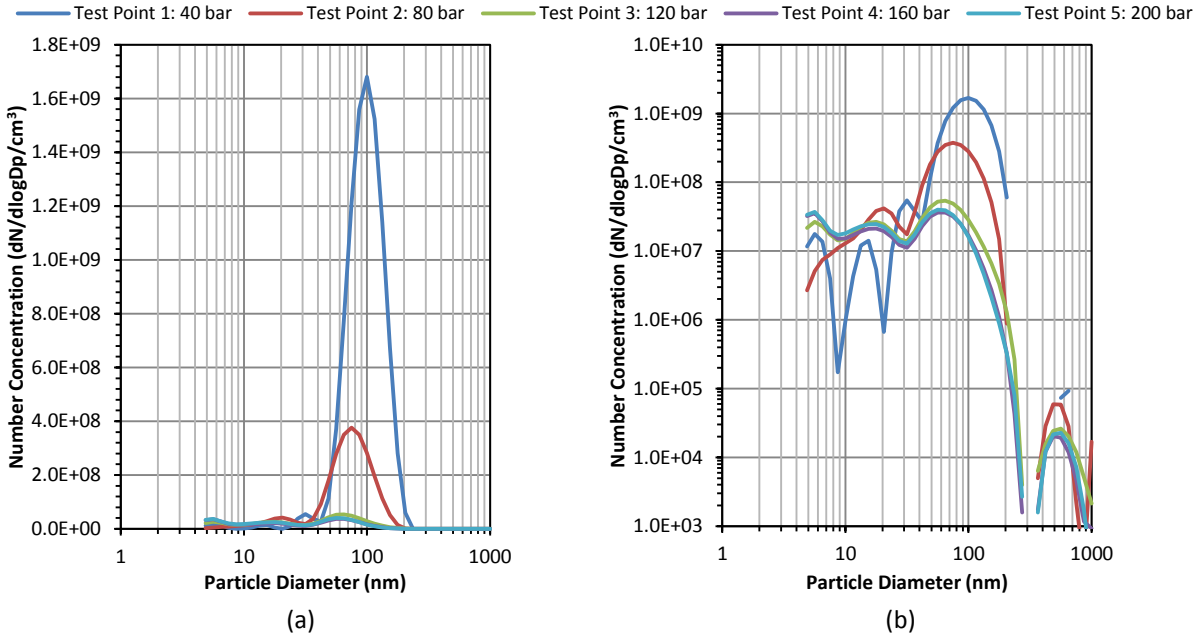

Figure 5.63: DMS500 size spectra for variable fuel injection pressures at stratified high load condition: (a) linear y-axis scale, (b) logarithmic y-axis scale.

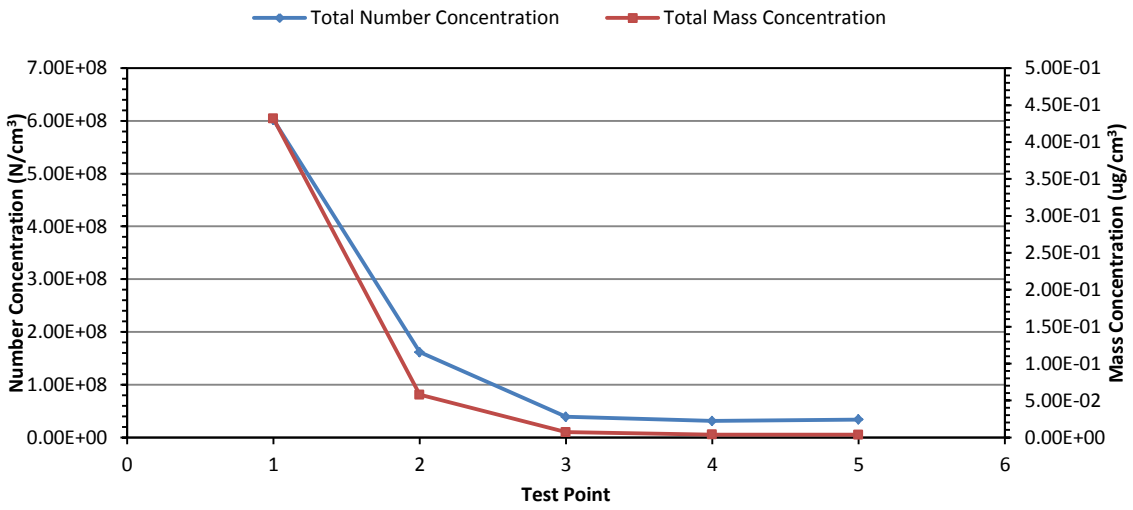

Figure 5.64: Number and mass concentrations measured for varying fuel injection pressures at stratified high load condition.

A summary of all total number and mass concentration measurements recorded during experimentation into how varying the fuel injection pressure affected the emission of PM during stratified charge operation is shown in Table 5.10.

Table 5.10: Summation of all number and mass concentrations at each engine load and fuel injection pressure condition during stratified charge operation.

Test Point	Total Number Concentration (N/cm^3)	Total Mass Concentration ($\mu g/cm^3$)
	Low Load	
1: 40 bar	4.11×10^{7}	9.46×10^{-3}
2: 80 bar	4.27×10^{7}	3.34×10^{-3}
3: 120 bar	7.04×10^{7}	3.35×10^{-3}
4: 160 bar	3.38×10^{7}	3.75×10^{-4}
5: 200 bar	2.11×10^{7}	3.12×10^{-4}
	Medium Load	
1: 40 bar	1.00×10^{8}	4.14×10^{-2}
2: 80 bar	9.05×10^{7}	5.55×10^{-3}
3: 120 bar	8.94×10^{7}	4.01×10^{-3}
4: 160 bar	6.93×10^{7}	1.18×10^{-3}
5: 200 bar	8.03×10^{7}	1.89×10^{-3}
	High Load	
1: 40 bar	6.02×10^{8}	4.32×10^{-1}
2: 80 bar	1.62×10^{8}	5.79×10^{-2}
3: 120 bar	3.92×10^{7}	7.04×10^{-3}
4: 160 bar	3.10×10^{7}	3.79×10^{-3}
5: 200 bar	3.38×10^{7}	3.56×10^{-3}

Figure 5.65 and Figure 5.66 show all the PM number and mass concentration measurement recorded during this series of experiments. As was seen in some test conditions during SCRE experimentation an increased in PM number concentration at medium load condition was observed during SOI variation. This reaffirms the hypothesis that PM generation is not only attributed to engine load, but also engine rpm. Total mass concentration increases steadily as engine loading is increased as the

fuel pressure is increased at each loading condition the observed mass concentration are significantly reduced.

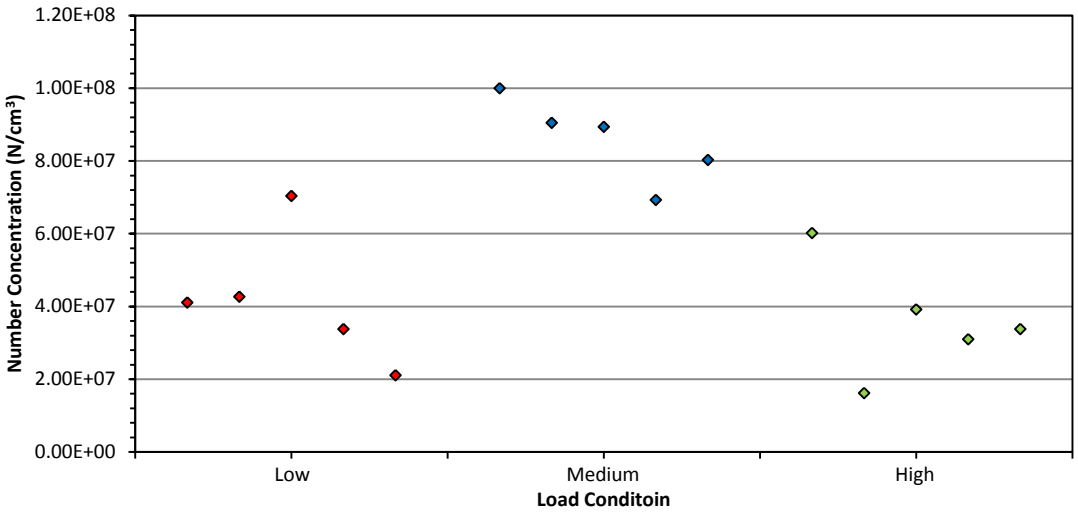

Figure 5.65: Total number concentration for low, medium, high engine load condition during stratified charge fuel injection pressure testing.

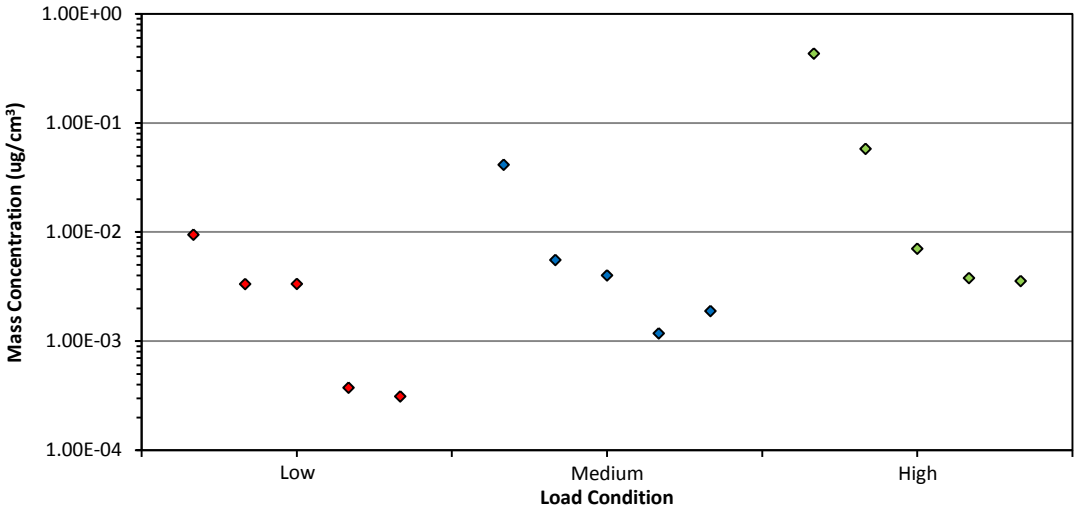

Figure 5.66: Total mass concentration for low, medium, and high engine load condition during stratified charge fuel injection pressure testing.

5.7 Start of Injection Time

Injection of the fuel charge into in the cylinder at the optimum time during the engine cycle is an important factor in establishing air-fuel mixing characteristics and ultimately

engine performance and combustion efficiency. In order to investigate how PM emissions altered depending on the start of injection (SOI) timing several test conditions were analysed where all other engine parameters were kept constant while the SOI was varied during homogeneous and stratified charge operation modes. Table 5.11 shows the engine conditions which were examined during homogeneous charge operation.

Table 5.11: Start of injection settings for homogeneous operation conditions.

Test Point	Engine Parameters			
	FP	**iVVT**	**eVVT**	**SOI**
1	140	20	20	330
2	140	20	20	300
3	140	20	20	270
4	140	20	20	240

5.7.1 Results: Homogeneous Charge Operation

5.7.1.1 Low Engine Loading (1500 rpm, 2.62 bar)

The size spectra produced during this set of experiments remained fairly unchanged throughout with a dominant size mode at ≈7nm which is almost certainly composed of volatile or semi-volatile material. There is a bi-modal element to these size spectra, as it appears that there is a larger size mode at approximately 100nm, this is likely to be the carbonaceous soot fraction of the PM distribution.

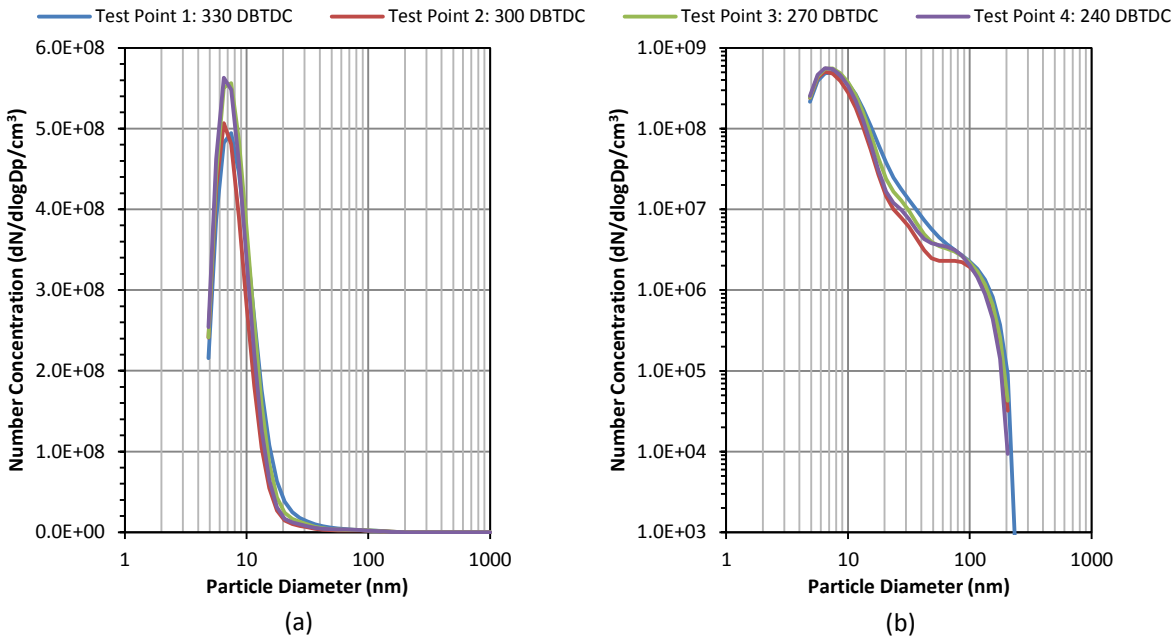

Figure 5.67: DMS500 size spectra for variable start of injection times at homogeneous charge low load condition: (a) linear y-axis scale, (b) logarithmic y-axis scale.

Figure 5.68 shows that PM mass and number concentrations remain fairly constant throughout the SOI test matrix at low loading, this would is consistent with the stable size spectra previously shown.

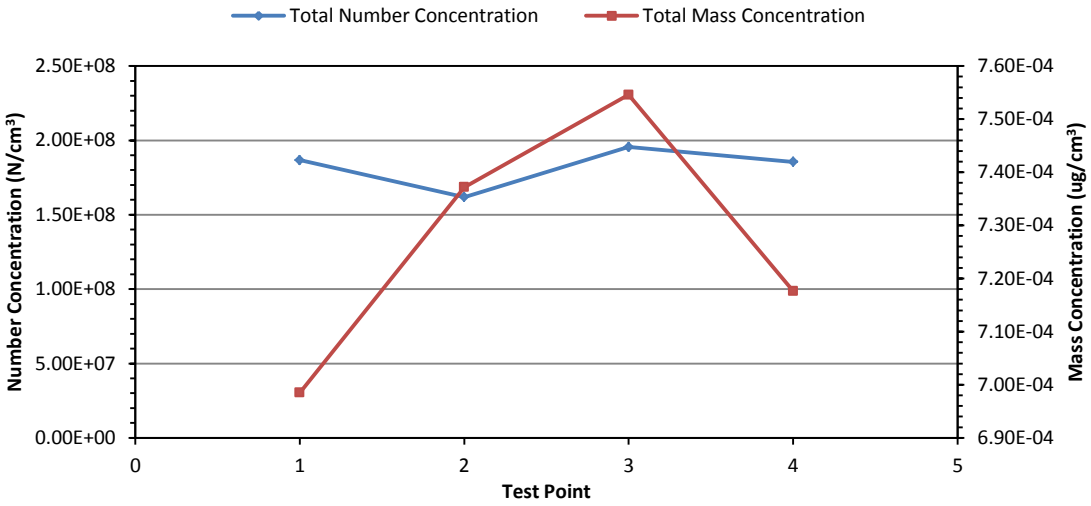

Figure 5.68: Number and mass concentrations measured for variable start of injection times at homogeneous charge low load condition.

5.7.1.2 Medium Engine Loading (2000 rpm, 2 bar)

The medium load condition generated similar size spectra as those produced at the low load condition with a very high concentration nucleation mode. The larger size particle range is sporadic with no obvious agglomeration mode present. It is possible that at these very high concentration levels the dilution required to remain in the operational range of the DMS500 affected the integrity of the sample to some degree when compared to the lower load condition.

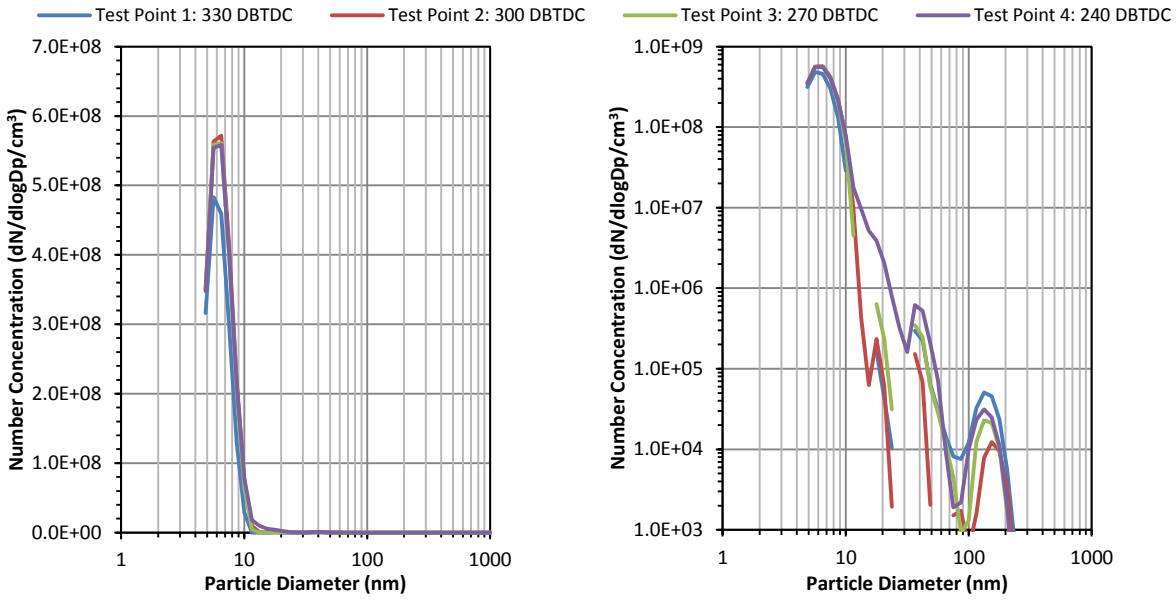

Figure 5.69: DMS500 size spectra for variable start of injection times at homogeneous charge medium load condition: (a) linear y-axis scale, (b) logarithmic y-axis scale.

Total number concentrations are slightly lower than those seen at low loading, however total mass concentrations are significantly lower suggesting that there may be a greater percentage of larger particles produced in the low load test range which are difficult to see on the size spectrum plot due to the concentration levels of the smaller particles.

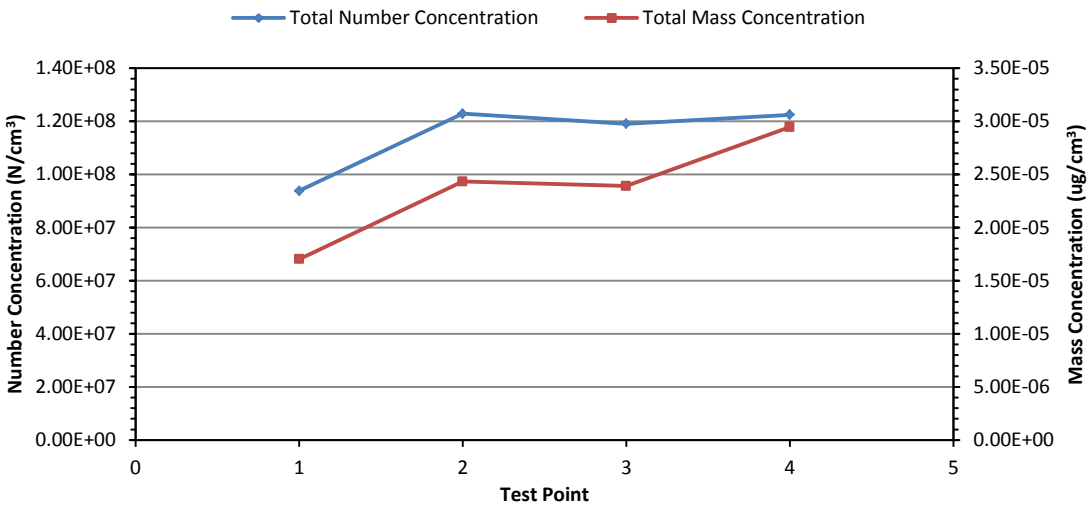

Figure 5.70: Number and mass concentrations measured for varying start of injection times at homogeneous charge medium load condition.

5.7.1.3 High Engine Loading (2000 rpm, 5 bar)

Clear tri-modal size spectra developed during the high load condition test experiments with peak positions at 6nm, 18nm and 70nm. These modes indicate that volatile particles, primary carbonaceous soot particle and particles agglomerations are present in the exhaust.

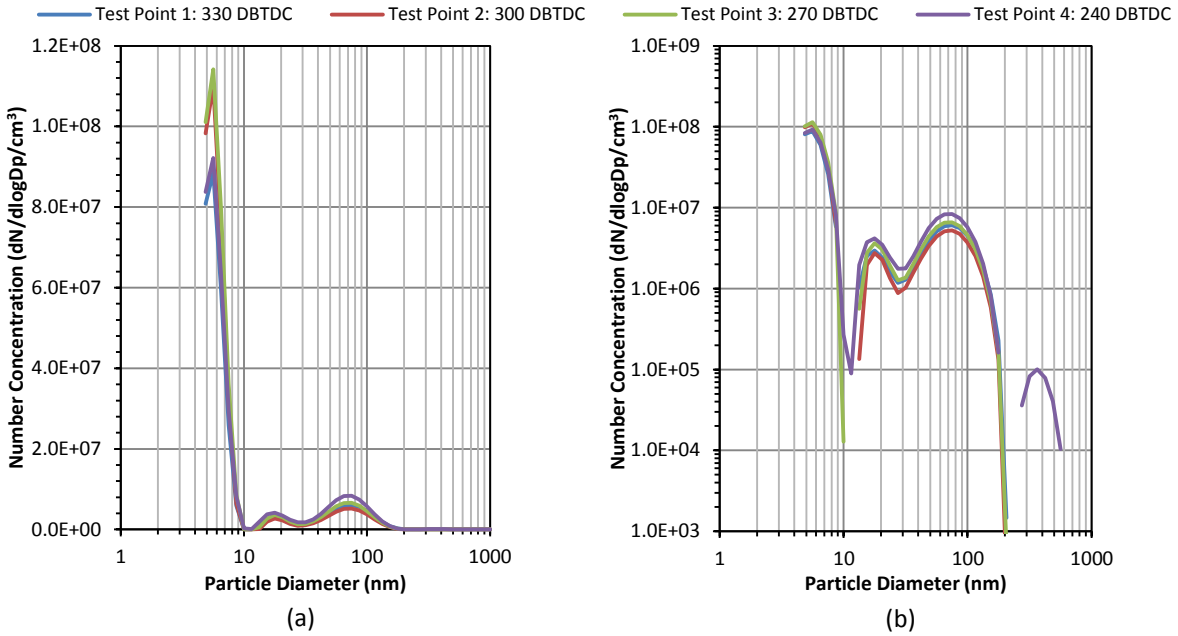

Figure 5.71: DMS500 size spectra for variable start of injection times at homogeneous charge high load condition: (a) linear y-axis scale, (b) logarithmic y-axis scale.

Total number concentrations have reduced again relative to the low and medium load conditions however total mass concentration has risen slightly, probably due to the presence of higher concentration larger size modes.

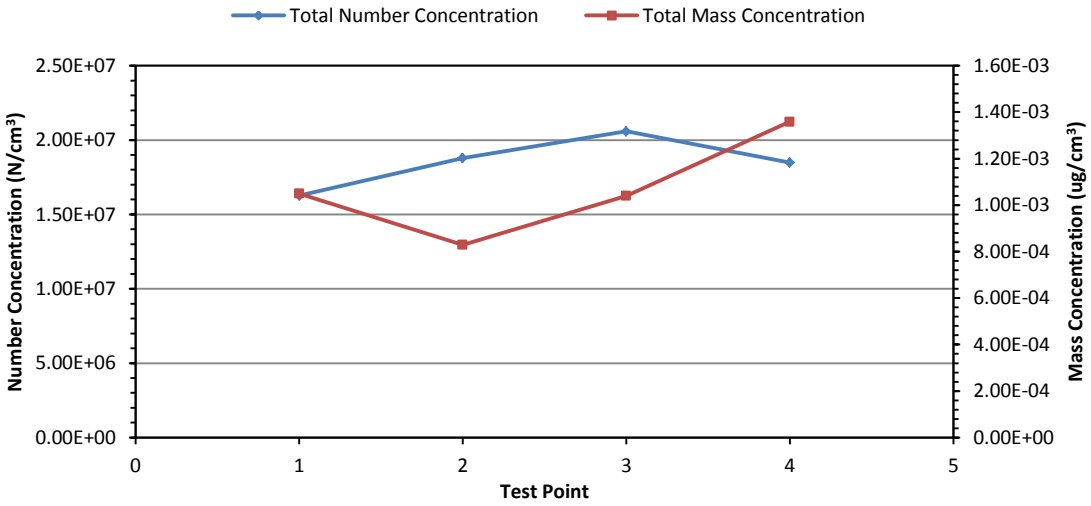

Figure 5.72: Number and mass concentrations measured for varying start of injection times at homogeneous charge high load condition.

5.7.1.4 Very High Engine Loading (2500 rpm, 10 bar)

The PM size spectra observed during the highest load condition also appear to show three size modes at similar particle sizes as those of the high load condition. At this condition there is a pronounced trend that as the SOI was reduced, the concentration levels of the larger size modes were also reduced.

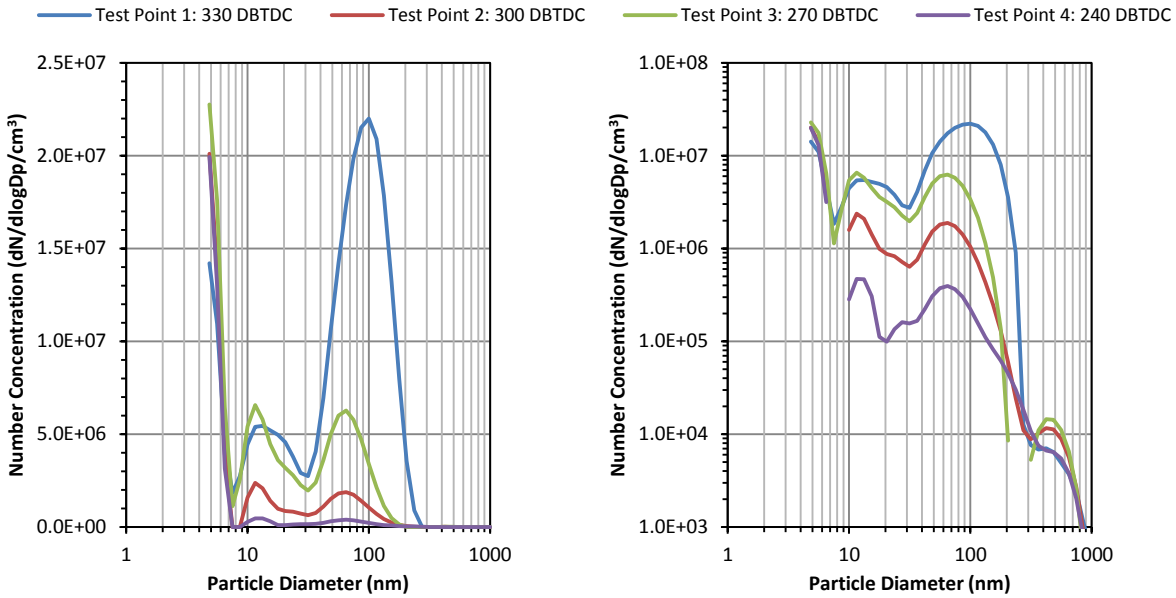

Figure 5.73: DMS500 size spectra for variable start of injection times at homogeneous charge very high load condition: (a) linear y-axis scale, (b) logarithmic y-axis scale.

Total number concentrations are similar to those measured at high load conditions experiments as are the total mass measurements.

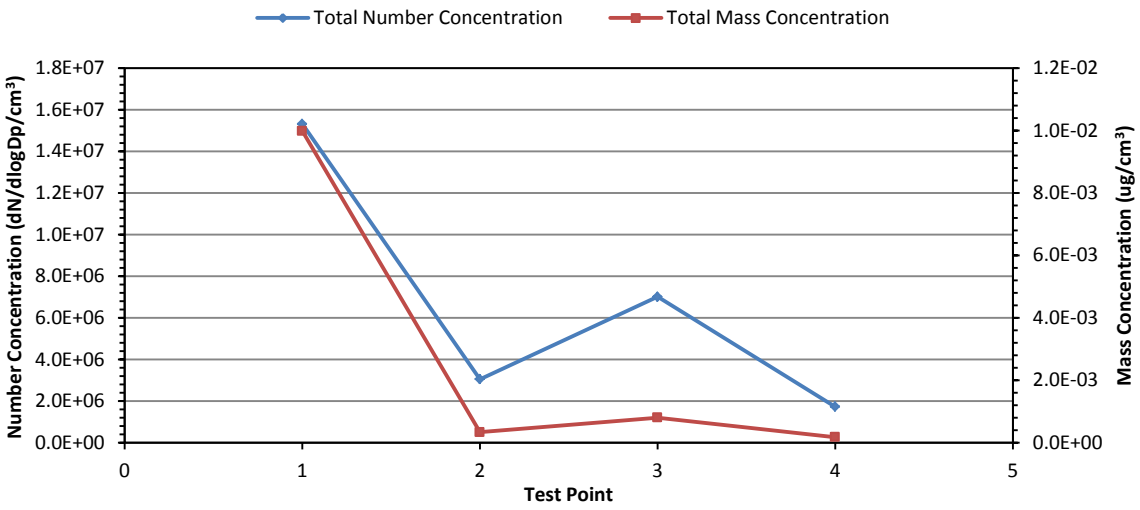

Figure 5.74: Number and mass concentrations measured for varying start of injection times at homogeneous charge very high load condition.

A summary of all the PM number and mass concentrations recorded during the experimentation into how varying the SOI affected the emissions on PM is shown in Table 5.12.

Table 5.12: Summary of all number and mass concentrations at each engine load and start of injection condition during homogeneous charge operation.

Test Point	Total Number Concentration (N/cm^3)	Total Mass Concentration ($\mu g/cm^3$)
	Low Load	
1: 330 DBTDC	1.87×10^{8}	6.99×10^{-4}
2: 300 DBTDC	1.62×10^{8}	7.37×10^{-4}
3: 270 DBTDC	1.95×10^{8}	7.55×10^{-4}
4: 240 DBTDC	1.85×10^{8}	7.18×10^{-4}
	Medium Load	
1: 330 DBTDC	9.38×10^{7}	1.70×10^{-5}
2: 300 DBTDC	1.23×10^{8}	2.43×10^{-5}
3: 270 DBTDC	1.19×10^{8}	2.39×10^{-5}
4: 240 DBTDC	1.22×10^{8}	2.94×10^{-5}
	High Load	
1: 330 DBTDC	1.63×10^{7}	1.05×10^{-3}
2: 300 DBTDC	1.88×10^{7}	8.30×10^{-4}
3: 270 DBTDC	2.06×10^{7}	1.04×10^{-3}

4: 240 DBTDC	1.85×10^{7}		1.36×10^{-3}
		Very High Load	
1: 330 DBTDC	1.53×10^{7}		9.98×10^{-3}
2: 300 DBTDC	3.05×10^{7}		3.40×10^{-4}
3: 270 DBTDC	7.01×10^{7}		8.04×10^{-4}
4: 240 DBTDC	1.73×10^{7}		1.82×10^{-4}

Changing the SOI time appears to have little impact on the PM number and mass concentration levels generated during each set of experiments at each load condition. The difference in engine loading does however result in a noticeable difference in the size PM distribution output, as has been shown in previous experiments with the SCRE. This reduction develops from the nucleation mode either reducing in concentration or the particle sizes within the mode are being reduced below the detection limit of the DMS500. This results in reduction in the PM number concentration as the engine load increases. Generally there is also a reduction in the mass concentration produced as the engine loading is increased. Further analysis of the medium load dataset indicated that the sample flow being supplied to the DMS500 was on the lower boundary considered acceptable for reliable results. This, in conjunction with the very high concentration of small particles, and therefore a need for high dilution, may have compromised the integrity of the sample and resulted in lower than expected concentration of larger size particles and therefore lower than expected mass concentration results.

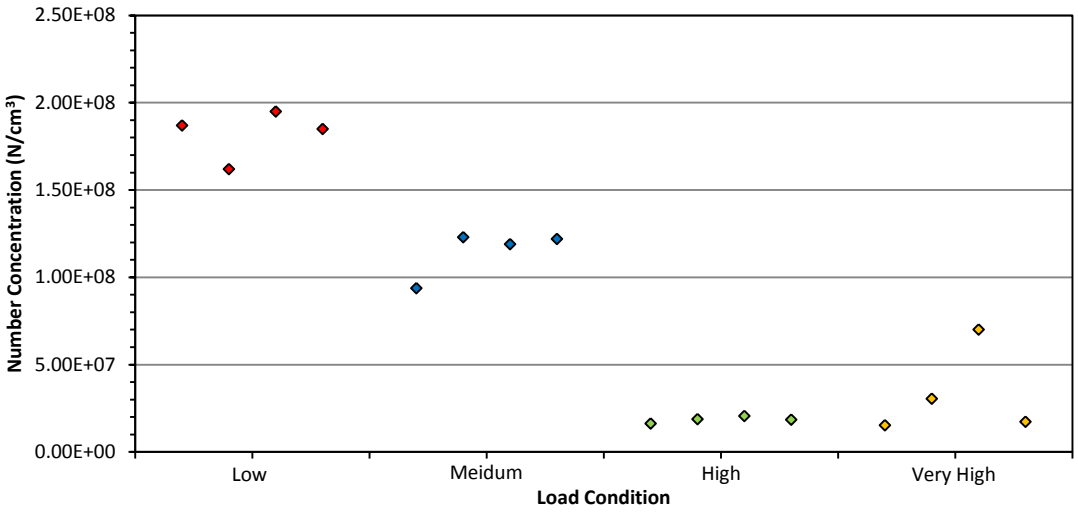

Figure 5.75: Total number concentration for low, medium, high, and very high engine load condition during homogeneous charge SOI testing.

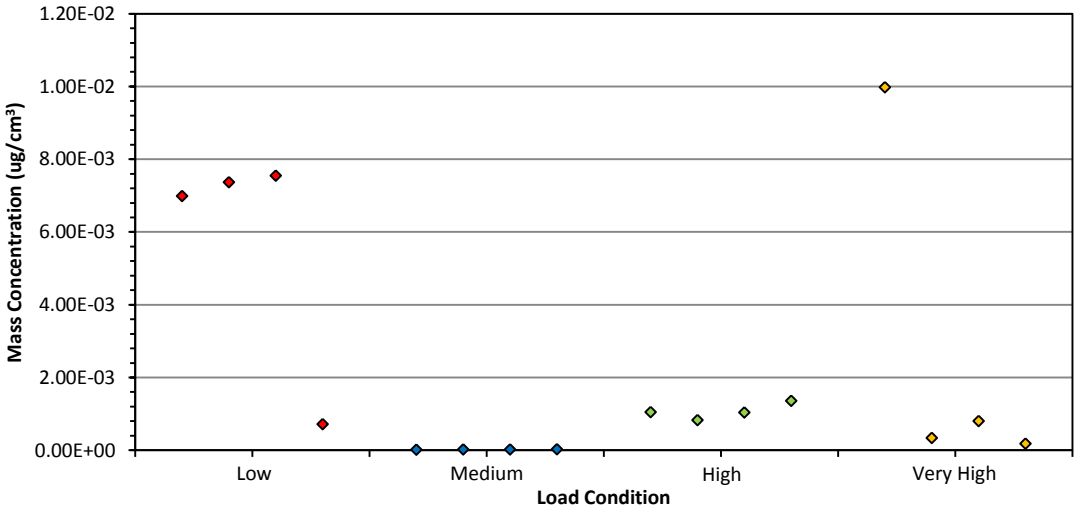

Figure 5.76: Total mass concentration for low, medium, high, and very high engine load condition during homogeneous charge SOI testing.

5.7.2 Results: Stratified Charge Operation

During stratified charge operation fuel injection occurs very late in the compression stoke of the piston. This is reflected in the operational conditions (low SOI values) listed in Table 5.13 which are identical in terms of fuel injection pressure to those used in the homogenous charge experimentation cycle. However for successful stratified

operation the number of fuel injections was increased to 2 and a quantity of EGR was applied. The SOI for these experiments was varied between 30 and 45 DBTDC.

Table 5.13: Start of injection settings for stratified operation conditions.

Test Point	Engine Parameters			
	FP	**Number of Injections**	**EGR Rate**	**SOI**
1	140	2	27	30
2	140	2	27	35
3	140	2	27	40
4	140	2	27	45

5.6.2.1 Low Engine Loading (1500 rpm, 2.62 bar)

The size spectra produced during the low load condition showed a sequence of bi-modal distributions which initially have a high concentration of small particles (≈10nm) and a secondary peak or larger particles (≈75nm).

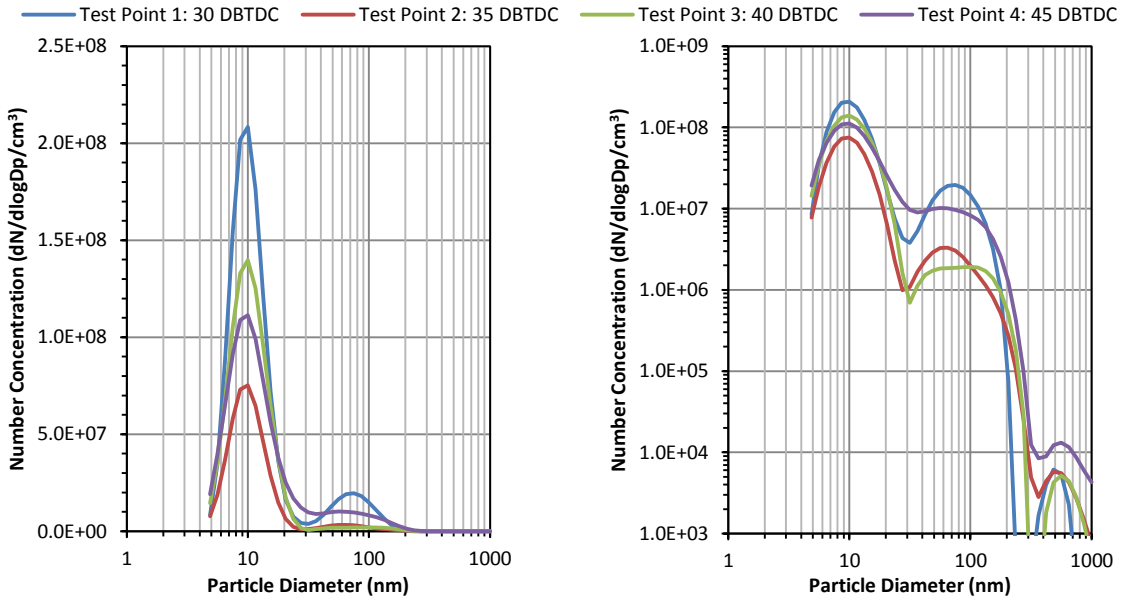

Figure 5.77: DMS500 size spectra for variable start of injection times at stratified charge low load condition: (a) linear y-axis scale, (b) logarithmic y-axis scale.

Total number and mass concentrations reflect the changing size spectra whereby concentration levels decrease before increasing again towards the initial starting levels.

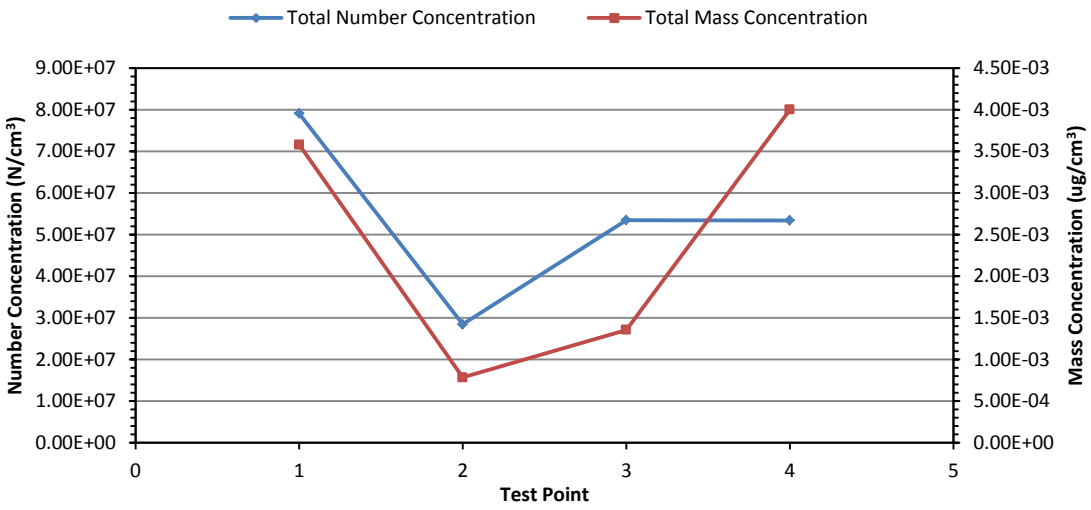

Figure 5.78: Number and mass concentrations measured for varying start of injection times at stratified low load condition.

Medium Engine Loading (2000rpm, 2bar)

During medium load operation bi-modality is again observed in the PM size spectra. As was observed during low load operation, the conditions operating with the minimum and maximum SOI values produce very different PM size distributions. Maintaining stability and optimisation of stratified charge engine modes can prove difficult and therefore extending SOI into these regions may be having a negative effect on engine performance (increased likelihood of knocking and smoke production).

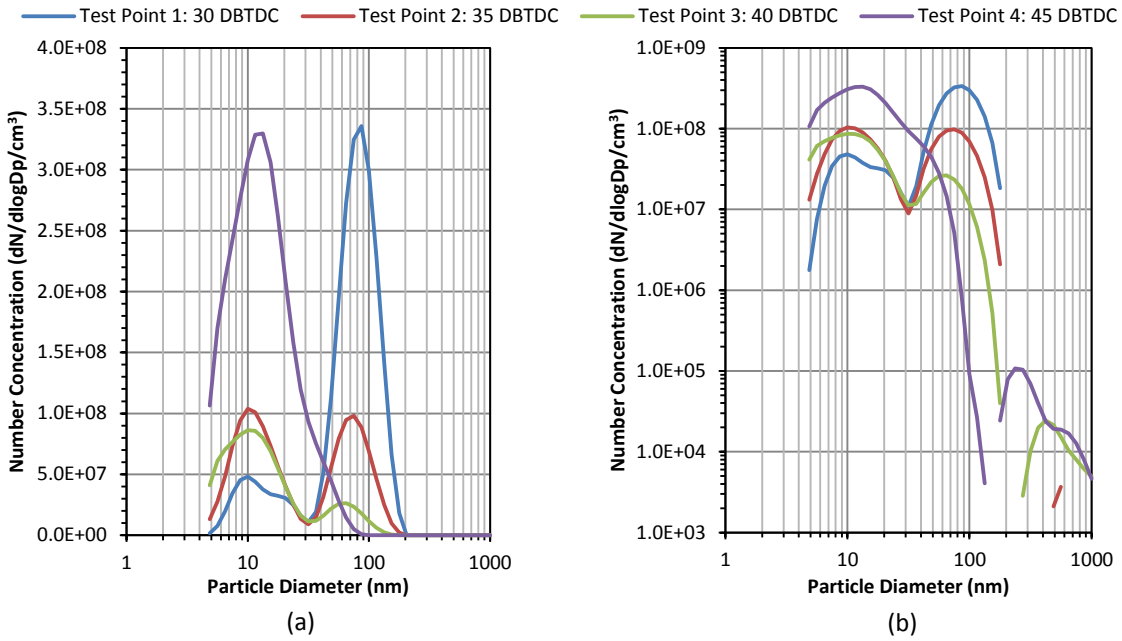

Figure 5.79: DMS500 size spectra for variable start of injection times at stratified medium load condition: (a) linear y-axis scale, (b) logarithmic y-axis scale.

Figure 5.80 shows that as the SOI is increased (earlier injection) the mass concentration generated is reduced. This is consistent with the production of reduced agglomeration mode particulates.

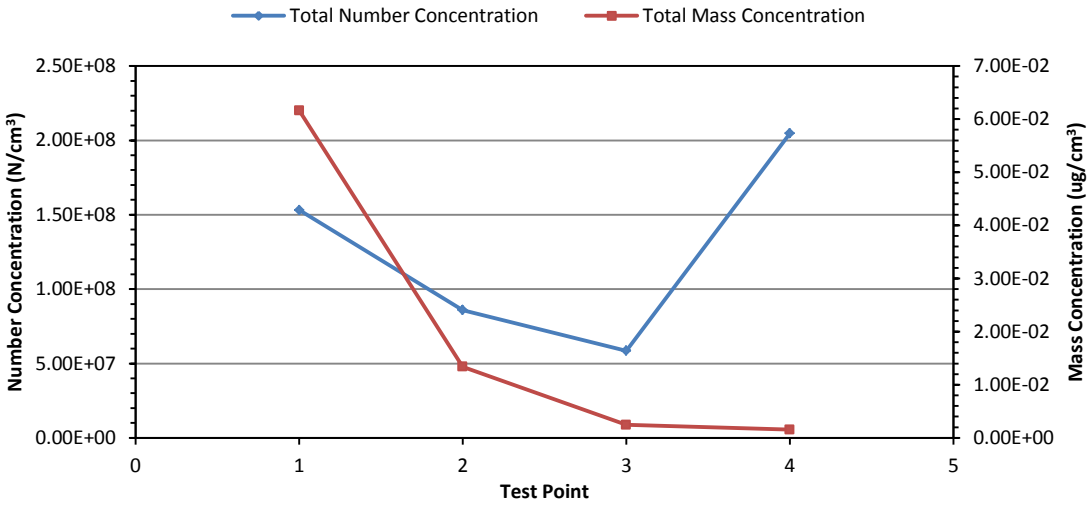

Figure 5.80: Number and mass concentrations measured for varying start of injection times at stratified charge medium load condition.

5.6.2.2 High Engine Loading (2000 rpm, 5 bar)

Two test points for the high engine load experimental range are significantly different from all other test points in terms of number and mass concentration. This may suggest that the engine settings used during these cycles are less stable than those previously observed. The size spectrums for test points 1 and 2 show a high concentration of large particles. This size mode decreases throughout the experimental range which reduces the number and mass concentration down to similar levels seen in the previous test conditions.

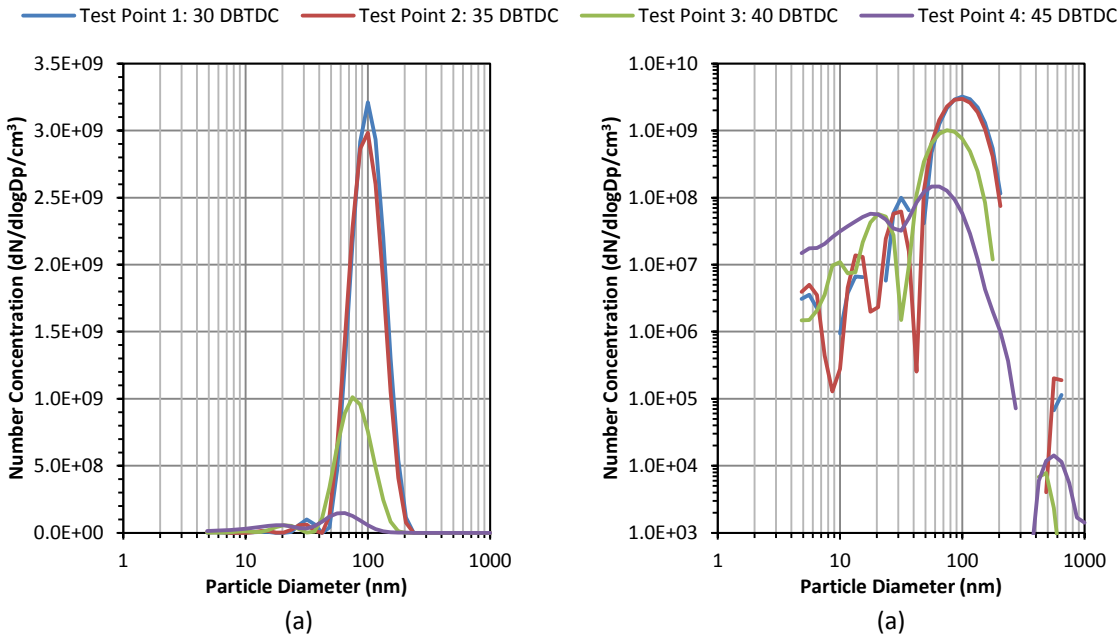

Figure 5.81: DMS500 size spectra for variable start of injection times at stratified charge high load condition: (a) linear y-axis scale, (b) logarithmic y-axis scale.

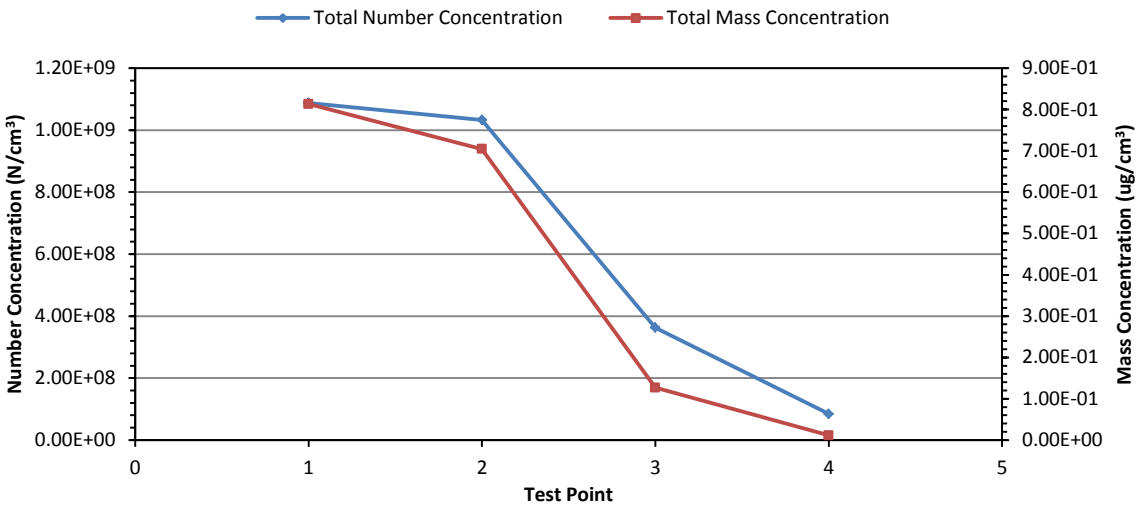

Figure 5.82: Number and mass concentrations measured for varying start of injection time at stratified charge high load condition.

A summary of the all the average number and mass concentrations which were recorded during experimentation into how varying the SOI timing affected the production of PM while operating in a stratified charge mode at multiple loading conditions is provided in Table 5.14.

Table 5.14: Summary of all number and mass concentrations at each engine load and start of injection condition during stratified charge operation.

Test Point	Total Number Concentration (N/cm^3)	Total Mass Concentration ($\mu g/cm^3$)
	Low Load	
1: 330 DBTDC	7.91×10^{7}	3.58×10^{-3}
2: 300 DBTDC	2.85×10^{7}	7.84×10^{-4}
3: 270 DBTCD	5.35×10^{7}	1.35×10^{-3}
4: 240 DBTDC	5.34×10^{7}	4.00×10^{-3}
	Medium Load	
1: 330 DBTDC	1.53×10^{8}	6.16×10^{-2}
2: 300 DBTDC	8.59×10^{7}	1.34×10^{-2}
3: 270 DBTCD	5.86×10^{7}	2.46×10^{-3}
4: 240 DBTDC	2.05×10^{8}	1.54×10^{-3}
	High Load	
1: 330 DBTDC	1.09×10^{9}	8.13×10^{-1}

2: 300 DBTDC	1.03 x10^{9}	7.04 x10^{-1}
3: 270 DBTCD	3.62 x10^{8}	1.27 x10^{-1}
4: 240 DBTDC	8.45 x10^{7}	1.15 x10^{-2}

Total number and mass concentrations measured at all experimental test conditions are shown in Figure 5.83 and Figure 5.84. Number concentration levels remain fairly stable across all engine loadings apart from the two test point previously discussed at high load. This is also true for the mass concentrations which are emitted during this series of experiments.

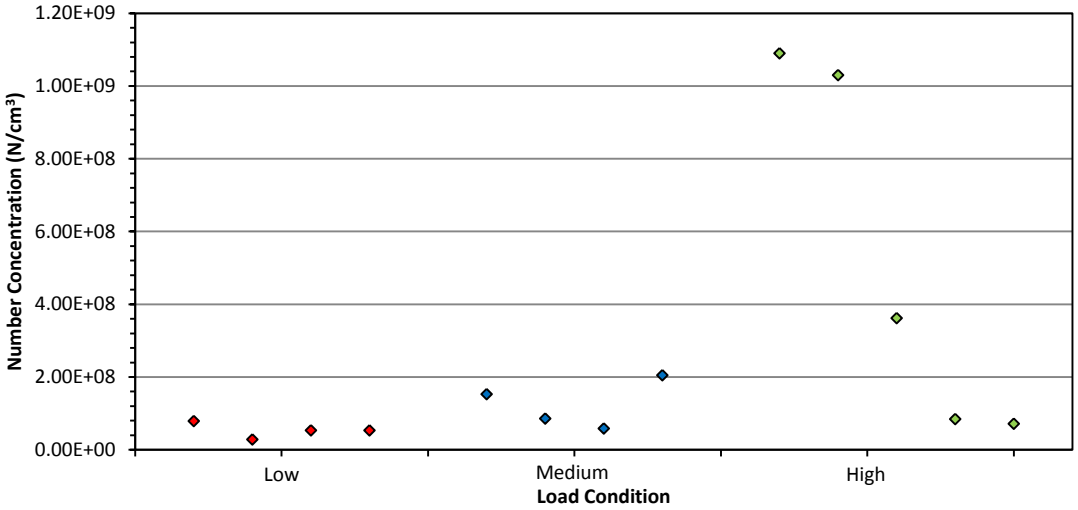

Figure 5.83: Total number concentration for low, medium, high engine load condition during stratified charge SOI testing.

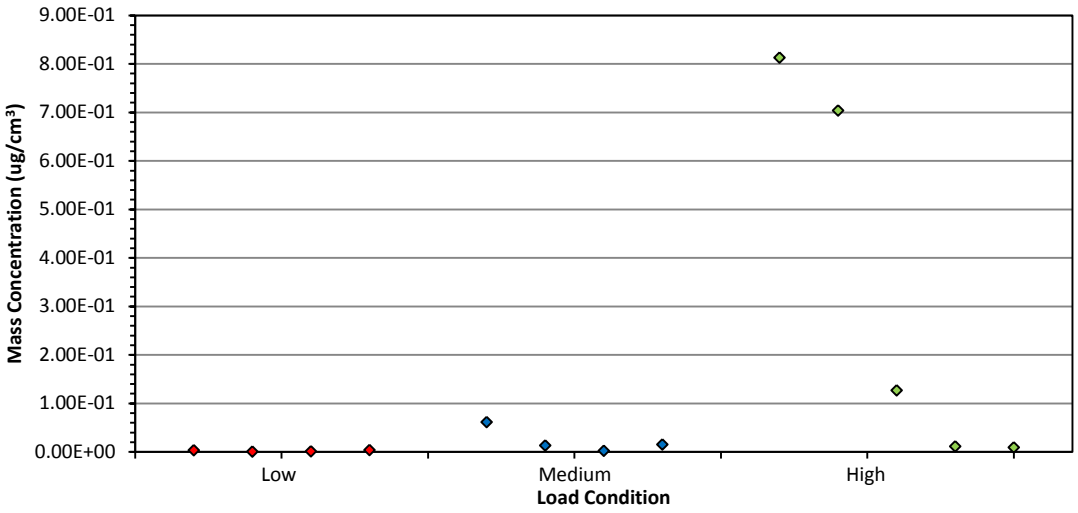

Figure 5.84: Total mass concentration for low, medium, and high engine load condition during stratified charge SOI testing.

5.8 Number of Fuel Injections

Another methodology of controlling air-fuel mixing in-cylinder conditions is to introduce fuel in a number of discreet injections. Increasing the number of fuel injections has been shown to give considerable reductions in fuel consumption at all engine loading when compared to homogenous charge operation [95]. In this experimental campaign PM analysis was performed during stratified charge operation of the MCRE at for three loading conditions, the details of which are listed in Table 5.15.

Table 5.15 Number of fuel injection settings for stratified charge mode operation conditions.

Test Point	Engine Parameters			
	FP	**Number of Injections**	**EGR Rate**	**SOI**
1	140	1	27	37
2	140	2	27	37
3	140	3	27	37
4	140	4	27	37
5	140	5	27	37

5.8.1 Result: Stratified Charge Operation

5.8.1.1 Low Engine Loading (1500 rpm, 2.62 bar)

As the number of injections is increased the PM size spectra produced show nucleation mode peaks at approximately 10 and 100nm respectively. At higher numbers of fuel injections (>3) there is a decreasing the nucleation mode and an increase in the agglomeration mode observed.

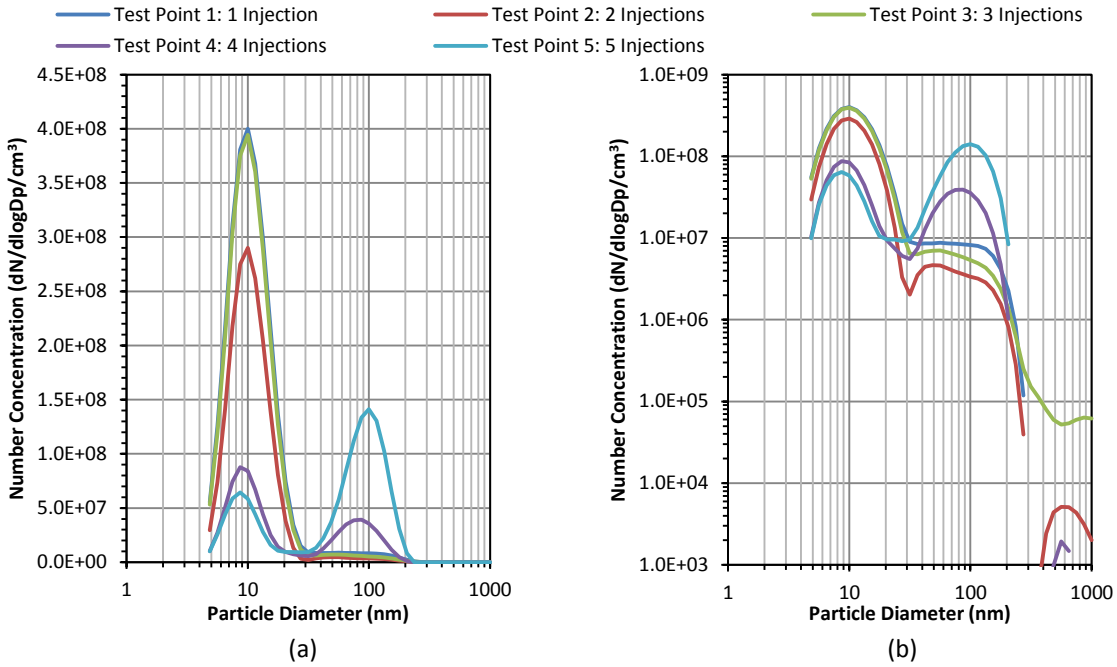

Figure 5.85: DMS500 size spectra for variable number of fuel injections at stratified charge low load condition: (a) linear y-axis scale, (b) logarithmic y-axis scale.

Variation in the PM size spectra is consequentially responsible for the increase in the mass concentration towards the end of the test range. Total number concentration generally decreases as number of fuel injections increases.

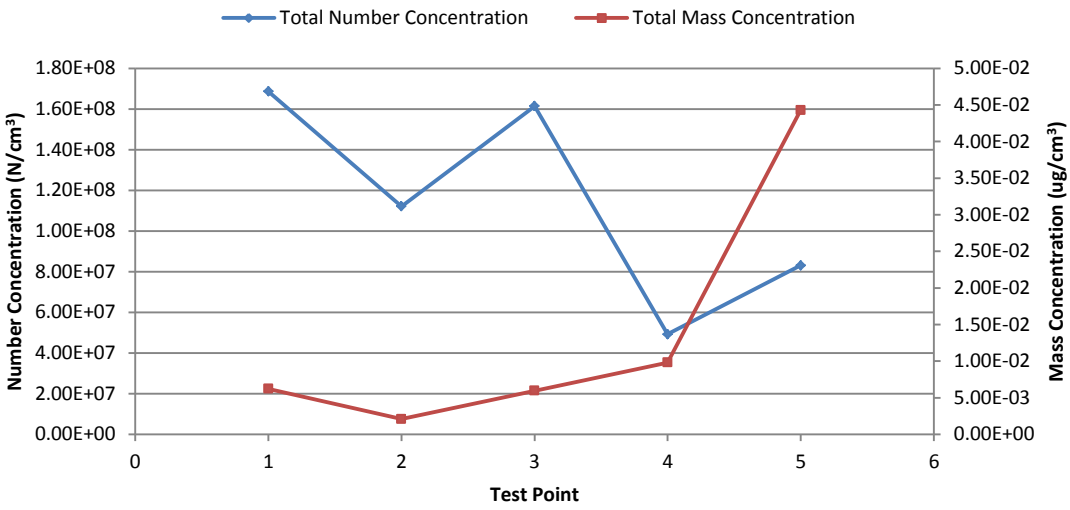

Figure 5.86: Number and mass concentrations measured for variable numbers of fuel injections at stratified charge low load condition.

5.8.1.2 Medium Engine Loading (2000 rpm, 2 bar)

Figure 5.87 shows that at the medium load condition similar PM size spectra as that observed at low loading were generated. As the number of fuel injection is increased the concentration of larger particles also increases.

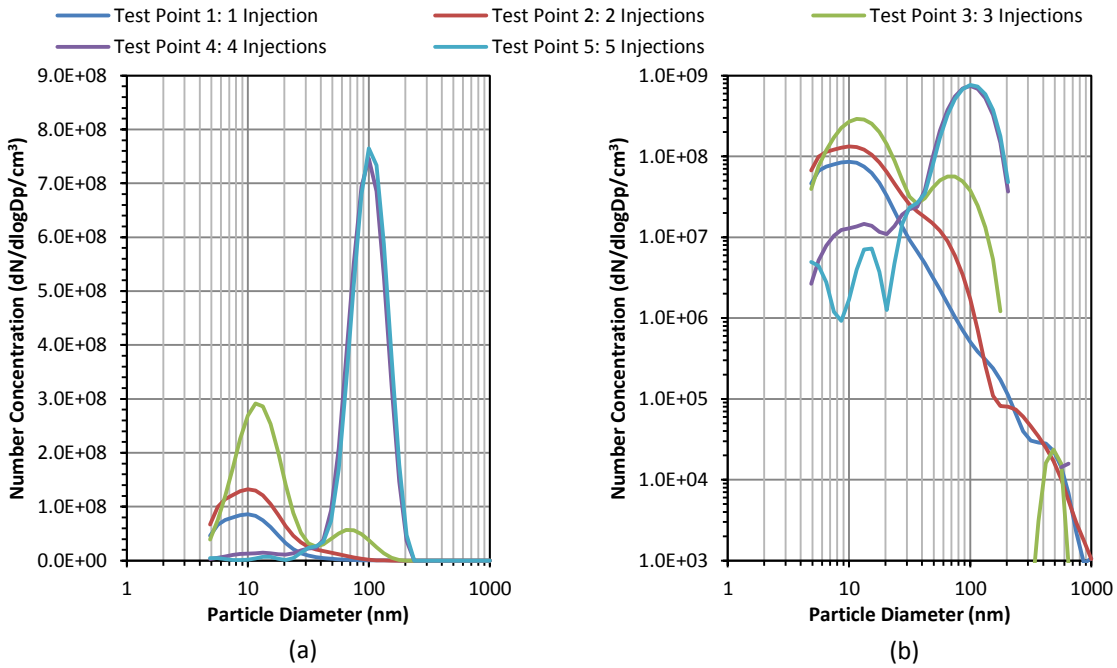

Figure 5.87: DMS500 size spectra for variable number of fuel injections at stratified charge medium load condition: (a) linear y-axis scale, (b) logarithmic y-axis scale.

As noted at the low load condition, the consequence of the increasing particle concentration in the ≈100nm size region produced a fairly significant increase in the PM mass and number concentration.

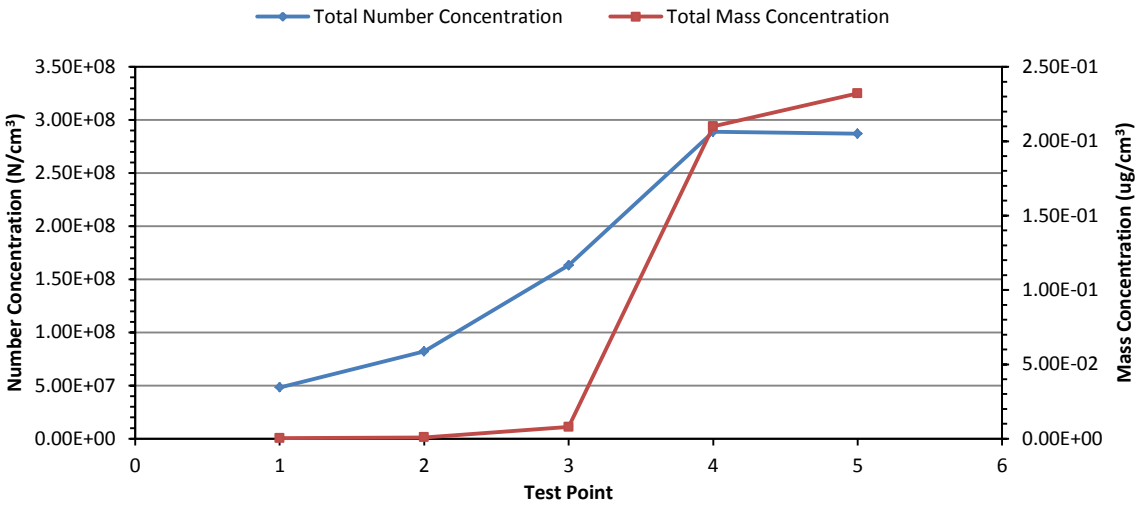

Figure 5.88: Number and mass concentrations measured for variable numbers of fuel injections at stratified charge medium load condition.

5.8.1.3 High Engine Loading (2000 rpm, 5 bar)

The size spectra produced at the highest tested loading were consistent and displayed bi-modality with a dominant peak in the larger particle size range of 70 - 90nm. As for the previous test conditions as the number of injection was increased the development of higher concentrations of agglomeration mode particles was observed.

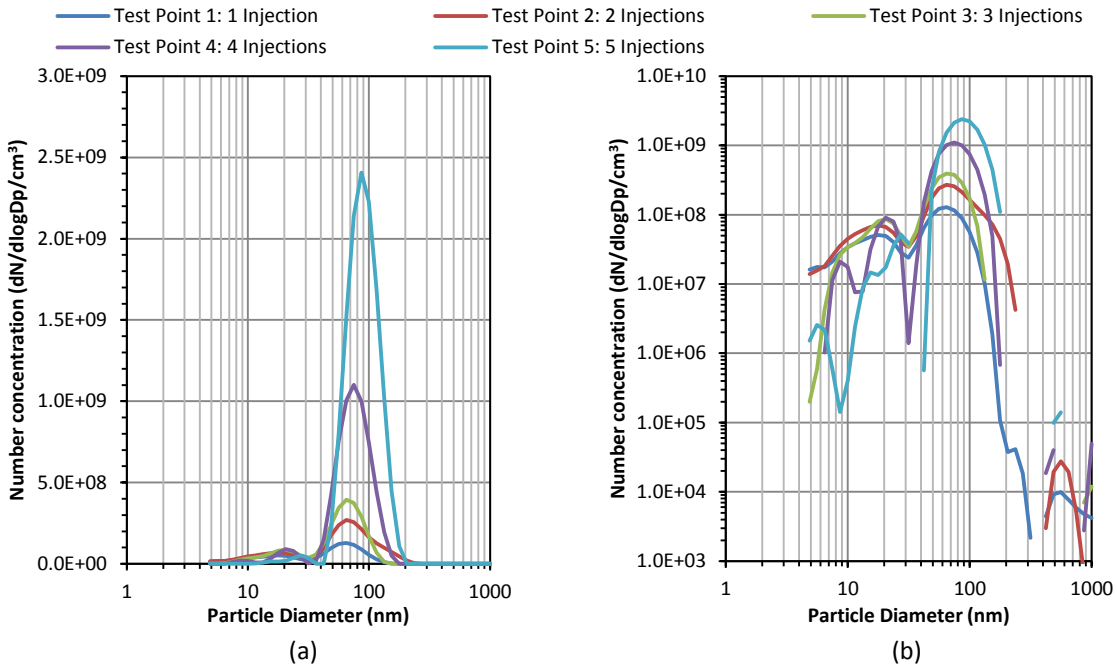

Figure 5.89: DMS500 size spectra for variable number of fuel injections at stratified charge high load condition: (a) linear y-axis scale, (b) logarithmic y-axis scale.

As a result of the concentration of the agglomeration mode increasing as the number of fuel injections increases the recorded mass and number output also increased.

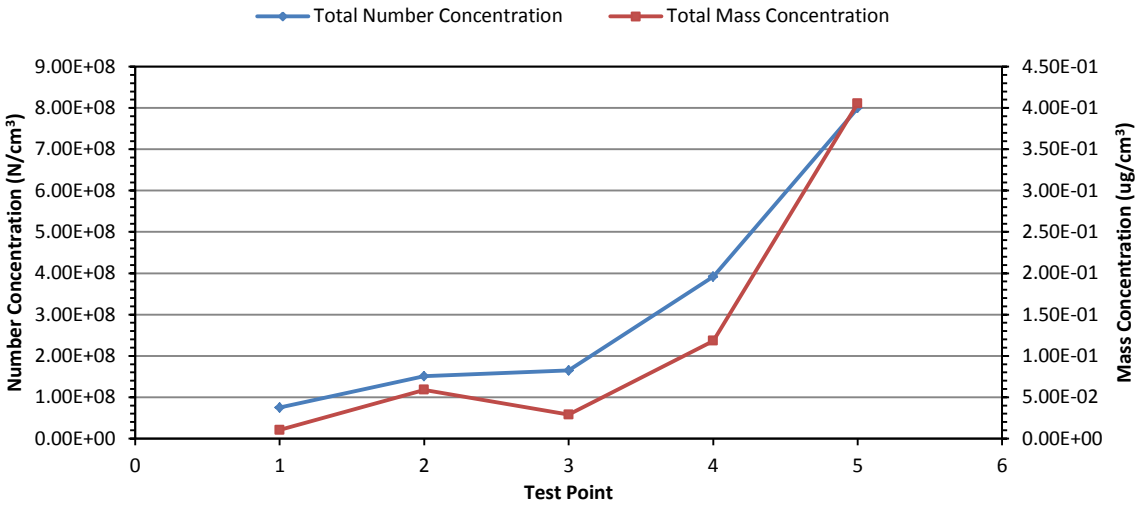

Figure 5.90: Number and mass concentrations measured for variable numbers of fuel injections at stratified high load condition.

A summary of all average number and mass concentrations measured experiments of how varying the number of fuel injections affected the production of PM while

operating in a stratified charge mode at multiple loading conditions is provided in Table 5.16.

Table 5.16: Summary of all number and mass concentrations at each engine load and number of injection condition during stratified charge operation.

Test Point	Total Number Concentration (N/cm^3)	Total Mass Concentration ($\mu g/cm^3$)
	Low Load	
1: 1 injection	1.69×10^{8}	6.23×10^{-3}
2: 2 injections	1.12×10^{8}	2.10×10^{-3}
3: 3 injections	1.61×10^{8}	5.96×10^{-3}
4: 4 injections	4.93×10^{7}	9.82×10^{-3}
5: 5 injections	8.31×10^{7}	4.43×10^{-2}
	Medium Load	
1: 1 injection	4.83×10^{7}	3.04×10^{-4}
2: 2 injections	8.21×10^{7}	8.74×10^{-4}
3: 3 injections	1.63×10^{8}	7.92×10^{-3}
4: 4 injections	2.89×10^{8}	2.10×10^{-1}
5: 5 injections	2.87×10^{8}	2.32×10^{-1}
	High Load	
1: 1 injection	7.47×10^{7}	1.04×10^{-2}
2: 2 injections	1.51×10^{8}	5.90×10^{-2}
3: 3 injections	1.65×10^{8}	2.89×10^{-2}
4: 4 injections	3.92×10^{8}	1.18×10^{-1}
5: 5 injections	8.00×10^{8}	4.05×10^{-1}

The average number concentration produced across all loading conditions were fairly consistent and in the $1x10^8$ to the $3x10^8$ N/cm^3 range with the exception of the highest number of injection conditions during high engine loading. Changing the number of injections had little effect on the PM number concentrations at low engine loading. At medium and high load conditions, as the number of injections was increased the PM number concentration also increased. The increase in number concentration development mainly from an increasing of particles in the 80nm range and therefore the result on PM mass output was affected considerably. For all engine loadings, as the

number of fuel injections was increased the mass concentrations produced also increased.

It is proposed that increasing the number of fuel injections number of fuel injections is inducing fuel rich zones to develop later in the injection cycle and there incomplete combustion of the fuel charge is occurring. It is also possible that as the later fuel injections are impinging on the cylinder walls and piston crown resulting in soot formation.

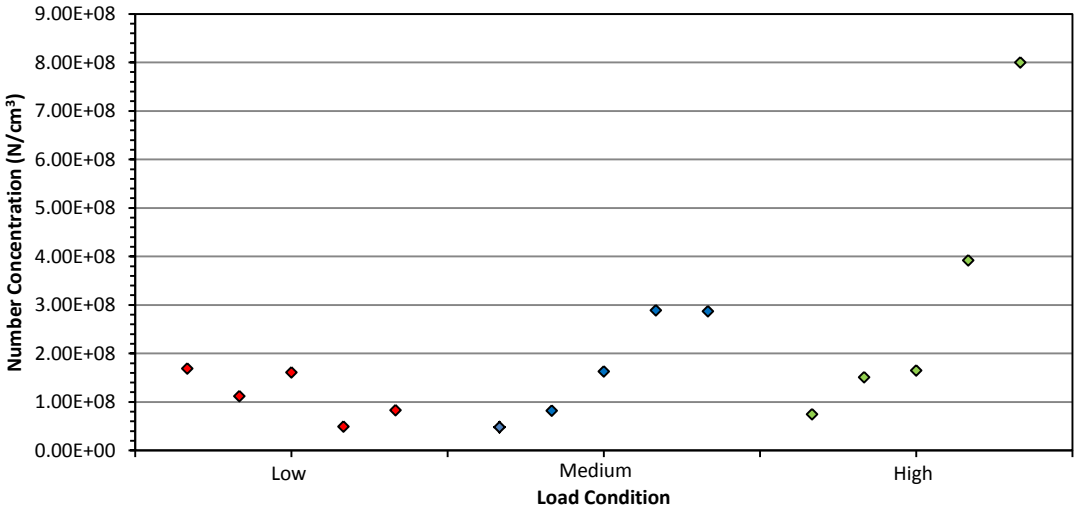

Figure 5.91: Total number concentration for low, medium, and high engine load condition during stratified charge number of fuel injection testing.

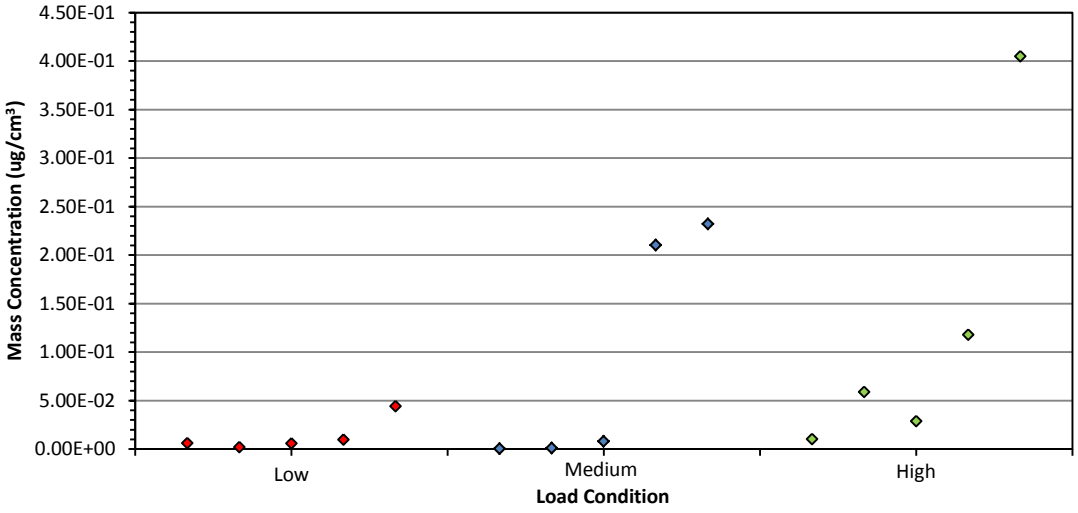

Figure 5.92: Total mass concentration for low, medium, and high engine load condition during stratified charge number of fuel injection testing.

5.9 Exhaust Gas Recirculation

EGR has been used extensively in the diesel automotive industry to reduced NO_x emissions through the reduction of in-cylinder temperature [114]. Studies have also shown NO_x reductions for GDI engines however maximum EGR rates have been presented as high cyclic variations, misfires, a decrease of total efficiency and an increase of HC emissions can result [115]. This problem can be improved by stratified charge EGR operation. This research project investigated how the introduction of higher rates of EGR influenced the PM emission from the MCRE.

Table 5.17: Exhaust gas recirculation settings for stratified charge mode operation conditions.

Test Point	Engine Parameters			
	FP	**Number of Injections**	**EGR Rate**	**SOI**
1	140	2	10	37
2	140	2	30	37
3	140	2	50	37
4	140	2	70	37

5.9.1 Results: Stratified Charge Operation

5.9.1.1 Low Engine Loading (1500 rpm, 2.62 bar)

The size spectra produced while operating at low loading EGR experiments show a bi-modal structure with peaks at approximately 10 - 15nm and 60 - 70nm. As the rate of EGR is increased the smaller size peak is reduced with little change in the larger size mode.

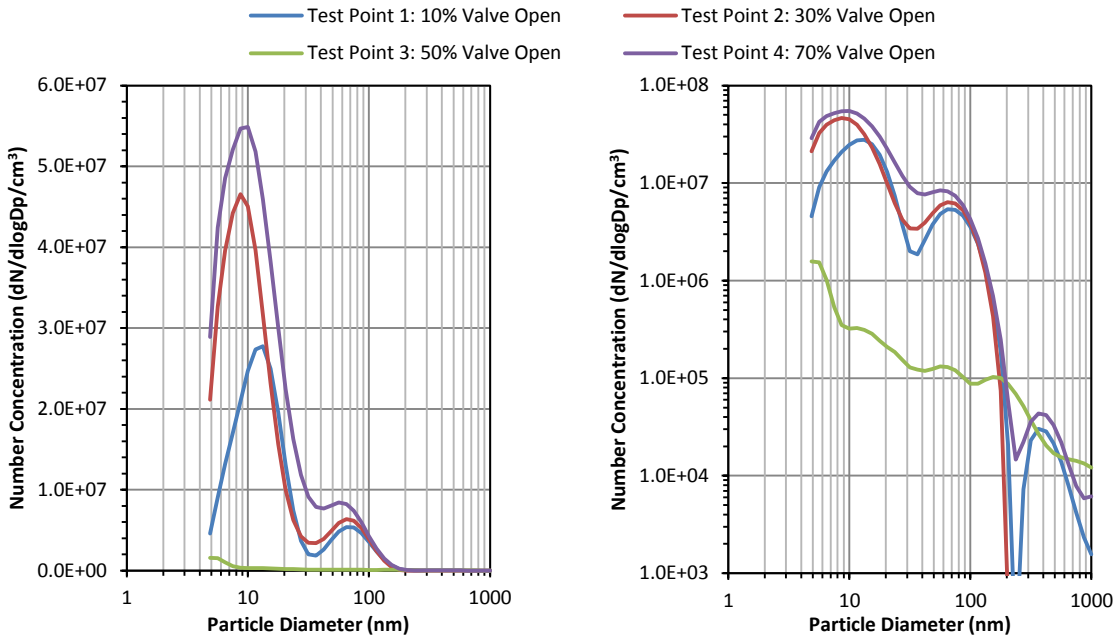

Figure 5.93: DMS500 size spectra for variable exhaust gas recirculation rates at stratified charge low load operation: (a) linear y-axis scale, (b) logarithmic y-axis scale.

There is an anomaly in this date set, that being Test Point 3 where the number concentration is unexpectedly low. Mass concentration values are fairly consistent throughout the test range at approximately $9x10^{-4}$ µg/cm^3.

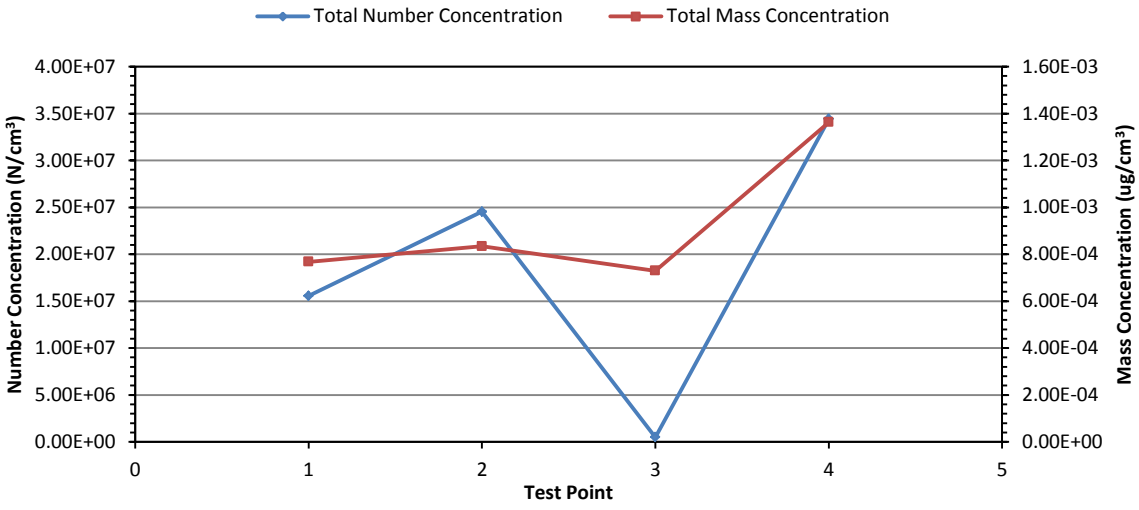

Figure 5.94: Number and mass concentrations measured for variable exhaust gas recirculation rates at stratified charge low load condition.

5.9.1.2 Medium Engine Loading (2000 rpm, 2 bar)

Figure 5.95 shows how PM size distributions varied throughout the medium load EGR experimentation. The size spectra remain fairly consistent in terms of shape and size mode peak position (10nm nucleation mode and 65nm agglomeration mode).

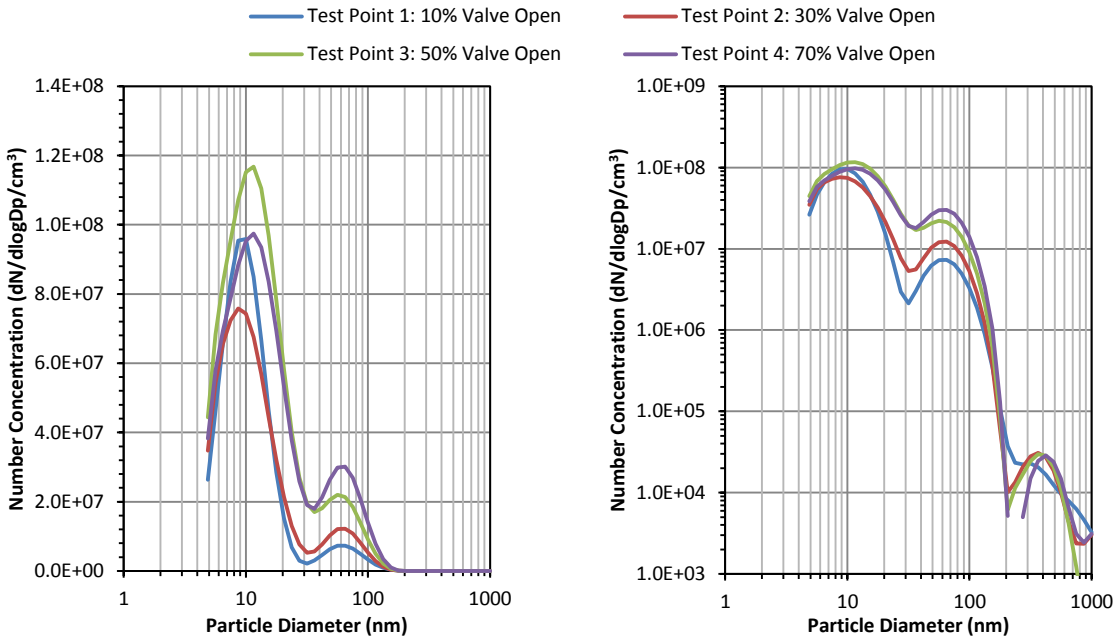

Figure 5.95: DMS500 size spectra for variable exhaust gas recirculation rates at stratified medium load operation: (a) linear y-axis scale, (b) logarithmic y-axis scale.

During the medium load operation as the EGR rate is increased the total number concentration recorded tends to increase. The mass concentration also increases as the presence of the larger size mode developed.

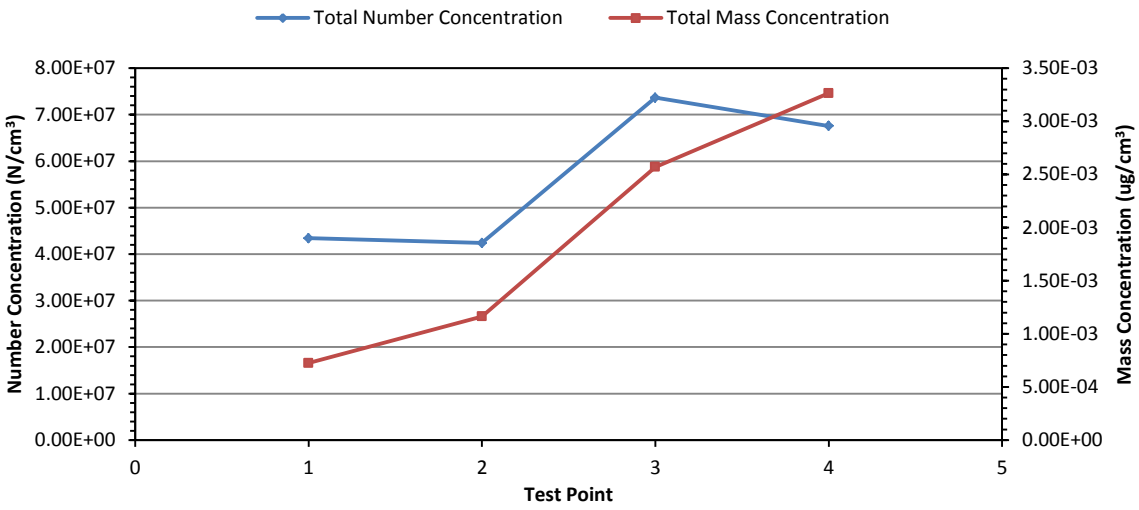

Figure 5.96: Number and mass concentrations measured for variable exhaust gas recirculation rates at stratified charge medium load condition.

5.9.1.3 High Engine Loading (2000 rpm, 5 bar)

The size spectral results from the high loading conditions test conditions are heavily affected by the unusually high concentration levels observed in test point 5. This test point is at the extremity of the test series and therefore the risk of engine instability is high. When plotted on a log-scale PM other test condition size distributions displayed high concentration of particle across a broad size range (10 - 200nm).

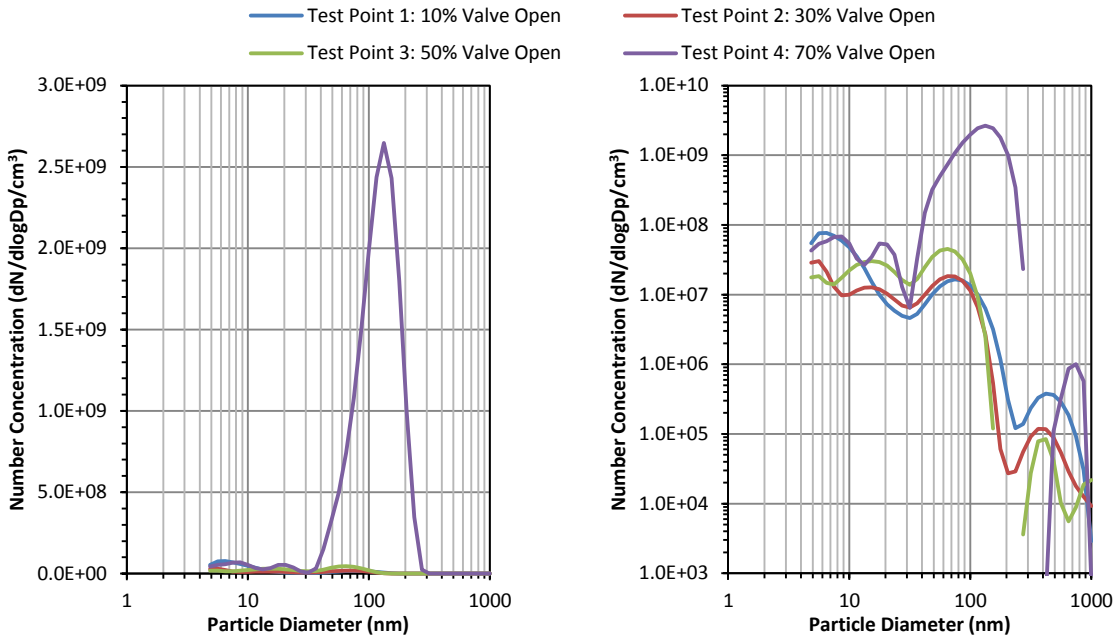

Figure 5.97: DMS500 size spectra for variable exhaust gas recirculation rates at stratified high load operation: (a) linear y-axis scale, (b) logarithmic y-axis scale.

With the exclusion of test point 4 from the EGR series data set the number and mass concentrations produced at this condition were observed to be stable at approximately $2x10^{7}$ N/cm^{3} and $8x10^{-3}$ µg/cm^{3} respectively.

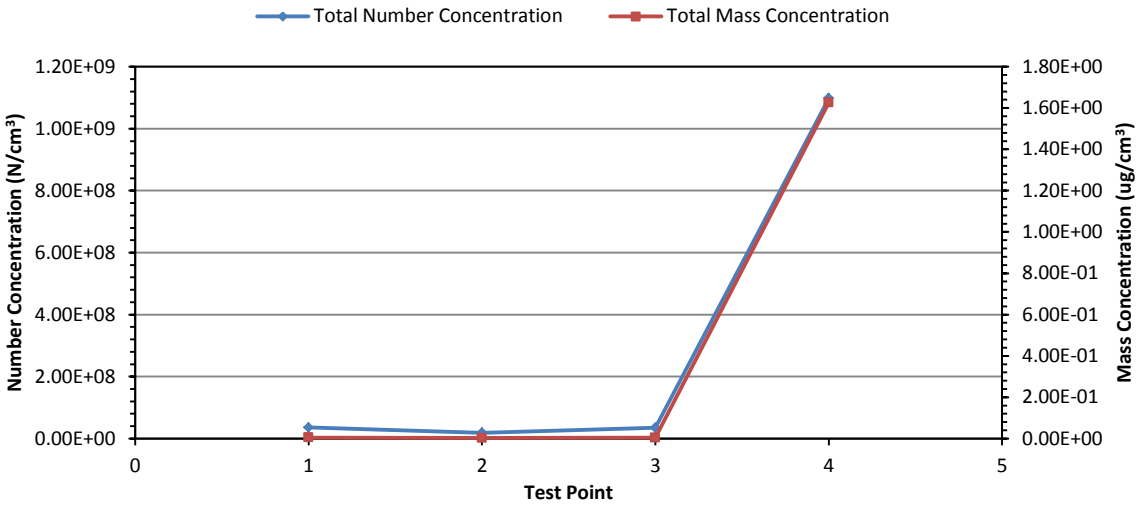

Figure 5.98: Number and mass concentrations measured for variable exhaust gas recirculation rates at stratified high load condition.

A summary of all average number and mass concentrations which were recorded during experimentation into how the rate of EGR affected the production of PM while

operating in a stratified charge mode at multiple loading conditions is provided in Table 5.18.

Table 5.18: Summary of all number and mass concentrations at each engine load and number of injection condition during stratified charge operation.

Test Point	Total Number Concentration (N/cm^3)	Total Mass Concentration ($\mu g/cm^3$)
	Low Load	
1: 10% valve open	1.56×10^{7}	7.67×10^{-4}
2: 30% valve open	2.45×10^{7}	8.34×10^{-4}
3: 50% valve open	4.88×10^{5}	7.30×10^{-4}
4: 70% valve open	3.44×10^{7}	1.36×10^{-3}
	Medium Load	
1: 10% valve open	1.56×10^{7}	4.34×10^{-4}
2: 30% valve open	2.45×10^{7}	4.24×10^{-3}
3: 50% valve open	4.88×10^{7}	7.36×10^{-3}
4: 70% valve open	3.44×10^{7}	6.76×10^{-3}
	High Load	
1: 10% valve open	3.59×10^{7}	7.67×10^{-3}
2: 30% valve open	1.85×10^{7}	8.34×10^{-3}
3: 50% valve open	3.47×10^{7}	7.30×10^{-3}
4: 70% valve open	1.10×10^{9}	1.36×10^{0}

All DMS500 total number and mass concentration results which were recorded during experimentation into how PM emission differed depending on the level of EGR employed during stratified charge operation on the MCRE are shown in Figure 5.99 and Figure 5.100. Total number concentrations throughout this series of experiments were stable excluding two anomalous test points. Mass concentration levels however were very sensitive to the increased EGR rates and rose considerably.

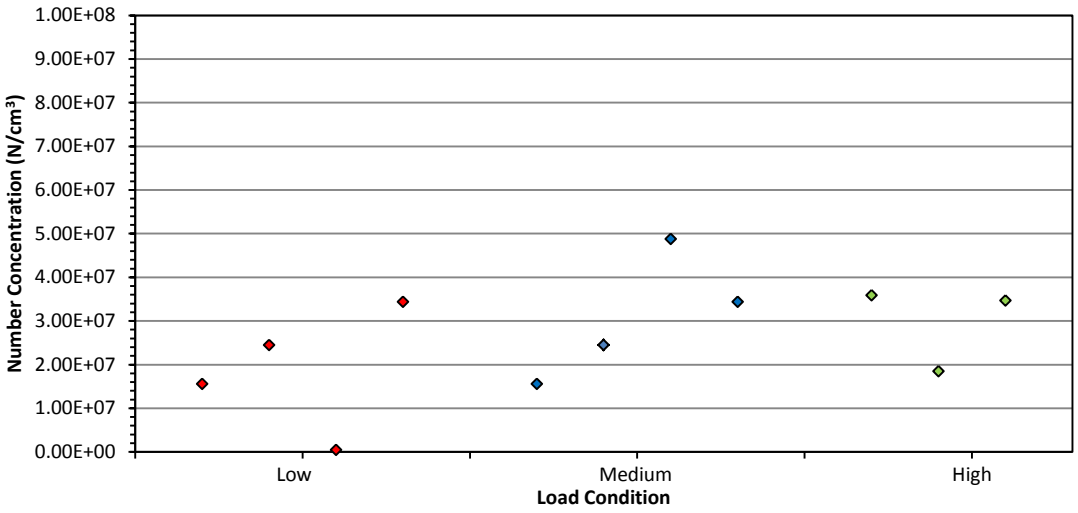

Figure 5.99: Total number concentration for low, medium, and high engine load condition during stratified charge number of fuel injection testing.

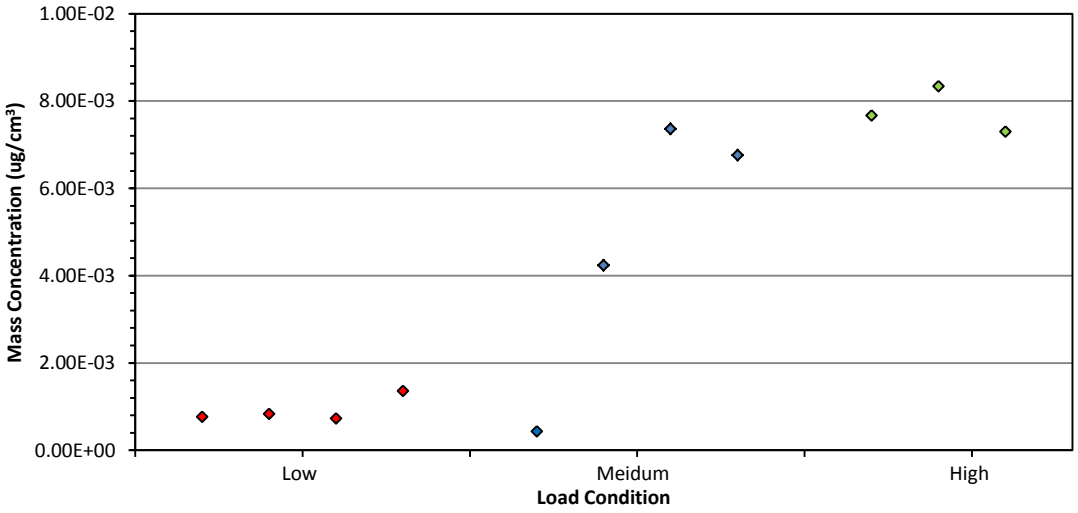

Figure 5.100: Total mass concentration for low, medium, and high engine load condition during stratified charge number of fuel injection testing.

5.10 Summary of Multi-Cylinder Hydra Engine Testing Results

This research programme has explored the variation in PM emission due to a number of different engine parameters. The first of the tested engine parameters was fuel injection pressure. As fuel injection pressure was increased during homogenous charge operation a reduction in both PM number and mass concentration was recorded for all

load conditions apart from the lowest evaluated test load. This is in agreement with experimentation of other researchers [77] and the result of improved fuel atomisation and therefore improved combustion efficiency. Consequentially DMS500 size spectral analysis of test conditions showed that as fuel injection pressure was increase the concentration of agglomeration mode particulate was reduced. When operating in a stratified charge engine mode there was not a significant effect on PM number output however PM mass concentration was reduced as fuel injection pressure was increased. Very high concentrations of small particles (<10nm) were recorded at all test conditions. These particles are considered to be organic carbon formations which have developed from unburnt fuel. When operating in a stratified charge mode the PM number concentrations some variation was observed deepening on the loading condition however no significant change was found as the fuel injection pressure varied. PM mass concentrations followed the same trend as that seen in the homogenous charge tests and decreased as the fuel injection pressure increased. Generally PM emissions were found to be higher when operating in a stratified charge configuration.

Experimentation into how SOI influenced PM emissions showed that during homogenous operation there was little change in the PM number concentration output as the injection was advanced or retarded. This was also true for the mass concentration produced however at the extreme ends of the operation test range (earliest and latest injection point) engine instability caused far higher or lower PM measurements to be recorded than the observed average. The same trends were true stratified charge operation however there was a notable difference in the PM size distributions produced in both engine configurations. Overall PM emissions were found to be higher when operating in a stratified charge mode.

Increasing the number of fuel injections during each fuel charge event was shown to cause an increase in PM number and mass concentration at all examined engine load conditions. Increasing agglomeration mode particles (soot) was the cause of this increase and therefore operating in this style would be unfavourable from an emission standpoint.

PM number concentrations were found to remain stable across all engine loading while the EGR was increased. At low loading there was no significant change in mass concentration however as engine load was increased high PM mass output was recorded. This is a common problem when trying to reduce NO_x emissions through the reduction of combustion zone temperature there is a likelihood of incomplete fuel burn occurring.

Chapter 6

Development of an International Emission Sampling System for the Aviation Industry

The PMP established a methodology for the sampling, conditioning and measurement requirements of automotive PM emissions. The aviation industry has historically relied upon Annex 16 and smoke number for the certification of aviation gas turbines, practices which have now become outdated. The International Civil Aviation Organisation (ICAO) aims to address this issue and through the Committee on Aviation Environmental Protection (CAEP) has tasked the SAE E-31 Committee to develop a new a non-volatile PM measurement standard which is to be implemented in 2016.

This Chapter presents experimental results collected during experimental testing campaigns which have contributed to the development of this new sampling system. The experimental campaigns discussed have been funded by the European Aviation Safety Agency (EASA) and are known as the SAMPLE (Studying, Sampling and Measuring of Aircraft Particulate Emissions) suite of research projects. This collaboration was commissioned originally in 2008 and consists of a consortium of academic and industrial organisations.

Elements of results presented in this Chapter have been used in the formation of the SAMPLE 3 SC.01 and SC.02 reports [93,94] been have been published at the European Combustion Meeting in 2013 [116], and the ASME Gas Turbo Expo in 2014 [117].

6.1 Exhaust Sampling Systems

One of the greatest difficulties when attempting to make quantitative assessments of an engine exhaust is creating an appropriate sampling system. A basic sampling system will include a sample probe, sample condition suite and a transportation network. There are many factors which will influence how a sampling system is designed the most important of which is the emission source which is being examined. This is highlighted perfectly by the discrepancies between the sampling systems used to measure emissions in the aviation industry and those used within the automotive industry. The following sections discuss what the current state of emission sampling within both industries and how future developments may be introduced to improve them.

6.2 Sampling Aviation Gas Turbine Exhaust

Emission sampling from a gas turbine engine is a very challenging task as the sampling environment within the exhaust stream is extremely hostile. Obtaining a gaseous sample via the introduction of a probe is a relatively simple element of a sampling system design in comparison to the transport network required to move that sample a safe distance away from the engine to undergo further analysis. In addition to transporting the sample, it is crucial that the sample quality is maintained thus ensuring measurements made downstream of the sampling system are reflective of the input exhaust composition. As highlighted previously in Chapter 2 historically aviation exhaust PM has been regulated using the visibility metric SAE smoke number. This is currently being phased out due to its shortcomings and is being replaced by a far more robust and repeatable sampling approach being developed by the SAE E-31 Committee.

6.3 SAE E-31 Committee: Aims, Development and Future

Participants of the SAE E-31 Committee include original equipment manufacturers (OEMs), suppliers, propulsion emissions measurement companies, consulting firms,

and Government and academic researchers. The scope of the Committee is stated as being:

a) *To develop standards for the measurement of emissions from aircraft engines and combustion systems.*
b) *Review and maintain cognisance of standards for the measurement of aircraft engine emissions as developed, issued and/or recommended by Government, private agencies, or technical societies.*
c) *Encourage open and frequent dialogue and communication between the various agencies, companies and individuals within the aircraft industry including Government, industry and the academic community.*
d) *Provide a forum for the free and open exchange and expression of ideas, opinions and viewpoints on the subject of aircraft engine emissions measurement technology.*
e) *E-31 will not address the question of aircraft engine emission levels as they affect the environment nor will E-31 consider the question of control strategies to meet international, national or local ambient air quality standards.*

The most recent timeline of the progress of the Committees objectives was published following a meeting in San Diego in 2012. The group were able to show a technology readiness level (TRL) for the major areas of the project which must be completed to deliverer the Aerospace Recommended Practice (ARP) to CAEP by 2016, as illustrated by Figure 6.1. A ballot ready ARP is expected to be produced by 2014 in order to allow for further validation of the proposed sampling methodology and to allow comparisons to be made with the alternative systems currently under development in the US.

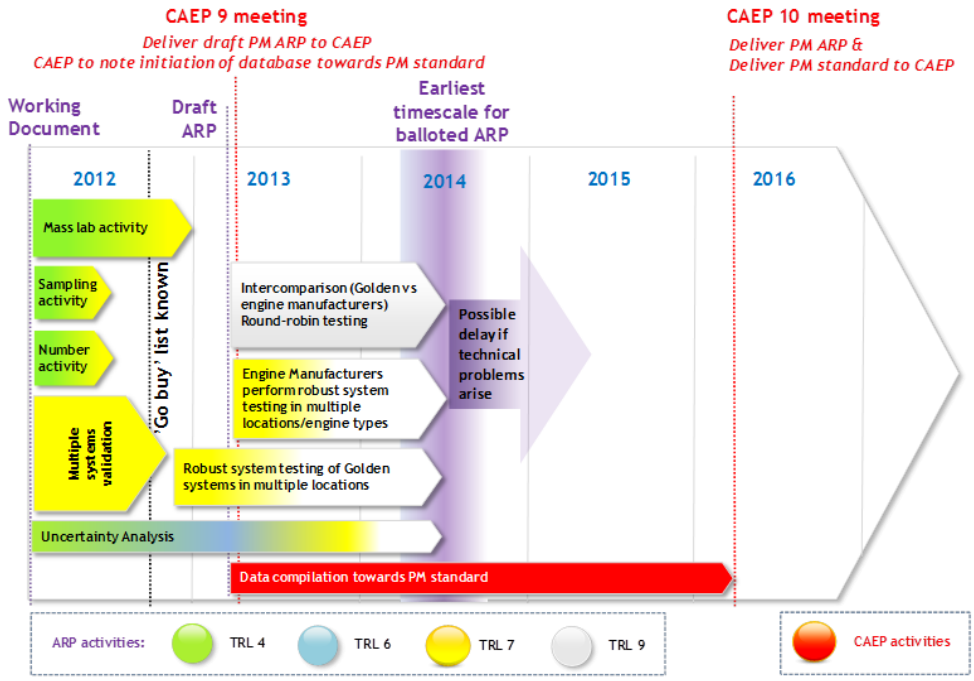

Figure 6.1: Timeline of the technology readiness levels of main objectives in the creation of a non-volatile PM sampling system ARP, reproduced from [94].

6.3.1 Current Iteration of the SAE E-31 Committee Sampling System

Progress on the development of a new aviation emission sampling system has been swift and thorough; a flow chart illustrating how the sampling system has been segmented into individual elements is shown in Figure 6.2. Splitting the system into three distinct sections has allowed for an element of operational flexibility in order to ensure the system can be utilised by all OEMs and regulating bodies. In this way the resulting ARP can stipulate how to produce a compliant sampling system that also allows a degree of tolerance to better suit OEMs current exhaust sampling setups. The most recent iteration of the sampling system which is being developed by the SAE E-31 Committee is shown in Figure 6.3.

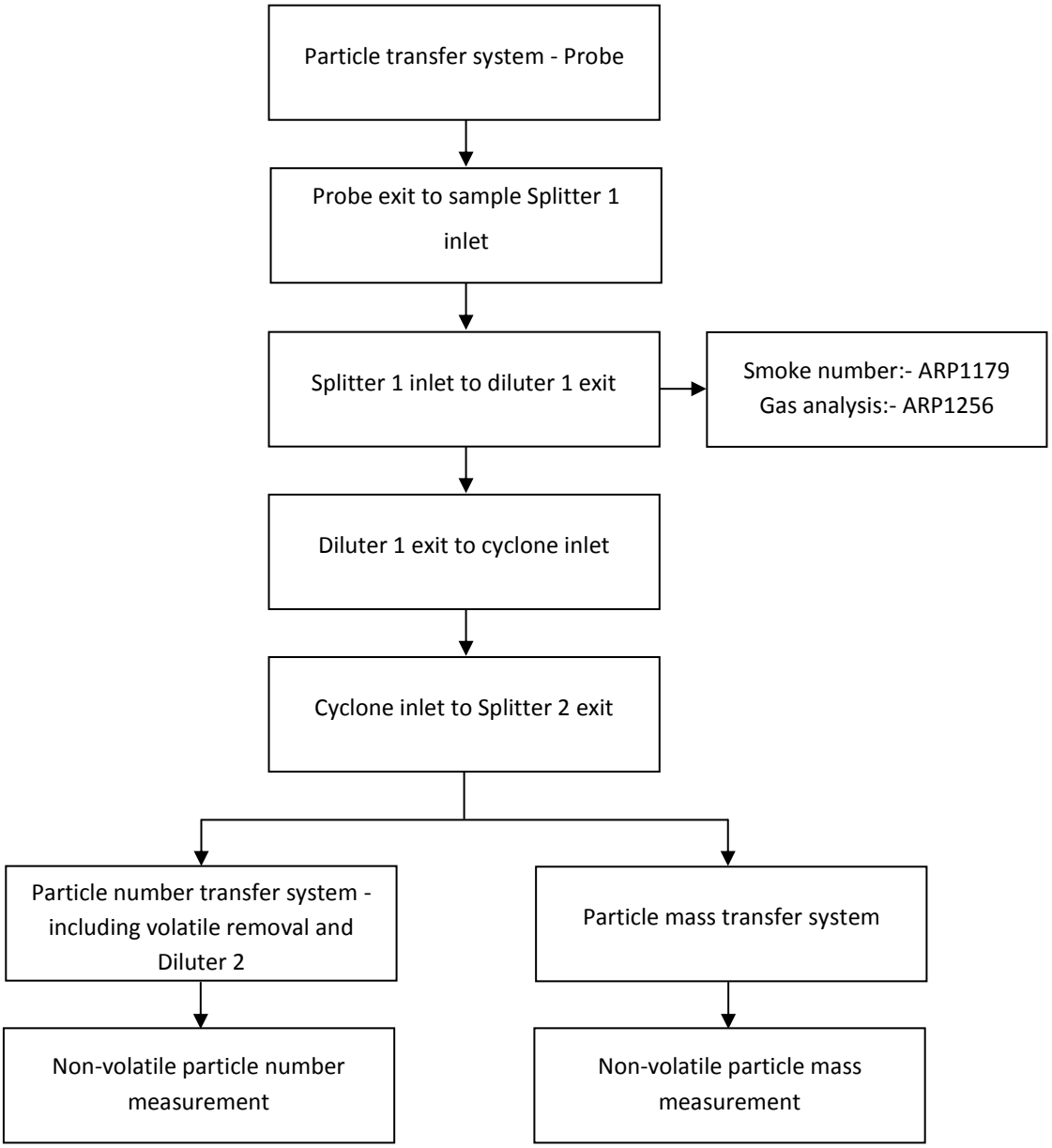

Figure 6.2: Flow chart of the SAE E-31 Committee sampling system methodology, adapted from [93].

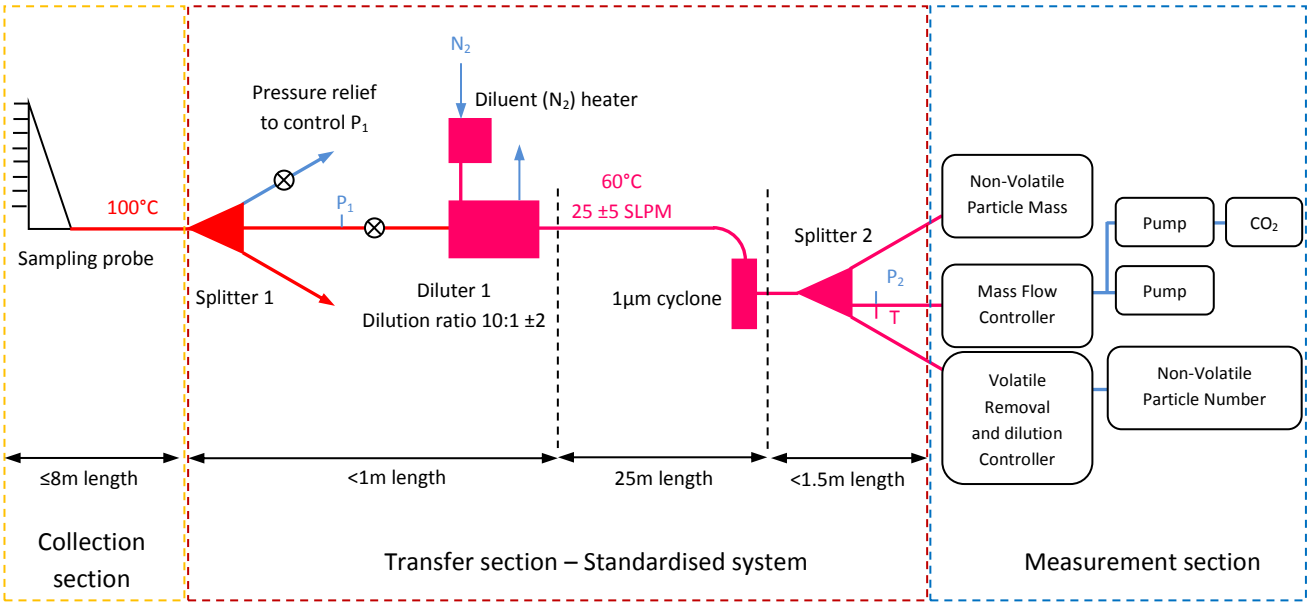

Figure 6.3: Schematic diagram of the most recent iteration of the SAE E-31 Committee sampling system.

Throughout the development of this sampling network design there have been large scale exhaust sampling campaigns designed to appraise the systems performance and investigation prospective designs concepts. Some of the experiments conducted as part of these campaigns is discussed hereafter.

6.4 PM Sampling from a Simulated Aviation Gas Turbine Exhaust

The HPCR in conjunction with the HES sector combustor rig located at the GTRC has been used extensively during the course of the EASA funded SAMPLE research projects as a means to produce a gas turbine exhaust segregate in order to validate the sampling system being developed by the SAE E-31 Committee. Only a portion of material gathered during the SAMPLE III experimentation will be discussed within this Thesis, however for all experimental campaign results readers are directed to the published SAMPLE reports [90,91,93,94].

6.4.1 Particle Characterisation for High and Low Sample Line and Dilutant Temperatures

One area of uncertainty which was explored during the development the SAE E-31 Committee emission sampling system was how sampling line and diluent temperature affected sample conditioning. This is an important consideration not only for ensuring that sample integrity is maintained but also as there are gas analysis and particle measuring instruments which are constrained to specific sample inlet temperatures.

For this experimentation the HPRC was fuelled with aviation grade kerosene (Jet-A) and configured such that the emissions produced were known to have an adequate organic and smoke content (smoke number of approximately 5) to thoroughly access any impact resulting from changing the sample temperature. Specific rig details are shown in Table 6.1.

Table 6.1: HPRC rig configuration details.

Mass Flow (kg/s)	Fuel Flow (g/s)	AFR	Pressure (bar)	Air Inlet Temp. (°C)
0.69	14.11	48.7	2.44	335

Three sample temperature conditions were selected for this experimentation:

- **High temperature**: 400°C initial sample line temperature, maintained at 400°C until the introduction of 200°C dilution (N_2) at a 10:1 dilution ratio, followed by further 20°C dilution (N_2) at a 10:1 dilution ratio.
- **Medium temperature**: 400°C initial sample line temperature, maintained at 200°C until the introduction of 60°C dilution (N_2) at a 10:1 dilution ratio, followed by further 20°C dilution (N_2) at a 10:1 dilution ratio.
- **Low temperature**: 400°C initial sample line temperature, cooled to 20°C until the introduction of 20°C dilution (N_2) at a 10:1 dilution ratio, followed by further 20°C dilution (N_2) at a 10:1 dilution ratio.

These temperatures were chosen in order to access the extent which rapid cooling of the sample prior to sample dilution induced condensation of the volatile fraction within the sample, which would have otherwise remained in the gaseous phase.

A schematic diagram of the sampling setup is shown in Figure 6.4.

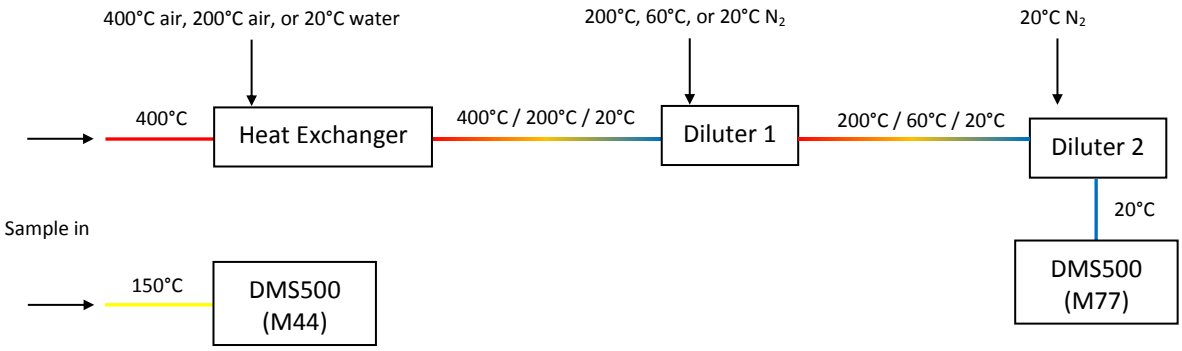

Figure 6.4: Schematic diagram of sample temperature experimentation setup.

A DMS500 (M44) sampling and undiluted exhaust flow was used as a reference instrument to ensure the sample characteristics had not changed significantly throughout the experiment. The particle size spectra of the undiluted sample are shown in Figure 6.5. The emissions source remained fairly stable throughout the experimentation with some slight variation in the smaller size mode for the medium temperature condition. This may have developed due to this test condition being the final set in the experiment programme. Changes in ambient conditions or sample system 'bed-in' could therefore have resulted in a higher proportion of volatile and primary carbon particulates being produced for this particular case.

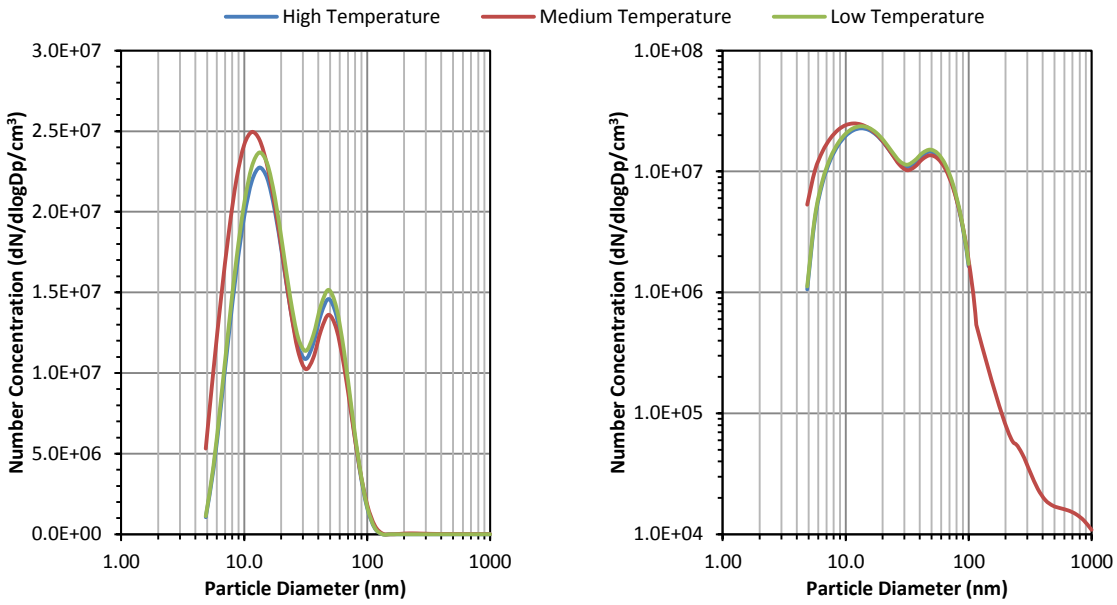

Figure 6.5: DMS500 particle size spectra of undiluted exhaust produced using the HPRC and HES: (a) linear y-axis scale, (b) logarithmic y-axis scale.

Size spectral analysis of the conditioned sample can be seen in Figure 6.6 where there were observable difference in the sample size distribution following the system heat exchanger and sample dilution phases. The peak location of the sample remains identical however the concentration level of these sizes modes has been reduced in a fashion uncharacteristic of solely dilution and line penetration losses. Decreasing the sample line and dilution temperature does not have a significant impact on the lower particle size mode. The number concentration of the small particle sizes was highest for the high temperature condition. This indicates that although a volatile fraction is very likely present within this sample, temperature reductions along the simple line do not introduce particle condensation from the gas phase.

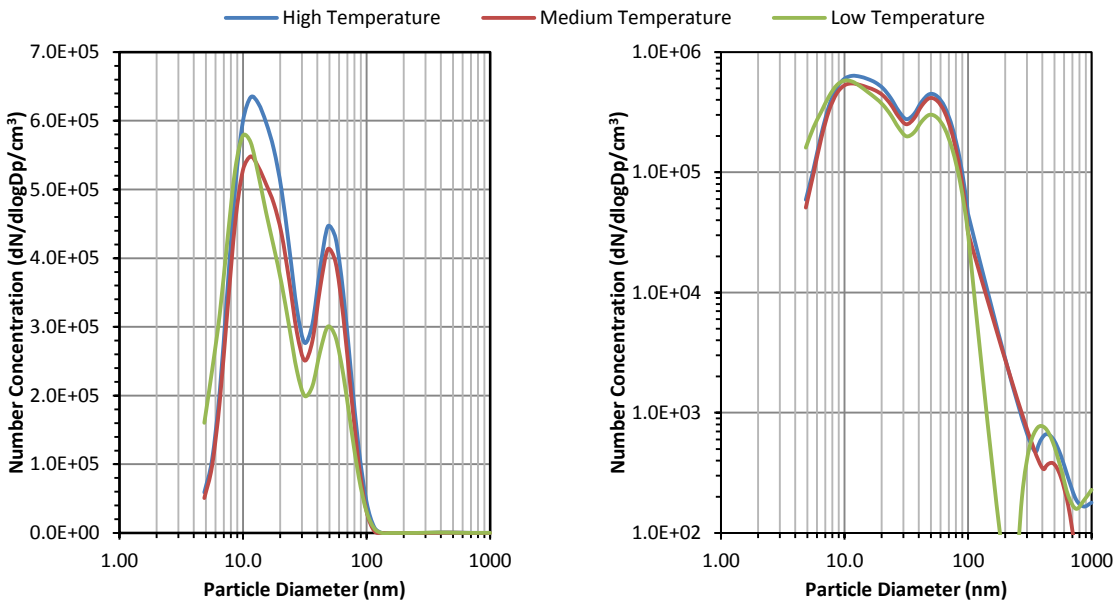

Figure 6.6: DMS500 particle size spectra following high, medium and low temperature dilution: (a) linear y-axis scale, (b) logarithmic y-axis scale.

It is the larger particle size mode which has been impacted most dramatically during this programme with the lowest temperature condition experiencing a number concentration reduction of approximately 36% at the spectrum peak location (49nm) when compared to that of the high temperature condition. As this sampling system is intended to measure only non-volatile PM it is important that the larger size particles which are more commonly associated with the solid carbonaceous fraction of the sample are maintained as closely as possible to the original emission source. It is likely that thermophoretic losses are responsible for this disparity as the temperature gradient between the 400°C initial sampling line and the 20°C heat exchanger is significantly large to drive particles towards the sample line walls.

It was found in the Sample 3 SC.02 project [94] that particle losses due to thermophoresis would be minimised if the temperature reduction of sample occurred during the primary dilution phase of the system. These results support this hypothesis and provide some justification of the decision to reduce the sample temperature from 160°C within the primary sample lines to 60°C via dilution using 60°C nitrogen.

6.5 PM Sampling from an Auxiliary Power Unit (APU)

This phase of the programme was conducted at the University of Sheffield's Low Carbon Combustion Centre (LCCC). An APU was used as an emission source as it provided a representative aviation gas turbine PM distribution, in-effect acting as an intermediary appraisal phase which did not require a full-scale gas turbine emission certification test. The APU which was employed was a Rolls-Royce Artouste Mk 113 previously described in Chapter 3 §3.3.1. The engine was fuelled with Jet A-1 aviation kerosene and emission characterisation was performed at two operating conditions, idle and full power. One of the main objectives of the APU exhaust sampling was to characterise how the PM emissions profile varied along the length of the sampling system.

6.5.1 APU operating conditions

Two engine operating conditions were employed. First an idle condition which exhibited relatively low smoke and fairly high volatile emissions and secondly a full power condition with higher smoke and lower volatile emissions.

In addition to the engine operation parameters typical emission index (IE) (g/kg), raw gaseous emissions, and smoke and particle emission data for each condition are shown in Table 6.2, Table 6.3, and Table 6.4.

Table 6.2: Typical engine index data for both idle and full power test conditions.

	AFR	EI CO_2	EI CO	EI NO_x	EI UHC
Idle	68.1	3061	71.3	1.8	9.2
Full Power	63.5	3155	25.8	4.1	1.1

Table 6.3: Typical gaseous emissions data for both idle and full power operating conditions.

	AFR	CO_2		CO		NO_x		UHC	
		%	σ	%	σ	%	σ	%	σ
Idle	68.1	2.9	0.3	1100	34	19.0	0.17	273.2	11.2
Full Power	63.5	3.2	0.04	409	9.3	37.6	1.03	34.5	1.4

Table 6.4: Typical smoke and particle emission data for both idle and full power conditions.

	SAE Smoke Number		Non-volatile particle mass		Non-volatile particle number	
	-	σ	mg/m^3	σ	N/cm^3	σ
Idle	7.5	1.1	0.297	0.011	$5.2x10^7$	$1.7x10^5$
Full Power	19.2	0.9	0.764	0.014	$7.8x10^7$	$2.4x10^5$

6.5.2 Sampling Setup

Sampling ports were distributed at significant points along the transfer system to allow particle measurement apparatus to be installed quickly during each engine test condition. Figure 6.7 shows a schematic of the sampling setup:

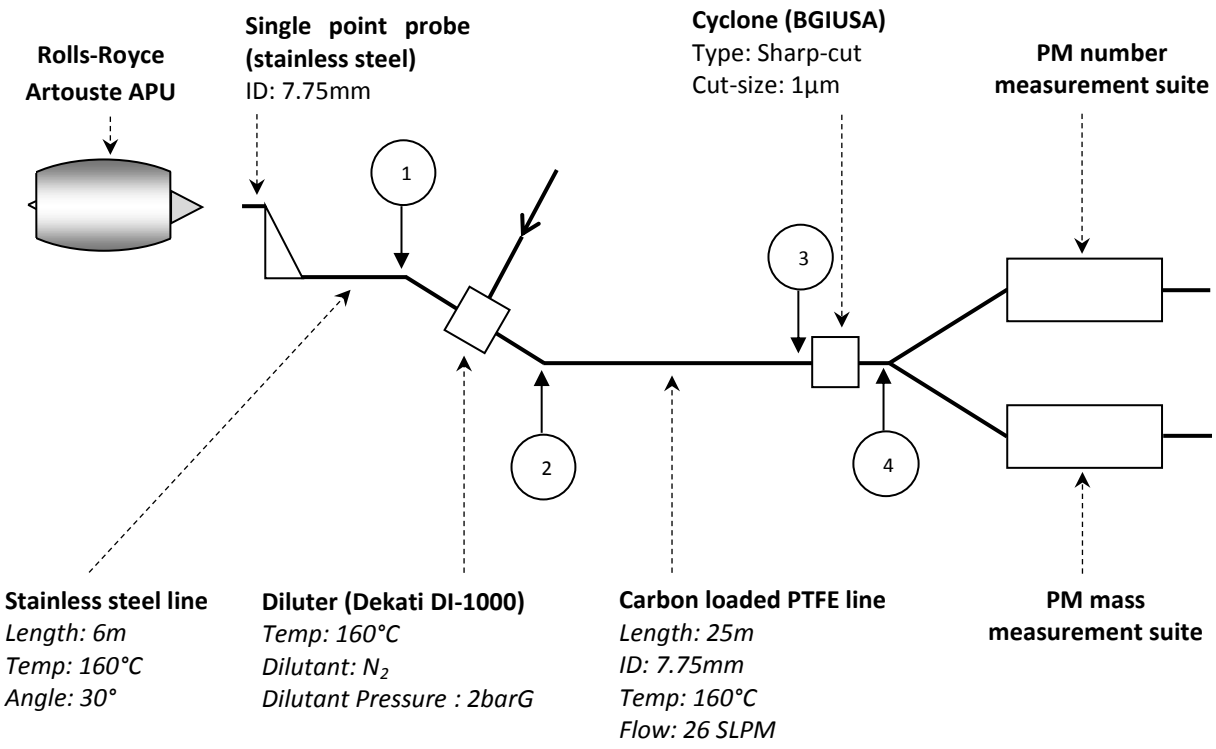

Figure 6.7: Schematic diagram of the APU emissions sampling system and the locations of each particle sampling point.

The exhaust sampling points chosen were such that they were positioned to include:

1) Pre-dilution exhaust.
2) Post-dilution (≈10:1, N_2, 160°C) exhaust.
3) Downstream of a 25m conductive PTFE sampling line (160°C, 7.75mm ID).
4) Downstream of a 1µm sharp-cut cyclone.

6.5.3 Undiluted APU Exhaust Particle Size, Number and Mass Characterisation

To provide an initial characterisation of the APU exhaust, Figure 6.8 shows DMS500 particle size spectra for both the low and high power conditions sampled from the undiluted Point 1 location. For both power conditions the particle size distributions are of a bi-modal nature with nucleation and accumulation mode peaks in approximately the same sizes positions (15 and 50nm). The concentration levels of the nucleation mode are also fairly consistent, both measuring approximately 1.25×10^8

dN/dlogDp/cm^3. There is a significant change in the accumulation mode of the high power condition where the concentration has risen to 1.97x10^8 dN/dlogDp/cm^3 compared to 7.56x10^7 dN/dlogDp/cm^3 at the low power condition.

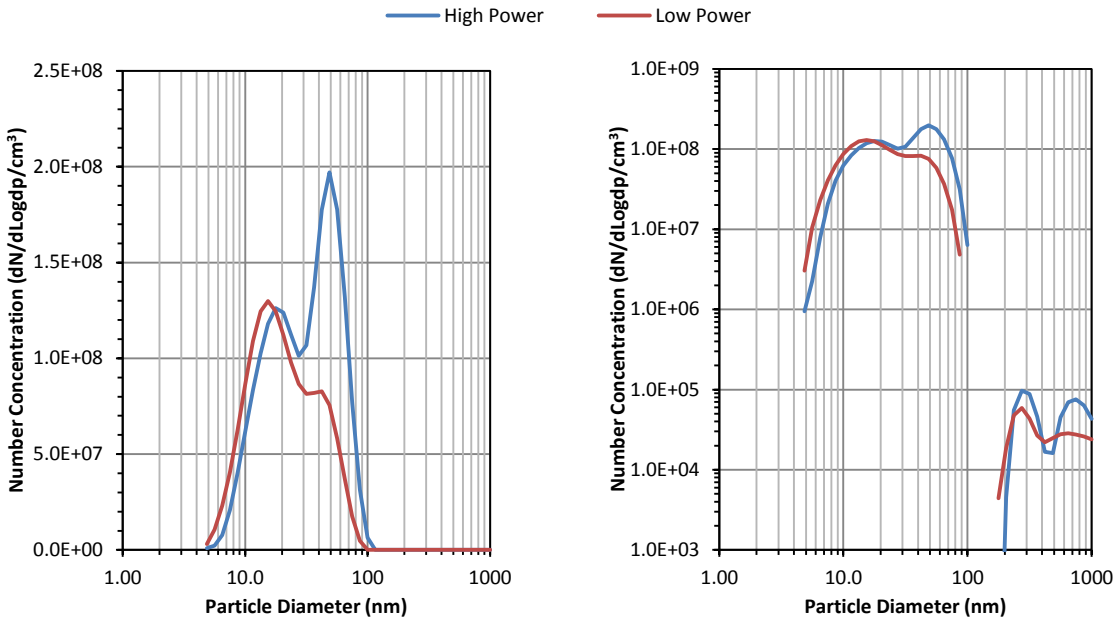

Figure 6.8: DMS500 particle size spectra for APU exhaust at high and low power conditions: (a) linear y-axis scale, (b) logarithmic y-axis scale.

This type of change in particle output is consistent with other gas turbine emission tests and results from higher soot formation during the increased fuel consumption required at the higher power conditions.

A higher concentration of large particles will inevitably have an impact on the PM mass concentration of the high power exhaust. In this case the mass of the sample has transitioned from 2.78x10^{-3} µg/cm^3 at low power to 1.05x10^{-2} µg/cm^3 at high power.

6.5.4 Particle Size Characterisation for Low to High Power Transition

Using a fast response instrument such as the DMS500 it is possible track how the particulate output of the APU exhaust changes as the engine increases from a low to high power. This enabled size spectral analysis to be performed during the transient phase of the condition changes rather than simply taking PM measurements during stable engine operation. During a 20-second transition in engine power, the particle

size spectra was significantly changed before finally stabilising with a profile similar to that of the high power condition displayed in Figure 6.8.

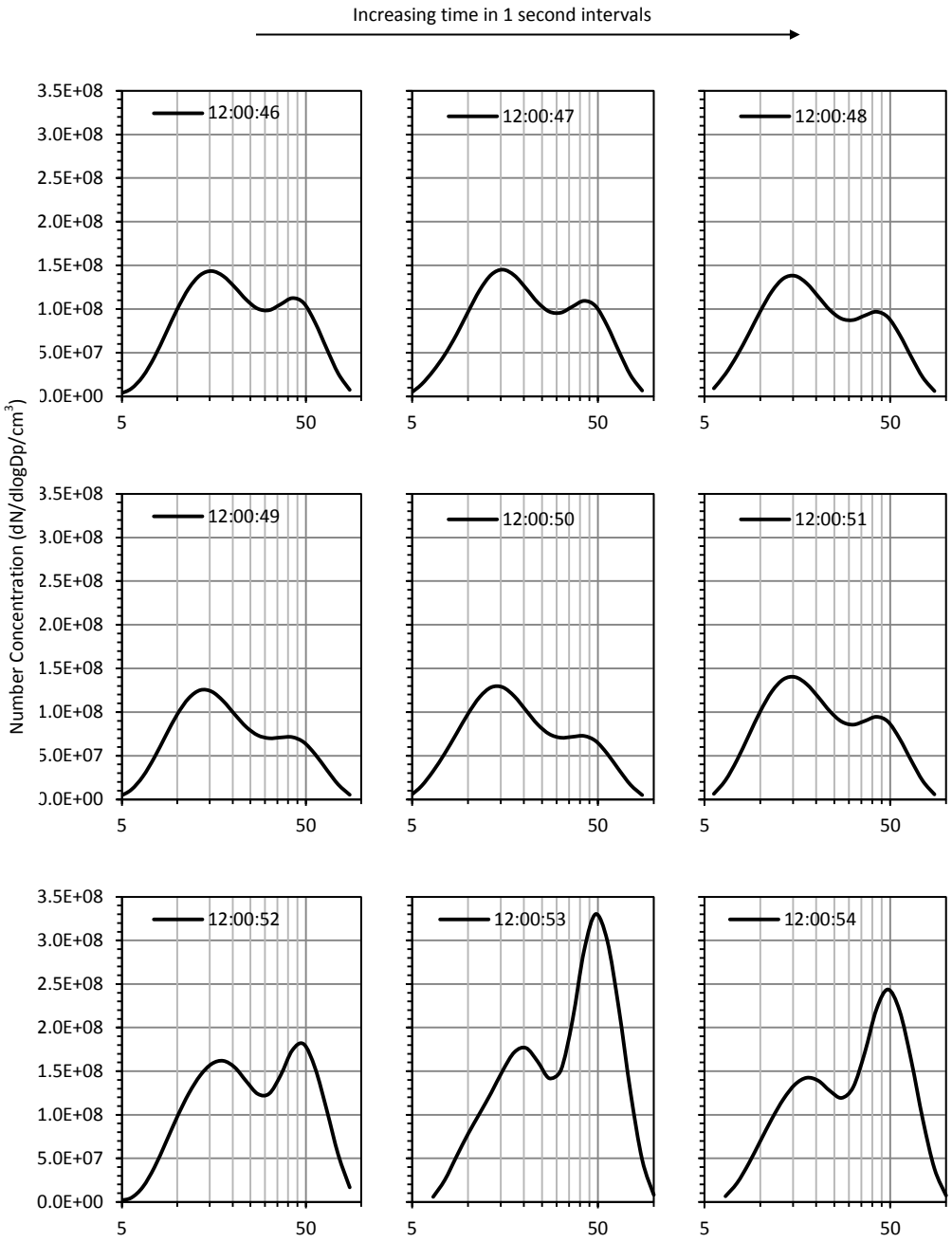

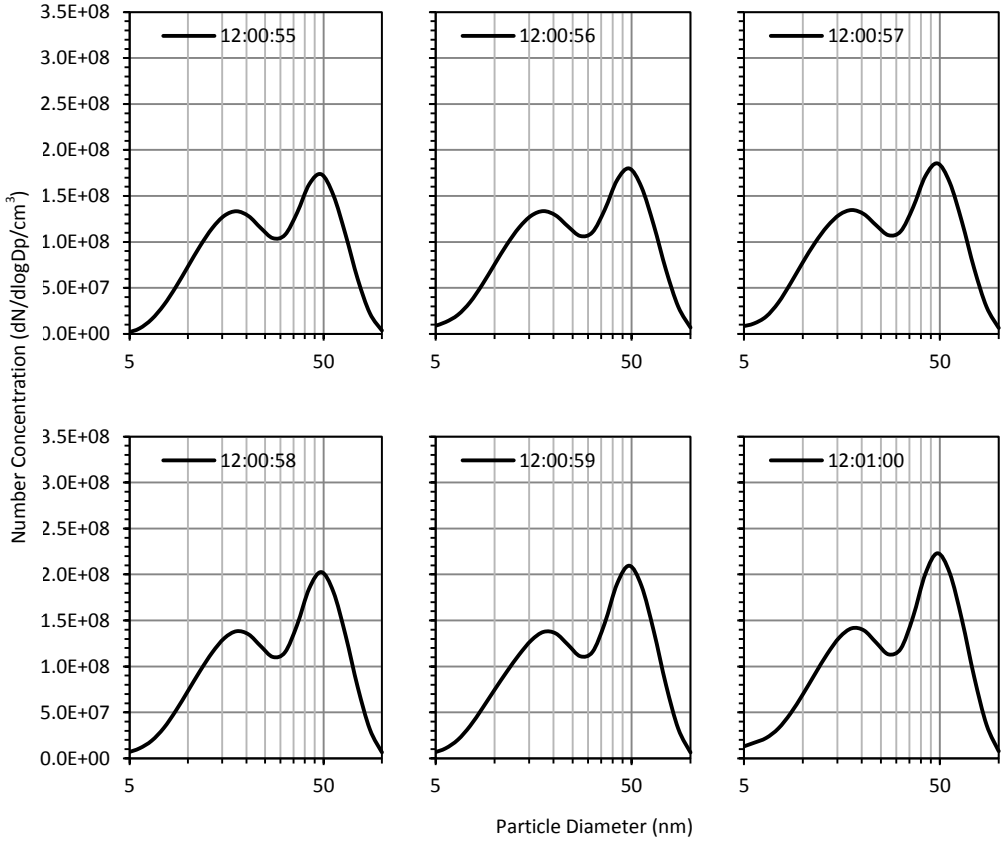

Figure 6.9: DMS500 size spectra of undiluted APU exhaust during low to high power transition.

The first indication of a change in the particle size spectrum occurs at 12:01:48 where a there is a drop in the nucleation and accumulation mode number concentrations. The slight delay noted in the changing PM size distribution recorded compared to the time for the change in engine condition is likely to be due the residence time of the sampling system. The accumulation mode subsequently becomes more pronounced up until 12:01:53, when there is a rapid increase in accumulation mode particle concentration, peaking at approximately 3.30×10^8 dN/dLogDp/cm^3. This accumulation mode peak then fluctuates for 6-7 seconds until stabilising at approximately double that of the concentration level previously measured at the idle condition.

This increase in accumulation mode is not unexpected as increasing engine power usually corresponds to an increase in soot production due to the increased fuel consumption and greater likelihood of fuel-rich zones developing in the primary combustor zone. There are exceptions to this influence of power such as emission characteristics from multi-stage combustion gas turbines which utilise different

combustion regimes at different power bands. An example of this type of emission profile is presented subsequently.

6.5.5 Assessment of Particle Loss across the Sampling System

For a low-power engine condition, multiple repeat exhaust samples were taken at each sampling point (Point 1, undiluted exhaust) during the two test runs. A comparison of all Point 1 undiluted particle size spectra measured with the DMS500 is shown in Figure 6.10. The exhaust composition remained fairly stable with the majority of the particle size distribution existing within the 5 - 100nm diameter size region. An average of all the measurements taken at each sampling point was used when making a comparative assessment of measured emissions spectra.

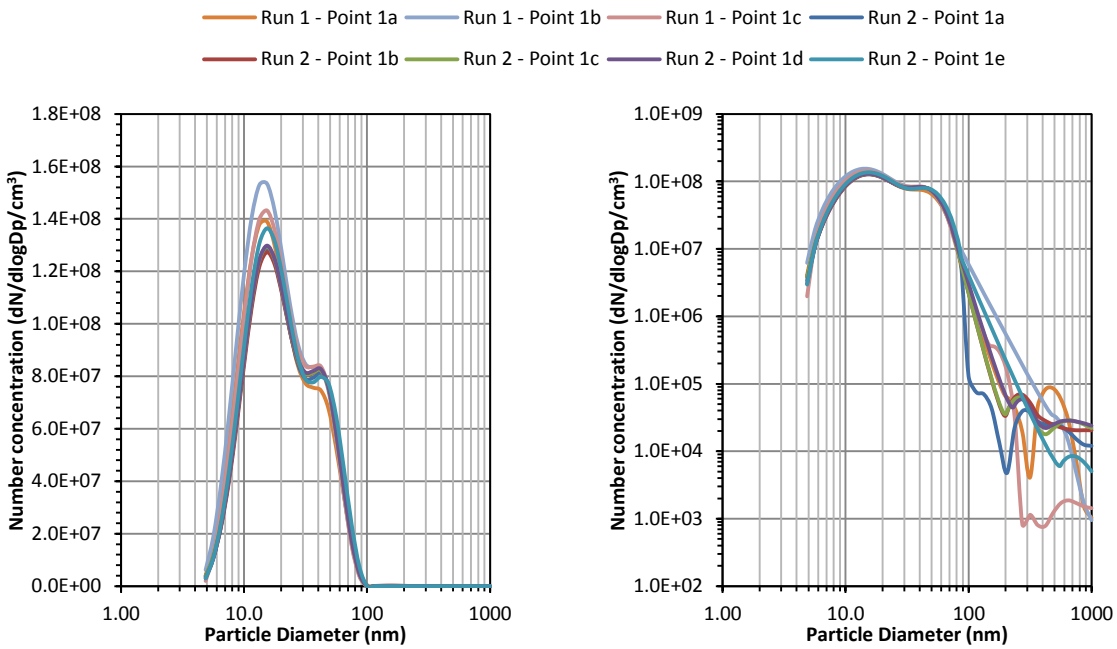

Figure 6.10: DMS500 size spectra of APU exhaust during low power condition sampled at Point 1: (a) linear y-axis scale, (b) logarithmic y-axis scale.

Clear differences are observed when samples from all of the sampling locations are compared. The size spectra shown in Figure 6.11 are from measurements made during both test run 1 and test run 2 compared to the undiluted Point 1 average data set. It is important to note that no correction has been made to the data sets to incorporate the 10:1 dilution applied directly after Point 1, and so there is an expectation of lower

concentration levels. However, it is also evident that subsequent differences exist between the Point 2, Point 3 and Point 4 spectra.

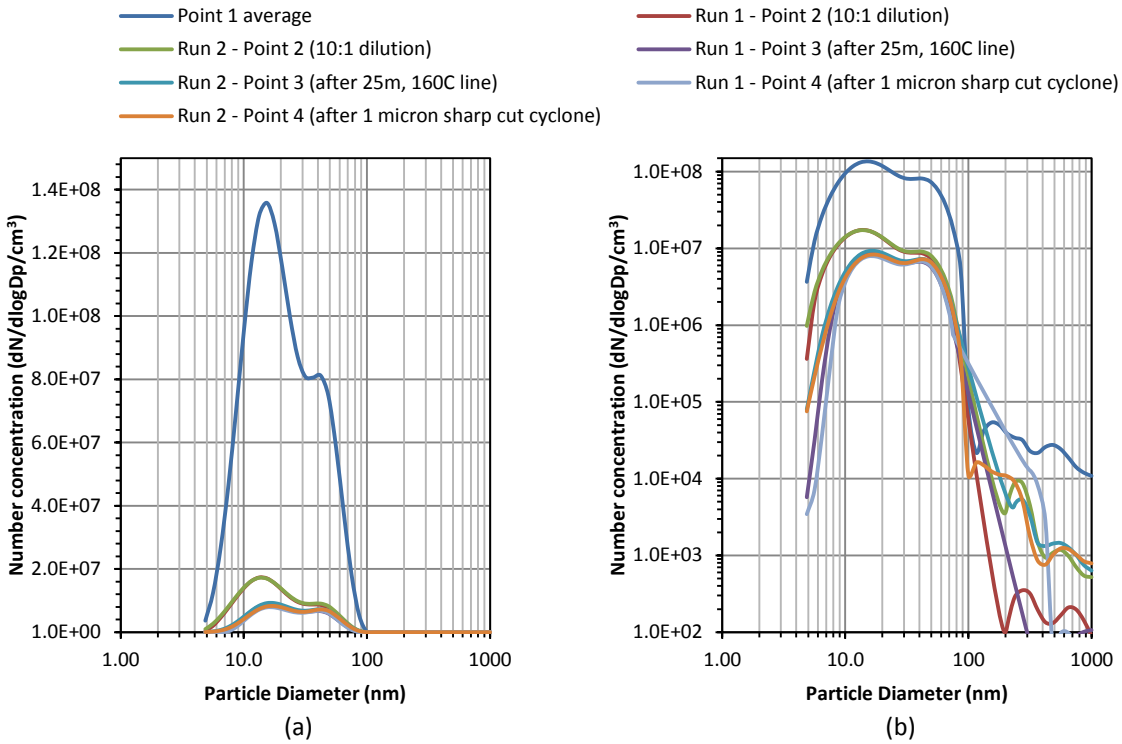

Figure 6.11: DMS500 particle size spectra for APU exhaust during low power condition at multiple points along the sampling line: (a) linear y-axis scale, (b) logarithmic y-axis scale.

When a dilution multiplication factor (10.5) is applied to the average Point 2 size spectra it is found that there is an unexpected small increase in particle number concentration within the nucleation mode. This discrepancy is also seen in Figure 6.11 as a difference between the size spectra of test run 1 and test run 2 and may therefore develop from the adoption of an average Point 1 size spectrum.

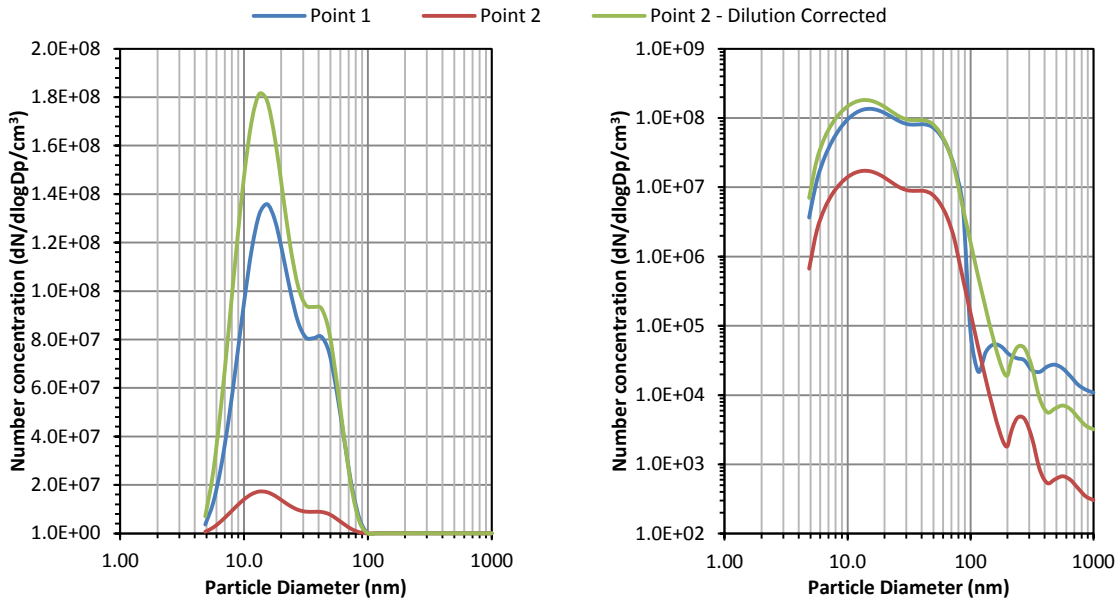

Figure 6.12: DMS500 size spectra for APU exhaust during low power condition sampled from Point 1, Point 2 and Point 2 with dilution correction applied: (a) linear y-axis scale, (b) logarithmic y-axis scale.

The total PM number concentration measured at Point 1 was 9.41×10^{7} N/cm^3 with a mass concentration of 2.47×10^{-4} µg/cm^3. The measured total number concentration at Point 2 was 1.17×10^{7} N/cm^3 with a mass concentration of 2.47×10^{-5} µg/cm^3. When dilution corrected, Point 2 number and mass concentration measurements become 1.23×10^{8} N/cm^3 and 2.59×10^{-4} µg/cm^3 respectively. These values compared well to the undiluted exhaust with the difference likely to have occurred due to very slight engine exhaust variance between test run conditions, coupled with uncertainty in the determination of the dilution ratio via measurement of upstream and downstream CO_2, which the authors approximate could summate to 6%.

In 2009 United Technologies Research Centre (UTRC) developed a Microsoft Excel based spreadsheet which allowed for fast assessment of particle line losses within a PM transportation system.

The fundamental operating principle of the UTRC transport model is to deconstruct a transport network into sections of variable physically characteristics. Each section is then assigned an unique penetration efficiency, with the summation of all sections giving an overall total penetration efficiency η_p, described in Equation 19.

$$\eta_p = \prod_{i=1}^{n} \eta_{pi}$$

Equation 19: Underpinning UTRC Model calculation.

In calculating penetration losses, the UTRC model takes the following considerations into account:

- Gas properties
- Aerosol properties
- Flow and heat transfer properties in a tube flow
- Penetration in a fully developed turbulent flow
- Thermophoretic penetration efficiency
- Turbulent, diffusive penetration efficiency
- Tube bending effects on penetration efficiency

In the constructing equations to describe the previously listed phenomena the authors of the UTRC model highlight the work of Yook and Pui [118] and Willeke and Baron [119]. A complete description of the UTRC model and the elements on which it is based the tool and user documentation are available for download online [120].

For simplicity the sampling setup was considered to be a continuous sampling line with no bends. Although this was not the case, it was ensured that bending radii were greater than ten times the internal sampling line diameters whilst it has been demonstrated that the sampling splitters which were have negligible losses across them. The complete input parameters applied to generate the particle penetration curve used to in this work are shown in Table 6.5.

Table 6.5: UTRC Model parameters for the long transport line between Point 2 and Point 3.

Parameter	Measured value
Actual gas temperature (K)	433.15
Actual gas pressure (atm)	1
Flowrate (slpm)	20.29

Line diameter (mm)	7.747×10^{-3}
Line length (m)	25
Wall temperature (K)	433.15
Total bending degrees (°)	0

Figure 6.13 shows the total transport efficiency curve generated using the parameters listed in Table 6.5 and the particle diameters used in the DMS500 electrometer size classifications as inputs for the UTRC model. It was anticipated that the dominant loss factor was diffusion to the line walls.

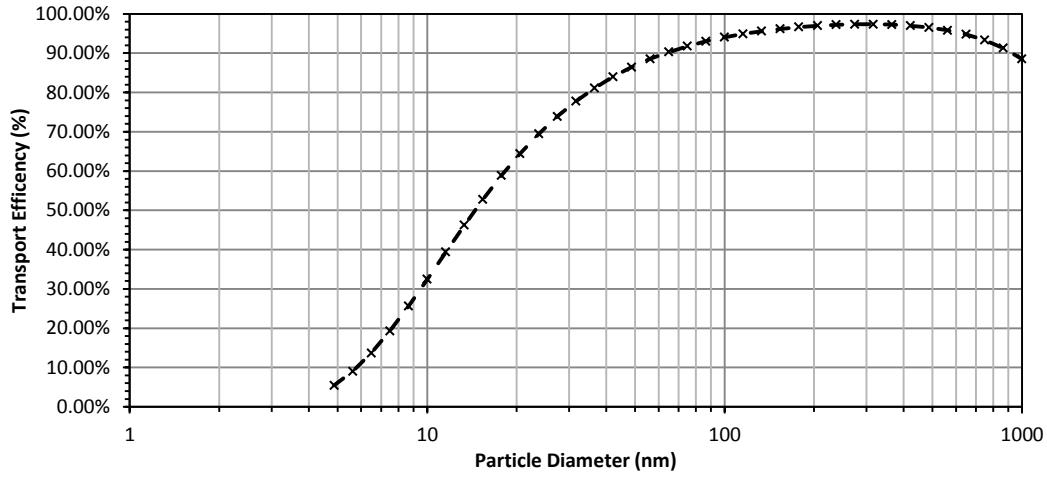

Figure 6.13: Transport efficiency curve formulated using the UTRC Model.

To determine if this transport efficiency curve could be used to reconstruct downstream sample measurements to be more representative of the upstream exhaust composition, transport efficiency values determined using the UTRC model were applied as multiplication factors to each of the DMS size and number concentration data values measured at sampling Point 3. This allowed a particle-size specific correction to be implemented.

Figure 6.14 shows that prior to the inclusion of these multiplication factors (green line), the size spectrum at Point 3 indicates significant losses occurring in the smaller size ranges (5-40nm). This is consistent with diffusion losses to the transport line walls, which was also predicted to be the main loss mechanism by the UTRC model. The number concentration measured at Point 3 was 6.31×10^{6} N/cm^{3}, approximately a 46%

decrease compared to the number concentration measured at Point 2 (red line), 25m upstream. As the particle loss occurs mainly within the smaller size region, the difference is less significant in terms of mass which was measured as 1.65×10^{-5} µg/cm^3 corresponding to a ≈7% loss in mass concentration.

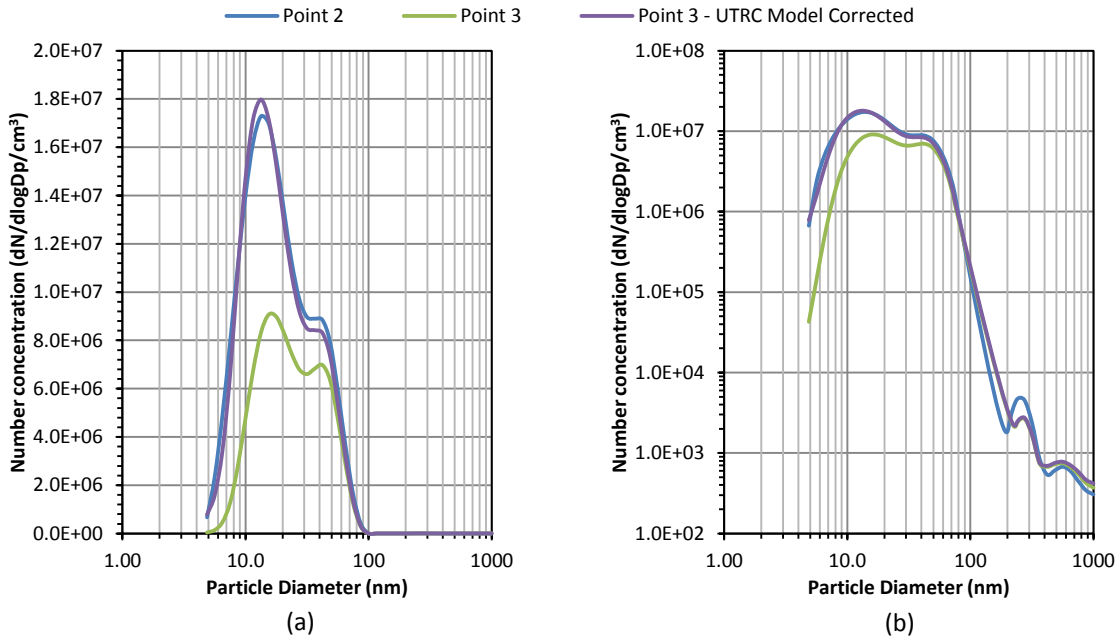

Figure 6.14: DMS500 size spectra for the APU exhaust during low power condition sampled from Point 2, Point 3 and Point 3 with UTRC loss correction applied: (a) linear y-axis scale, (b) logarithmic y-axis scale.

When transport efficiency is considered the particle size spectrum which is generated is far more reflective of that which was measured at Point 2. The total number concentration for the corrected data was calculated as 1.13×10^{7} N/cm^3 which compares well with the 1.17×10^{7} N/cm^3 measured at Point 2.

DMS500 measurements were also made at sampling Point 4, located downstream of a 1µm 'sharp-cut' cyclone. Some losses in particle number were again observed; likely due to additional transport line losses with number and mass concentrations being 5.77×10^{6} N/cm^3 and 2.32×10^{-5} µg/cm^3 respectively. The size spectra of Point 3 and Point 4, shown in Figure 6.15, show good agreement although there is again some variance in number concentration values for particle sizes >100nm. This reaffirms the proposition that as the measured number concentrations in this size range are sufficiently low, they are more susceptible to instrumentation noise and inaccuracy

due to calibration sensitivity. This may explain the slight differences observed in this dataset.

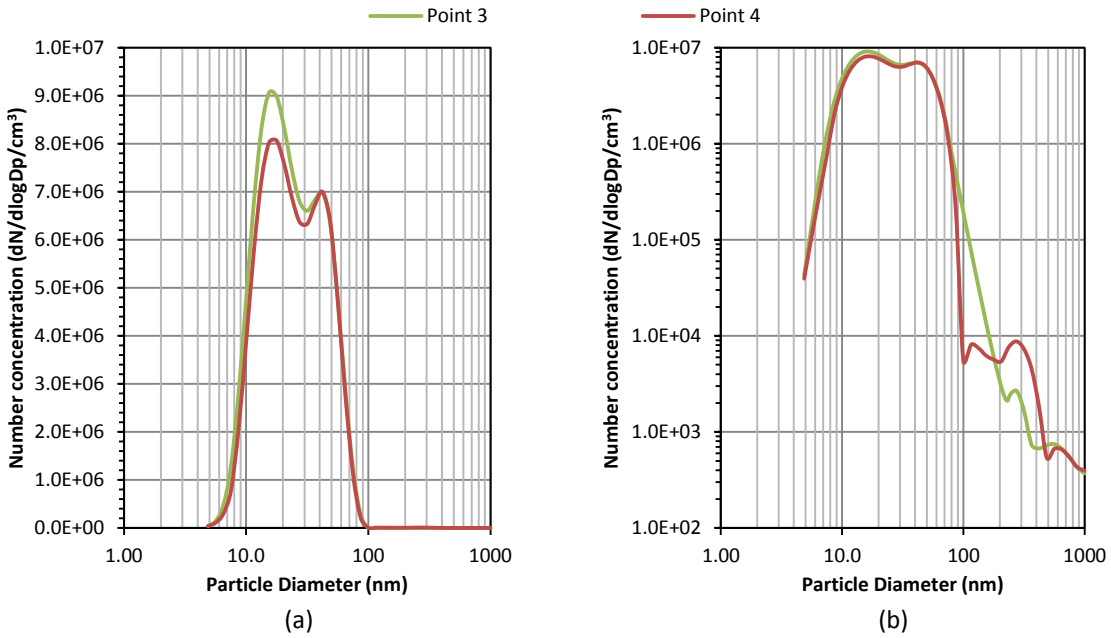

Figure 6.15: DMS500 size spectra for APU exhaust during low power condition sampled from Point 3 and Point 4: (a) linear y-axis scale, (b) logarithmic y-axis scale.

Applying the UTRC particle loss tool to the size spectrum data measured at Point 4 - with the inclusion of an additional 1m of heated sample line into the calculations - generated the corrected spectrum shown in Figure 6.16.

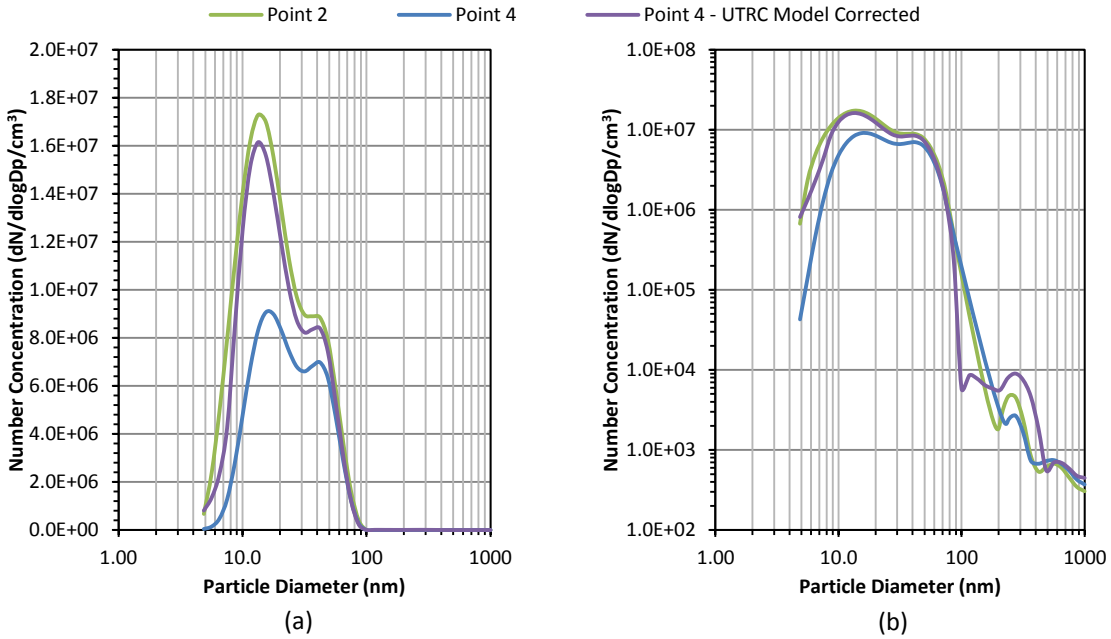

Figure 6.16: DMS500 size spectra for APU exhaust during low power condition sampled from Point 2, Point 4 and Point 4 with UTRC correction applied: (a) linear y-axis scale, (b) logarithmic y-axis scale.

A ratio of the Point 2 and UTRC corrected data for Point 3 and Point 4 is shown in Figure 6.17. The UTRC model appears to perform very well for the particle size ranges corresponding to where the majority of PM number concentration from aviation gas turbine exhausts (10-75nm) exist. The model starts to under predict losses at higher size ranges. At this time this under-prediction cannot be fully appraised as there is also a higher variation in the repeated test points at these higher sizes, thought to be an artefact of the sensitivity of the DMS500 discussed earlier. Hence this variation may simply be a function of altering engine conditions. Further experimentation with a spectrum of mono-dispersed particles generated from a repeatable source, such as those produced using a DMA in conjunction with a PALAS soot generator or CAST propane diffusion flame, would be required to fully appraise this particle loss model.

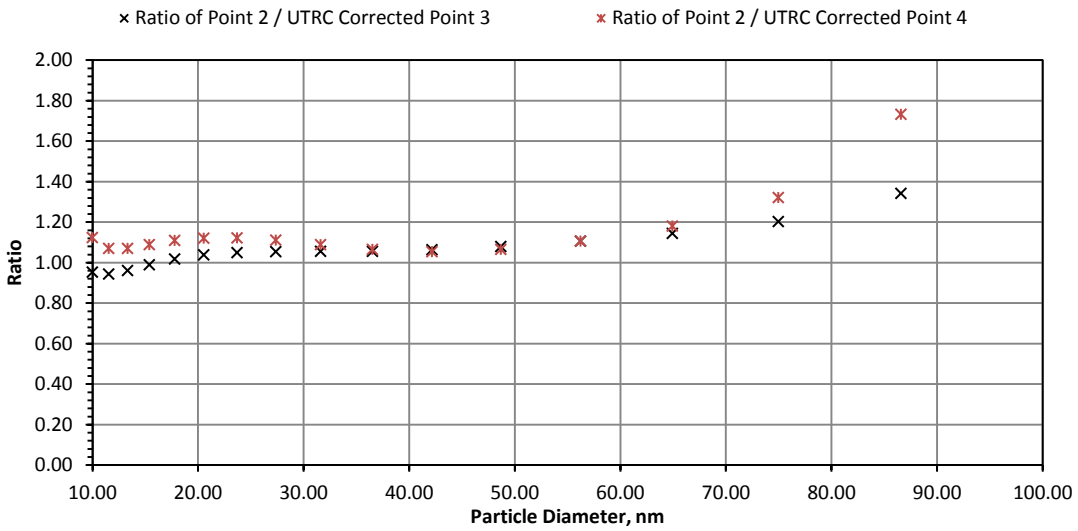

Figure 6.17: Ratios of the measured Point 2 and UTRC corrected Point 3 and Point 4 data sets.

This data shows that significant particle loss does occur over a long heated exhaust transportation line, particularly in the sub-40nm size region. Losses were less significant following initial sample conditioning with 160°C N_2 and after a 1µm 'sharp-cut' cyclone; however it was noted that caution is required when applying dilution ratio correction, as this may potentially add further uncertainty to the final non-volatile PM measurement.

The UTRC particle line loss model, when configured to accept DMS500 particle diameters as input criteria, does appear to be applicable to aviation gas turbine PM emissions measured using the DMS500. Measurements taken at the outlet of a 25m heated sample line and then corrected using this model show excellent agreement with upstream measurements across the particle size range associated with aircraft engine exhausts. Differences observed between the measured and UTRC corrected spectrums, are within the DMS500 and dilution ratio measurement uncertainties. In addition, the uncertainty in the inversion fitting software may also be influencing the comparison.

6.6 PM Sampling from Multiple Large Civil Gas Turbine Engines

Developing systematically on from the analysis of the PM data obtained from the GTRC HPCR fitted with the HES, followed by that of the APU, a final assessment was undertaken on a full scale engine and was performed at the SR Technics aircraft engine maintenance facility located at Zürich Airport. The transfer network which was used during testing was based upon that previously described in Figure 6.3, which presents the most recent iteration of the SAE E-31 concept sampling system. In addition to this system, two other systems were employed for comparison purposes in this experimental programme. These systems were the current regulatory standard detailed in Annex 16, and a transfer system designed by the Federal Office of Civil Aviation (FOCA) which was previously installed on-site. A schematic of the final sampling system set-up is shown in Figure 6.18, which followed the concept of having both the established current regulatory methodology (Annex 16) and the newly developed SAE E-31 system integrated enabling concurrent measurements.

Although the SAMPLE III and FOCA sample network designs were slightly different specifically concerning sample line diameter and temperature, the overall concept of this sampling system construction was to ensure that whenever possible the measurement suite at the end of each line was identical. Performing measurements in this way increase the level of confidence to the final results.

Exhaust samples were collected using an 8mm ID single point probe manufactured from stainless steel. The internal sample line is enclosed within a secondary larger diameter (25mm) stainless steel surround which during testing allowed un-sampled exhaust gases to enter via 2 inlet holes. This overflow of hot exhaust gases ensured the line sample line temperature did not fall below the 160°C stipulated in the SAE E-31 methodology. The probe was held in an elevated position out of the engine exhaust core while not in use and vertically traversed into a selected sampling zone for testing.

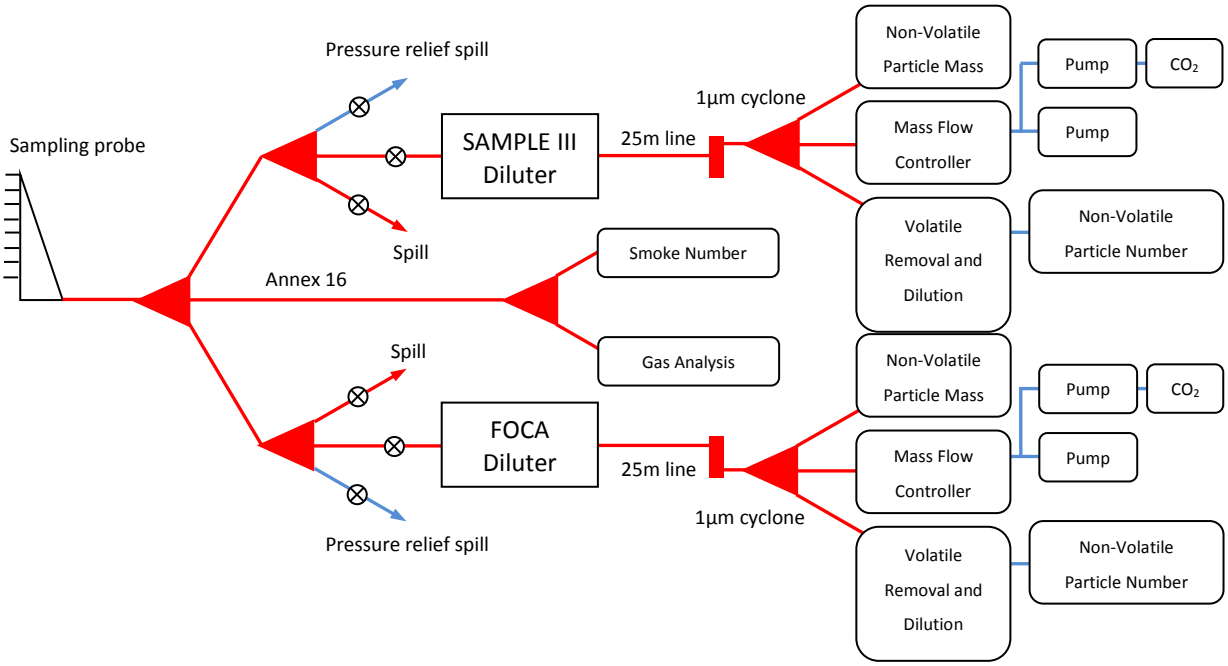

Figure 6.18: Schematic diagram of the sample transfer system design used for appraisal of the SAE E-31 sampling methodology at SR Technics.

It should be noted that although the probe sample line temperature criteria adhere to the SAE E-31 methodology elements of the probe design and functionality do not. Much of this stems from the fact the SAE E-31 sampling methodology builds upon transfer system details established in the Annex 16 specifications. For this reason the probe does not meet the requirements of:

1) Being within ½ a nozzle diameter of the engine exhaust plane in all configurations due to the fixed position of the probe and engine housing assembly.
2) Having a minimum of 12 iso-kinetic, i.e an 80% pressure drop across the probe, sampling locations positioned across the engine exit plane.

This does not negate the finding of these experiments as they were designed to appraise the sampling system design rather than provide and engine emission certification data.

Figure 6.19: Front and side views of the SR Technics 8mm single point sampling probe.

6.6.1 Sample Line Comparison

Following the primary sampling probe, a 6m long, 8mm ID flexible stainless steel sampling line, heated and insulated at 160°C, supplied both of the main sample line configurations which were installed during the experimental testing at the SR Technics facility. These were designated as the SAMPLE and FOCA sampling lines and each were installed in accordance with the standards specified by each investigating group, i.e. the SAMPLE Consortium and the Federal Office of Civil Aviation.

To ensure that the exhaust sample integrity was maintained and that a representative PM sample was being supplied to both of the sample line configurations, a bespoke sample splitter was installed to allow simultaneous sampling. Two and three-way sample splitter designs which have been a developed component of SAMPLE research programme. In addition to splitting the exhaust sample into the separate sampling lines, primary dilution was also introduced prior to the main 25m sample network which transported the sample out of the engine testing bay and into the experimental test zone. This primary dilution system consisted of an eductor diluter supplying 60°C nitrogen at a dilution ratio of 10±2:1. Full details of the sample dilution and splitting apparatus which was specially designed and constructed for this purpose can be found in the SAMPLE 3 SC.02 report [94].

6.6.2 DMS500 Comparison

As part of the experimental setup at the SR Technics facility, three DMS500 systems were used, primarily to establish comparative PM size distribution measurements on each of the installed sample lines - those corresponding to Annex 16, SAMPLE and FOCA. The DMS500s used will be referenced by their instrument production number as the M44, M77 and M125 unit. Both the M44 and M77 systems were upgraded first generation system, while the M125 was a newer first generation unit.

The sampling location of the M77 was located on a gantry within the engine test bay for the duration of the testing performed at the SR Technics facility. In contrast the M44 and M125 system were installed some distance away and sampled from either the SAMPLE or FOCA sample lines depending on the experimental sampling period.

Prior to gas turbine exhaust sampling a comparison of DMS results taken from the same source was performed. The source used for this comparison was the PALAS soot generator which was configured to emit particles of approximately 10, 20 and 30nm. Samples of each aerosol were taken for 5 minutes and an average across this period taken to determine the size distribution, number and mass concentration, and geometric mean diameter (GMD). The size distributions generated at each of the sample conditions are shown in Figure 6.20, Figure 6.21 and Figure 6.22.

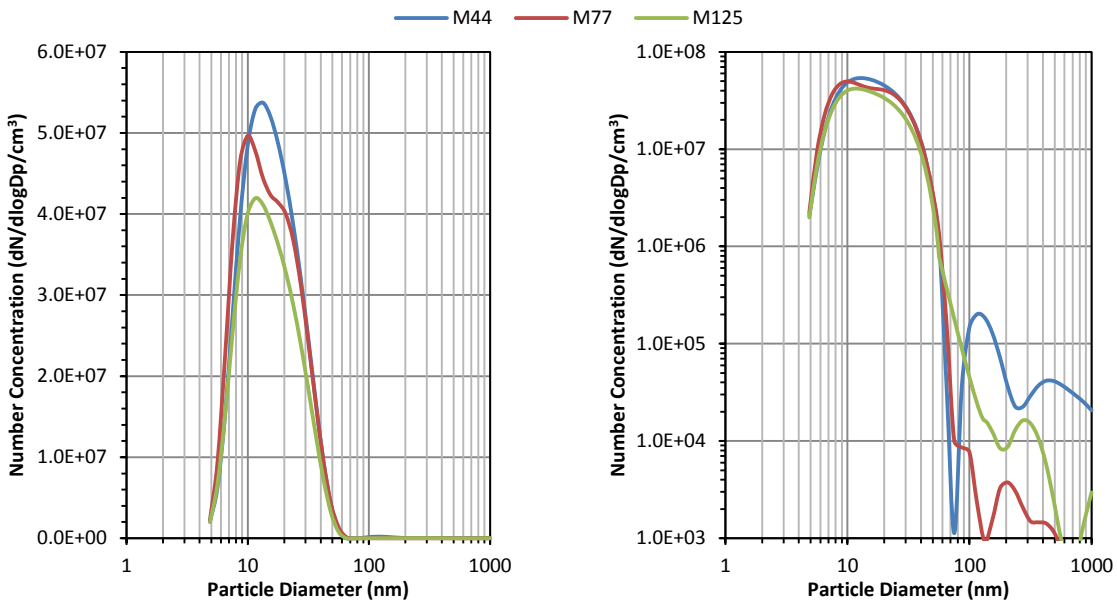

Figure 6.20: DMS500 size spectra for M44, M77 and M125 systems sampling 10nm solid particles generated using the PALAS soot generator: (a) linear y-axis scale, (b) logarithmic y-axis scale.

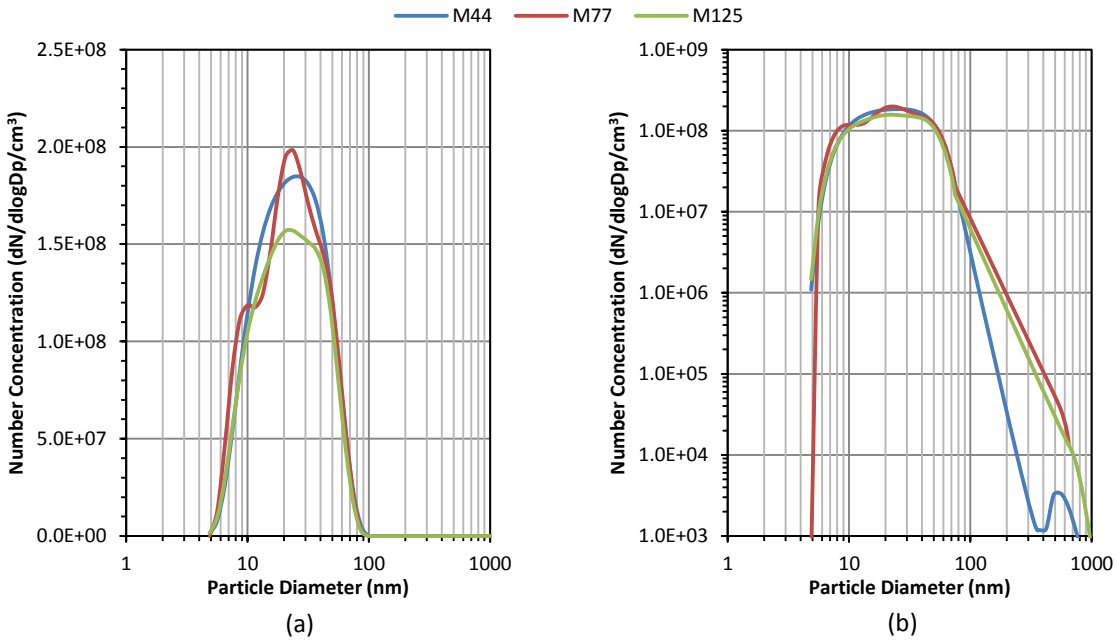

Figure 6.21: DMS500 size spectra for M44, M77 and M125 systems sampling 20nm solid particles generated using the PALAS soot generator: (a) linear y-axis scale, (b) logarithmic y-axis scale.

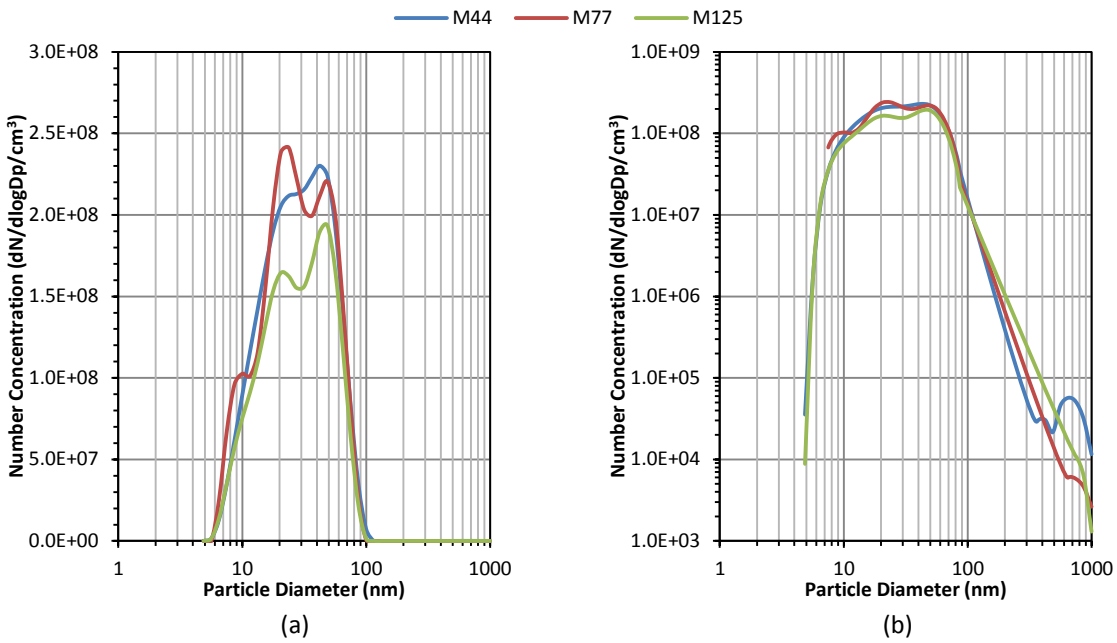

Figure 6.22: DMS500 size spectra for M44, M77 and M125 systems sampling 30nm solid particles generated using the PALAS soot generator: (a) linear y-axis scale, (b) logarithmic y-axis scale.

The size distributions which were measured by each of the DMSs were fairly consistent with one another at all of the sample particle sizes. It would be expected that aerosols of this nature would exhibit a mono-modal size distribution centred on the target particle size (10, 20 or 30nm). It can be seen that all of the DMSs experience a certain level of bi-modality, particularly at the 30nm condition. This may be an artefact of how the DMS500 uses an inversion matrix to generate number and size distribution from the electrical charge fluctuations on the electrometer rings. Alternatively, there is also a possibility an agglomeration process occurring which is inducing additional size modes. This type of process may also explain some of the variation in the measured concentrations of particles >100nm, however the relatively low concentrations of particles in this size range would also induce measurement error.

A summation of number concentration, mass concentration and GMD results generated by each DMS model for each of the sampled aerosols is compiled in Table 6.6.

Table 6.6: Summation of number concentration, mass concentration and GMD results for 10, 20 and 30nm solid particle measured with the M44, M77 and M125 DMS units.

DMS Model	Number Concentration (N/cm^3)	Mass Concentration ($\mu g/cm^3$)	GMD (nm)
		10nm Particles	
M44	$3.23x10^{7}$	$7.38x10^{-4}$	15
M77	$3.16x10^{7}$	$2.16x10^{-4}$	15
M125	$2.55x10^{7}$	$1.98x10^{-4}$	15
		20nm Particles	
M44	$1.42x10^{8}$	$4.70x10^{-3}$	22
M77	$1.43x10^{8}$	$4.29x10^{-3}$	22
M125	$1.24x10^{8}$	$4.05x10^{-3}$	22
		30nm Particles	
M44	$1.75x10^{8}$	$1.07x10^{-2}$	28
M77	$1.79x10^{8}$	$9.11x10^{-3}$	26
M125	$1.39x10^{8}$	$8.25x10^{-3}$	27

These results reinforce what is observed in the size spectral analysis, in that the main difference in the systems is that between the M44 and M125 units. For the 10, 20 and 30nm aerosols, the M44 measured 27, 15 and 26% higher number concentration respectively than that of the M125. Similar percentage differences exist in the mass concentration outputs, although due the variation in the >100nm particle concentrations discussed previously, this is to be expected. The instruments all produced comparable GMD measurements for each of the samples.

Generally the three DMS did compare well when measuring from the same regular PM source. It is possible that as the M44 and M77 systems were upgraded first generation units compared to the newer M125 model, some differences in the configuration of the units, or improved hardware may contribute to the observed variation. Although relatively small, the discrepancy between systems should be noted as it will influence all the subsequent measurements and therefore will need to be taken into account when drawing conclusions.

6.6.3 Particle Characterisation for Multiple Gas Turbines

Exhaust sampling within the Sample III SC.02 [94] experimental programme was determined by one of two factors: either where test conditions were stipulated by the SAMPLE Consortium management, or in a parasitic mode, when sampling was allowed by the SR Technics facility leaders at non-performance critical stages of their engine certification operations. Hence, PM measurements were taken from other gas turbine engines in addition to the scheduled CFM56-5B4-2P dedicated engine test periods.

In total 5 gas turbine engines were tested at comparable engine power settings. These included four variations of engines manufactured by CFM International - a joint venture between GE and Snecma - and one Pratt and Whitney engine. The details of all the tested gas turbines are listed in Table 6.7.

Table 6.7: Specifics of the gas turbine engines tested at low and high power conditions at the SR Technics facility.

Engine	Maximum thrust	Combustor type	Other information
PW4000-94-44623	62000 lb (276 kN)	Phase 3	
CFM56-5B3P	33000 lb (147 kN)	Standard	
CFM56-7B263	26300 lb (117 kN)	Tech Insertion	
CFM56-5C4	34000 lb (151 kN)	Standard	Mixed exhaust nozzle
CFM56-5B4-2P	27000 lb (127 kN)	Double annular combustor	

Particle size spectral analysis plots were produced from stable testing periods measured using the M77 DMS500 situated on a gantry within the gas turbine test cell, as close as possible to the exhaust sample point. Positioning a particle size and mass measurement instrument at this location on the Annex 16 sampling line ensured that uninterrupted measurements would be recorded from the undiluted exhaust source at all times during tests. In addition to providing a constant point of comparison and measure of uniformity of all measurements at the final stage of the sample line, these instruments would also experience a minimum amount of particle losses.

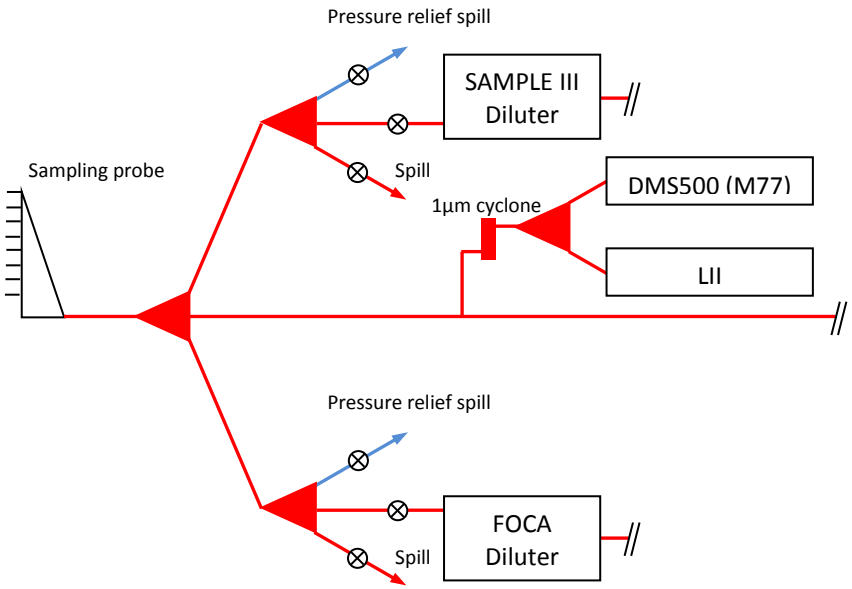

Figure 6.23: Schematic diagram illustrating the positioning of the DMS500 and LII within the SR Technics engine testing bay.

Under low power conditions, all of the exhaust samples comprised a bi-modal particle distribution with nucleation and accumulation mode peaks at approximately 10 and 25nm respectively.

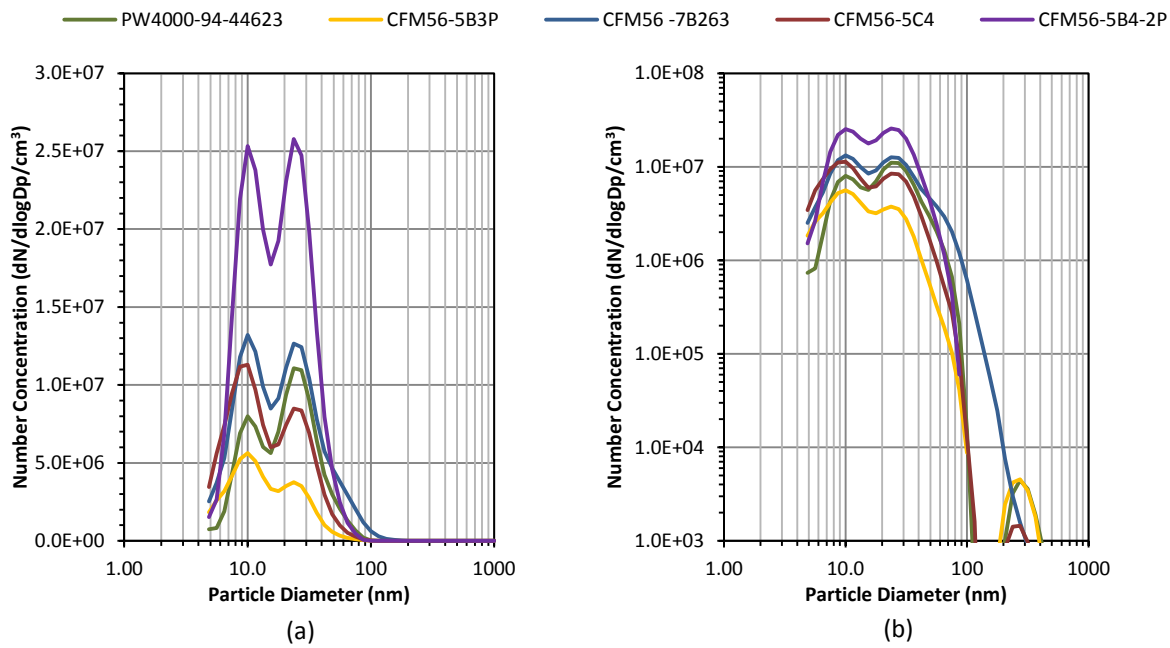

Figure 6.24: Particle size spectra for multiple gas turbine engines at low power conditions: (a) linear y-axis scale, (b) logarithmic y-axis scale.

At high power conditions there is a much more pronounced accumulation mode peak, a common occurrence as higher levels of soot particles are produced. There are indications that the size distribution is now of a tri-modal nature with the peak positions at approximately 10, 30 and 55nm.

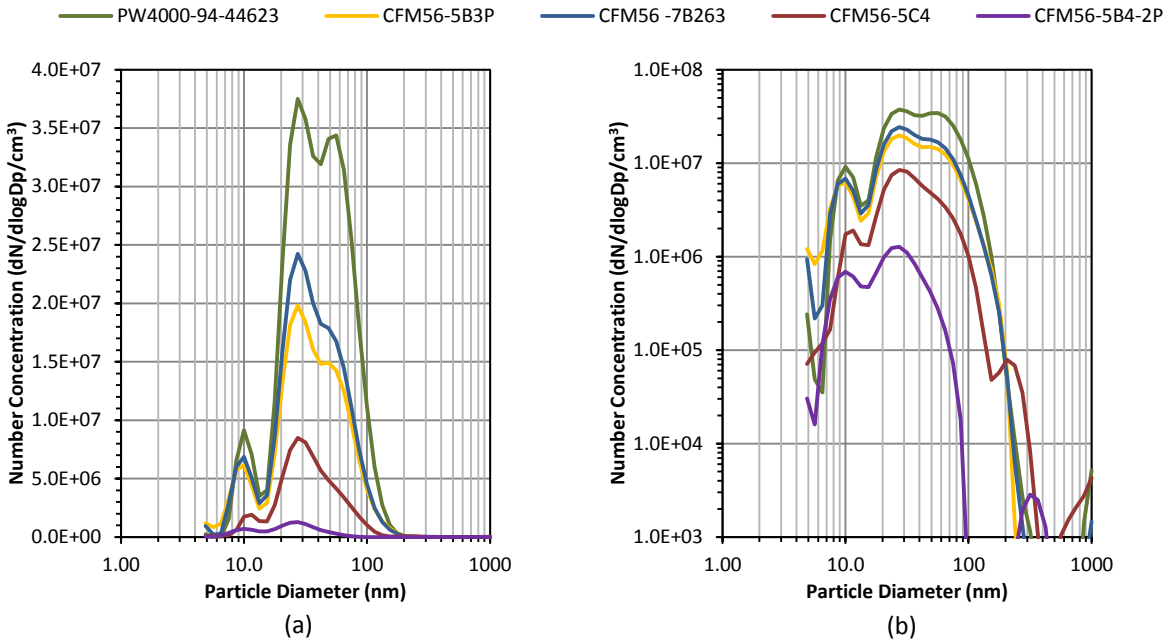

Figure 6.25: Particle size spectra for multiple gas turbine engines at high power conditions: (a) linear y-axis scale, (b) logarithmic y-axis scale.

The particle concentration levels for the majority of the engines at low power are very similar, with the notable exception of the CFM56-5B4-2P. This is an interesting result of the engines combustor design, the double annular combustor (DAC), which has 2 distinct combustion modes depending on the engine RPM. Figure 6.26 and Figure 6.27 show number and mass concentrations measured across a range of engine RPM settings. It is clear that following 2550 RPM the engine combustor switches from its initial mode to a secondary mode better suited for higher engine power output. This step change is seen in both total number and mass concentration charts and results in significantly lower, approximately 2 orders of magnitude, emission levels. Take-off and max-continuous settings do exhibit slight increases in particle mass output with some small variance also in number concentration. It is possible that these points do not follow the trends due to additional operational parameters which may be in place for these safety critical, regularly used engine modes.

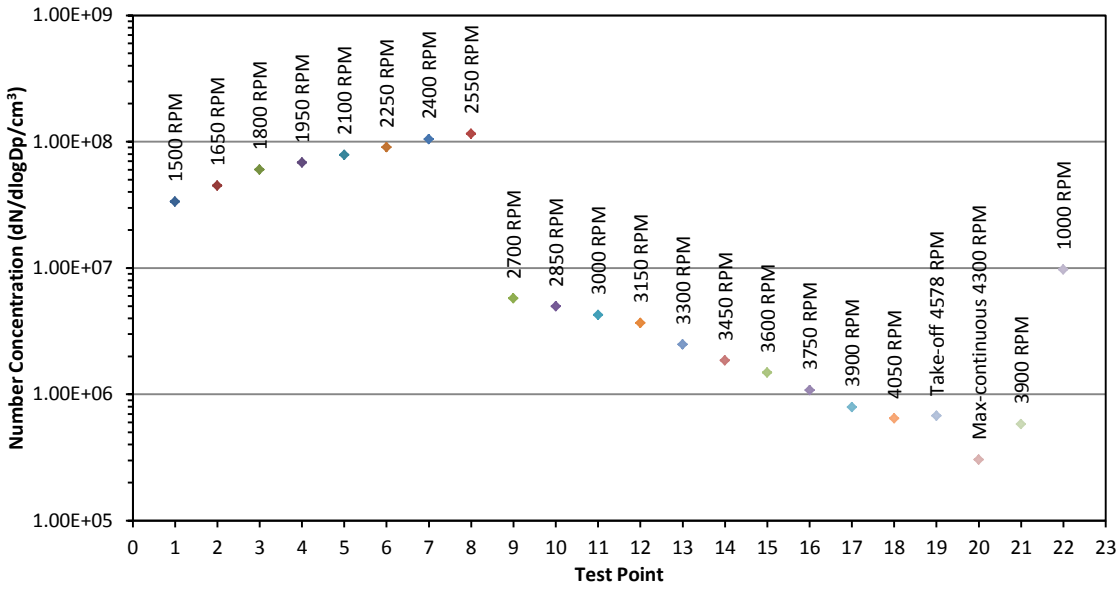

Figure 6.26: Total number concentration for CFM56-5B4-2P engine at various RPM settings.

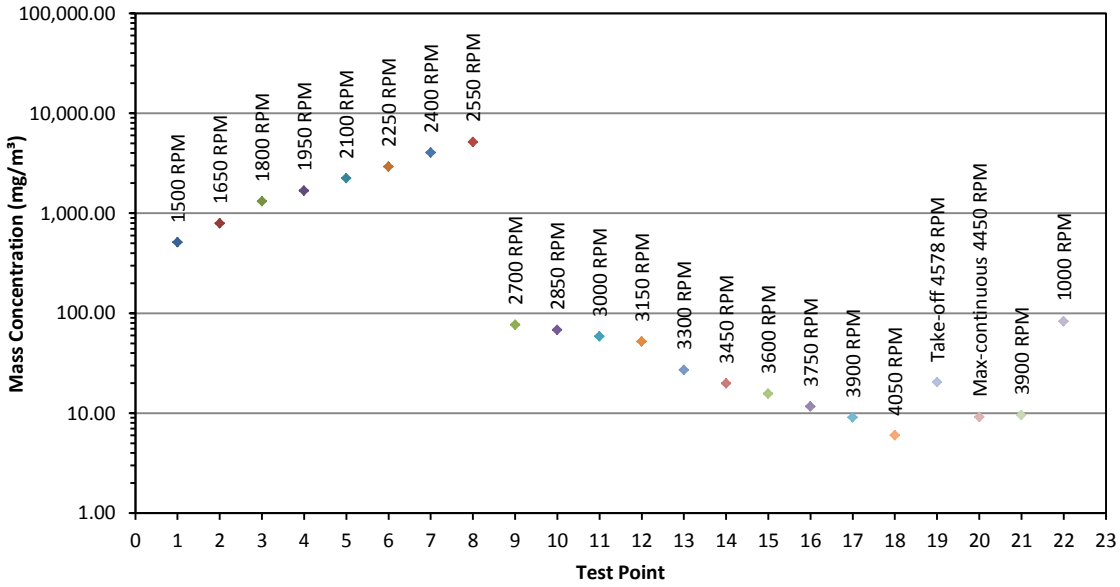

Figure 6.27: Total mass concentration for CFM56-5B4-2P engine at various RPM settings.

6.6.4 Influence of Sample Line Length on PM Measurement

As emphasised previously, the inclusion of long sample lines in aviation gas turbine emission sampling systems is essential for practical purposes of delivering gaseous

exhaust away from the exit plane of an engine and to the sampling instrumentation situated a safe distance away. Characterisation of how these transfer lines effect final PM measurement is critical to determine if PM downstream of the sample transfer system is representative of the actual engine exhaust. The sample line installation at the SR Technics facility was such that the FOCA sample line network comprised of two 12.5m heated lines, fixed end-to-end, to form the required 25m sample line stipulated by SAE E-31. This sample line configuration enabled appraisal of how the FOCA and SAMPLE 3 sample lines differed during sampling when the FOCA line was 12.5m or 25m, long as the sampling arrangement included 2 DMS500 capable of sampling on each line.

Three engine conditions were tested during this experimental programme comprising a low, medium and high PM condition, which had previously been identified during preliminary testing on the CFM56-5B4-2P gas turbine. Figure 6.28 shows DMS500 size spectra of the low, medium and high PM exhaust conditions sampled during this programme. These results were generated using data collected by the M77 DMS which was located on the gantry within the engine test cell. Sampling using the full length 25m sampling lines was conducted during each of the first PM conditions. This was followed by further sampling with the shortened 12.5m sampling line for the second set of exhaust condition. There is some slight variation in the low PM condition where slightly higher concentrations of ≈25nm particles were recorded, however the medium and high PM conditions remained very stable during both sampling periods.

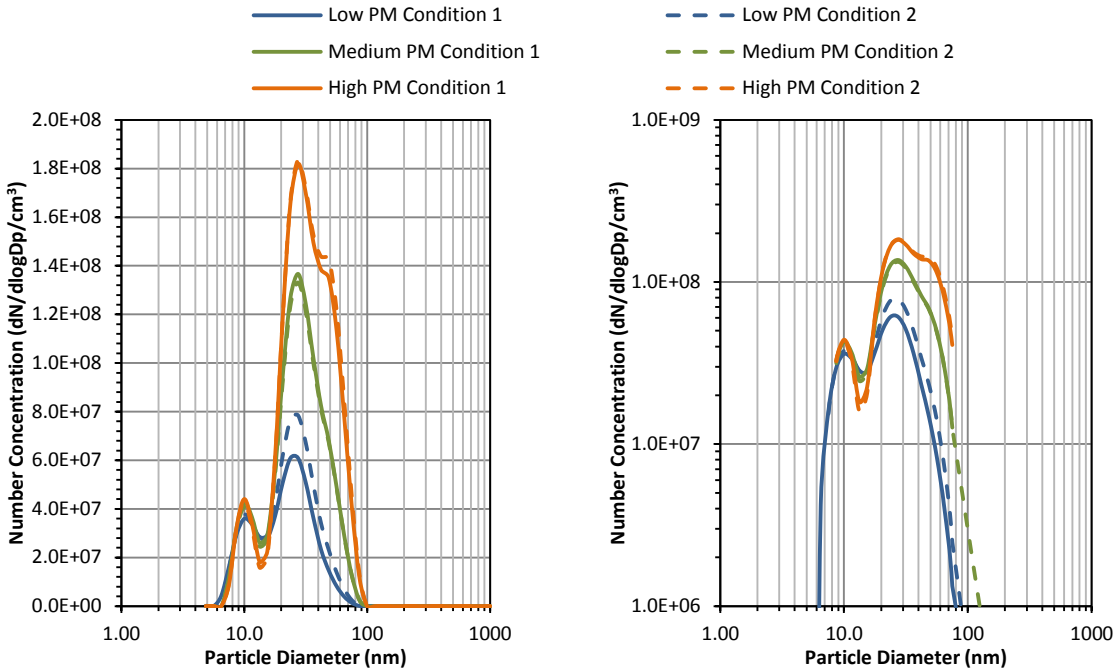

Figure 6.28: DMS500 size spectra of the low, medium and high PM conditions were sampled from the CFM56-5B4-2P gas turbine at the SR Technics facility: (a) linear y-axis scale, (b) logarithmic y-axis scale.

Assuming the bi-modality of the spectra to be correct, the nucleation mode of the particle composition, likely to contain a majority of volatile organic compounds, remains virtually identical for all three conditions. It is clear that the higher PM conditions (higher engine RPMs) produce higher concentrations of larger particles.

During the first sampling period of each PM condition, both the SAMPLE 3 and FOCA main sample lines were 25m long. In the second phase of testing the FOCA main sample line was shortened to 12.5m in length while the SAMPLE 3 main line remained 25m. The particle size distributions generated for each of the PM conditions previously described are shown in Figure 6.29 (low PM condition), Figure 6.30 (medium PM condition), and Figure 6.31 (high PM condition).

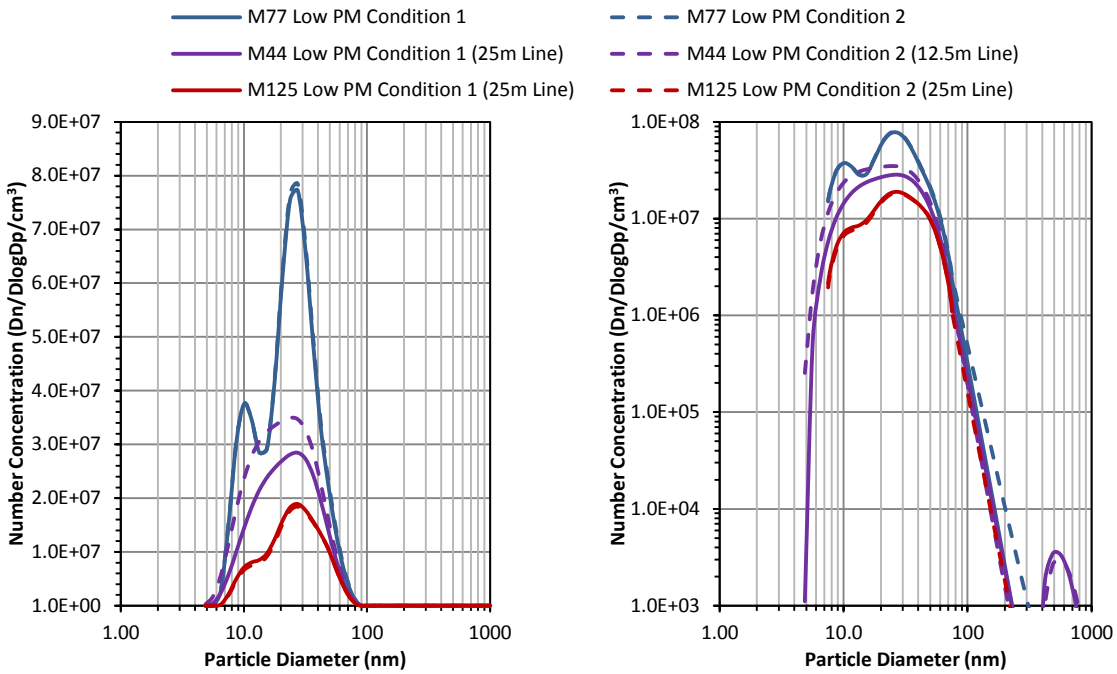

Figure 6.29: DMS500 size spectra generated from three DMS units utilising different sample line lengths during the low PM exhaust condition from CFM56-5B4-2P: (a) linear y-axis scale, (b) logarithmic y-axis scale.

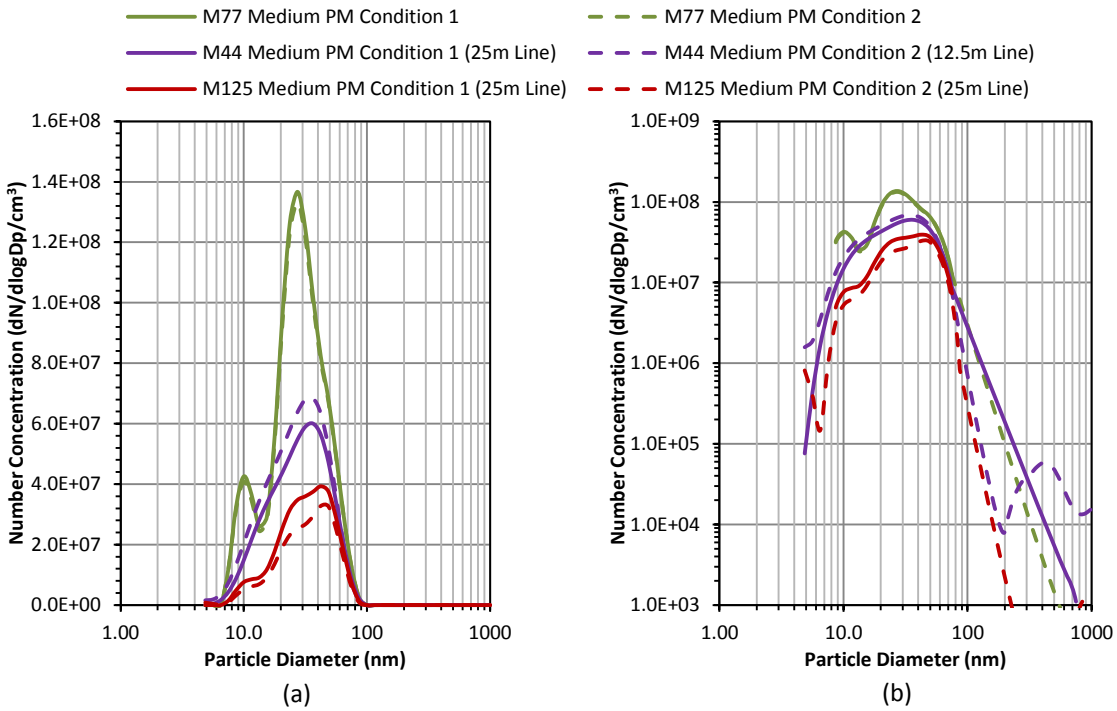

Figure 6.30: DMS500 size spectra generated from three DMS units utilising different sample line lengths during the medium PM exhaust condition from CFM56-5B4-2P: (a) linear y-axis scale, (b) logarithmic y-axis scale.

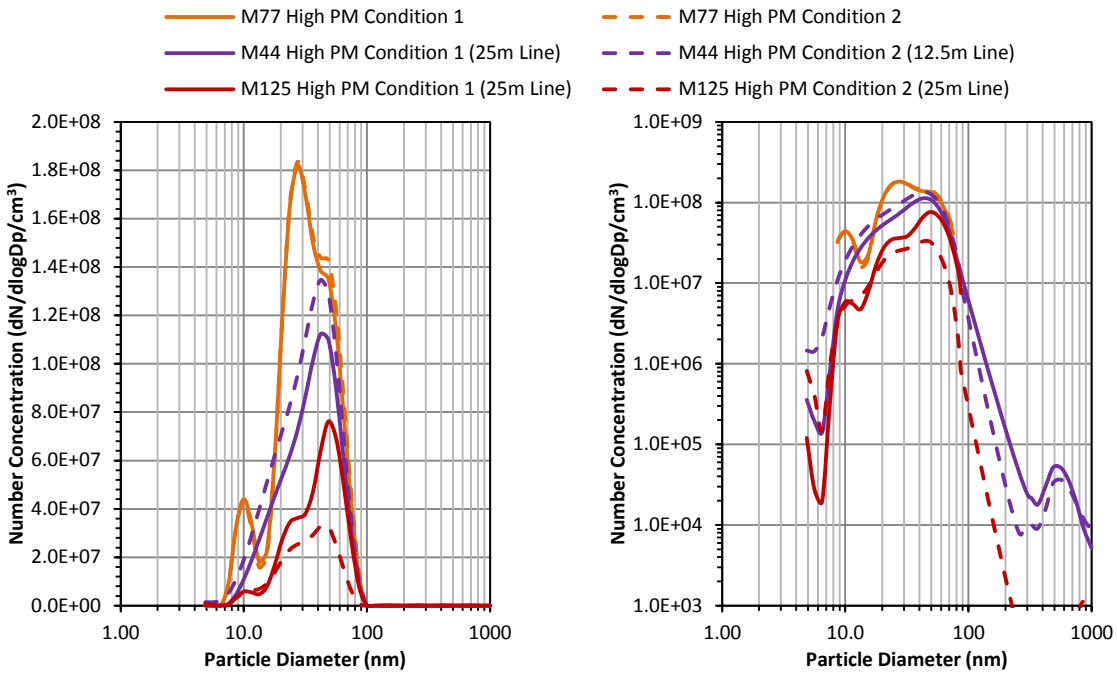

Figure 6.31: DMS500 size spectra generated from three DMS units utilising different sample line lengths during the high PM exhaust condition from CFM56-5B4-2P: (a) linear y-axis scale, (b) logarithmic y-axis scale.

First it should be noted that the results of the PM size spectral analysis show that there is a large difference between the concentration levels recorded by the M77 DMS500 (undiluted, close to probe tip) and the M44 and M125 DMS500 (downstream of sample network, 10:1 diluted). This reduction in PM concentration is most apparent at low and medium PM exhaust condition where ≈20% reduction in total PM number was observed. This is an inevitable consequence of the diffusional and thermophoretic losses that develop in long sample lines. The M125 also recorded lower PM concentration than the M44 however this was also witnessed during comparison of the instruments with the PALAS soot generator and when this is taken into account the number concentration results are comparable.

The main conclusion of these results is that of halving the main sample line length to 12.5m there was approximately 22% increased PM penetration compared to the 25m line. This highlights the requirement for a standardised PM sampling methodology as variations such as these lead to very different results and therefore unrepresentative

final emissions measurement. This problem could also be reduced through the inclusion on PM line loss compensation into final PM measurements.

6.6.5 Influence of Sample Line Temperature on PM Measurement

Currently SAE E-31 recommend that sample line temperatures should be maintained at 60°C in order to minimise particle losses due to thermophoresis and to reduce the possibility of re-condensation of volatile and semi-volatile organic compounds. During gas turbine exhaust analysis at the SR Technics facility this protocol was still under consideration and therefore the potential for PM measurement variability due to sample line temperature was investigated. This experimentation consists of PM analysis using the DMS500 systems downstream of the main SAMPLE sample line network which was heated to 160°C, and the FOCA main sample line network which was heated to 60°C. For this experiment a high power condition on a CFM56-7B26 gas turbine engine was used as an exhaust source. Figure 6.32 shows the DMS size spectra generated from a DMS placed within the engine test cell as close as possible to the sample probe (M77), and two DMS units downstream of the SAMPLE 3 and FOCA line networks (M44 and M125).

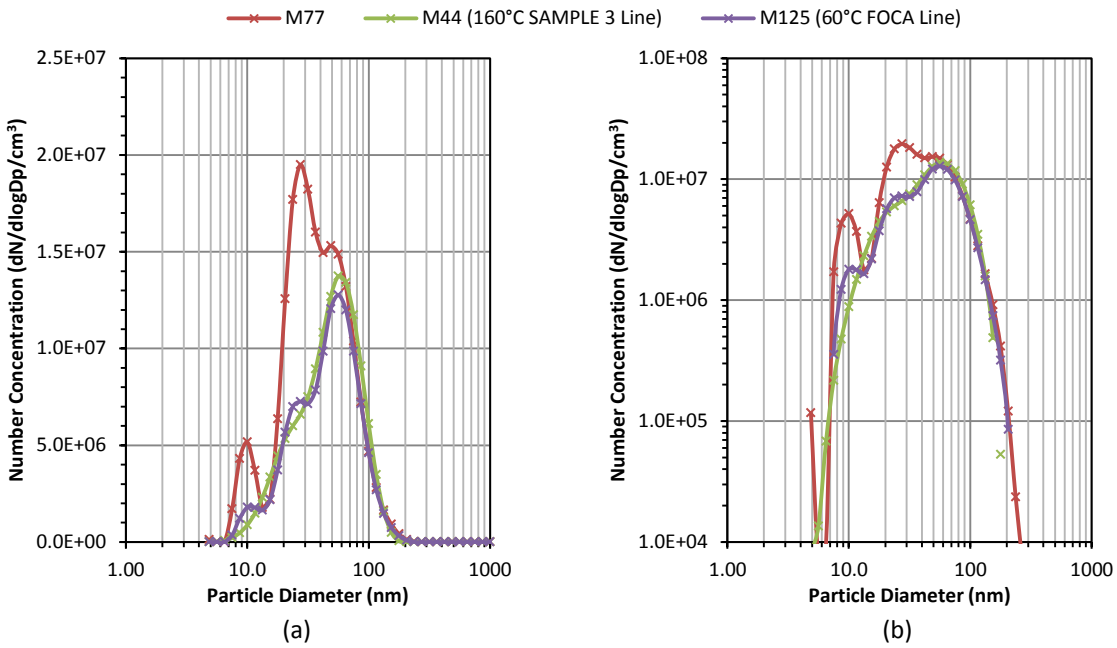

Figure 6.32: DMS500 size spectra generated from three DMS units utilising different sample line temperature for CFM56-5B4-2P at high power: (a) linear y-axis scale, (b) logarithmic y-axis scale.

The undiluted exhaust which was sampled by the M77 produced what appears to be a tri-modal distribution of with peak positions at approximately 10, 27 and 50nm with a total measured number and mass concentration averaged over the sample duration of $1.22x10^{7}$ N/cm^3 and $1.40x10^{-3}$ µg/cm^3 respectively. The spectra produced by the M44 and M125 have both been corrected for the 10:1 dilution which was applied to each sample line (160°C nitrogen dilution for the SAMPLE line and 60°C nitrogen dilution for the FOCA line) and generate far more mono-modal distributions than that of the M77. There is still an indication of the 10 and 27nm peaks which were recorded by the M44 and M125 DMS500 instruments, however these are far less pronounced than for the M77. Generally the PM spectra produced by M44 and M125 compare very well and the temperature difference between the two sample line networks has no significant on the final PM distribution. The total number and mass concentration recorded by the M44 and M127 are also consistent although as would be expected due to losses in the sampling systems they are significantly less than that measured by the M77 with values of $8.17x10^{5}$ N/cm^3 and $1.22x10^{-4}$ µg/cm^3, and $7.57x10^{5}$ N/cm^3 and $1.13x10^{-4}$ µg/cm^3 respectively. This difference can be attributed mainly to diffusional losses as clearly the thermophoretic impact is minor in comparison.

6.7 Chapter Summary

Using the HPCR and HES rig analysis of the impact variation of the sample conditioning parameters had on the PM size distribution was performed. Three test conditions were evaluated, those being a;

- **High temperature**: 400°C initial sample line temperature, maintained at 400°C until the introduction of 200°C dilution (N_2) at a 10:1 dilution ratio, followed by further 20°C dilution (N_2) at a 10:1 dilution ratio.
- **Medium temperature**: 400°C initial sample line temperature, maintained at 200°C until the introduction of 60°C dilution (N_2) at a 10:1 dilution ratio, followed by further 20°C dilution (N_2) at a 10:1 dilution ratio.
- **Low temperature**: 400°C initial sample line temperature, cooled to 20°C until the introduction of 20°C dilution (N_2) at a 10:1 dilution ratio, followed by further 20°C dilution (N_2) at a 10:1 dilution ratio.

The results showed that changes in the sample line and dilution temperature did not have a significant effect on the nucleation mode of the PM distribution. The larger accumulation mode however was reduced by approximately 36% when the line dilution temperatures were reduced to the lowest appraised values.

The overall assessment of this experimentation was that as the sampling system being designed by the SAE-E31 Committee intends to only measure non-volatile PM it is the larger size mode which must be maintained. As the medium temperature condition did not experience the same magnitude of PM losses across the size spectrum reducing the sample line and dilution temperatures to these levels may be appropriate. There are potential benefits to using a reduced temperature profile across the sampling system such as a reduced likelihood of thermophoresis occurring due to ‘cold-spots’ developing on sample line fittings.

Several interesting conclusions can be made from the experimentation conducted using the Rolls-Royce Artouste APU. First, the differences observed between the PM size spectra produced at high and low power conditions were consistent with those generated from large scale aviation gas turbines. This validates the use of a small scale gas turbine such as an APU for the purpose of sampling system appraisal. Introducing

an intermediary emission source between that of a synthetic aircraft exhaust produced at the GTRC and a full scale gas turbine certification test can be beneficial in terms of logistics, cost control and operational flexibility.

Second, at high power the emission of larger size particles was increased by approximately 62% significantly increasing the overall PM number and mass output. These high number and mass concentration are particularly concerning as it is the APUs which can remain running for longer periods of time while an aircraft is located in an airport. At low altitude it is these emissions which are directly related to human health in and around airport grounds.

Third, to capture transient PM emission events a fast particle analyser such as the DMS500 must be used. When the rate of change between two test conditions, in this case low and high power, is rapid the change in the PM composition is equally as fast. In this research programme in approximately 5 seconds the initial condition size spectra had transitioned and become fairly stable with the PM characteristics of the new condition. Utilising PM diagnostics apparatus which do not have a response time of 1 second of less will be unable to track these occurrences.

Exhaust sampling from the APU has shown that significant particle loss does occur over a long heated exhaust transportation line, particularly in the sub-40nm size region. Losses were less significant following initial sample conditioning with 160°C nitrogen and after a 1µm sharp-cut cyclone; however it was noted that caution is required when applying dilution ratio correction as this may potentially add further uncertainty to the final non-volatile PM measurement.

The UTRC particle line loss model was shown to be applicable to aviation gas turbine PM emissions measured using the DMS500. Measurements taken at the outlet of a 25m heated sample line and then corrected using this model showed excellent agreement with upstream measurements across the particle size range associated with aircraft engine exhaust. Differences observed between the measured and UTRC corrected spectrums, are within the DMS500 and dilution ratio measurement uncertainties. In addition, the uncertainty in the inversion fitting software may also be impacting the comparison.

The results gained from this experiment have aided the development and validation of the new non-volatile PM sampling methodology being developed by the SAE E-31 Committee. Although correction for particle line loss is not expected to be included as part of the final SAE Aerospace Recommended Practice (ARP), the consideration of particle loss theory is required in order to establish sample transport performance differences between engine manufacture systems. The understanding that particle losses will occur within a sampling system, and how best to mitigate and standardise these losses, is important. In addition, the ability to compare particle measurements taken from different experimental set-ups is something which this type of size methodology may be used for in the future, so as a better understanding of overall measurement uncertainty can be assessed.

Further work is required to improve understanding into the true nature of aviation exhaust PM composition (including volatile gaseous precursors). This will aid in further development of improved PM sampling methodologies and ensure that particulate measurements obtained following a complex transportation sampling system are representative of measurements at the engine exit plane.

Three DMS500 instruments were assessed for comparability using the same particle generation source. The results of this experiment showed that there is potential for some variation in the interpreted size distribution when operating DMS500 which have slightly different internal configurations. In these isolated circumstances employing the algorithm generated log-normal fitting profiles that are possible with the DMS500 would be appropriate and would potential provide even better correlation between the measured data sets.

The PM distributions which were obtained during multiple gas turbine sample at the SR Technics facility in Zürich displayed high degrees of bi-mobility across all gas turbine sizes, designs, and manufactures. PM modes consistent with volatile and soot agglomeration particulates are present at 10 and 30nm at lower power and 10 and 30 - 60nm at high power. There is a possibility that the DMS500 software inversion process may be introducing a higher probability of bi-modal emission profiles and it may therefore be worthwhile maintaining an element of scientism over the precise peak

locations. Future re-inversion of the data-sets with updated inversion matrices would be beneficial in fully understanding this topic.

PM number and mass concentration results obtained when sampling from the CFM56-5B4-2P gas turbine which employed a fuel-staged combustor design clearly displayed the potential PM reduction benefits of operating in a fuel-staged configuration. This is seen as a sudden drop in the measured PM at a set engine rpm at which time the engine has transitioned into a different combustion mode. Using this engine as an example reduction in number and mass concentrations of approximately 100% are achievable when comparing the measured emissions at the highest original un-staged condition lowest fuel-staged condition.

Approximately a 22% increase in PM penetration was observed when the main sample line was reduced from 25m to 12.5m in length.

No significant change in number or mass concentration was observed when comparing PM measurements taken from sample lines heated to 60 and 160°C. This further validates the decision to of the SAE E-31 Committee to limit sample line temperature to 60°C in order to reduce the likelihood of thermophoretic losses.

Chapter 7

PM Characterisation for a Fully Annular Gas Turbine Combustors Operating at Rich and Lean Combustion Modes

One of the recent advances in the commercial aviation gas turbine industry is the introduction of combustors designs which are able to operate in a lean-burning regime. The potential fuel saving and emission reduction benefits which these technologies can bring mean this is a trend which is likely to continue.

In this Chapter analysis of PM emissions which were sampled from both rich and lean combustor sections of modern large civil aviation gas turbines are presented. These results were collected as part of ongoing research collaboration between Cardiff University and Rolls-Royce into gas turbine particle emissions.

A fully annular combustor rig was used to generate the exhaust emissions presented in this Chapter. The main objective of the measurements conducted on this rig was to characterise the PM produced from two combustors, of rich-burning and lean-burning designs which were operated in multiple distinct combustion modes. These consisted of a high, medium and low power condition during experimentation with the rich-burn combustor and a pilot-only high and low power, and fuel-staged power condition while operating the lean-burning combustor.

Combustor exhaust was sampled using a traversing probe system which was capable of making a 360° rotation around the annulus of the combustor exit plane. Emissions measurements were made using an optical smoke meter, DMS500 and full gas analysis suite.

7.1 PM Measurements Using Traversing Probe

An important consideration during the development of any gas turbine combustor section is the evaluation of the pollutant emission production. One methodology used to study the exhaust characteristics of the combustion section of a gas turbine prior to full scale engine testing is to isolate this section on a testing rig and operate it with inlet and outlet conditions representative of those seen on a complete gas turbine.

PM measurements of this nature were obtained at Rolls-Royce combustion rig facility in Derby where characterisation of the combustion sections of a rich and lean-burning combustor were undertaken. An element of the combustion rig is that it allows fully annular particle and gas analysis measurements to be taken over a range of combustion inlet conditions. This was achieved using a specially design sampling probe and system of sample lines which made it possible to traverse the probe tips around the circumference of the annular combustor exit. A schematic diagram describing the probe rotation and the experimental set-up is shown Figure 7.1.

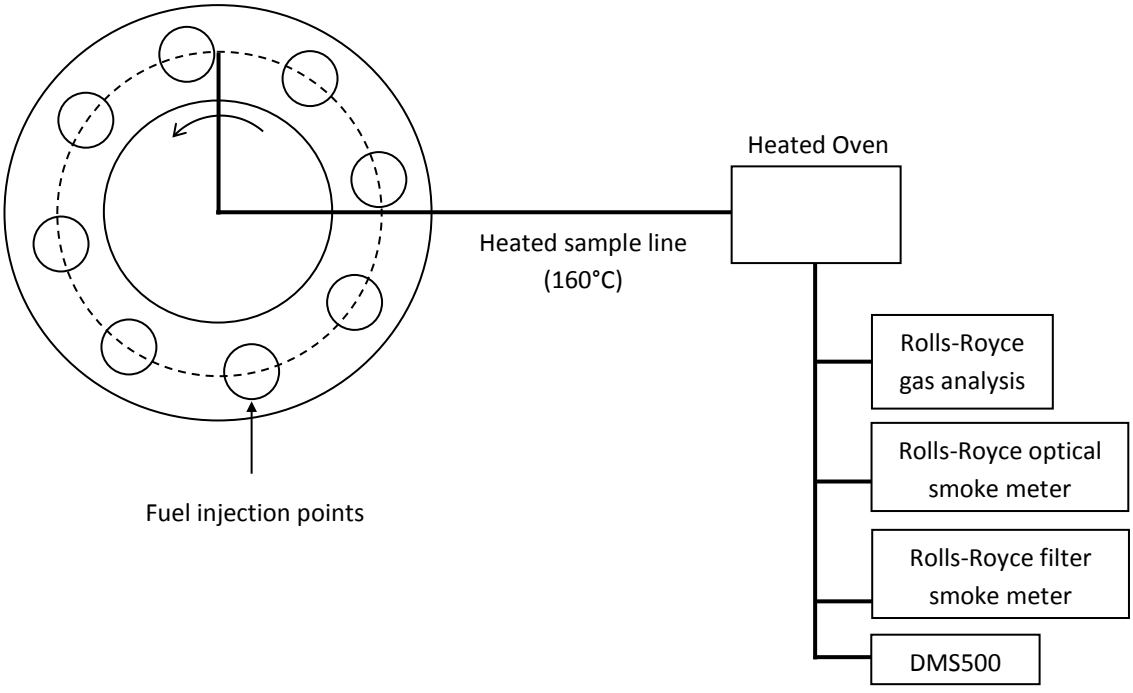

Figure 7.1: Schematic diagram of the experimental set-up for the rich-burn combustor test.

PM and gaseous emission samples for several combustor operating mode and power configurations were taken using this traversing probe set-up. Results from of each

sampling instruments were time-synchronised in post processing of the data to remove the detection delay caused by the variable sample line lengths connecting the measurement apparatus.

It is important to note that the results obtained when using the traverse probe which are presented in the forthcoming discussions do not show the absolute smoke number, particle number concentration or mass concentration across the entire annulus of the combustor exit. Due to confidentiality obligations the presented results were recorded over an undisclosed portion of the complete annulus. These data-sets show the observed trends, similarities and differences between the PM produced at various combustor configurations and are not intended to disclose or relate to any specific design or operational characteristics of this combustor system.

7.2 PM Sampling from a Rich-Burn Combustor

Most modern aviation gas turbines are designed such that the primary stage of the combustor operates either at or near the stoichiometric air fuel ratio (AFR of ≈15:1) or fuel-rich depending on the power level [121]. As described in Chapter 2 air is introduced into a combustor at different locations along its length and hence a distribution of air-fuel ratios develops along the length of the combustor. This has led to the traditional combustors being referred to as rich-quench-lean (RQL) combustors. In such designs the front portion of the combustor is operating fuel-rich, this mixture is subsequently diluted (quenched) by additional airflow downstream resulting in a final fuel-lean mixture at the combustor exit, as illustrated in Figure 7.2.

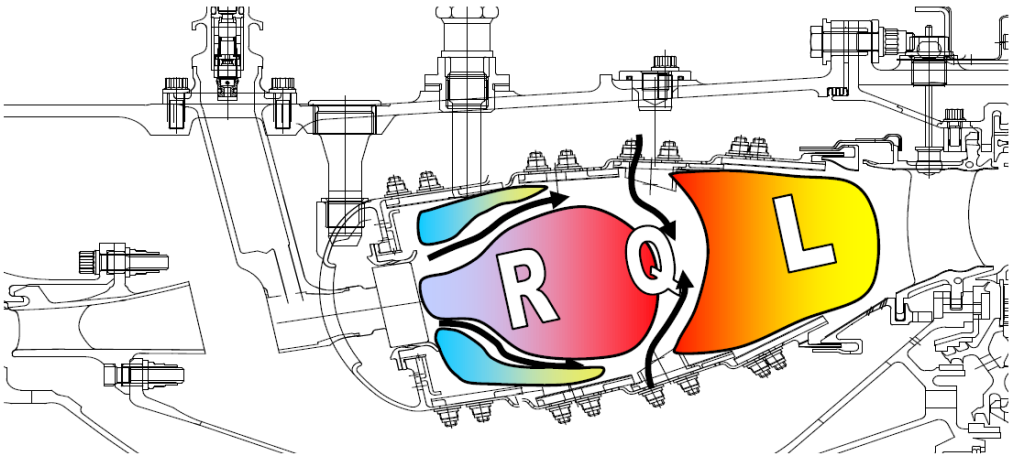

Figure 7.2: Illustration of an RQL combustor where a high temperature fuel-rich zone is maintained at the front of the combustor before quenching and diluting the combustion mixture with additional airflow, reproduced from [122].

7.2.1 Ambient PM Assessment

Prior to PM characterisation of the combustor exhaust samples, an analysis of the compressed ambient air which was being supplied to the combustor was performed to ensure that any artefacts of the ambient inlet air could be distinguished from the combustion exhaust PM. The resultant size spectrum showed the composition of the ambient PM distribution consisted mainly of large ≈200nm particulates (GMD of 148nm). This is consistent with the expected ambient conditions in an industrial location where concentration of dust, silica and other non-combustion related particulates are likely to be fairly high.

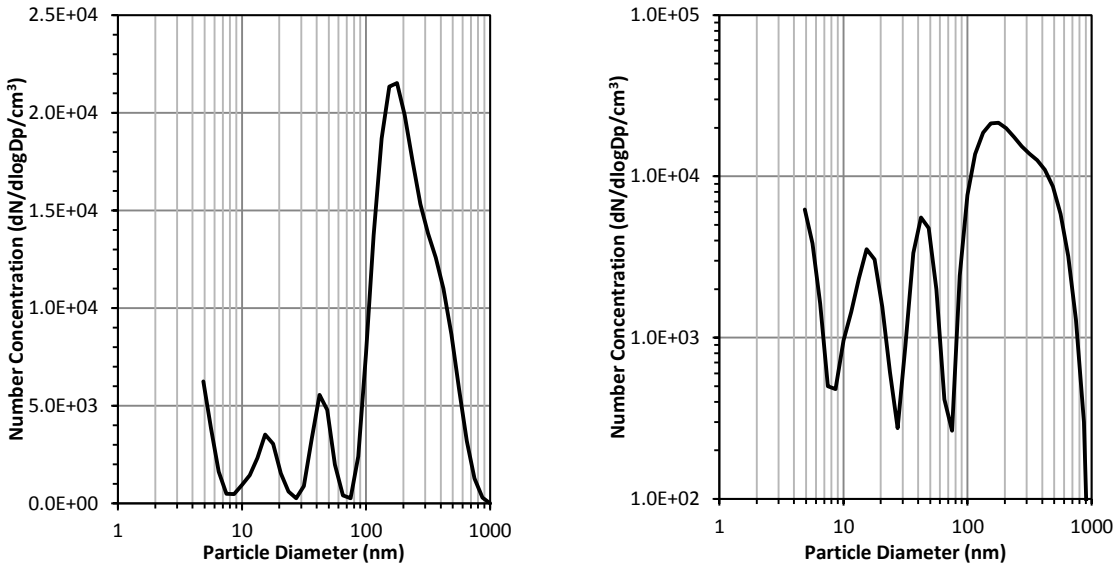

Figure 7.3: DMS500 size spectrum produced for ambient air: (a) linear y-axis scale, (b) logarithmic y-axis scale.

The measured total number concentration and mass concentrations for this ambient sample were recorded as 1.46×10^{4} N/cm^3 and 2.29×10^{-4} µg/cm^3 respectively. These are also fairly typical of ambient PM measurements [7,123].

7.2.2 Emissions at High, Medium and Low Power Combustor Conditions

Through variation of the combustor temperature, pressure and AFR several combustion configurations which were representative of those which would be used on a full gas turbine engine were achieved. For confidentiality reasons these conditions will only be referred to as being of low, medium and high power settings. In addition, the smoke number results have been normalised such that the trends in the results are maintained, however specific smoke number values have been removed.

As smoke number is the current aircraft engine exhaust regulatory standard, a comparative assessment of smoke number at each of the power conditions is an important benchmark. Figure 7.4 shows that the highest smoke number measurements are recorded at the highest power condition. The measured smoke number is of a similar magnitude at medium and low power conditions.

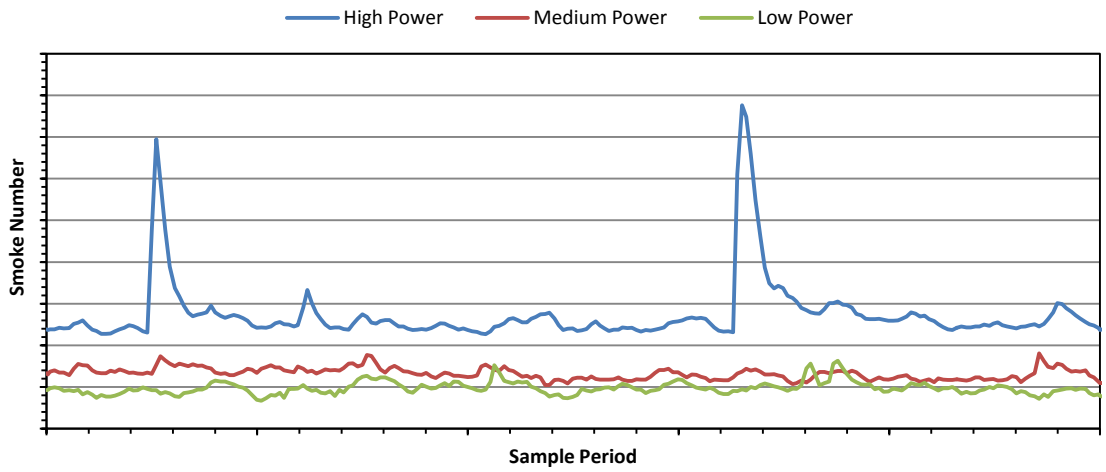

Figure 7.4: Comparison of recorded smoke number for high, medium and low combustor power conditions.

Higher smoke number at higher power conditions is a typical trend for RQL combustors, as illustrated in Figure 7.5. The higher fuel flows and normally higher equivalence ratios which develop at higher power conditions make smoke formation more likely.

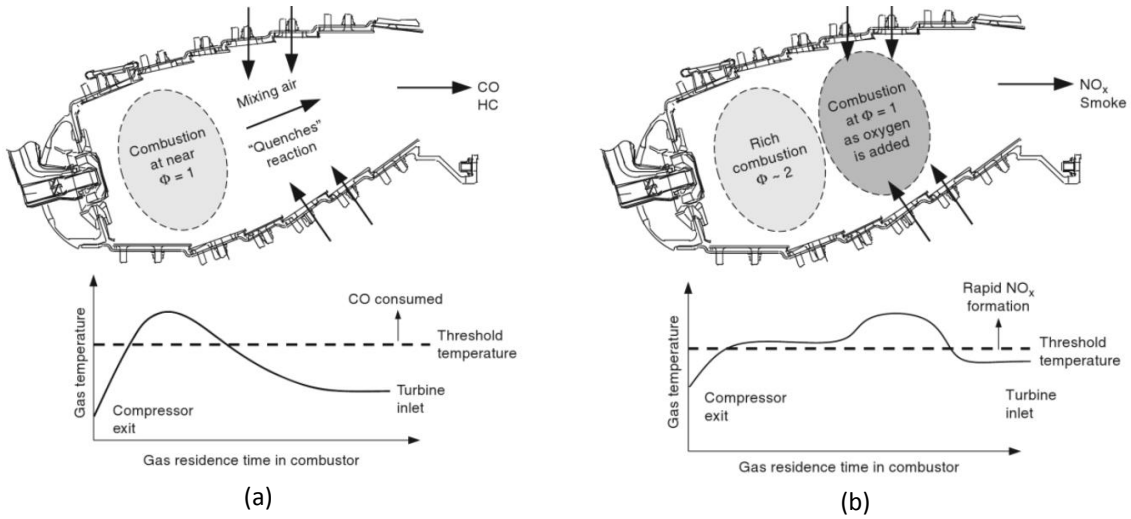

Figure 7.5: Typical emission formation trends for (a) low power, and (b) high power combustor conditions when operating a RQL combustor, reproduced from [121].

The correlation between the DMS500 mass calculation and the smoke number in terms of temporal resolution is excellent, as shown in Figure 7.6.

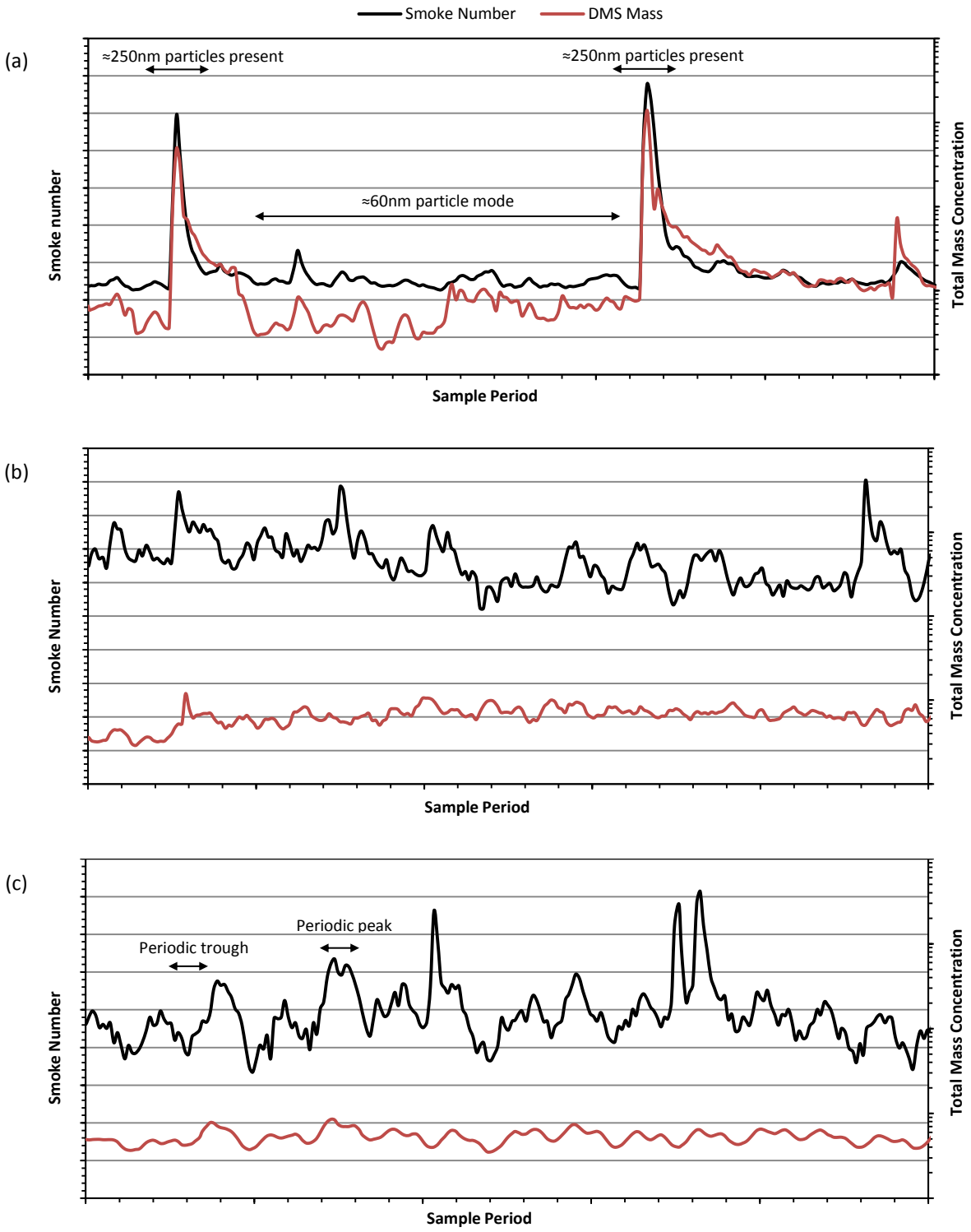

Figure 7.6: DMS500 total mass concentrations and optical smoke number comparisons at (a) high, (b) medium and (c) low power conditions.

Consistent with the DMS500 data the periodic increases in PM number concentration which occurred when the sample probe passed across fuel injection regions are mainly produced by particles in the 50 to 60nm size region. Particles in this size range do not

contribute a large proportion of total PM mass concentration and hence, whilst noticeable in the total mass output, are far less pronounced than that recorded in the number concentration measurements. These fluctuations are most apparent at medium and low power combustor conditions, where the two peaks in mass concentration which were recorded during the high power condition partially obscure the lower average condition magnitude concentrations.

The periodic peaks and troughs which are clearly identifiable in the smoke number, and to a lesser extend the DMS500 mass measurement arise when the sample probe passes the combustor fuel injectors. It is expected that in these regions where extremely fast paced chemical reactivity and fuel combustion is occurring that there will be higher than average concentrations of PM being recorded. To distinguish precisely which areas around the injector locations are responsible for the higher and lower PM recordings (centre of the injector core of outer edges of the fuel spray) a target single point emission sampling cycle would be required around the annulus of the combustor exit rather than a complete 360° traverse.

The large sudden spikes in the smoke number and DMS500 mass signals recorded during the high power condition were likely to have occurred due to the emissions sampling probe used and arise from shedding of particle build-up on the sample line walls.

The presence of the peaks and troughs in the exhaust emission profiles is also shown by the number concentration measurements which were recorded by the DMS500 at each combustor power condition. It is clearly observed that as the probe passes fuel injection locations there is a corresponding increase in PM number concentration.

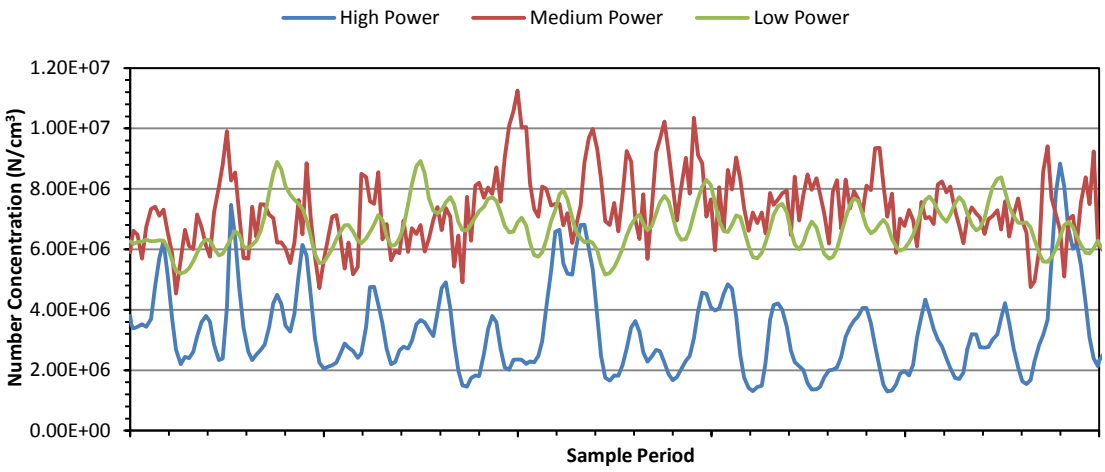

Figure 7.7: Comparison of the DMS500 number concentrations recorded during high, medium and low power combustor conditions.

As previously mentioned there is a disparity between the fairly stable smoke-meter readings across the probe traverse and oscillating PM number concentrations recorded by the higher sensitivity DMS500. It is interesting to note from the DMS500 data that there is a fairly consistent 'double peak' in number concentration close to each of the injection positions. Visualisation and computational fluid dynamics (CFD) models of fully annular gas turbine combustors in the literature [124,125] show that there are distinct flame regions surrounding each fuel injector. The presence of these peaks is therefore likely to be related the boundary of the flame or the distribution of the injector fuel at each injector position.

The presence of sudden peaks in the recorded smoke number during the high power condition illustrates one of the main limitations of the current regulatory standard for aircraft PM emissions. The lack of any data relating to the PM size or number distributions which are causing of these sudden increases prohibits analysis of these anomalies. This lack of detailed PM characterisation shows the benefit of understanding the size distribution which is being considered within SAE E-31 with the development of a new PM measurement and sampling system.

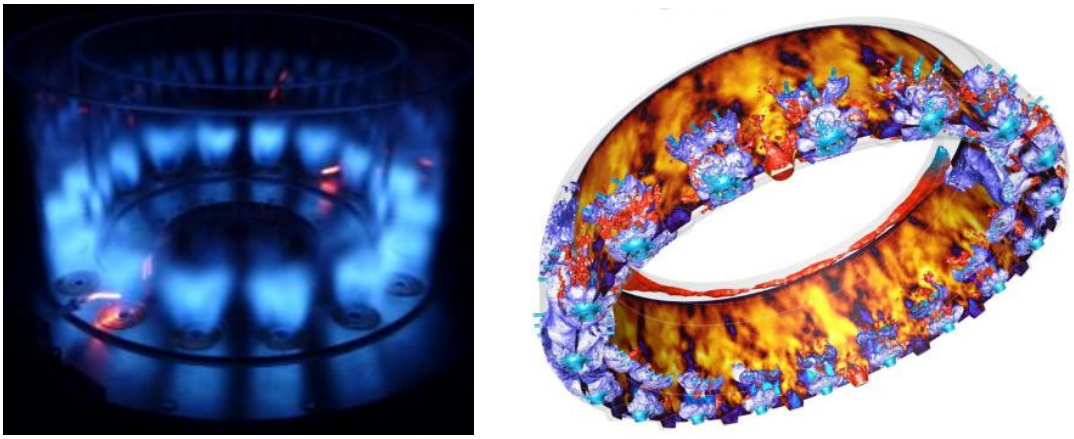

Figure 7.8: (a) Image of swirling flames for an annular chamber in a 200mm quartz tube, reproduced from [124], (b) CFD visualisation of a fully annular combustor ignition sequence, reproduced from [125].

A fast response particle measuring instrument, such as the DMS500, which is able to measures particle size distributions in real-time facilitates a better understanding of these types of anomalies. Figure 7.9 shows the smoke number signals overlaid onto particle size spectra contour plots. First, it is observed - most clearly for the high power condition - that there are periodic increases in particle concentration in the 50-60nm size range (whiter regions). This increased sensitivity enabling identification of PM source terms contrast with smoke number measurements which show only slight deviation from the condition average. At approximately the time of the sudden spikes in the measured smoke number during the high power condition there were also increases in the number concentration of particles in the 250nm size range. These increases in large size particles suggest that at these points particle shedding is occurring in the sample transport network and therefore at these periods the measurements are not representative of the overall combustor PM emissions. Occurrences such as these can develop for a number of reasons, in this case it is possible that pressure fluctuations in the sample arising from the high exhaust flow rate may have led to an increased potential for particle shedding. Without the PM size measurement data a combustion engineer could easily misinterpret that the smoke number emissions profiles are resulting from issues with the fuel injectors. It is also notable that the PM shedding events dissipate across a small period of time and

therefore this would need to be incorporated into any corrective post-processing technique.

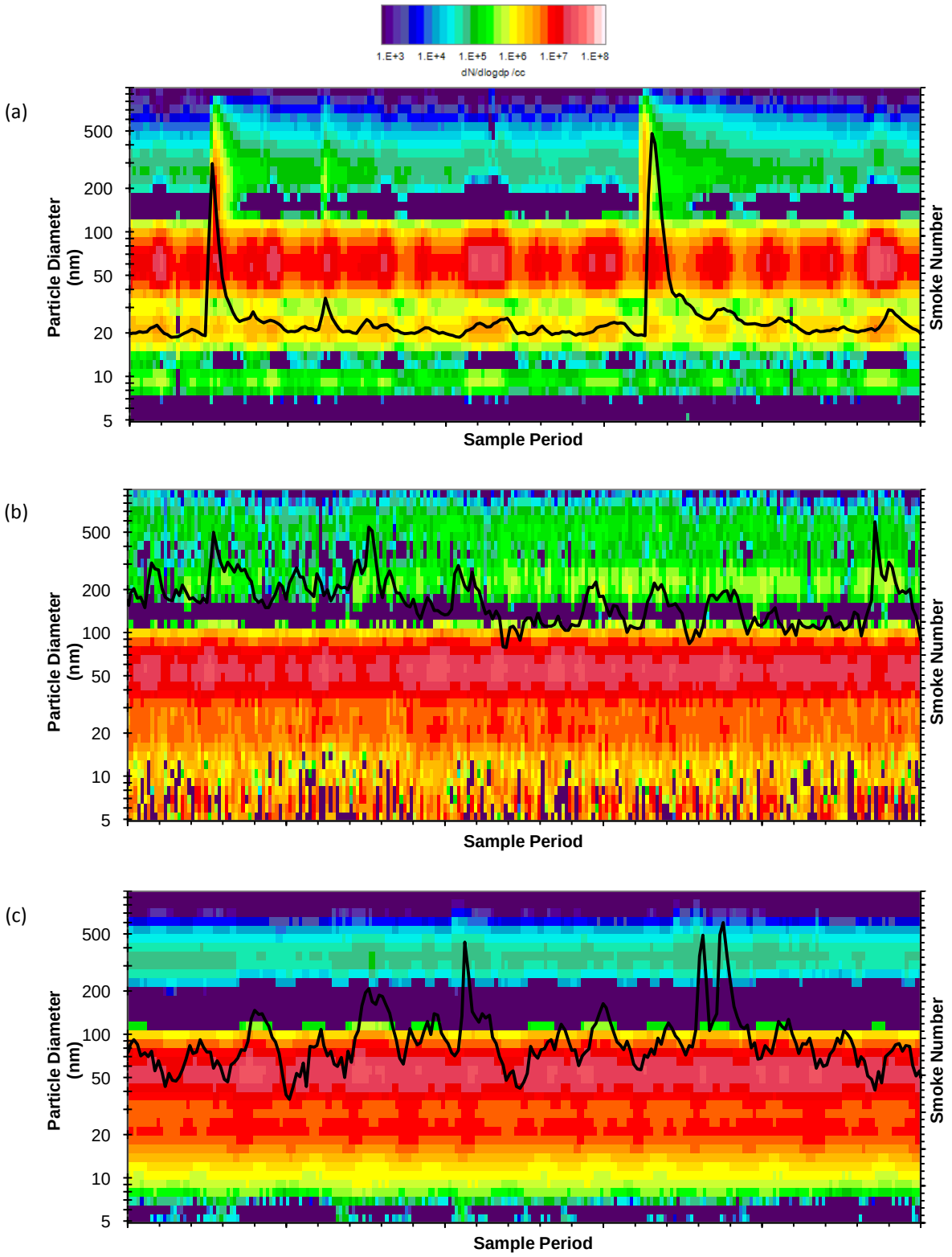

Figure 7.9: DMS500 size spectra contour plots with smoke number overlaid at (a) high, (b) medium and (c) low power conditions: smoke number shown by solid black line.

The DMS500 was used to analyse the PM size distribution of the exhaust at each of the combustor power conditions. These DMS500 results are presented in Figure 7.10 with the average size spectrum across the annulus of the exhaust exit plane, and a typical maximum PM distribution as the probe traverses a fuel injection location and a minimum PM distribution as the probe is traversed between two injectors.

It may also be observed at this condition that there are multiple lognormal particle size modes present in positions similar to those noted in previous aero-combustor and aviation gas turbines PM experiments (average size spectrum across the probe traverse). Multiple modes are detected by the DMS500, located at approximately 8, 20, 60nm, larger particle sizes stem from the non-combustion related particulates in the ambient inlet air or particle shedding from sampling system walls. It is possible that the smaller size modes consist of volatile and primary solid particles and that the larger size modes are agglomerates of smaller sized particulates.

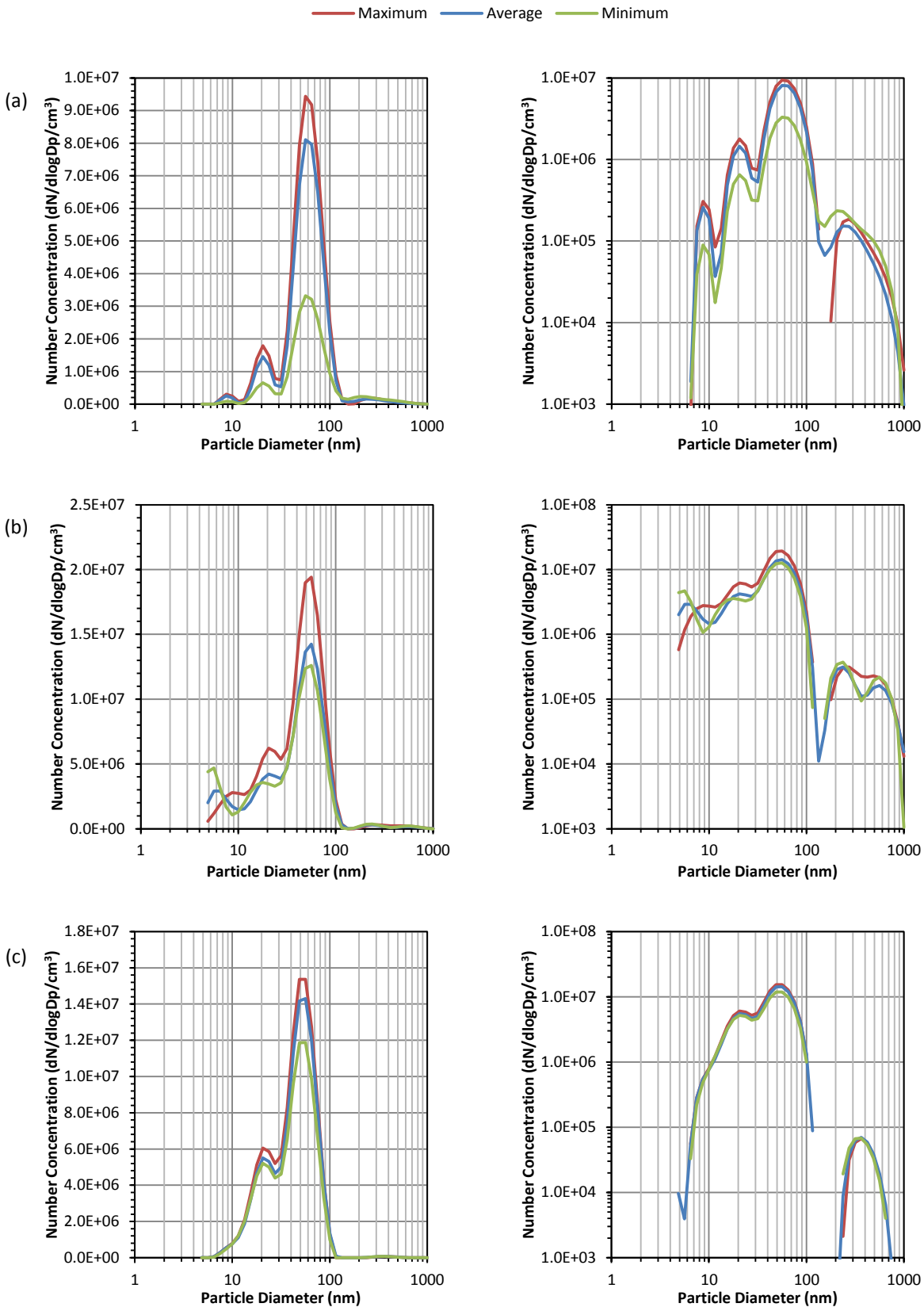

Figure 7.10: DMS500 size spectra at (a) high, (b) medium and (c) low power conditions: (left) linear y-axis scale, (right) logarithmic y-axis scale.

Average size spectra produced during each of the combustor conditions were also compared to the sample of ambient combustion air which was previously presented. Figure 7.11 shows that there is an appreciable difference in the particle size spectra produced at each of the combustor conditions and the ambient sample. This is most apparent for particle sizes below 100nm where the concentration levels are much higher than those measured in the ambient sample.

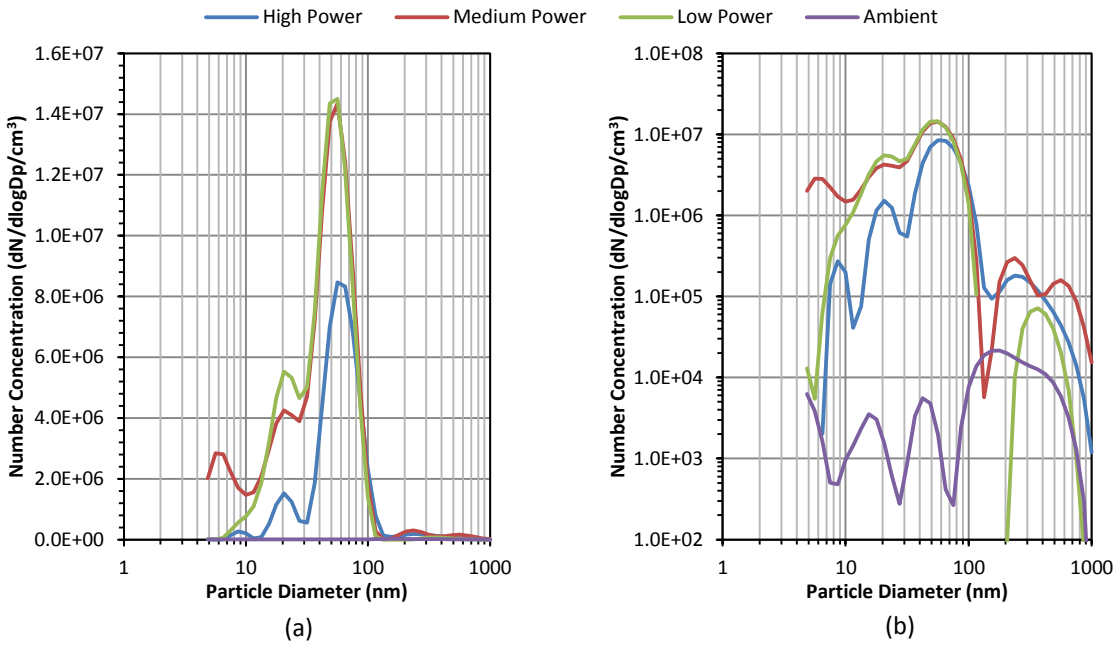

Figure 7.11: Comparison of DMS500 size spectra at ambient and high, medium and low power conditions: (a) linear y-axis scale, (b) logarithmic y-axis scale.

To assess how well the measured smoke number and DMS500 mass calculations correlate, each of the data sets collected at the three combustor conditions was compared to the FOA3 predicted mass for a each given smoke number. The FOA3 is based upon the empirical relationship between smoke number and the gravimetric measure of PM in engine exhaust emissions [126]. The correlation used to make the FOA3 mass prediction (mg/m^3) is shown in Equation 20 [126]:

$$FOA3_{mass} = 2.6156x10^{-6}SN^4 - 1.0998x10^{-4}SN^3 + 2.2367x10^{-3}SN^2 + 0.10955SN + 1.2842x10^{-3}$$

Equation 20: FOA3 mass correlation with smoke number.

The results of this comparison (Figure 7.12) display a very good correlation between the DMS500 calculated mass and the FOA3 prediction during the high and low power conditions. Post processing of the medium power condition showed that the DMS500 secondary rotating dilution system had remained set at a dilution ratio of 100:1 when it was intended to be at 1:1, and so is not presented.

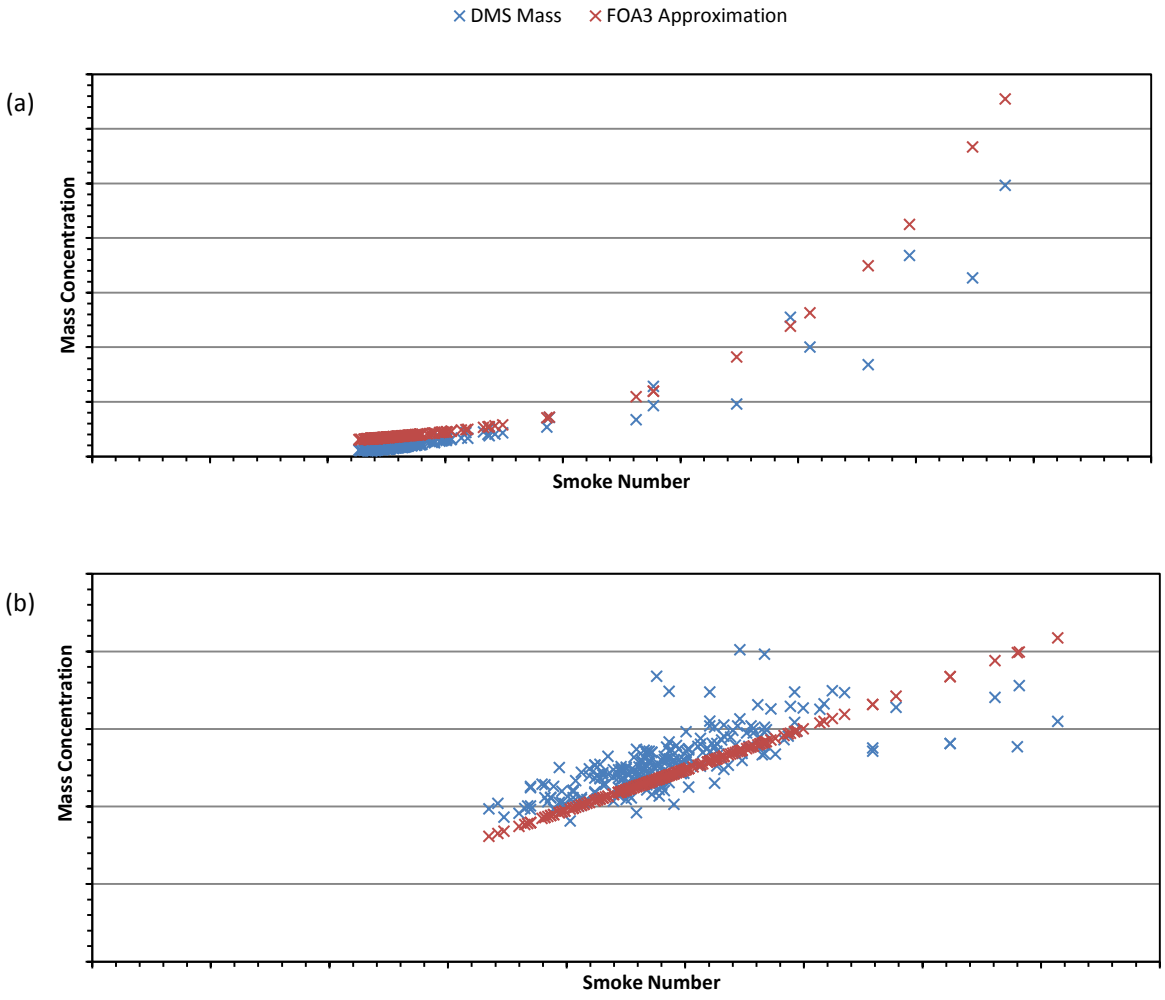

Figure 7.12: Correlation between DMS500 mass concentration and predicted mass using the FOA3 approximation for each smoke number measurement recorded at (a) high power and (b) low power combustor conditions.

Analysis of the gaseous emissions present in the combustor exhaust was also undertaken during this experiment. This enabled the calculation of the Emission Indices (EI) for each of the emission datasets. This can be particularly beneficial when discussing the PM number and mass concentration in an aircraft exhaust as they

provide details on the emission rate per kg of fuel. EIs can therefore enable greater comparison of emissions data from different engines operating at different conditions.

A EI for PM number concentration (EI_N (g/kg fuel)) and PM mass concentration (EI_M (#/kg fuel)) has been calculated for each combustor conditions considered, using the methodology and formulae outlined in the SAE gaseous emissions guidelines for aircraft emissions [127]. The formulae used to calculate EI_N and EI_M are shown in Equation 21 and Equation 22; the full derivation may be found in the SAE AIR6241 [128].

$$EI_N = \frac{PM_{number} \times 10^6}{([CO_2] + [CO] - T + X[C_xH_y] - U)(M_c + \propto M_h)} \frac{0.082T_{number}}{P_{number}}$$

Equation 21: Emission index for PM number concentration (EI_N)

$$EI_M = \frac{PM_{mass}}{([CO_2] + [CO] - T + X[C_xH_y] - U)(M_c + \propto M_h)} \frac{0.082T_{mass}}{P_{mass}}$$

Equation 22: Emission index for PM mass concentration (EI_M)

where PM_{number} and PM_{mass} are the number and mass concentrations measured by the DMS500 respectively, $[CO_2]$ is the mole fraction concentration of carbon dioxide in the exhaust, [CO] is the mole fraction concentration of carbon monoxide in the exhaust, T is the mole fraction of carbon dioxide in dry inlet air (0.00038), X is the moles of dry air/mole of fuel, $[C_xH_y]$ is the mole fraction concentration of total hydrocarbon in the exhaust expressed in ppmC, U is the mole fraction of Methane in the dry inlet air (0), M_c is atomic weight of Carbon (12.001), α is the atomic hydrogen-carbon ratio in the fuel (1.917), M_h is the atomic weight of hydrogen (1.008), T_{number} and P_{number} are the temperature and pressure defining the condition for the PM number concentration (273K and 1atm respectively), and T_{mass} and P_{mass} are the temperature and pressure defining the condition for the PM mass concentration (273K and 1atm respectively).

The results of the EI_N and EI_M calculations for the three combustor conditions are presented in Figure 7.13.

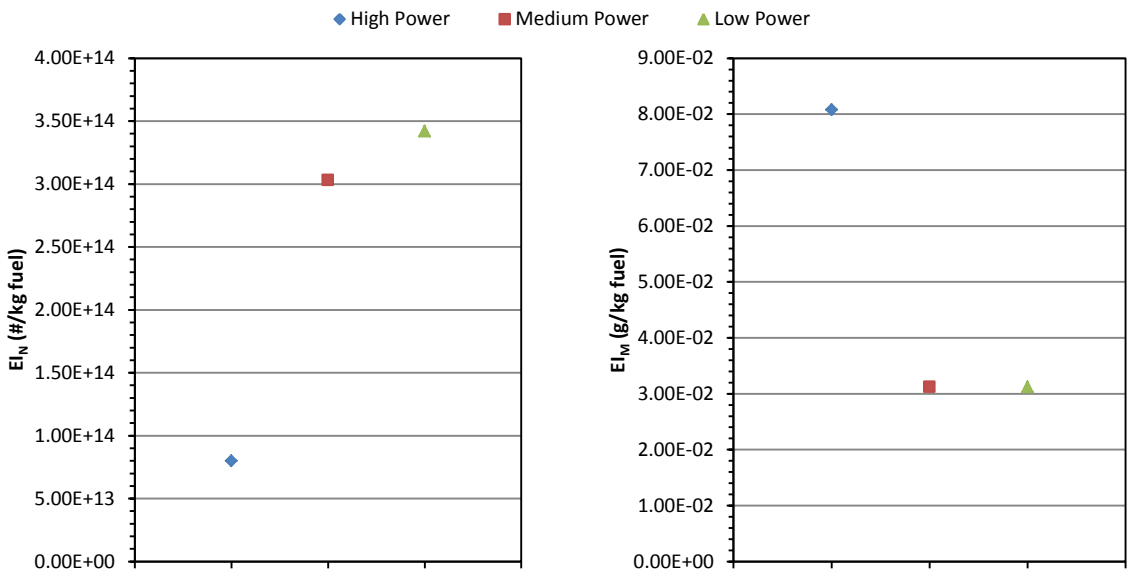

Figure 7.13: EI_N and EI_M values for high, medium and low power combustor conditions.

Gas analysis of the measured NO_x levels in the combustor exhaust is also noteworthy. As would be expected in the higher temperature and pressure conditions generated at higher power conditions the production of NO_x is far higher.

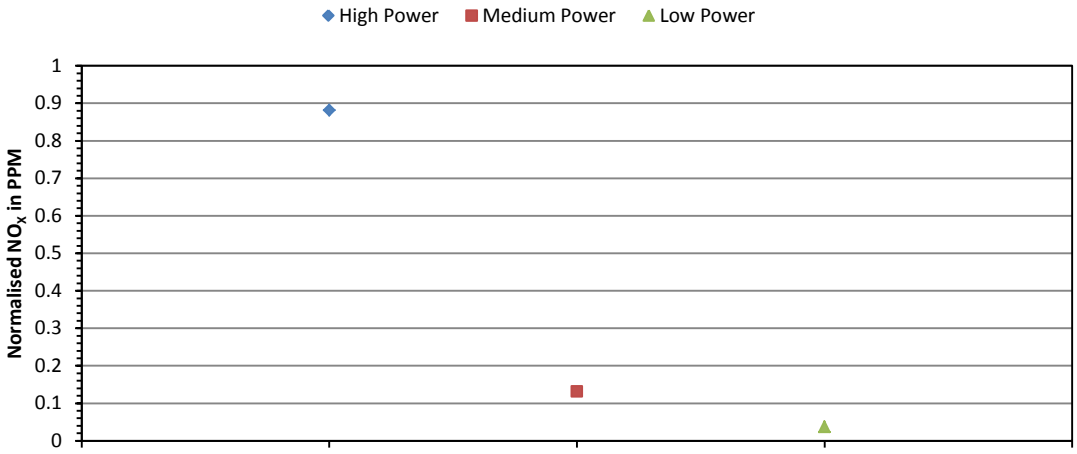

Figure 7.14: Normalised NO_x measured at high, medium and low power combustor conditions.

For some while there has been a movement in the aviation gas turbine manufacturing industry towards the production of combustor technologies which operate in lean-burning mode. One of the benefits of operating in a fuel lean mode is that the reduced localised temperatures and increased airflows can help reduce NO_x formation.

Additionally potential reduction of fuel-rich zones which can lead to inefficient combustion with reduced oxygen can establish other pollutant emission reduction benefits. This was something which was investigated during the second stage of combustor research at the Rolls-Royce facilities in Derby.

7.3 PM Sampling from a Lean-Burn Combustor

In the aviation gas turbine industry primary factors which have driven the development of lean-burn combustor technologies include regulatory pressure for lower pollutant emissions (lower NO_x), desire for improved engine performance, and engine reliability considerations. There are also additional benefits; such as the financial rewards for aircraft owners that could be achieved from lower airport NO_x landing charges with and for Original Engine Manufacturers (OEMs) new combustion technologies are also appealing as they are keen to promote their environmentally friendly credentials.

Lean-burning combustor designs have seen limited use in commercial aviation gas turbines since they were first introduced in the 1990s. The most successful implementation of lean-burn technology has been made by adoption of fuel-staged combustors.

In contrast to the RQL combustors, the overall approach of a fuel-staged combustor is to control combustion stoichiometry by either selective injection of fuel at multiple combustor locations [129] or through the use of novel injector design and variable injection regimes [121]. The final result is the same, that being in a staged combustor multiple airflow and fuel flow zones are allowed to develop rather than employing a uniform fuel and air flow at the front of the combustor as in a RQL design. By doing this a small volume of stoichiometric air-fuel mixture undergoes combustion near the injector and is surrounded by a larger volume of very lean combustion air. This general concept of a fuel-stage combustor is illustrated in Figure 7.15.

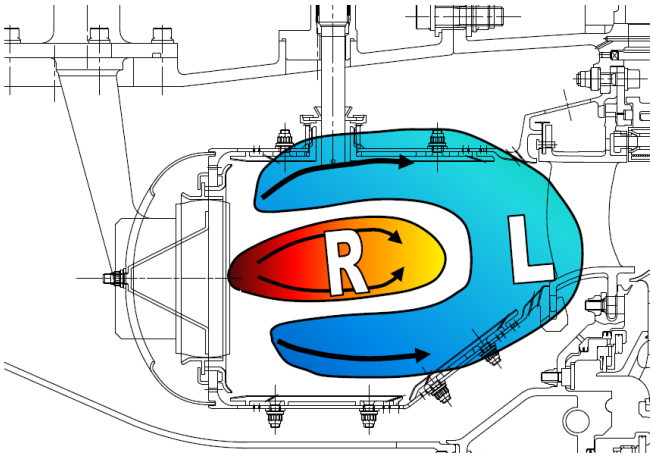

Figure 7.15: Illustration of a fuel staged combustor showing the small isolated high temperature fuel-rich or stoichiometric zone near the fuel injector is surrounded by a low temperature fuel-lean region, reproduced from [122].

The main benefits of operating a combustor in a fuel-lean configuration are the potential pollutant emissions reductions which can be achieved. The lower combustion temperatures and fuel-lean conditions mean that NO_x emissions can be significantly reduced when the combustor is operating in a staged configuration, as illustrated in Figure 7.16. Fuel-staging will often be designed such that it occurs prior to an engine's cruise operational range, as this is the power condition at which an engine operates for the majority of its lifetime.

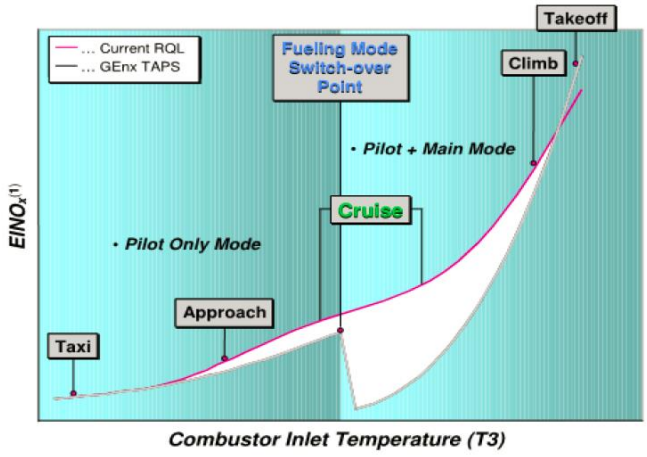

Figure 7.16: Comparison of NO_x production for conventional RQL combustor and a General Electric (GE) fuel-staged combustor across the engine operating range, reproduced from [130].

Additionally by reducing the probability of fuel-rich zones developing in the combustor PM production is likely to be reduced and therefore smoke emissions can be minimised.

The disadvantage of operating in a lean-burn combustion mode is that combustion stability issues can arise, particularity at low power conditions, due to the high airflow which is required to achieve fuel-lean operation. One methodology to mitigate these risks is to switch off some injectors at low power conditions. Alternatively, fuel injectors can be designed such that they operate with a pilot fuel and air flow and a main fuel and air flow, an example of such a design is shown in Figure 7.17.

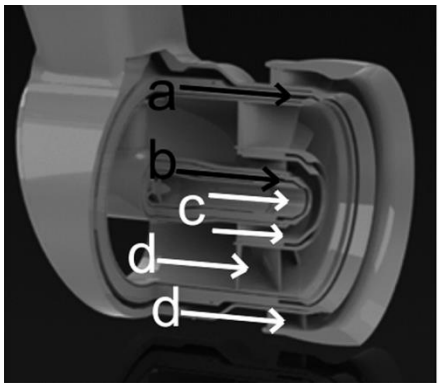

Figure 7.17: Rolls-Royce LDI fuel injector with concentric arrangement; pilot injector in the centre, (a) main fuel flow, (b) pilot fuel flow, (c)pilot air flow, and (d) main air flow, reproduced from [131].

The Rolls-Royce Lean Direct Injection (LDI) fuel injector has been developed primarily to reduce NO_x emissions.

7.3.1 Ambient PM Assessment

As was performed during sampling on the rich-burn combustor, an initial assessment of the compressed ambient air which was used as combustion air was undertaken. The ambient PM size distribution is similar to that recorded prior to the rich-burn combustor programme, with a dominant peak at approximately 200nm, and an overall GMD of 100nm. Number and mass concentrations were slightly lower than those observed during the rich-burn tests, as 7.68×10^{3} N/cm^3 and 6.42×10^{-5} µg/cm^3

respectively. Again these characteristics are consistent with what would be expected at an industrial facility in an urban location.

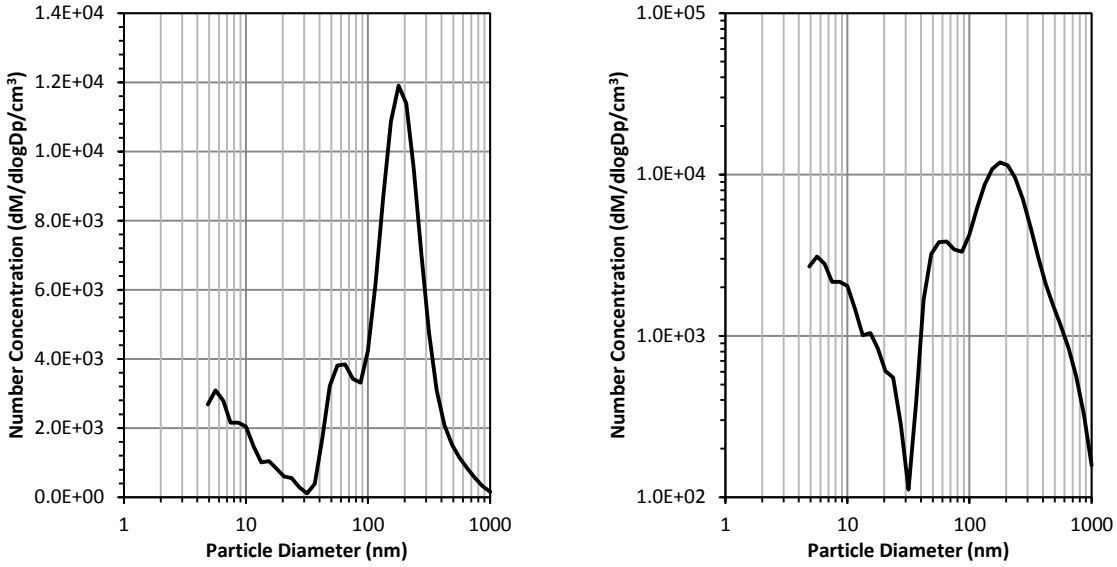

Figure 7.18: DMS500 size spectrum produced for ambient air: (a) linear y-axis scale, (b) logarithmic y-axis scale.

7.3.2 Emissions at Medium and Low Power Pilot-Only and Fuel-Staged Power Combustor Conditions

The purpose of a fuel-staged combustor is to vary the fuel injection and air flow characteristics to establish control over the combustion stoichiometry with the main goal of achieving lean-burning operational modes. Variation in these operational parameters will inevitably have an effect on the exhaust composition and therefore the overall PM distribution.

PM generated at three combustor conditions were analysed to investigate how the PM emissions changed as the operating mode of the lean-burn combustor varied. These conditions included a medium (top of the pilot-only injector mode range) and low (bottom of the pilot-only injector mode range) power condition when the combustor was operating in a pilot-only flame configuration; and a high power fuel-staged condition when the combustor had transitioned into a lean-operating mode.

Comparing the recorded smoke number measurements for each combustor condition shows a large difference between the smoke emissions of the high power conditions and those of the low power and staged combustor conditions. The medium power pilot-only condition in this combustor configuration produced the highest of all the recorded smoke number measurements, even those produced during the rich-burn combustor experiments.

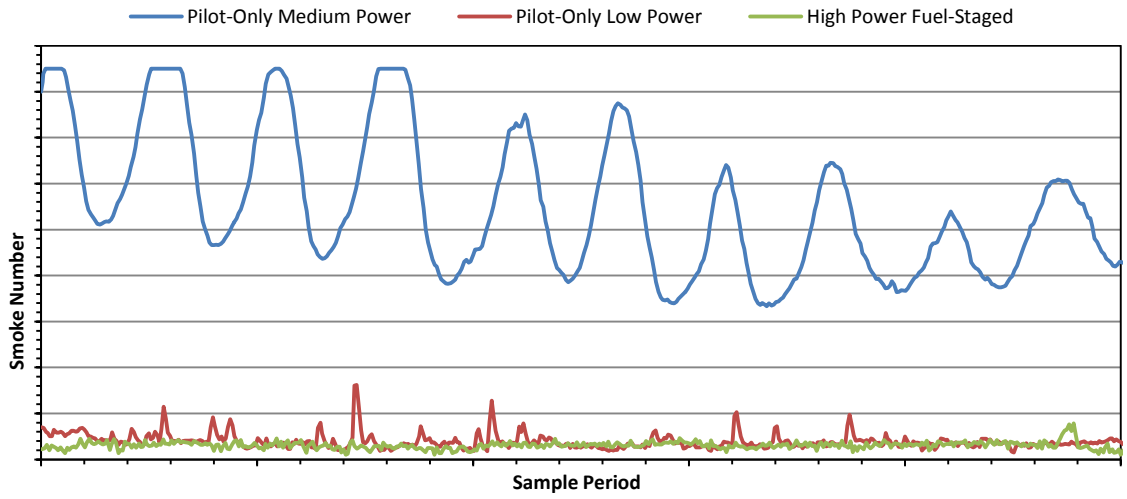

Figure 7.19: Comparison of recorded smoke number for high, low and staged combustor power conditions.

The periodic increases and decreases in the measured smoke data at the high power condition again reflect the traversing probe passing over fuel injection locations.

The DMS500 mass calculations correlate well with measurements of smoke number at the highest power condition during sampling of lean-burn combustor emissions. The flattened smoke number peaks represent periods when the optical smoke number instrument had reached its maximum measurement range. The smoke number and DMS500 mass concentration values which were generated by the pilot-only low power and fuel-staged conditions show some agreements at positions were there are sudden variations. However as has been previously discussed it should be noted that at these emission levels both the optical smoke-meter and DMS500 are within their respective measurement uncertainty zones.

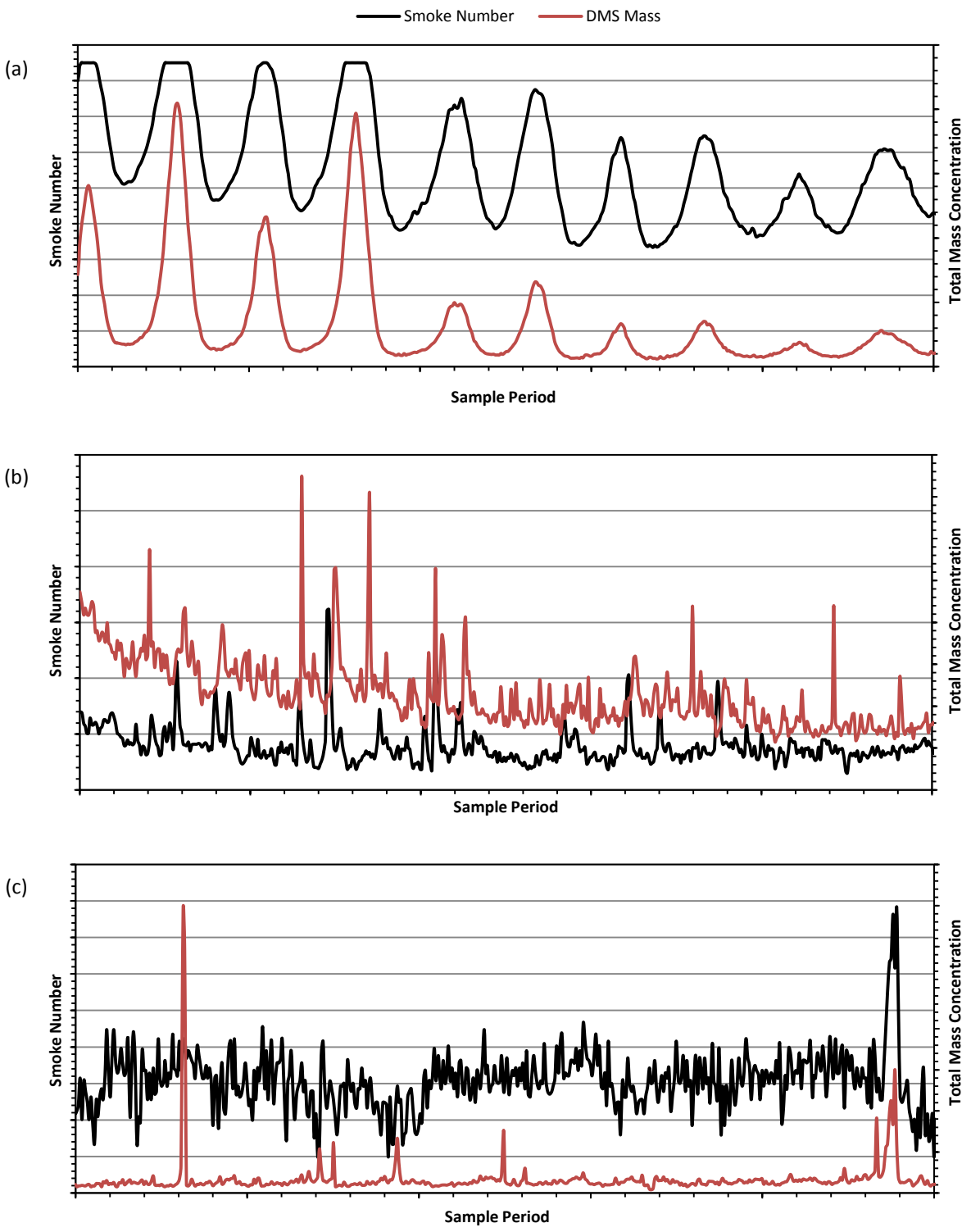

Figure 7.20: DMS500 total mass concentrations and optical smoke number comparisons at (a) pilot-only medium, (b) pilot-only low and (c) fuel-staged power conditions.

Total number concentrations measured using the DMS500 (Figure 7.21) show the same trends as those seen in the smoke number measurements. As would be expected the medium power condition operating in a pilot-only combustor stage configuration resulted highest measured number concentrations, followed by the low power condition, and finally the lean high power fuel-staged condition. The PM number concentration levels of the fuel-staged condition are very low for a combustion system, and illustrate the potential PM reduction benefits of operating a combustor in such a combustion mode.

These results also highlight the growing need for new non-volatile PM regulations and sampling methodologies for the aviation industry as discussed in the previous Chapter. The average smoke number values of the pilot-only low power and the fuel-staged conditions were typically less than 3, while the accuracy of the smoke number measurement is generally considered to be ±3. As future combustor technologies including fuel-staged combustors and potentially alternative aviation fuels begin to be introduced into the commercial aviation market in a continuing effort to reduce pollutant emissions and fuel consumption, there will be an increased demand for appropriate, accurate regulatory standards and sampling methodologies for engine certification.

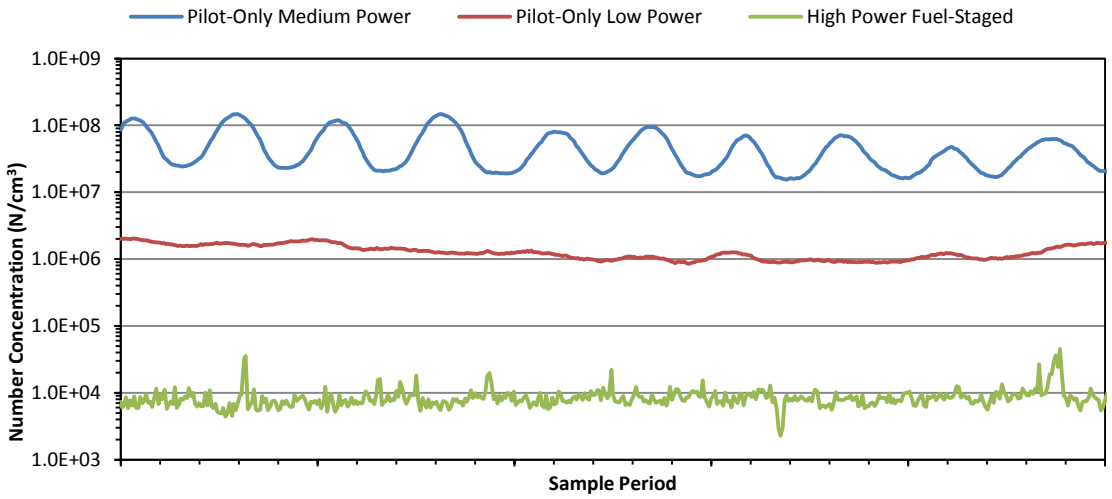

Figure 7.21: Comparison of the DMS500 number concentrations recorded during pilot-only high and low power, and fuel-staged combustor conditions.

The DMS500 PM data was also processed in the form of PM number and particle size contour plots from exhaust samples produced at all operating conditions tested on the lean-burn combustor rig; these are shown in Figure 7.22. The scale used to present this data is consistent with that used in the analysis of the rich-burn dataset in order to allow direct comparison between the results.

Possibly the best illustration of the periodic PM generation fluctuations was produced during the sampling of the pilot-only high power condition exhaust. It is interesting that not only are there increases in the concentration of particles in the 50 - 200nm range but also regions of high concentration of smaller ≈20nm particles detected. These formations were recorded at positions between the fuel injection points and therefore could be regions where volatile or small solid material has not been burnt off. Growth of the larger particles (≈400nm) may also be occurring due to agglomeration of particles generated during combustion to the surface of large particles entrained in the ambient combustion air. The increasing concentration of particles >200nm can also be observed in Figure 7.24.

The contour plot produced for the pilot-only low power condition is very different to that of the high-power condition. The majority of the particle number concentration has shifted to lower sized particulates and although still slightly visible the periodic increases in number concentration are less well defined.

During fuel-staged operation the PM concentration levels are so low it is difficult to discern any obvious trends in the PM output. The highest concentrations of particles are in the 50 - 500nm size region, consistent with the spectral analysis of the ambient combustion air prior to combustion tests.

As in the previous rich-burn testing the smoke number measurements were found to compare well with the DMS500 in terms of temporal characteristics, with increases in large particles concentrations recorded by the DMS500 occurring concurrently with increases in the measured smoke number.

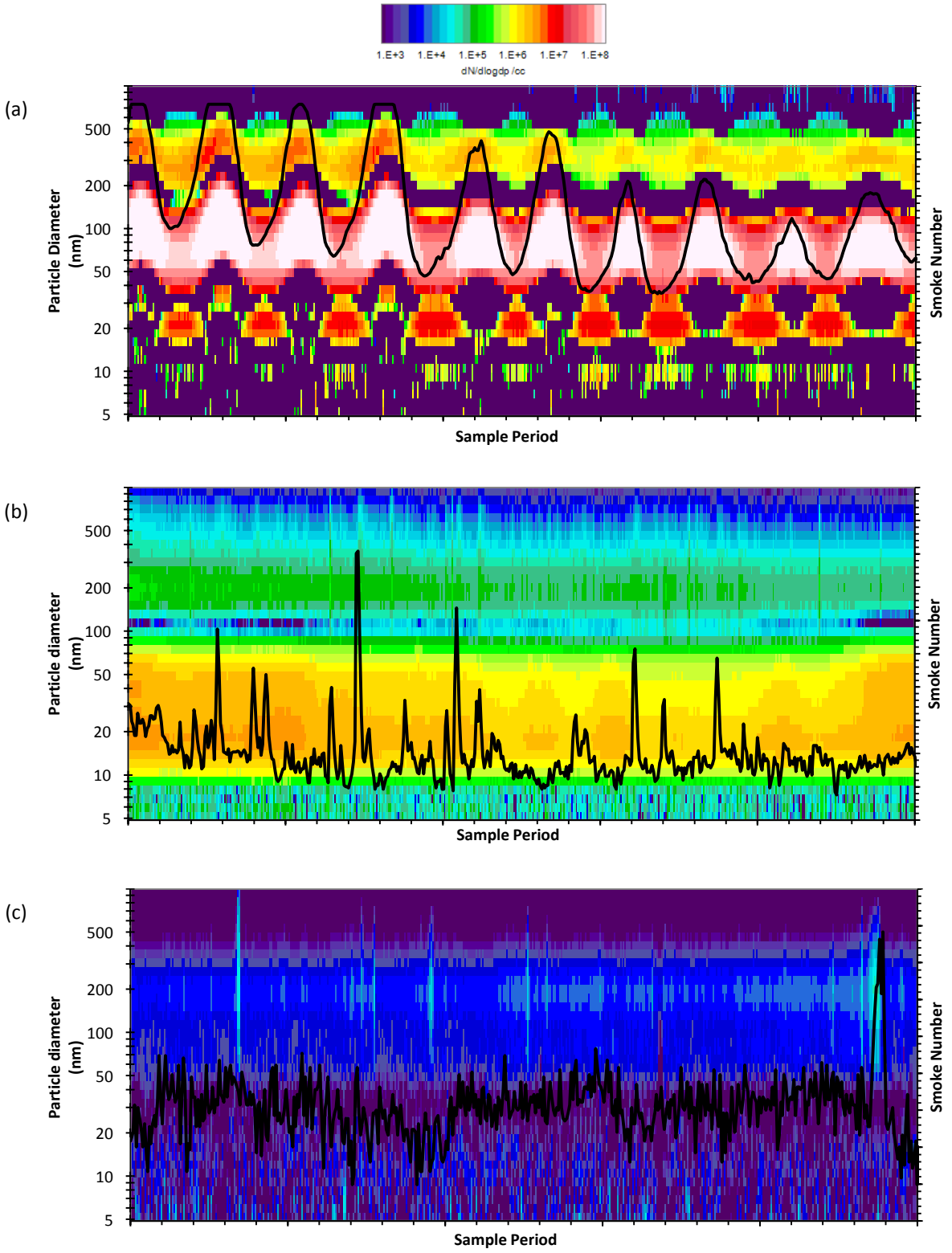

Figure 7.22: DMS500 size spectra contour plots with smoke number overlaid at (a) pilot-only medium, (b) pilot-only low and (c) fuel-staged power conditions: smoke number shown by solid black line.

The PM size distributions generated at each combustor condition are shown in Figure 7.23. During the pilot-only high power condition the particle generation is consistent with a typical rich-burn combustor configuration shown earlier. This is to be expected as the combustor will be operating at stoichiometric or fuel-rich conditions to ensure combustion stability.

The transition to the pilot-only low power condition is accompanied by a drastic change in the PM size distribution. PM concentrations and primary size mode have reduced with a new peak position at approximately 20nm.

The final size spectrum for the fuel-staged condition produced PM concentration levels which were beginning to enter the uncertainty level of the DMS500's detection range ($1x10^{-4}$ $dN/dlogDp/cm^3$). These levels are typical of those observed at ambient conditions and are extremely low for a combustion system.

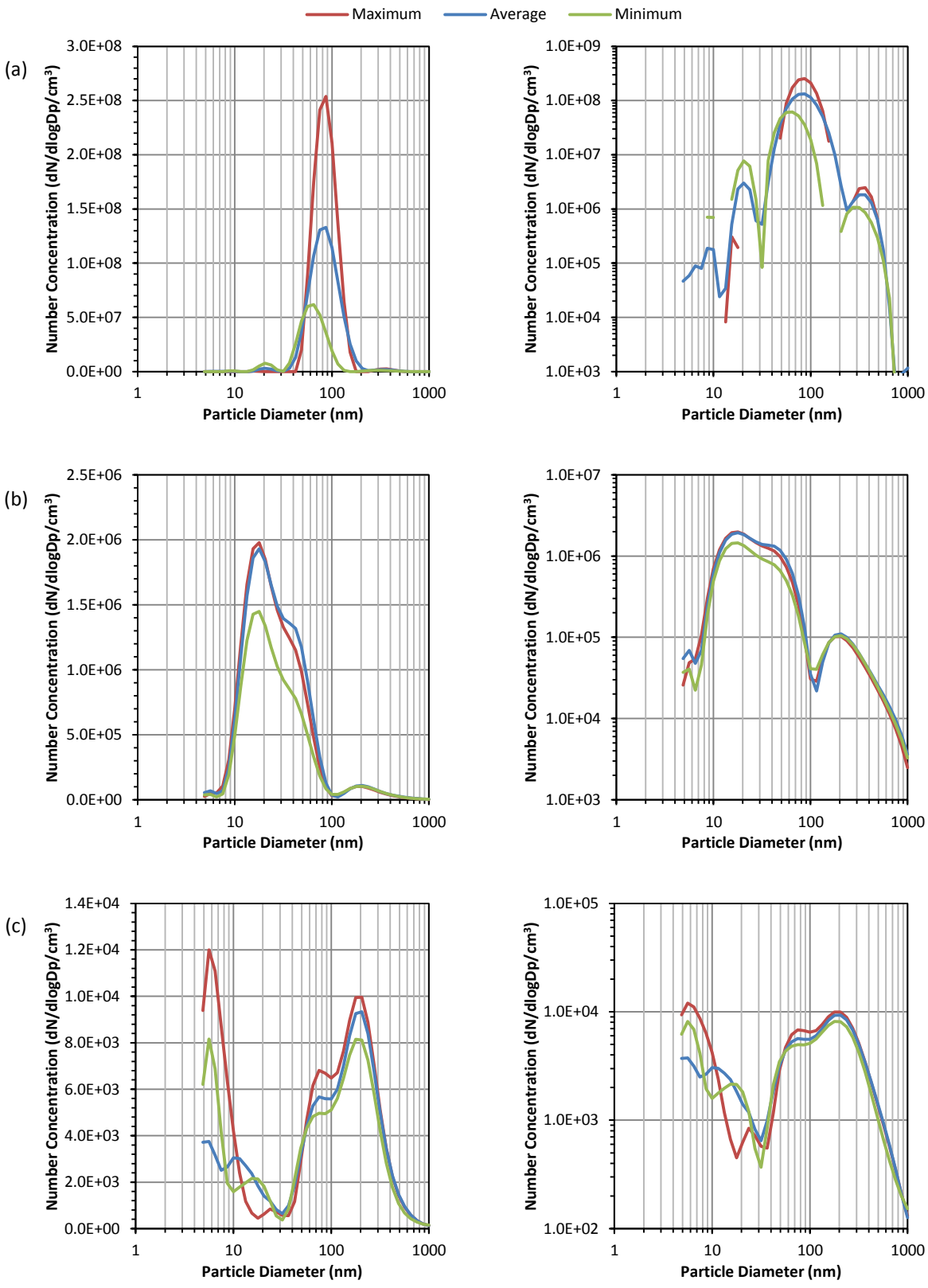

Figure 7.23: DMS500 size spectra at (a) pilot-only high, (b) pilot-only low and (c) fuel-staged conditions: (left) linear y-axis scale, (right) logarithmic y-axis scale.

When the average size spectra are compared to the ambient combustion air which was being supplied to the combustor rig the variation in the PM produced while operating at the different combustor conditions is clearly observed.

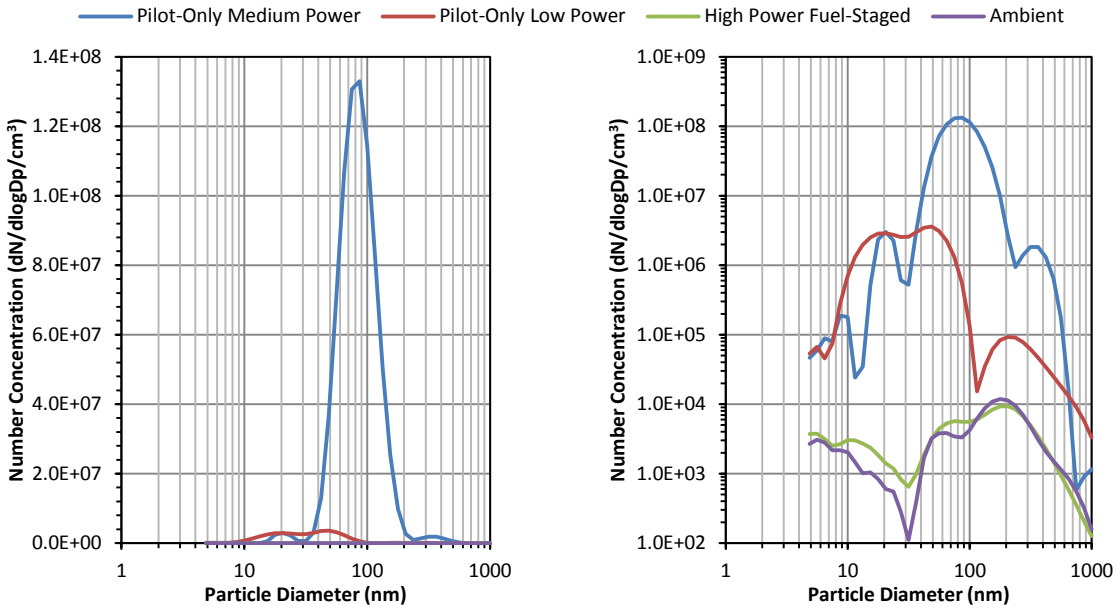

Figure 7.24: DMS500 size spectra at high, low fuel-staged and ambient conditions: (a) linear y-axis scale, (b) logarithmic y-axis scale.

On a linear scale the higher concentration of particles around 80nm produced at the medium power condition dominate the other datasets. The presence of high smoke concentrations at this non-fuel-staged condition is not uncommon.

As the power reduces under the pilot-only condition the presences of the larger sized particle mode is reduced which is consistent with reduced smoke production. The relatively high concentrations of particles in the 20 - 50nm size region remain however and these are likely to be associated with volatile material or smaller early-life carbonaceous particles.

Finally, the high power fuel-staged condition shows an almost identical PM size distribution to that measured for the ambient combustion air. This is remarkable in terms of emission reductions benefits of this technology and illustrates why OEM's are focused on lean-burning combustion systems for future engine designs.

The limitations of the smoke number diagnostic to approximate mass concentration are displayed in Figure 7.25 which compares the FOA3 correlation for predicted mass against the calculated DMS500 mass concentrations at each combustor condition. For the pilot-only high power condition the correlation between the predicted and actual mass concentrations is excellent, up until the point where the smoke number reaches the maximum detection limit of the optical smoke-meter.

At the lower smoke producing conditions, the correlations are poor with the FOA3 values under predicting those of the DMS5000 for the pilot-only low power condition and the over predicting those of the fuel-staged condition. Correlations other that FOA3 relating smoke number and particle mass concentrations have recently been proposed within set upper and lower bounds [126,132].

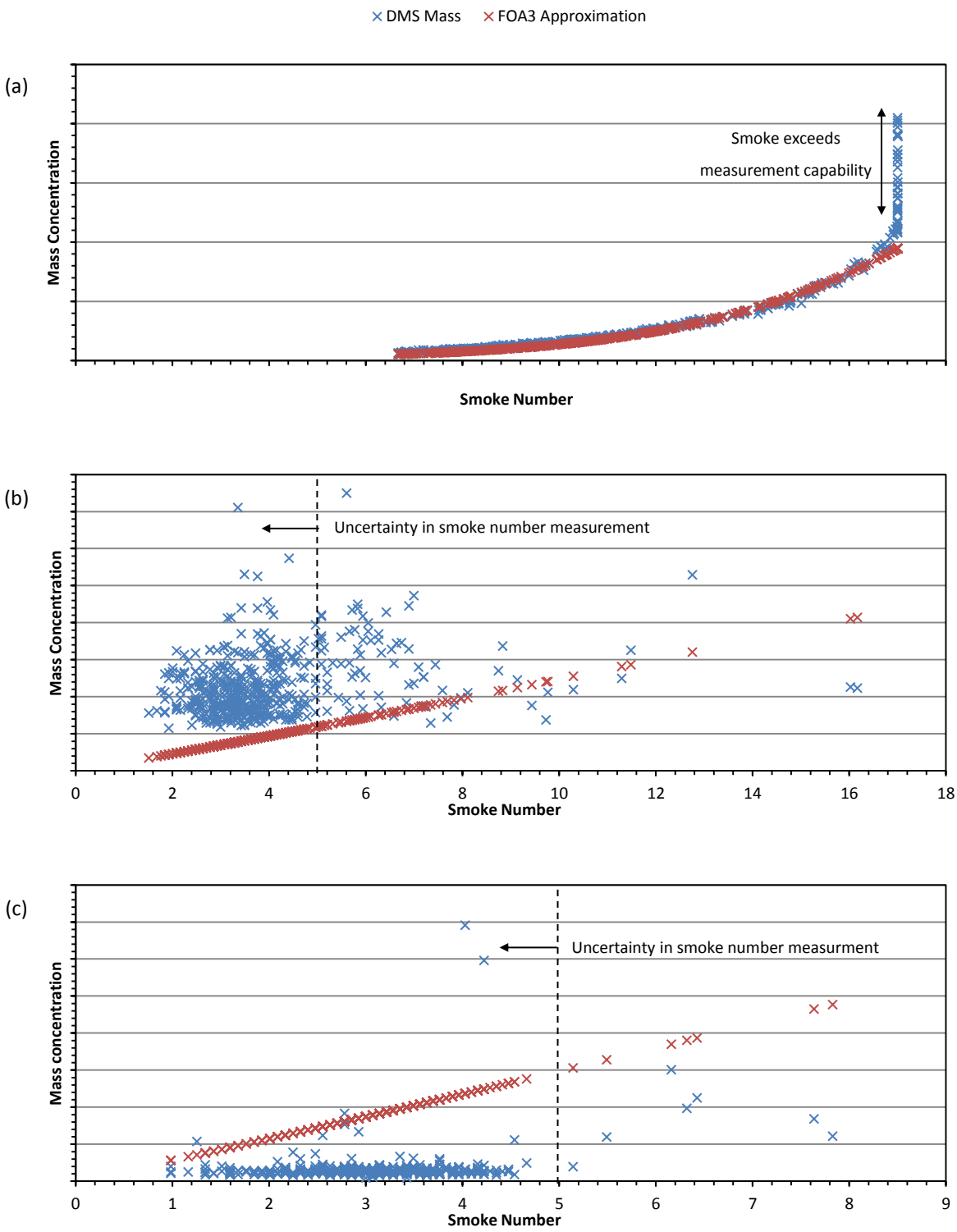

Figure 7.25: Correlation between DMS500 mass concentration and predicted mass using the FOA3 approximation for each smoke number measurement recorded at (a) pilot-only medium power, (b) pilot-only low power, and (c) high power fuel-staged conditions.

EI_N and EI_M values which were calculated for conditions specified on the lean-burn combustor are shown in Figure 7.26. Significant reductions in the particle number concentration and mass concentrations are noted as the combustor power is when the combustor is operated in a fuel-staged configuration.

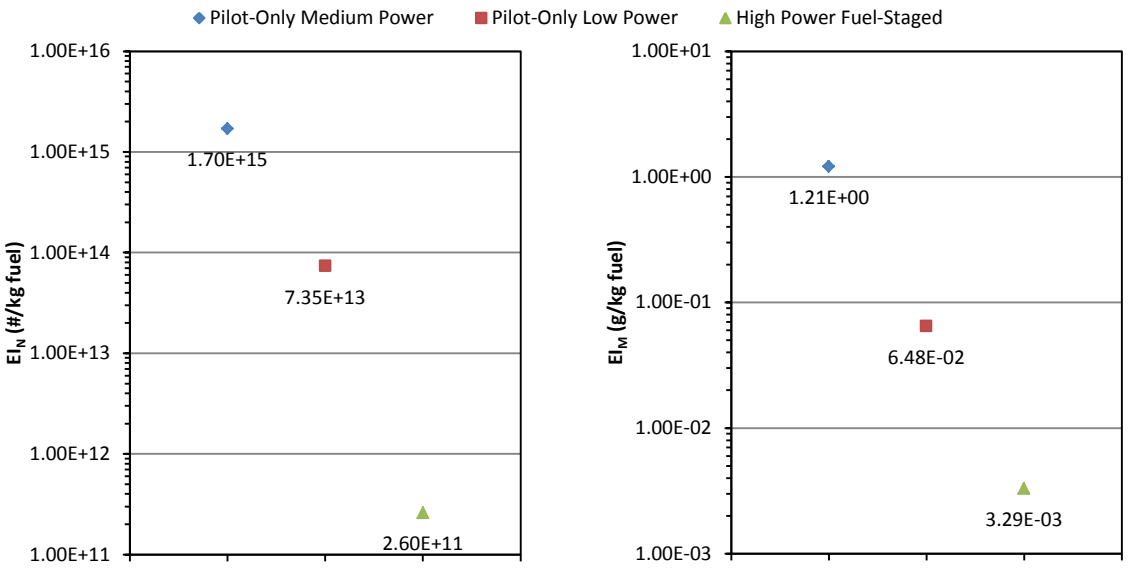

Figure 7.26: EI_N and EI_M values at pilot-only high power, pilot-only low power and fuel-staged combustor conditions.

Similar reductions in NO_x output are also noted, shown in Figure 7.27. It is interesting that the NO_x levels seen at the pilot-only low power and the fuel-staged conditions are very similar yet the particle generation of the fuel-staged conditions is so significantly reduced. The reduction in the NO_x of the pilot-only combustor condition is likely to have developed as a result of the lower fuel consumption and lower combustion temperature. The NO_x reductions produced at the fuel-staged condition are more likely to have arisen directly from the improved combustion efficiency and reduced localised combustion temperatures which are generated from the higher airflows.

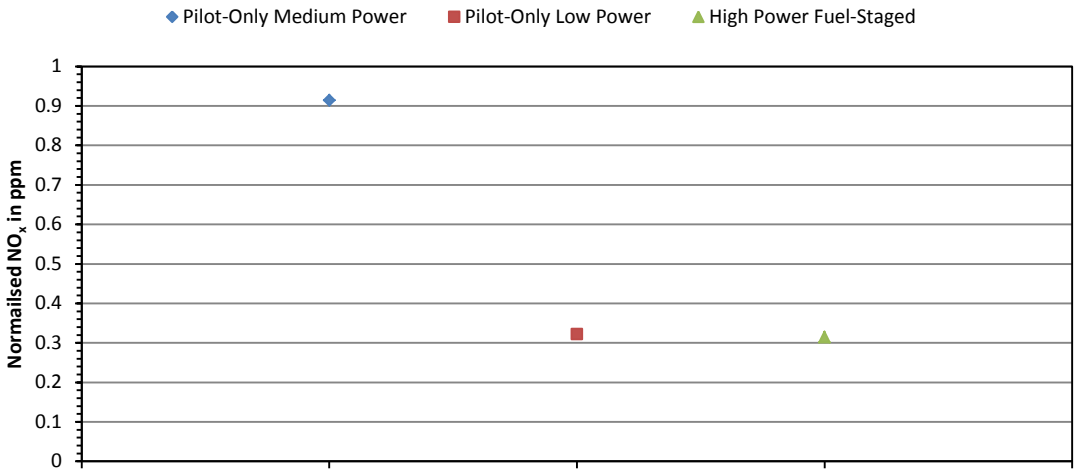

Figure 7.27: Normalised NO_x measured at pilot-only medium power, pilot-only low power and fuel-staged combustor conditions.

7.4 Chapter Summary

In this Chapter unique PM analysis on rich and lean-burn configurations of a Rolls-Royce combustor rig have been presented. The opportunity to sample the exhaust of multiple combustor conditions which were operating different combustor modes has allowed not only individual dataset comparison but also the possibility to explore how future combustor technologies may advance the reduction of pollutant generation. Some of the results have been normalised due to their commercially sensitive nature.

The fast-response DMS500 PM analyser enabled the measurement of real-time PM emissions. This, in conjunction with the novel traversing probe which was installed on the combustor rig, enabled fully annular PM together with gaseous emission analysis. Periodic fluctuations in the both the smoke number, DMS500 number and mass concentrations were observed during the majority of the reported test conditions as the sample probe past fuel injection regions. In these combustor zones the elevated concentrations of PM which were recorded by the traditional smoke number and DMS500 systems compared very well.

Assessment of the correlation between the smoke number and DMS500 mass calculation using the FAO3 approach showed very good agreement for combustor

conditions which produced higher smoke numbers (>10). However when the smoke number measurements reached the maximum instrument recording level or became so low they were within the range of measurement uncertainty (±3) unsurprisingly the correlation broke down.

Online diagnostics of incidents of instability in the PM diagnostics, such as those shown in Figure 7.28, where sudden spikes in the measured PM concentration were identified, could aid in the valuable detection and understanding of a potential fault or inefficiency within the combustor. The optical smoke-meter was also able to detect sudden changes in PM production however it lacks the sensitivity to interpret why these increases are occurring i.e. both small increase large particle production or large increase in smaller particle production could result in the same smoke number measurement , whereas the causes would be completely different.

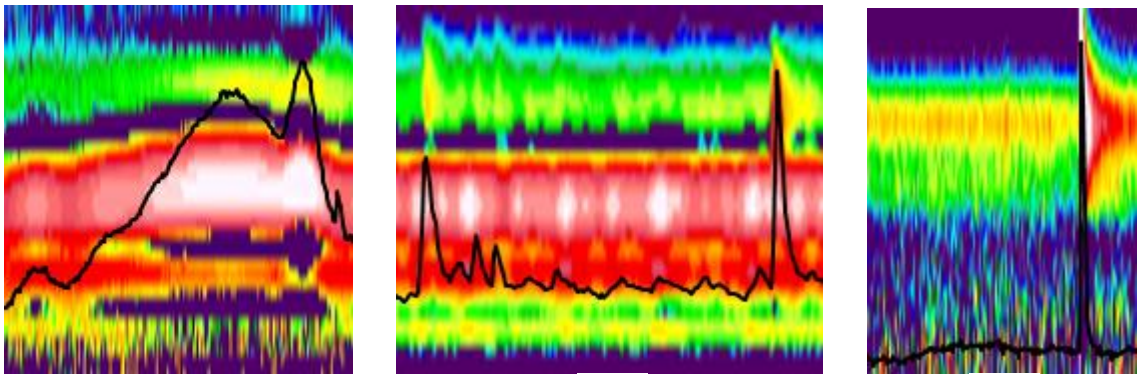

(a) (b) (c)

Figure 7.28: Examples of unstable PM generation, (a) inefficiency in combustor sector, (b) particle shedding events recorded during rich-burn combustor sampling and (c) particle shedding event recorded during lean-burn combustor sampling.

The addition of a fast-response instrument particle analysis instrument which is capable of provide size spectral analysis of the PM to a diagnostics setup allows for improved interpretation of data.

The main conclusion from the results presented in this Chapter is the great potential for pollutant emission reduction which could be achieve through the adoption of lean-burning combustor technology in the aviation gas turbine industry. The main focus of this research has been on PM, with some additional discussion on NO_x formation. A

summation of the normalised average smoke number and NOx concentration recorded for each of the rich and lean-burn conditions is shown below:

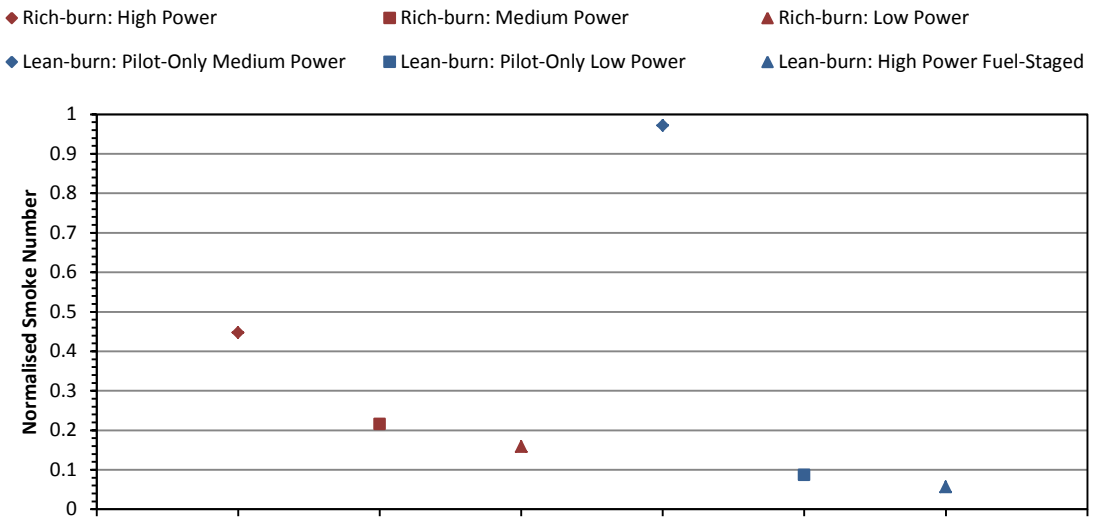

Figure 7.29: Normalised smoke number for all power conditions tested on the rich and lean-burn combustor configurations.

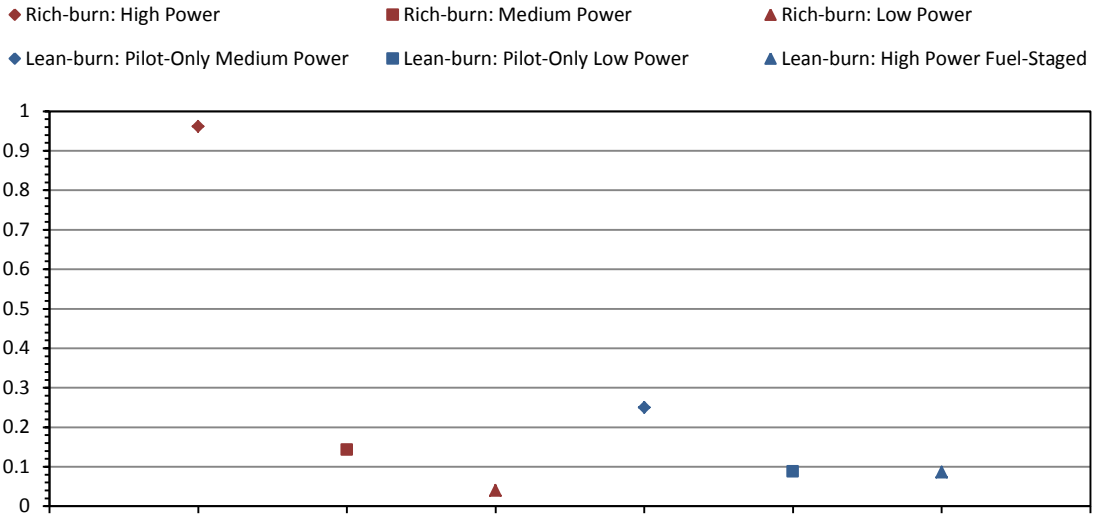

Figure 7.30: Normalised NO_x for all power conditions tested on the rich and lean-burn combustor configurations.

The ability of lean-burn combustors to develop smoke and NO_x emissions at fairly high power fuel-staged conditions (a typical cruise condition) which are characteristic of those produced at low powers (a typical idle condition) by a traditional RQL combustor could result in much lower overall emissions on a typical flight.

The reductions in PM emissions are probably best illustrated when a comparison is made between the EI_N and EI_M values calculated for the rich and lean-burn combustor configurations, this is shown in Figure 7.31 and Figure 7.32 .

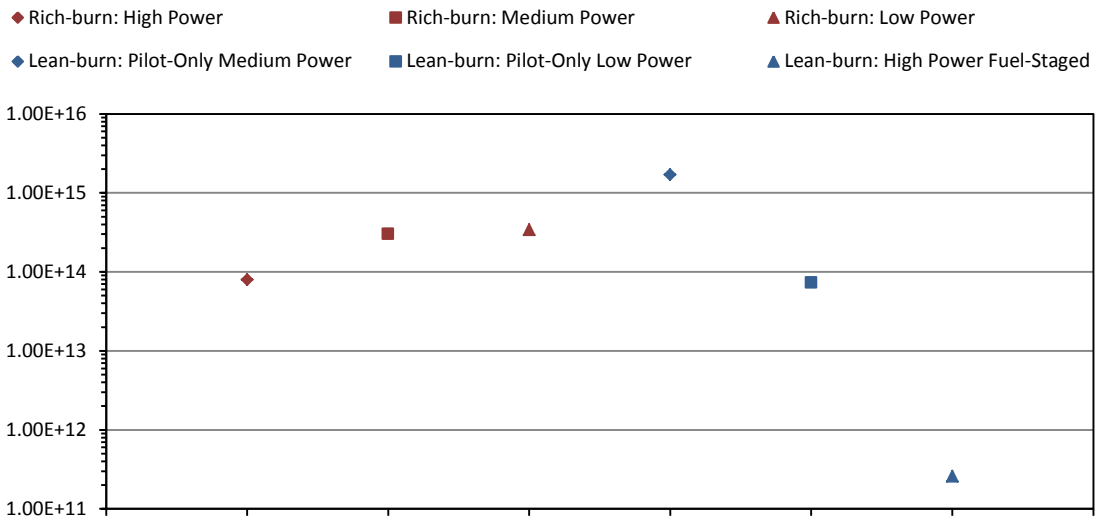

Figure 7.31: EI_N values for all power conditions tested on the rich and lean-burn combustor configurations.

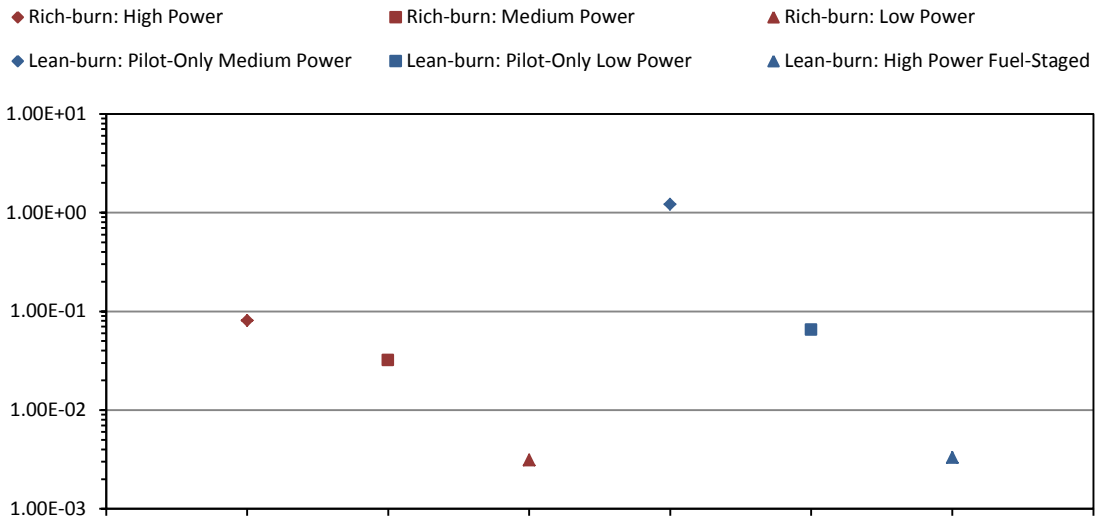

Figure 7.32: EI_M values for all power conditions tested on the rich and lean-burn combustor configurations.

Chapter 8

Conclusions

In this Chapter a summary of the main conclusions which can be drawn from this research project will presented. In addition to review of this Thesis, potential future research areas associated with PM are presented with brief reasoning as to why they would add to the current understanding of combustion related PM.

8.1 Volatile PM and the Removal of Volatile-Only and Volatile Coated Solid Core Particle 'Challenge' Aerosols

Two commercially available VPR systems, one which met the PMP specifications and one which did not, were evaluated to determine how they performed when exposed to very high concentrations of volatile material. The results showed the DEKATI EDD system (PMP compliant) was able to remove 90% of the 100nm and greater than 99% of the 50, 30 and 15nm volatile only 'challenge' aerosols. The GRIMM ESS (non-PMP compliant) system did not perform as well as the DEKATI EDD and was even found to increase the recorded number concentration of the 100nm challenge aerosol following exposure to the VPR. Size spectral analysis showed that this result occurred because the volatile material was only reduced in size and was likely to have fractured into smaller particle formations within the VPR. As the GRIMM ESS relies solely on hot dilution (200°C) to evaporate the volatile material compared the DEKATI EDD which employs hot dilution (150°C) and an evaporation tube (350°C), this poor performance at very high particle concentrations was not unexpected. When the particle size of the 'challenge' aerosol was decreased to 50, 30 and 15nm the GRIMM ESS removal efficiency improved resulting in 66%, 99.8% and 99.9% volatile removal respectively.

The volatile remove effectiveness of both VPRs appraised was therefore good enough to surpass the PMP requirement for >99% removal of 30nm volatile PM.

Appraisal of the VPRs with volatile coated solid core particles resulted in good overall volatile removal efficiency however the solid particles appear to have reduced in size compared to their initial input sizes (100, 50 and 30nm). It is possible that this reduction could have developed as a direct result of the temperature gradient created in the dilution and evaporation tube stages of the VPRs. Alternatively, as the PALAS GFG 1000 has been previously shown to produce agglomerate particle formations [44], and in these experiments the volatile coating which was applied to them may have caused the structure to collapse and contract in size.

It can therefore be concluded that it is not only important to adopt a PMP compliant VPR which is capable of removing higher than required volatile PM but also that

inclusion of a VPR system have an impact on the final PM size distribution of the solid particle which do penetrate through the instrument.

8.2 PM Characterisation for Spray-Guided GDI Single-Cylinder Research Engine

PM distribution from both the Bosch and Transonic fuel injection systems proved to be highly dependent on the engine operating load conditions. The potential change in the PM production which occurred from relatively small increases in engine load or RPM were dramatic and as a result the PM number concentration reflect these changes.

When operating in a homogeneous charge mode the PM number concentrations were highest at low load conditions when for both the Bosch and Transonic fuel injectors. At higher engine loads PM concentrations were reduced significantly.

PM number concentration measurements made using the DMS500 were found to be consistently higher than those measured by the SPCS. This was expected as the SPCS system is insensitive to volatile PM and was further downstream of the emission source (PM line losses). However, attempts made to correct for the most influencing of these factors (volatile PM) using a CS still resulted in a disparity in PM number concentration for results generated using the Bosch fuel injector.

Although moderate PM emission reduction benefits have been reported for the Transonic injection system [112] in the series of experiments performed during this Thesis PM number concentrations produced by the Bosch and Transonic fuel injection system were comparable.

8.3 PM Characterisation for Spray-Guided GDI Multi-Cylinder Research Engine

As fuel injection pressure was increased during homogenous charge operation a reduction in both PM number and mass concentration was recorded for all load conditions apart from the lowest evaluated test load. This is in agreement with

experimentation of other researchers [77] and the result of improved fuel atomisation and therefore improved combustion efficiency. Consequentially DMS500 size spectral analysis of test conditions showed that as fuel injection pressure was increased the concentration of agglomeration mode particulate was reduced. When operating in a stratified charge engine mode there was not a significant effect on PM number output however PM mass concentration was reduced as fuel injection pressure was increased. Very high concentrations of small particles (<10nm) were recorded at all test conditions. These particles are considered to be organic carbon formations which have developed from unburnt fuel. When operating in a stratified charge mode the PM number concentrations some variation was observed depending on the loading condition however no significant change was found as the fuel injection pressure varied. PM mass concentrations followed the same trend as that seen in the homogenous charge tests and decreased as the fuel injection pressure increased. Generally PM emissions were found to be higher when operating in a stratified charge configuration.

Experimentation into how SOI influenced PM emissions showed that during homogenous operation there was little change in the PM number concentration output as the injection was advanced or retarded. This was also true for the mass concentration produced however at the extreme ends of the operation test range (earliest and latest injection point) engine instability caused far higher or lower PM measurements to be recorded than the observed average. The same trends were true stratified charge operation however there was a notable difference in the PM size distributions produced in both engine configurations. Overall PM emissions were found to be higher when operating in a stratified charge mode.

Increasing the number of fuel injections during each fuel charge event was shown to cause an increase in PM number and mass concentration at all examined engine load conditions. Increasing agglomeration mode particles (soot) was the cause of this increase and therefore operating in this style would be unfavourable from an emission standpoint.

PM number concentrations were found to remain stable across all engine loading while the EGR was increased. At low loading there was no significant change in mass concentration however as engine load was increased high PM mass output was recorded. This is a common problem when trying to reduce NO_x emissions through the reduction of combustion zone temperature there is a likelihood of incomplete fuel burn occurring.

8.4 The Development of an Emissions Sampling System for the Aviation Industry

It was shown that changes in the sample line and dilution temperature did not have a significant effect on the nucleation mode of the PM distribution. The larger accumulation mode however was reduced by approximately 36% when the line dilution temperatures were reduced to the lowest appraised values. As the medium appraised temperature condition did not experience the same magnitude of PM losses across the size spectrum reducing the sample line and dilution temperatures to these levels may be appropriate. There are potential benefits to using a reduced temperature profile across the sampling system such as a reduced likelihood of thermophoresis occurring due to 'cold-spots' developing on sample line fittings.

Differences were observed between the PM size spectra produced at high and low power conditions when sample APU exhaust which were consistent with those generated from large scale aviation gas turbines. This validates the use of a small scale gas turbine such as an APU for the purpose of sampling system appraisal. Introducing an intermediary emission source between that of a synthetic aircraft exhaust produced at the GTRC and a full scale gas turbine certification test can be beneficial in terms of logistics, cost control and operational flexibility.

At high power the emission of larger size particles by the sampled APU was increased by approximately 62% significantly increasing the overall PM number and mass output. These high number and mass concentration are particularly concerning as it is the APUs which can remain running for longer periods of time while an aircraft is located

in an airport. At low altitude it is these emissions which are directly related to human health in and around airport grounds.

In order to capture transient PM emission events a fast particle analyser such as the DMS500 must be used. When the rate of change between two test conditions, in this case low and high power, is rapid the change in the PM composition is equally as fast. In this research programme in approximately 5 seconds the initial condition size spectra had transitioned and become fairly stable with the PM characteristics of the new condition. Utilising PM diagnostics apparatus which do not have a response time of 1 second of less will be unable to track these occurrences.

Exhaust sampling from the APU has shown that significant particle loss does occur over a long heated exhaust transportation line, particularly in the sub-40nm size region. Losses were less significant following initial sample conditioning with 160°C nitrogen and after a 1µm sharp-cut cyclone; however it was noted that caution is required when applying dilution ratio correction as this may potentially add further uncertainty to the final non-volatile PM measurement.

The UTRC particle line loss model was shown to be applicable to aviation gas turbine PM emissions measured using the DMS500. Measurements taken at the outlet of a 25m heated sample line and then corrected using this model showed excellent agreement with upstream measurements across the particle size range associated with aircraft engine exhaust. Differences observed between the measured and UTRC corrected spectrums, are within the DMS500 and dilution ratio measurement uncertainties. In addition, the uncertainty in the inversion fitting software may also be impacting the comparison.

Although correction for particle line loss is not expected to be included as part of the final SAE Aerospace Recommended Practice (ARP), the consideration of particle loss theory is required in order to establish sample transport performance differences between engine manufacture systems. The understanding that particle losses will occur within a sampling system, and how best to mitigate and standardise these losses, is important. In addition, the ability to compare particle measurements taken from different experimental set-ups is something which this type of size methodology

may be used for in the future, so as a better understanding of overall measurement uncertainty can be assessed.

Three DMS500 instruments were assessed for comparability using the same particle generation source. The results of this experiment showed that there is potential for some variation in the interpreted size distribution when operating DMS500 which have slightly different internal configurations. In these isolate circumstances employing the algorithm generated log-normal fitting profiles that are possible with the DMS500 would be appropriate and would potential provide even better correlation between the measured data sets.

The PM distributions which were obtained during multiple gas turbine sampled at the SR Technics facility in Zürich displayed high degrees of bi-mobility across all gas turbine sizes, designs, and manufactures. PM modes consistent with volatile and soot agglomeration particulates are present at 10 and 30nm at lower power and 10 and 30 - 60nm at high power. There is a possibility that the DMS500 software inversion process may be introducing a higher probability of bi-modal emission profiles and it may therefore be worthwhile maintaining an element of scientism over the precise peak locations. Future re-inversion of the data-sets with updated inversion matrices would be beneficial in fully understanding this topic.

PM number and mass concentration results obtained when sampling from the CFM56-5B4-2P gas turbine which employed a fuel-staged combustor design clearly displayed the potential PM reduction benefits of operating in a fuel-staged configuration. This is seen as a sudden drop in the measured PM at a set engine rpm at which time the engine has transitioned into a different combustion mode. Using this engine as an example reduction in number and mass concentrations of approximately 100% are achievable when comparing the measured emissions at the highest original un-staged condition lowest fuel-staged condition.

Approximately a 22% increase in PM penetration was observed when the main sample line was reduced to 12.5m in length. This improved penetration is a result of the reduced diffusional sample line losses. This finding reaffirms the need for a

standardised sampling methodology in which all sample line dimensions are equivalent.

No significant change in number or mass concentration was observed when comparing PM measurements taken from sample lines heated to 60 and 160°C. This further validates the decision to of the SAE E-31 Committee to limit sample line temperature to 60°C in order to reduce the likelihood of thermophoretic losses.

8.5 PM Characterisation for Rich and Lean-Burn Combustion Modes for a Large Civil Aviation Gas Turbine Combustor Section

A novel traversing probe which was installed on the Roll-Royce combustor rig enabled fully annular PM and gaseous emission analysis. Periodic fluctuations in the both the smoke number, DMS500 number and mass concentrations were observed during the majority of the reported test conditions as the sample probe past fuel injection regions. In these combustor zones the elevated concentrations of PM which was recorded by the traditional smoke number and DMS500 systems compared very well.

Assessments of the correlation between the smoke number and DMS500 mass calculation using the FAO3 approach showed very good agreements for the combustor conditions which produced higher smoke numbers (>10). However when the smoke number measurements reached the maximum instrument recording level or became so low they were within the range of uncertainty (±3) of the measurement the relationship was not so strong.

As was observed during the sampling of APU exhaust throughout a transition from low to high engine power, the generated PM size distribution can change rapidly in response to different combustion characteristics. Using a fast response particle analyser (DMS500) similar dramatic changes in PM distributions where detected during sampling across the annulus of the combustor exit plane. These fluctuations in PM size distribution produced distinct increases in PM number and mass concentration which were also recorded by as optical smokemeter. This instrument however lacked the sensitivity to interpret why these increases occurred i.e. a small increase large

particle production or large increase in smaller particle production may result in the same smoke number recording. The potential for rudimental combustor fault or combustion inefficiency diagnostics through the use of fast response particle analysers mean it could prove beneficial for OEMs to consider the inclusive of such apparatus in future emissions sampling suite designs.

8.6 Potential Future Research

Most analysis of PM size distribution in the Thesis has been performed using the DMS500. The DMS500 has been used extensively to record aviation and automotive emissions and has been shown to produce bi-modal PM distributions [123]. In this Thesis there have been occasions when different DMS500 instruments produced variable multi-modal distributions and a possible cause for this has been determined to be particles in the ≈30nm size region becoming doubly changed [94]. These charging characteristic can be difficult to interpret by the DMS500 fitting algorithms and produce erroneous results. New inversion matrices produced by Cambustion Ltd. have shown a high propensity to generate mono-modal PM distributions consistent with those of SMPS systems. Re-inversion of data sets presented in this Thesis would be beneficial to understand the true nature of the nucleation and agglomeration mode peaks presented in the Thesis.

There are many reasons as to why volatile particulates can form in the exhaust of combustion systems (i.e. unburnt fuel and oil leakage). There is less certainty over the formation mechanisms of volatile PM during exhaust transportation in sample lines. A number of ‘best practices’ have developed from the implantation of the PMP which are now commonly employed such as heated sample lines and hot and cold dilution at the sample inlet. These techniques seek to minimise the potential of volatile PM formation. Additional research into the formation mechanisms of volatile PM along a sampling network would be beneficial in improving PM sample transportation systems, however there are now commercially available instruments designed to remove volatile particles (VPRs) prior to final PM measurement. Therefore from a reliability standpoint installation of VPR is a preferred however alternative VPR technologies

than the PMP compliant systems (dilution and evaporation tube) may be more appropriate choice and have less impact on the sample integrity. New volatile insensitive CPC systems [133] are being developed as are catalytic removal solutions based on the CS system discussed in Chapter 5 . Evaluation of how these new systems compare to the current PMP compliant designs would be very beneficial.

This research programme assessed the PM output from traditional and a prototype novel fuel injection system. It is likely that GDI engine technologies will be adopted in increasing numbers in the future and therefore PM research on such technologies will be highly topical. With the introduction of the EURO6 Standard and the inclusion of limits on PM number and mass output research in PM mitigation technologies, particularly GPF's would be beneficial.

Lastly, the decision to limit the newly developed SAE-31 aviation gas turbine PM sampling methodology to only nvPM number and mass concentration, although far improved that the original smoke number quantification, could be extended. The DMS500 has been shown to be extremely valuable in deriving a better understanding in PM emissions, especially during transient (traverse combustor rig work). Inclusion of a fast response PM size measurement instrument into the next iteration of the aviation regulatory standard or any new PM measurement methodology would prove very valuable. As PM limits and increasing are attaching importance to PM size (PM_{10} and $PM_{2.5}$) further appraisal of the applicability of commercially available PM size measurement instruments should be conducted.

References

[1] C.A. Pope 3rd, D.W. Dockery, Health effects of fine particulate air pollution: lines that connect, J. Air Waste Manag. Assoc. 1995. 56 (2006) 709–742.

[2] D.S. Lee, D.W. Fahey, P.M. Forster, P.J. Newton, R.C.N. Wit, L.L. Lim, et al., Aviation and global climate change in the 21st century, Atmos. Environ. 43 (2009) 3520–3537. doi:10.1016/j.atmosenv.2009.04.024.

[3] M. Pilling, H. ApSimon, D. Carruthers, D. Carslaw, R. Colvile, R. Derwent, et al., Particulate Matter in the United Kingdom: Summary, Department for the Environment, Food and Rural Affairs, London, 2005. http://archive.defra.gov.uk/environment/quality/air/airquality/publications/particulate-matter/documents/pm-summary.pdf.

[4] A. Seaton, J.G. Ayres, P.J. Baxter, P.G. Burney, R.L. Carter, J.W. Cherrie, et al., Expert Panel on Air Quality Standards 6th Report: Particles, Department for the Environment, Transport and Regions, 1995. http://webarchive.nationalarchives.gov.uk/20060715141954/http://www.defra.gov.uk/environment/airquality/aqs/particle/index.htm.

[5] K.T. Whitby, The physical characteristics of sulfur aerosols, Atmospheric Environ. 1967. 12 (1978) 135–159. doi:10.1016/0004-6981(78)90196-8.

[6] K. Klejnowski, A. Krasa, Rogula-Koz&#x142, W. Owska, B&#x142, B. Aszczak, Number Size Distribution of Ambient Particles in a Typical Urban Site: The First Polish Assessment Based on Long-Term (9 Months) Measurements, Sci. World J. 2013 (2013) e539568. doi:10.1155/2013/539568.

[7] Air Quality Criteria for Particulate Matter: Volume I of II, Environmental Protection Agency, 2004.

[8] Review of the National Ambient Air Quality Standards for Particulate Matter: Policy Assessment of Scientific and Technical Information., Environmental Protection Agency, 2005.

[9] J. Evelyn, Fumifugium; Or, the Inconvenience of the Aer and Smoake of London, Humphries, 1772.

[10] 50 Years On: The Struggle for Air Quality in the UK, Greater London Authority, London, 2002. http://legacy.london.gov.uk/mayor/environment/air_quality/docs/50_years_on.pdf.

[11] E.T. Wilkins, Air pollution aspects of the London fog of December 1952, Q. J. R. Meteorol. Soc. 80 (1954) 267–271. doi:10.1002/qj.49708034420.

[12] M.L. Bell, D.L. Davis, T. Fletcher, A retrospective assessment of mortality from the London smog episode of 1952: the role of influenza and pollution., Environ. Health Perspect. 112 (2004) 6–8.

[13] Clean Air Act 1956, 1956. http://www.legislation.gov.uk/ukpga/Eliz2/4-5/52/contents.

[14] Clean Air Act 1968, 1968. http://www.legislation.gov.uk/ukpga/1968/62/contents.

[15] Use of the Ringelmann and miniature smoke charts (BS 2742:1969), (1969).

[16] Clean Air Act 1993, 1993. http://www.legislation.gov.uk/ukpga/1993/11/contents.
[17] Environment Protection Act 1990, 1990. http://www.legislation.gov.uk/ukpga/1990/43/contents.
[18] Environment Act 1995, 1995. http://www.legislation.gov.uk/ukpga/1995/25/contents.
[19] H.I.H. Saravanamuttoo, G.F.C. Rogers, H. Cohen, Gas Turbine Theory, 5th ed., Pearson Education Limited, England, 2001.
[20] C. Soares, Gas Turbines: A Handbook of Air, Land, and Sea Applications, Butterworth-Heinemann, 2008.
[21] S. Samuelsen, Conventional Type Combustion, in: Gas Turbine Handb., 2006.
[22] A.H., Ballal, Dilip R Lefebvre, Gas turbine combustion: alternative fuels and emissions, CRC Press, Boca Raton, Fla. [u.a., 2010.
[23] J. Rhode, Overview of the NASA AST and UEET emissions reduction projects, (2002). http://adg.stanford.edu/aa241/emissions/NASAUEETemissions.pdf.
[24] Air BP: Handbook of products, (2000). http://www.bp.com/liveassets/bp_internet/aviation/air_bp/STAGING/local_assets/downloads_pdfs/a/air_bp_products_handbook_04004_1.pdf.
[25] Aviation fuels technical review, Chevron, 2004. http://www.skybrary.aero/bookshelf/books/2478.pdf.
[26] C.L. Cummins, Early IC and Automotive Engines, SAE International, Warrendale, PA, 1976. http://papers.sae.org/760604/ (accessed November 13, 2013).
[27] J.B. Heywood, Internal combustion engine fundamentals, McGraw-Hill, New York, 1988.
[28] V. Wagner, EU Fuels: Diesel and Gasoline, EU Fuels Diesel Gasol. (2013). http://transportpolicy.net/index.php?title=EU:_Fuels:_Diesel_and_Gasoline (accessed February 4, 2014).
[29] R.K. Rajput, Internal Combustion Engines, Laxmi Publications, 2005.
[30] G.. Richards, M.. McMillian, R.. Gemmen, W.. Rogers, S.. Cully, Issues for low-emission, fuel-flexible power systems, Prog. Energy Combust. Sci. 27 (2001) 141–169. doi:10.1016/S0360-1285(00)00019-8.
[31] D. Dunn-Rankin, Lean Combustion: Technology and Control, Academic Press, 2011.
[32] Exhaust Gas Analysers, Emission Tests and Lean-Burn Engines, (2010).
[33] J.E. Penner, Aviation and the Global Atmosphere: A Special Report of IPCC Working Groups I and III in Collaboration with the Scientific Assessment Panel to the Montreal Protocol on Substances that Deplete the Ozone Layer, Cambridge University Press, 1999.
[34] D. Wuebbles, M. Gupta, M. Ko, Evaluating the impacts of aviation on climate change, Eos Trans. Am. Geophys. Union. 88 (2007) 157–160. doi:10.1029/2007EO140001.
[35] 2012 UK Greenhouse Gas Emissions, Provisional Figures and 2011 UK Greenhouse Gas Emissions, Final Figures By Fuel Type and End User, (2012). https://www.gov.uk/government/uploads/system/uploads/attachment_data/file/193414/280313_ghg_national_statistics_release_2012_provisional.pdf.
[36] New Car CO2 Report 2014: The 13th Report, The Society of Motor Manufacturers and Traders Limited, 2014.

[37] Government Responce to the Commitee on Climate Change Report on Reducing CO2 Emissions from UK Aviation 2050, Department of Transport, 2011.
[38] J. MacCarthy, G. Thistlewaite, E. Salisbury, Y. Pang, T. Misselbrook, Air quality pollutant inventories for England, Scotland, Wales and Northern Ireland: 1990 - 2010, National Atmospheric Emission Inventory, 2012. http://uk-air.defra.gov.uk/reports/cat07/1209130947_DA_AQPI_2010_MainBody_v1.pdf.
[39] London Atmospheric Emissions Inventory 2010, (2010). http://data.london.gov.uk/datastore/package/london-atmospheric-emissions-inventory-2010.
[40] J. Kagawa, Evaluation of biological significance of nitrogen oxides exposure, Tokai J. Exp. Clin. Med. 10 (1985) 348–353.
[41] A.J. Chauhan, M.T. Krishna, A.J. Frew, S.T. Holgate, Exposure to nitrogen dioxide (NO2) and respiratory disease risk, Rev. Environ. Health. 13 (1998) 73–90.
[42] C.A. Amann, D.C. Siegla, Diesel Particulates—What They Are and Why, Aerosol Sci. Technol. 1 (1981) 73–101. doi:10.1080/02786828208958580.
[43] D.R. Tree, K.I. Svensson, Soot processes in compression ignition engines, Prog. Energy Combust. Sci. 33 (2007) 272–309. doi:10.1016/j.pecs.2006.03.002.
[44] H.G. M. Wentzel, Transmission electron microscopical and aerosol dynamical characterization of soot aerosols, J. Aerosol Sci. 34 (2003) 1347–1370. doi:10.1016/S0021-8502(03)00360-4.
[45] Soot Formation in Combustion - Mechanisms and Models, n.d.
[46] D.A. Jones, Characterisation and fundamental studies of particulate matter from combustion processes, Cardiff University, 2003.
[47] W. Bartok, A.F. Sarofim, Fossil fuel combustion: a source book, Wiley, 1991.
[48] O.I. Smith, Fundamentals of soot formation in flames with application to diesel engine particulate emissions, Prog. Energy Combust. Sci. 7 (1981) 275–291. doi:10.1016/0360-1285(81)90002-2.
[49] I. Glassman, Soot formation in combustion processes, Symp. Int. Combust. 22 (1989) 295–311. doi:10.1016/S0082-0784(89)80036-0.
[50] F. Arnold, L. Pirjola, H. Aufmhoff, T. Schuck, T. Lähde, K. Hämeri, First gaseous sulfuric acid measurements in automobile exhaust: Implications for volatile nanoparticle formation, Atmos. Environ. 40 (2006) 7097–7105. doi:10.1016/j.atmosenv.2006.06.038.
[51] A. Mayer, J. Czerwinski, M. Kasper, A. Ulrich, J.J. Mooney, Metal Oxide Particle Emissions from Diesel and Petrol Engines, SAE International, Warrendale, PA, 2012. http://www.sae.org/technical/papers/2012-01-0841 (accessed May 19, 2014).
[52] D.B. Kittelson, Engines and nanoparticles: a review, J. Aerosol Sci. 29 (1998) 575–588. doi:10.1016/S0021-8502(97)10037-4.
[53] R. Hitzenberger, H. Giebl, A. Petzold, M. Gysel, S. Nyeki, E. Weingartner, et al., Properties of jet engine combustion particles during the PartEmis experiment. Hygroscopic growth at supersaturated conditions, Geophys. Res. Lett. 30 (2003) n/a–n/a. doi:10.1029/2003GL017294.
[54] O.B. Popovicheva, N.M. Persiantseva, E.E. Lukhovitskaya, N.K. Shonija, N.A. Zubareva, B. Demirdjian, et al., Aircraft engine soot as contrail nuclei, Geophys. Res. Lett. 31 (2004) n/a–n/a. doi:10.1029/2003GL018888.

[55] S. Blakey, L. Rye, C.W. Wilson, Aviation gas turbine alternative fuels: A review, Proc. Combust. Inst. 33 (2011) 2863–2885. doi:10.1016/j.proci.2010.09.011.
[56] T.-Q. Thach, C.-M. Wong, K.-P. Chan, Y.-K. Chau, Y.-N. Chung, C.-Q. Ou, et al., Daily visibility and mortality: Assessment of health benefits from improved visibility in Hong Kong, Environ. Res. 110 (2010) 617–623. doi:10.1016/j.envres.2010.05.005.
[57] W.L. Chameides, H. Yu, S.C. Liu, M. Bergin, X. Zhou, L. Mearns, et al., Case study of the effects of atmospheric aerosols and regional haze on agriculture: An opportunity to enhance crop yields in China through emission controls?, Proc. Natl. Acad. Sci. 96 (1999) 13626–13633. doi:10.1073/pnas.96.24.13626.
[58] A.J. Cohen, H. Ross Anderson, B. Ostro, K.D. Pandey, M. Krzyzanowski, N. Künzli, et al., The global burden of disease due to outdoor air pollution, J. Toxicol. Environ. Health A. 68 (2005) 1301–1307. doi:10.1080/15287390590936166.
[59] The Mortality Efects of Long-Term Exposure to Particulate Air Pollution in the United Kingdom, Committee on the medical effects of ait pollution, 2010.
[60] A.C. Rohr, R.E. Wyzga, Attributing health effects to individual particulate matter constituents, Atmos. Environ. 62 (2012) 130–152. doi:10.1016/j.atmosenv.2012.07.036.
[61] L.W. Stanek, J.D. Sacks, S.J. Dutton, J.-J.B. Dubois, Attributing health effects to apportioned components and sources of particulate matter: An evaluation of collective results, Atmos. Environ. 45 (2011) 5655–5663. doi:10.1016/j.atmosenv.2011.07.023.
[62] S.H.L. Yim, S.R.H. Barrett, Public Health Impacts of Combustion Emissions in the United Kingdom, Environ. Sci. Technol. 46 (2012) 4291–4296. doi:10.1021/es2040416.
[63] International Agency for Research on Cancer: Diesel Engine Exhaust Carcinogenic, (2012). http://www.iarc.fr/en/media-centre/pr/2012/pdfs/pr213_E.pdf.
[64] M.E.J. Stettler, S. Eastham, S.R.H. Barrett, Air quality and public health impacts of UK airports. Part I: Emissions, Atmos. Environ. 45 (2011) 5415–5424. doi:10.1016/j.atmosenv.2011.07.012.
[65] S.H.L. Yim, M.E.J. Stettler, S.R.H. Barrett, Air quality and public health impacts of UK airports. Part II: Impacts and policy assessment, Atmos. Environ. 67 (2013) 184–192. doi:10.1016/j.atmosenv.2012.10.017.
[66] L.W. Jian Zhang, Formation, characterization, and fate of inhaled drug nanoparticles., Adv. Drug Deliv. Rev. 63 (2010) 441–55. doi:10.1016/j.addr.2010.11.002.
[67] C. Mühlfeld, P. Gehr, B. Rothen-Rutishauser, Translocation and cellular entering mechanisms of nanoparticles in the respiratory tract, Swiss Med. Wkly. 138 (2008) 387–391. doi:2008/27/smw-12153.
[68] X.M. Zeng, G.P. Martin, C. Marriott, Particulate Interactions in Dry Powder Formulations for Inhalation, Taylor & Francis, 2001.
[69] C. Darquenne, G.K. Prisk, Deposition of inhaled particles in the human lung is more peripheral in lunar than in normal gravity, Eur. J. Appl. Physiol. 103 (2008) 687–695. doi:10.1007/s00421-008-0766-y.
[70] Human respiratory tract model for radiological protection. A report of a Task Group of the International Commission on Radiological Protection, Ann. ICRP. 24 (1994) 1–482.

[71] International Civil Aviation Organization, ICAO Annex 16: Environmental Protection, Volume II -- Aircraft Engine Emissions, 2008. http://archive.org/details/gov.law.icao.annex.16.v2.2008 (accessed March 24, 2014).
[72] Regulation No. 83 - Emissions of M1 and N1 vehicles : Uniform provisions concerning the approval of vehicles with regard to the emission of pollutants according to engine fuel requirements, (n.d.).
[73] M. Johnson, Aero Turbine Emission Measurements – State-of-the-art Review, (2013).
[74] ARP1179D: Aircraft Gas Turbine Engine Exhaust Smoke Measurement, (2011).
[75] ARP1256D: Procedure for the Continuous Sampling and Measurement of Gaseous Emissions from Aircraft Turbine Engines., (2011).
[76] W. Piock, G. Hoffmann, A. Berndorfer, P. Salemi, B. Fusshoeller, Strategies Towards Meeting Future Particulate Matter Emission Requirements in Homogeneous Gasoline Direct Injection Engines, SAE International, Warrendale, PA, 2011. http://www.sae.org/technical/papers/2011-01-1212 (accessed May 21, 2014).
[77] Q.P. Heng, A.K. Jasuja, A.H. Lefebvre, Influence of air and fuel flows on gas turbine sprays at high pressures, Symp. Int. Combust. 26 (1996) 2757–2762. doi:10.1016/S0082-0784(96)80113-5.
[78] A.H.L. K. K. Rink, Influence of fuel drop size and combustor operating conditions on pollutant emissions, (1985).
[79] K. Tsuneyoshi, K. Yamamoto, Experimental study of hexagonal and square diesel particulate filters under controlled and uncontrolled catalyzed regeneration, Energy. 60 (2013) 325–332. doi:10.1016/j.energy.2013.07.069.
[80] E. Wirojsakunchai, E. Schroeder, C. Kolodziej, D.E. Foster, N. Schmidt, T. Root, et al., Detailed Diesel Exhaust Particulate Characterization and Real-Time DPF Filtration Efficiency Measurements During PM Filling Process, SAE International, Warrendale, PA, 2007. http://digitallibrary.sae.org/content/2007-01-0320 (accessed April 15, 2014).
[81] K. Tsuneyoshi, O. Takagi, K. Yamamoto, Effects of Washcoat on Initial PM Filtration Efficiency and Pressure Drop in SiC DPF, SAE International, Warrendale, PA, 2011. http://www.sae.org/technical/papers/2011-01-0817 (accessed April 15, 2014).
[82] R. Allansson, P.G. Blakeman, B.J. Cooper, H. Hess, P.J. Silcock, A.P. Walker, Optimising the Low Temperature Performance and Regeneration Efficiency of the Continuously Regenerating Diesel Particulate Filter (CR-DPF) System, SAE International, Warrendale, PA, 2002. http://digitallibrary.sae.org/content/2002-01-0428 (accessed April 28, 2014).
[83] A. Mamakos, N. Steininger, G. Martini, P. Dilara, Y. Drossinos, Cost effectiveness of particulate filter installation on Direct Injection Gasoline vehicles, Atmos. Environ. 77 (2013) 16–23. doi:10.1016/j.atmosenv.2013.04.063.
[84] I. Mikulic, H. Koelman, S. Majkowski, P. Vosejpka, A Study about Particle Filter Application on a State-of-the-Art Homogeneous Turbocharged 2L DI Gasoline Engine, (2010).
[85] C. Saito, T. Nakatani, Y. Miyairi, K. Yuuki, M. Makino, H. Kurachi, et al., New Particulate Filter Concept to Reduce Particle Number Emissions, SAE

International, Warrendale, PA, 2011. http://www.sae.org/technical/papers/2011-01-0814 (accessed April 28, 2014).
[86] P. Forzatti, Status and perspectives of catalytic combustion for gas turbines, Catal. Today. 83 (2003) 3–18. doi:10.1016/S0920-5861(03)00211-6.
[87] R.J. Farrauto, R.M. Heck, Catalytic converters: state of the art and perspectives, Catal. Today. 51 (1999) 351–360. doi:10.1016/S0920-5861(99)00024-3.
[88] R.M. Heck, R.J. Farrauto, Automobile exhaust catalysts, Appl. Catal. Gen. 221 (2001) 443–457. doi:10.1016/S0926-860X(01)00818-3.
[89] A. Petzold, R. Marsh, M. Johnson, Y. Sevcenco, D. Delhaye, X. Vancassel, et al., SAMPLE I: Studying, sampling and measurment of aircraft particulate emissions I, European Aviation Safety Agency, 2009. http://www.easa.europa.eu/safety-and-research/research-projects/environment.php.
[90] R. Marsh, A. Crayford, A. Petzold, M. Johnson, P. Williams, A. Ibrahim, et al., SAMPLE II: Studying, sampling and measurement of aircraft particulate emissions II, European Aviation Safety Agency, 2011. http://www.easa.europa.eu/safety-and-research/research-projects/environment.php.
[91] W. Lazik, T. Doerr, S. Bake, R. v. d. Bank, L. Rackwitz, Development of Lean-Burn Low-NOx Combustion Technology at Rolls-Royce Deutschland, (2008) 797–807. doi:10.1115/GT2008-51115.
[92] A. Crayford, M. Johnson, R. Marsh, Y. Sevcenco, D.M. Walters, P. Williams, et al., SAMPLE III SC.01: Studying, sampling and measurement of aircraft particulate emissions III (specific contract 1), European Aviation Safety Agency, 2011. http://www.easa.europa.eu/safety-and-research/research-projects/environment.php.
[93] A. Crayford, M. Johnson, R. Marsh, Y. Sevcenco, D.M. Walters, P. Williams, et al., SAMPLE III SC.02: Studying, sampling and measurement of aircraft particulate emissions III (specific contract 2), European Aviation Safety Agency, 2012. http://www.easa.europa.eu/safety-and-research/research-projects/environment.php.
[94] J. King, O. Böcker, Multiple Injection and Boosting Benefits for Improved Fuel Consumption on a Spray Guided Direct Injection Gasoline Engine, in: Proc. FISITA 2012 World Automot. Congr., Springer Berlin Heidelberg, 2013: pp. 229–241. http://link.springer.com/chapter/10.1007/978-3-642-33841-0_18 (accessed November 15, 2013).
[95] Rotadata Optical Smoke Meter Operation Manual, (1990).
[96] J. Binnig, J. Meyer, G. Kasper, Calibration of an optical particle counter to provide mass for well-defined particle materials, J. Aerosol Sci. 38 (2007) 325–332. doi:10.1016/j.jaerosci.2006.12.001.
[97] M. Heim, B.J. Mullins, H. Umhauer, G. Kasper, Performance evaluation of three optical particle counters with an efficient “multimodal” calibration method, J. Aerosol Sci. 39 (2008) 1019–1031. doi:10.1016/j.jaerosci.2008.07.006.
[98] Scanning Mobility Particle Sizer Spectrometer(SMPS) Model 3936: Highly Accurate, Real-time Nanoparticle Sizing Systems You Can Rely On For Years, (n.d.).
[99] J.P.R. Symonds, K.S.J. Reavell, J.S. Olfert, B.W. Campbell, S.J. Swift, Diesel soot mass calculation in real-time with a differential mobility spectrometer, J. Aerosol Sci. 38 (2007) 52–68. doi:10.1016/j.jaerosci.2006.10.001.

[100] G. Biskos, K. Reavell, N. Collings, Unipolar diffusion charging of aerosol particles in the transition regime, J. Aerosol Sci. 36 (2005) 247–265. doi:10.1016/j.jaerosci.2004.09.002.
[101] P. Kumar, Measurements and Modelling of the Dispersion of Nanoparticles in the Urban Environment, Cambridge, 2008.
[102] A.G. Prashant Kumar, Comparative study of measured and modelled number concentrations of nanoparticles in an urban street canyon, Atmos. Environ. 43 (2009) 949–958. doi:10.1016/j.atmosenv.2008.10.025.
[103] Cambustion DMS500 Fast Particulate Spectrometer with Heated Sample Line High Ratio Diluter: User Manual, (2011).
[104] Volatile Particle Remover Calibration and Validation Procedures, AEA Energy & Environment, 2007.
[105] U. Mathis, R. Kaegi, TEM analysis of volatile nanoparticles from particle trap equipped diesel and direct-injection spark-ignition vehicles, Atmos. Environ. (2004) 4347–4355. doi:10.1016/j.atmosenv.2004.04.016.
[106] I.M. Kennedy, The health effects of combustion-generated aerosols, Proc. Combust. Inst. 31 (2007) 2757–2770. doi:10.1016/j.proci.2006.08.116.
[107] Dekati Engine Exhaust Diluter DEED Specification Sheets, (n.d.).
[108] GRIMM Emission Sampling System (ESS) Model 7.917 Specification Sheets: Hot gas sampler and diluter for airborne nanoparticles., (n.d.).
[109] P.J. Bowen, D.M. Walters, A.P. Crayford, J. Andersson, R. Osbrone, Parametric Analysis of Particulate Matter from a GDI Research Engine using DMS, in: Bonn, 2013.
[110] D.B. Kittelson, W.F. Watts, J.C. Savstrom, J.P. Johnson, Influence of a catalytic stripper on the response of real time aerosol instruments to diesel exhaust aerosol, J. Aerosol Sci. 36 (2005) 1089–1107. doi:10.1016/j.jaerosci.2004.11.021.
[111] C.D. Boer, J. Chang, S. Shetty, Transonic Combustion - A Novel Injection-Ignition System for Improved Gasoline Engine Efficiency, SAE International, Warrendale, PA, 2010. http://papers.sae.org/2010-01-2110/ (accessed February 21, 2014).
[112] P.J. Kay, P.J. Bowen, H.W.M. Witlox, Sub-cooled and flashing liquid jets and droplet dispersion II. Scaled experiments and derivation of droplet size correlations, J. Loss Prev. Process Ind. 23 (2010) 849–856. doi:10.1016/j.jlp.2010.07.006.
[113] D. Agarwal, S.K. Singh, A.K. Agarwal, Effect of Exhaust Gas Recirculation (EGR) on performance, emissions, deposits and durability of a constant speed compression ignition engine, Appl. Energy. 88 (2011) 2900–2907. doi:10.1016/j.apenergy.2011.01.066.
[114] H. Wei, T. Zhu, G. Shu, L. Tan, Y. Wang, Gasoline engine exhaust gas recirculation – A review, Appl. Energy. 99 (2012) 534–544. doi:10.1016/j.apenergy.2012.05.011.
[115] D.M. Walters, Y.A. Sevcenco, A.P. Crayford, M. Johnson, R. Marsh, P.J. Bowen, Characterising Particulate Line Losses Through A New Proposed Aircraft Engine Sampling System, in: Lund, 2013.
[116] D.M. Walters, Y.A. Sevcenco, A.P. Crayford, M. Johnson, R. Marsh, P.J. Bowen, Differential Mobility Spectrometer Particle Emission Analysis for Multiple Aviation

Gas Turbine Engine Exhaust At High and Low Power Conditions and a Simulated Gas Turbine Engine Exhaust, in: Dusseldorf, 2014.
[117] S.-J. Yook, D.Y.H. Pui, Estimation of Penetration Efficiencies through NASA Sampling Lines, NASA Glenn Research Center, 2005.
[118] P.A. Baron, K. Willeke, Aerosol measurement: principles, techniques, and applications, Wiley, 2001.
[119] User Manual for UTRC Particle Transport Spreadsheet Tool, (2009).
[120] T.C. Lieuwen, V. Yang, Gas Turbine Emissions, Cambridge University Press, 2013.
[121] R. Parker, Engine Technology: the Key to Reducing Aviations Climate Impact, (2011).
[122] Y. Sevcenco, Measurement Techniques and Characterisation of Combustion Species at Operating Conditions Relevant to Gas Turbines, Cardiff University, 2010.
[123] J.-F. Bourgouin, D. Durox, T. Schuller, J. Beaunier, S. Candel, Ignition dynamics of an annular combustor equipped with multiple swirling injectors, Combust. Flame. 160 (2013) 1398–1413. doi:10.1016/j.combustflame.2013.02.014.
[124] M. Boileau, G. Staffelbach, B. Cuenot, T. Poinsot, C. Bérat, LES of an ignition sequence in a gas turbine engine, Combust. Flame. 154 (2008) 2–22. doi:10.1016/j.combustflame.2008.02.006.
[125] R.L. Wayson, G.G. Fleming, R. Iovinelli, Methodology to Estimate Particulate Matter Emissions from Certified Commercial Aircraft Engines, J. Air Amp Waste Manag. Assoc. 59 (2009) 91–100. doi:10.3155/1047-3289.59.1.91.
[126] ARP1533B: Procedure for the Analysis and Evaluation of Gaseous Emissions from Aricraft Engines, (2013).
[127] Aerospace Information Report AIR6241: Procedure for the Continuous Sampling and Measurement of Non-Volatile Particle Emissions from Aircraft Turnine Engines., SAE International, 2013.
[128] D.W. BAHR, Technology for the design of high temperature rise combustors, J. Propuls. Power. 3 (1987) 179–186. doi:10.2514/3.22971.
[129] L. Maurice, M. Ralph, J. Tilston, P. Kuentzmann, Report of the Independent Experts to CAEP/8 on the second NOx Review & Lonf Term Technology Goals, London, 2009.
[130] U. Meier, S. Freitag, J. Heinze, L. Lange, E. Magens, M. Schroll, et al., Characterization of Lean Burn Module Air Blast Pilot Injector With Laser Techniques, J. Eng. Gas Turbines Power. 135 (2013) 121508–121508. doi:10.1115/1.4025148.
[131] I., Meredith B. Colket, R.J. Hall, S.D. Stouffer, Modeling Soot Formation in a Stirred Reactor, (2004) 673–678. doi:10.1115/GT2004-54001.
[132] N. Collings, K. Rongchai, J.P.R. Symonds, A condensation particle counter insensitive to volatile particles, J. Aerosol Sci. 73 (2014) 27–38. doi:10.1016/j.jaerosci.2014.03.003.

Appendices

The following details and datasets were used during the formation of the results presented in this Thesis. However, for the purposes of conciseness and readability they were not included within the main body of the Chapters to which they relate.

Appendix 1: Additional DMS500 Information

Appendix 1.1 Division of DMS500 size measurement range

Table A.1: Division of DMS500 size measurement range.

Spectral Size Bin	Particle Size (nm)	Spectral Size Bin	Particle Size (nm)
1	4.87	21	86.60
2	5.62	22	100
3	6.49	23	115.48
4	7.50	24	133.35
5	8.66	25	153.99
6	10.00	26	177.83
7	11.55	27	205.35
8	13.34	28	237.14
9	15.40	29	273.84
10	17.78	30	316.23
11	20.54	31	365.17
12	23.71	32	421.70
13	27.38	33	486.97
14	31.62	34	562.34
15	36.52	35	649.38
16	42.17	36	749.89
17	48.70	37	865.96
18	56.23	38	1000
19	64.94		
20	74.99		